SHAPE MEMORY POLYURETHANES. APPLICATION IN SMART FABRICS

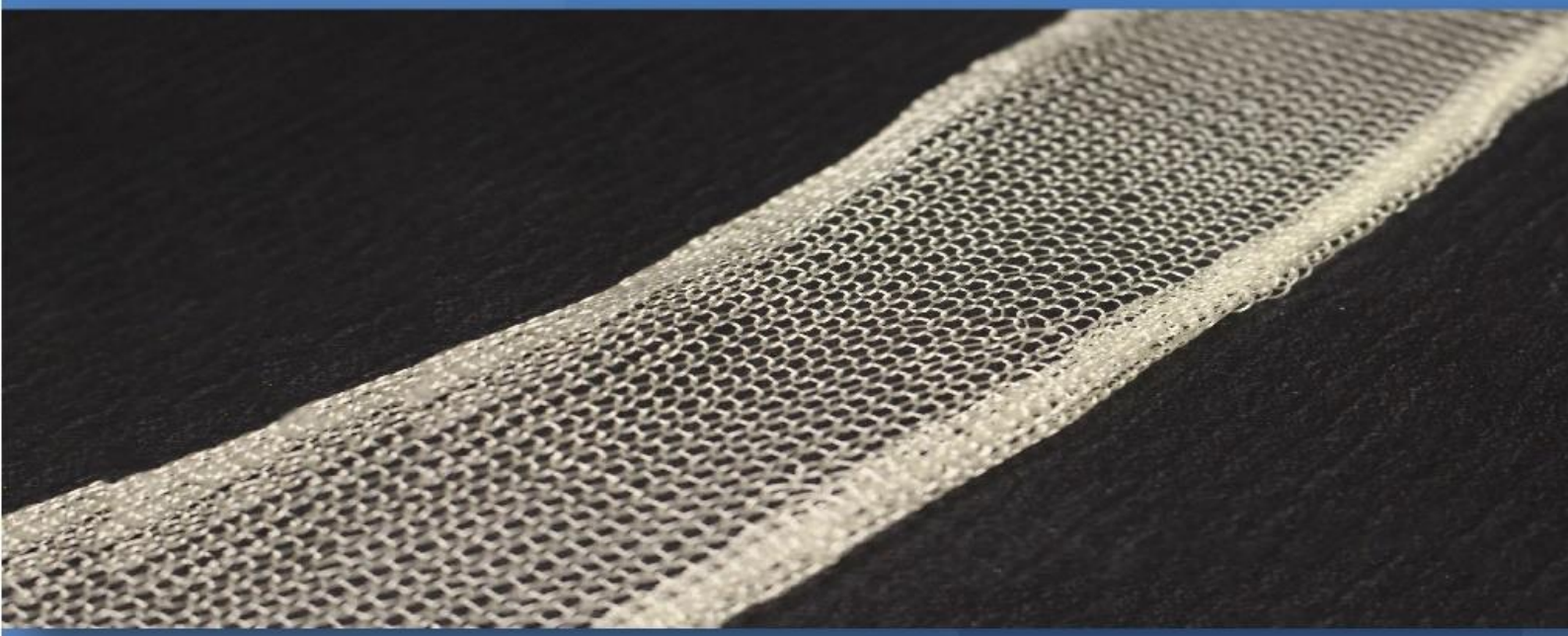

PhD THESIS

Míriam Sáenz Pérez

Leioa 2018

eman ta zabal zazu

Universidad del País Vasco

Euskal Herriko Unibertsitatea

CENTRO TECNOLÓGICO DEL CALZADO DE LA RIOJA

eman ta zabal zazu

Universidad del País Vasco

Euskal Herriko Unibertsitatea

SHAPE MEMORY POLYURETHANES. APPLICATION IN SMART FABRICS.

Memoria para optar al Grado de Doctor por la Universidad del País Vasco (UPV/EHU) presentada por

Míriam Sáenz Pérez

Directores: Prof. Luis Manuel León Isidro

Dr. Jorge García Barrasa

Tesis doctoral

Leioa, 2018

(c)2018 MIRIAM SAENZ PEREZ

Este trabajo de investigación para optar al Grado de Doctor por la Universidad del País Vasco (UPV/EHU) se ha realizado en colaboración entre el Centro Tecnológico del Calzado de La Rioja (CTCR) y el Grupo del Laboratorio de Química Macromolecular (LABQUIMAC) del Departamento de Química Física de la Facultad de Ciencia y Tecnología de la UPV/EHU.

Agradezco sinceramente a la Universidad del País Vasco (UPV/EHU), al Centro Tecnológico del Calzado de La Rioja, a la Universidad de Borås y al Gobierno de la Rioja por el apoyo financiero recibido para la realización de esta Tesis Doctoral.

A mi familia

Abstract

Shape memory polymers (SMPs) have attracted extensive attention from basic research to industrial applications because they have emerged as a cheap and efficient alternative to shape memory alloys. Shape memory polymers present the ability of modifying their shape in a predefined manner in response to externally imposed stimuli. More precisely, shape memory polyurethanes (SMPUs) include a class of polyurethanes that are different from conventional polyurethanes in that they exhibit a hard and soft-segment phase, forming a two-phase heterogeneous structure and morphology. Therefore, a wide variety of polyurethanes can be synthesized with different types of molecular architectures by manipulating their composition and choosing properly the chemical structure of their components, which in turn would be beneficial for their different applications. Among them, adhesives, coatings, automotive, biomedicine, construction and textile and footwear industry are the most important.

In this Thesis, a thorough study of shape memory polyurethanes (SMPUs) for applications in smart fabrics was presented. First, all SMPUs were synthesized by the prepolymer method. Soft-segment was composed of a polyol and hard-segment was composed of a diisocyanate and a chain extender. Second, relevant shape memory properties such as themogravimetric behavior, thermomechanical properties, permeability, and shape memory effect were characterized. Besides, fibers and fabrics were created from shape memory polyurethanes in order to provide deeper understanding towards the use of polyurethanes in the field of textile.

In conclusion, polyurethanes with tunable thermal and mechanical properties were obtained just by varying the hard to soft-segment content. Overall, the obtained experimental findings through this work highlight the potential of both MDI and TDI-based SMPUs for a wide range of applications. Moreover, shape memory effect of SMPUs shows that almost all SMPU samples have been characterized by shape fixity ratios higher than 85% and shape recovery ratios near 99%. Relating to permeability behavior, the conclusion is that these shape memory polyurethane films have potential applications in different fields such as in textile sector that could promote sweat evaporation and humidity control. Finally, it has demonstrated that synthesized and commercial fibers were successfully fabricated and possesses stable thermal properties. Moreover, SMPUs in the form of fabrics show excellent recovery (more than 99.9% in almost samples). Furthermore, it can be concluded that synthesized polyurethane fibers are good enough for future applications in textile industry or medical areas among others.

Resumen

En los últimos años, los polímeros con memoria de forma (Shape Memory Polymers, SMPs) han sido foco de atención, tanto en investigaciones básicas, como en sectores tecnológicamente avanzados, debido a su destacada funcionalidad y a las posibilidades que ofrecen como materiales inteligentes. Estos polímeros han surgido como una alternativa eficaz a las aleaciones metálicas con memoria de forma. Los polímeros con memoria de forma tienen la capacidad de modificar su forma desde un estado 'A' (denominado también original o permanente) a otro estado 'B' (conocido como transitorio o deformado) al aplicar sobre ellos un estímulo externo. Entre ellos, los poliuretanos con memoria de forma (Shape Memory Polyurethanes, SMPUs) son una clase de polímeros que se pueden sintetizar con diferentes tipos de arquitecturas moleculares mediante la variación de su composición y la elección adecuada de la estructura química de sus componentes. Esto da lugar a diversas aplicaciones en automoción, biomedicina, adhesivos, la industria textil o del calzado.

En esta Tesis Doctoral se presenta un estudio sobre los poliuretanos con memoria de forma para aplicaciones en tejidos inteligentes. En primer lugar, se describe la síntesis de SMPUs mediante el método del prepolímero. Los poliuretanos, así sintetizados, poseen una estructura segmentada constituida, por un lado, por segmentos rígidos (diisocianatos y un extendedor de cadena) y, por otro lado, por segmentos flexibles formados por polioles. A continuación, se ha analizado el comportamiento térmico, las propiedades termomecánicas, la permeabilidad y el efecto de memoria de forma. Además, se han creado fibras y tejidos a partir de los SMPUs con el fin de aportar una comprensión más profunda sobre los poliuretanos en la industria textil.

Finalmente, tras los resultados obtenidos, se puede concluir que los poliuretanos con memoria de forma sintetizados poseen aplicaciones prometedoras en la industria textil. Asimismo, el efecto de memoria de forma demuestra que la mayoría de SMPUs poseen valores de recuperación mayores del 99%. Respecto a la permeabilidad, se puede concluir que los films de SMPUs poseen la capacidad de promover la evaporación del sudor y el control de la humedad. Por último, se ha demostrado que las fibras se han obtenido satisfactoriamente y que poseen estabilidad térmica. También, los SMPUs en forma de tejido presentan una recuperación mayor del 99%, por lo que se puede concluir que las fibras y los tejidos se podrán usar en futuras aplicaciones en el campo textil.

Laburpena

Azken urteetan, formazko memoria duten polimeroak (Shape Memory Polymers, SMPs) interes handia izan dute, bai oinarrizko ikerkuntzan eta baita teknologi aurreratuzko sektoreetan ere, eskaintzen duten funtzionaltasun nabariak eta material adimentsuak egiterako orduan ahalbidetzen dituzten aukerengatik, besteak beste. Polimero hauek formazko memoria duten metal aleazioen hautabide gisa azaldu dira. Formazko memoria duten polimeroek 'A' egoeratik (egoera original edo behin betiko egoera bezala ezagutua), 'B' egoerara (trantsiziozko edo behin-behineko egoera bezala ezagutua) forma aldatzeko gaitasuna dute kanpo-estimulu bat aplikatzean heureengan. Horien artean, formazko memoria duten poliuretanoak (Shape Memory Polyurethanes, SMPUs) aurkitzen dira eta polimero hauek arkitektura molekular ezberdinekin sintetizatu daitezke osagaien neurriak aldatuz eta osagaien egitura kimikoen aukeraketa egokia eginez. Ezaugarri horiek, automozio-industria, biomedizina, eranskailu, textil-industria, edo zapatu-industrian hainbat aplikazio ahalbidetzen dituzte.

Doktorego-tesi honek, formazko memoria duten poliuretanoek ehun-adimendunen eremuko aplikazioei buruzko azterketa aurkezten du. SMPUen sintesia deskribatzen da lehenik, prepolimero teknika erabiliz. Honela sintetizaturiko poliuretanoek segmentutan banaturiko egitura osatzen dute, alde batetik segmentu zurrunak (diisozianatoez eta kate-luzatzaile batez osatuak) eta bestetik poliolez osaturiko segmentu malguak. Ondoren, jokamolde-termikoa, ezaugarri termo-mekanikoak, iragazkortasuna eta formazko memoria efektua aztertu dira. Gainera, zuntz eta ehunak sortu dira SMPUak erabiliz, poliuretanoak textil-industrian sakon ulertzeko asmoz.

Azkenik, lorturiko emaitzen harira, formazko memoria duten sintetizaturiko poliuretanoek etorkizun handiko aplikazioak dituztela textil-industrian ondoriozta daiteke. Hala nola, SMPUek formazko memoria efektuaren %99ko berreskuratze-maila baino handiagoak erakusten dituztela frogatzen da. Iragazkortasunaren inguruan, SMPU filmek izerdiaren lurrunketa sustatu eta hezetasuna kontrolatzen dutela ondoriozta daiteke. Amaitzeko, zuntzak behar bezala lortu direla eta egonkortasun termikoa aurkezten dutela erakutsi da. Gainera, SMPUek ehun-forman %99koa baino errekuperatze handiagoa azaltzen dute, beraz, aurkezturiko zuntz eta ehunek textil-eremuan erabilgarriak izango dira zenbait aplikaziotan.

Table of contents

List of tables

List of figures

List of symbols and abbreviations

Symbol	Definition
A	The area of the film
a_{ext}	The humidity outside the cell
a_{int}	The humidity inside the cell
ATR	Attenuated total reflection
BD	1,4-butanediol
C_p	Specific heat capacity
DMA	Dynamic Mechanical Analysis
DR	Draw ratio
DSC	Differential scanning calorimetry
DTA	Differential thermal analysis
DTG	Derivative Thermogravimetric
ε_b	Elongation at break
ε_m	Maximum deformation at T_{high}
ε_p	Residual deformation at T_{high}
ε_u	Deformation after unloading at T_{low}
ε_y	Strain at yield
E'	Storage modulus
F	Force (N)
FE-SEM	Field emission scanning electron microscope
IPNs	Interpenetrating polymer networks
IR	Infrared
l	Thickness of the film
LVR	Linear viscoelastic region
LVTR	Limonene Vapor Transmission Rate

m	The gradient of a line
M_n	Molecular weight
MDI	4,4'-methylenediphenyl diisocyanate
σ_b	Stress at break
σ_y	Stress at yield
OTR	Oxygen Transmission Rate
PO_2	Permeability Oxygen Measurements
PEG	Poly (ethylene glycol) (PEG)
PTMG	Poly(oxytetramethylene) glycol
PUs	Polyurethanes
R_f	Fixing ratio
R_r	Recovery ratio
RH	Relative humidity
SEM	Scanning electron microscope
SMAs	Shape Memory Alloys
SMCs	Shape Memory Ceramics
SME	Shape Memory Effect
SMMs	Shape Memory Materials
SMPs	Shape Memory Polymers
SMPUs	Shape Memory Polyurethanes
v_{r1}, v_{r2}	Roller speeds
tanδ	The loss factor
$T_{5\%}$	Initial decomposition temperature
T_d	Temperature degradation
T_g	Glass transition temperature
$T_{g,DSC}$	Glass transition temperatures measured in DSC
$T_{g,DMA}$	Glass transition temperatures measured in DMA
T_i	Initial temperature

T_{high}	High temperature, programming temperature
T_{low}	Low temperature
T_m	Melting temperature
T_{max}	Maximum degradation rate
T_{onset}	Onset temperature
T_{pist}	Piston temperature
T_{trans}	Transition temperature of shape memory effect
TDI	Toluene 2,4-diisocyanate
TGA	Thermogravimetric analysis
TMA	Thermo-mechanical analysis
U_T	Fracture toughness
V_{pist}	Volumetric flow rate
WVTR	Water Vapor Transmission Rate

Chapter I.
INTRODUCTION

"La calidad radica siempre en la capacidad de afrontar retos diferentes"

Kilian Jornet

Chapter I
INTRODUCTION

1.1. Definition and general aspects of smart materials

The research on smart materials is growing all over the globe due to their potential future benefits, and their intelligent structures and systems. Since the 19th century, revolutionary changes have been occurring at an unprecedented rate in many fields of science and technology, which have profound impacts on every human being. Later, during the second half of the 20th century, the majority of materials were developed for specific purposes, focusing the research on their performance, hence the name 'performative materials'.[1]. In this way, high quality materials were developed for industries such as aerospace, biomedical, industrial, automotive, etc. Due to this increasing awareness of unique material capabilities and properties, material development was taken to another level [2]. Nowadays, the ongoing

development is mainly focused on exploring the different functionalities of these materials and finding out what new added value they can contribute compared to existing materials.

Smart materials are the common name for a wide group of different substances. A smart material was defined as the material which responds to its environment in a timely manner and one or more properties might be altered under controlled conditions. However, the definition of smart materials has been expanded to the materials that receive, transmit or process a stimulus and respond by producing a useful effect [3]. Therefore, smart materials are a new generation of materials which overtake the conventional structural and functional materials.

Many researchers have employed the term 'smart material' in different fields, so that, some definitions are presented here to clarify what a smart material is. In 1989 *Rogers et al.* [4,5] defined smart materials as materials which possess the ability to change their physical properties in a specific manner in response to specific stimulus input. The stimuli could be pressure, temperature, electric and magnetic fields, chemicals, hydrostatic pressure or nuclear radiation. The associated changeable physical properties could be shape, stiffness, viscosity or damping.

Takagi [6] in 1990 defined the smart materials as materials that respond to environmental changes at the most optimum conditions and reveal their own functions according to the environment. The kind of 'smartness' shown by these materials is generally programmed by the material composition, a special processing, the introduction of defects or by modifying the micro-structure, so as to adapt to the various levels of stimuli in a controlled way. Like smart structures, the terms 'smart' and 'intelligent' are used interchangeably for smart materials. These materials possess adaptive capabilities to external stimuli, such as loads or environment, with inherent intelligence. The feedback functions within the material are combined with properties and functions of the materials.

In 1999, *Fairweather* [7] defined active smart materials as those materials which possess the capacity to modify their geometric or material properties under the application of electric, thermal or magnetic fields, thereby acquiring an inherent capacity to transduce energy.

Described in even more detail by *Xiaoming Tao* [8] in 2001, the term smart material is used to refer to materials that can sense and respond in a controlled or

predicted manner to environmental stimuli, which can be delivered in mechanical, thermal, chemical, magnetic or other forms. The responses of smart materials could be visible direct responses including automatic changes in shape, color, geometry, volume and other visible physical properties. Besides these definitions, *Karana & Kandachar* [9] in 2006 defined a smart material as "a material that has the capability to both sense and respond to environmental stimuli, as well as being capable of active control of its response".

Tao [8] further stated, "according to the manner of reaction, the smart materials can be divided into passive smart, active smart and very smart materials", *Figure 1.1*. Passive smart materials can only sense environmental conditions or stimuli; active smart materials will sense and react to the conditions or stimuli; very smart materials can sense, react and adapt themselves accordingly. In other words, passive smart materials are 'smart' in being responsive to their environment, but they lack the inherent capability to transduce energy. Fiber optic material is a good example of a passive smart material. An even higher level of intelligence can be achieved from active smart materials which transduce their stimuli energy into some other form of energy, those intelligent materials and structures are capable of responding or activated to perform a function in a manual or pre-programmed manner [10]. Sensors and actuators may be present in such materials. The sensors provide a nerve system to detect signals, thus in a passive smart material, the existence of sensors is essential. The actuators act upon the detected signal either directly or from a central control unit; together with the sensors, they are the essential element for active smart materials. Piezoelectric materials, shape memory alloys, shape memory polymers, electro-rheological fluids or magneto-strictive materials are considered to be active smart materials and therefore, they can be used as force transducers and actuators. At even higher levels, like very smart or intelligent materials, another kind of unit is essential, which works like the brain, with cognition, reasoning and activating capacities. They are adapted as smart material systems or smart textiles and can respond in any desired way to any desired stimuli by integrating electronics.

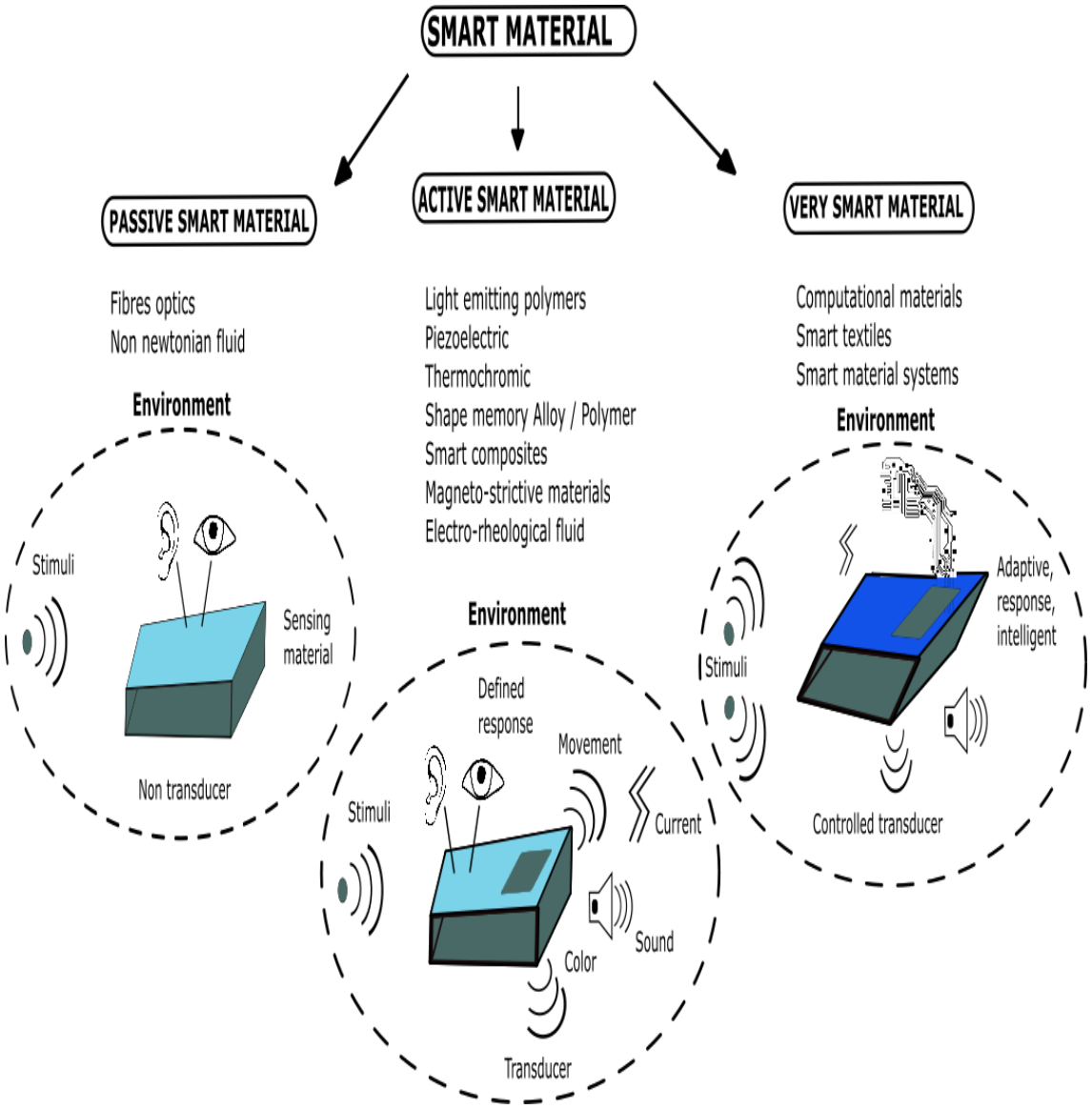

Figure 1.1. *Classification of smart materials by Tao* [8] *(2001)*

As mentioned above, some smart materials need electronic stimuli in order to function, others need to be chemically altered by adding certain 'smart' elements. Other classification about the different types of smart material was given by *Poelman and Tempelman* [11] in 2014. They classified the current smart materials according to their working principles on three levels (*Figure 1.2*):

1) New material systems on molecular level. They can be seen as intrinsic smart materials because they contain characteristics on a molecular level which they can respond to a certain stimulus. There is no need for any external electronic component nor software to make the material respond to the stimuli.

2) New material systems on particle level. The smart component in these materials is thus perceived from an external factor as seen from the original material.

3) New material systems on structural level. This group has a far wider range of applications since they also include materials that are controlled via integrated microprocessors and other electronic devices.

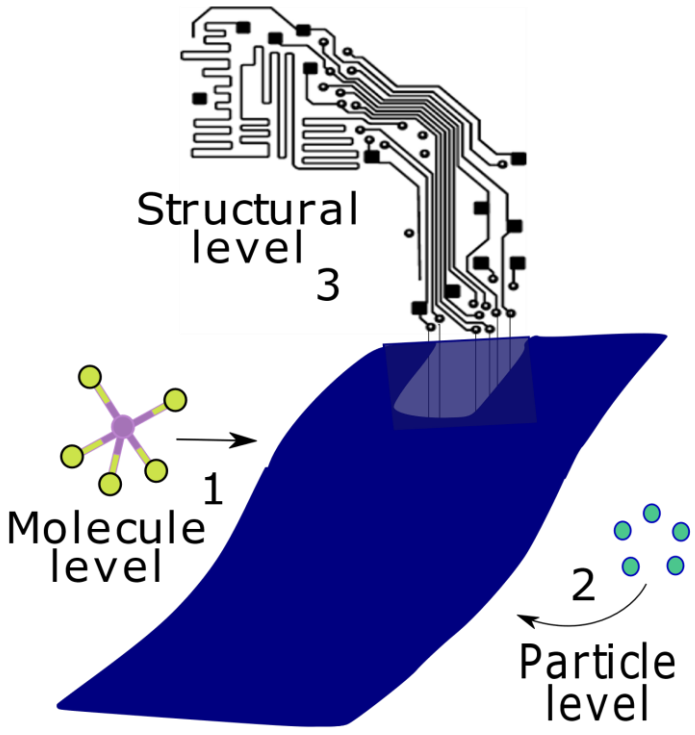

Figure 1.2. *The three levels on which a smart material effect works* [11]

To sum up, the concept of smart materials implies materials that are able to appropriately respond to changes in external factors such as temperature, pH, pressure, electric or magnetic field… by changing their structure and functions. In this way, it can be assumed that the smart materials have their own sensor, which is able to change the materials characteristics. This definition is then consistent with the behavior of shape memory materials, with potential applications as smart materials and new functional materials in many fields such as aerospace, civil engineering applications, biomedicine and textile industry.

1.2. Shape memory materials

Shape memory materials (SMMs) are one of the main groups of smart materials because of their unusual properties, such as the shape memory effect (SME), the pseudoelasticity or large recoverable stroke, the high damping capacity and the adaptive properties which are due to phase transitions in the materials. SMMs may sense thermal, mechanical, magnetic or electric stimuli and exhibit actuation or some pre-determined response, making it possible to tune some technical parameters such as shape, position, strain, stiffness, natural frequency, damping, friction and other static and dynamical characteristics of material systems in response to the environmental changes. However, shape memory materials have to overcome some shortcomings before they become more widely recognized in the industrial world [12–14]. SMMs have been extensively developed and applied in smart structure technology. SMMs have the capability to memorize a permanent shape and to be programmed for one or many temporary shapes, while spontaneously recovering their original permanent shape from temporary deformations upon exposure to an external stimulus [15,16]. As one of the most important branches of smart materials, the most common shape memory materials are shape memory alloys (SMAs), shape memory ceramics (SMCs) and shape memory polymers (SMPs).

a) Shape Memory Alloys

SMAs are metals that exhibit two unique properties. The first one is superplasticity, which is the ability of a material to exhibit large recoverable strains (up to approximately 15%), while deformed within a range of temperature which is characteristic of every specific alloy. The second one is the shape memory effect, characterized by the capability of a material to be deformed at a low temperature and then to revert to its prior shape upon heating above the temperature associated with every particular alloy [17,18].

Shape memory alloys are metal compounds, which can memorize a predetermined shape, and then can be bent, stretched or otherwise mechanically deformed so they can return to this predetermined shape under certain temperature conditions. This shape memory effect is due to a phenomenon known as a thermoelastic martensitic transformation, which is a reversible, diffusionless transformation between two different crystal microstructures that occurs when a shape memory alloy is heated or cooled beyond alloy specific transition temperatures. These temperature-dependent crystal structures or phases are called martensites (low temperature) and austenites (high temperature) [19]. Shape memory alloys are quite strong and hard in their austenite form, but in the martensite form SMAs are soft and ductile and can be easily deformed. SMAs also exhibit superelasticy (or pseudoelasticity) giving the material like a rubber behavior. In other words, the stress-induced strain on SMA can be recovered by heating the alloy up to the austenite finish temperature by transforming the low stiffness martensite phase to the high stiffness austenite phase. This reversible phase transformation is only temperature and stress dependent. The molecular structure of this phase is illustrated in *Figure 1.3.*

The discovery of the shape memory effect dates back to the 1930s when a Swedish chemist, Arne Ölander, discovered the pseudoelastic behavior of Au–Cd alloy in 1932 [20]. Major breakthrough discovery in the field of SMAs came in the earlies 1960s, when Buehler and his coworkers at the US Naval Ordnance Laboratory discovered the shape memory effect in an equi-atomic alloy of nickel and titanium [21]. This alloy was named Nitinol (Nickel–Titanium Naval Ordnance Laboratory) and nowadays it is the most widely used. Since that time, intensive investigations have been made to elucidate the mechanics of its basic behavior. Along with Nitinol, other important SMAs are copper–zinc–aluminum–nickel and copper–aluminum–nickel;

furthermore, SMAs can also be manufactured by alloying zinc, copper, gold and iron, which modifies the SME and superelastic effect as needed [22–24]. As they have a very high energy density and are usable in a variety of shapes, including rods, plates, ribbons, springs and wires, SMAs have been used in a wide variety of applications. For instance, SMA elements have been used in the medical and structural vibration control fields due to their superelastic properties when the temperature is above the austenite transition temperature, allowing them to constantly apply a force to regain their original configuration [25].

Shape memory alloys (SMAs) exhibit outstanding properties such as small size, high strength, easy to shape and work, hold the molded shape very well and have found wide technical applications. However, they have obvious disadvantages, such as high manufacturing cost, limited recoverable force and appreciable toxicity [26]. Therefore, ceramic-based and polymer-based shape memory materials have been explored.

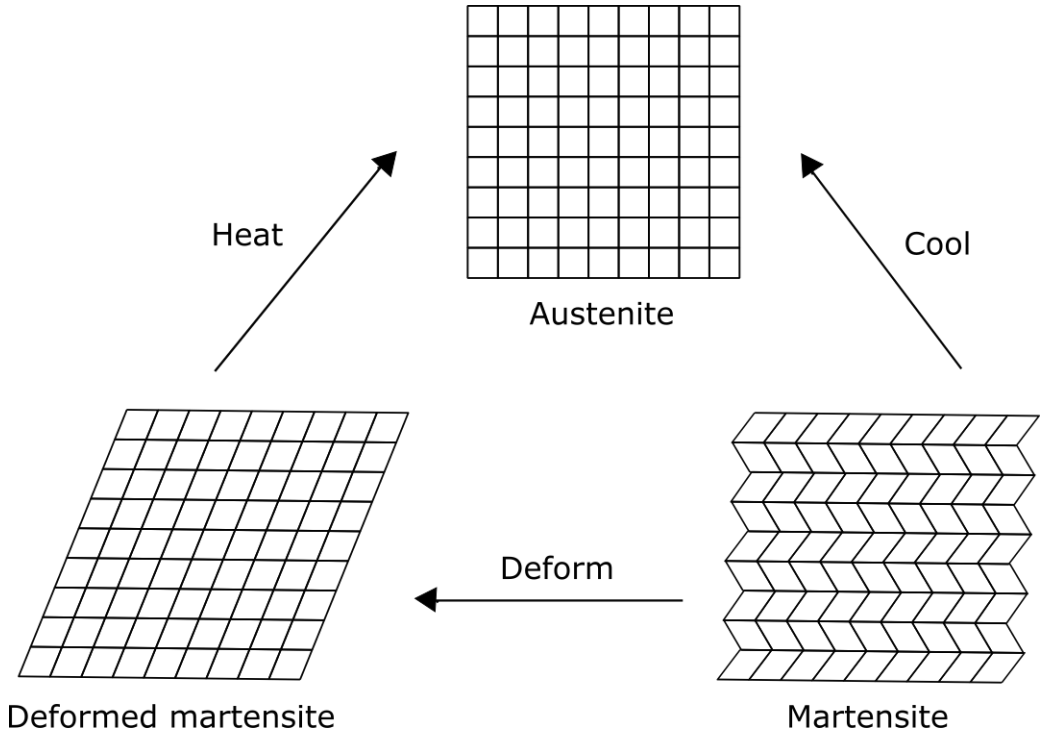

Figure 1.3. *Microscopic and macroscopic views of the two phases of SMAs*

b) Shape Memory Ceramics

Shape memory effect can also be found in ceramic materials. Shape memory ceramics (SMCs) can be classified as viscoelastic, martensitic, ferroelectric or ferromagnetic depending on their activation mechanism [27,28]. SMCs can tolerate much higher operating temperatures than other shape memory materials, but their recoverable strain is quite small. On the other hand, the actuation by electric field, for instance, can be much faster than by heat [29–32].

c) Shape Memory Polymers

Shape memory polymers (SMPs) are another emerging class of SMMs. Unlike SMAs, which can only recover between 1 and 10% strain, SMPs have the capacity to recover strain on the order of 100% [33]. SMPs exhibit a radical change from a normal rigid polymer to a highly flexible elastic polymer and then quickly revert back by application of heat. This change can be repeated multiple times without degradation of the material [34–37].

The term 'SMP' was not officially used until 1984, when the CFG Chimie Company (France) developed a polynorbornene based SMP [38,39]. Since then, the rapid development and wide investigation of SMPs has made their features more and more prominent, particularly compared with SMAs. In this way, one of the major application of SMPs was in robotics to develop an adaptive grip for robots [40]. Moreover, SMPs have been used in medicine and other fields [26,41]. SMPs have several advantages [42,43]:

- they can use diverse external stimuli: in addition to heat, there are many alternative ways to trigger the shape recovery (light, magnetic field, chemical, electricity…).
- they can show highly flexible programming: polymers can be programmed with different stimuli through single and multi-step processes.
- they have a broad range of structural designs: there is an abundance of approaches for designing net-points and switches for various types of SMPs.
- they possess tunable properties: the properties of SMPs can be engineered very easily and accurately tuned using composites, blends and different synthesis methods.

- they can be well-suited for responses to human senses/tissues and also can be biodegradable: SMPs are made from polymers, which are soft materials that provide an abundant array of choices for making highly biodegradable, biocompatible and comfortable devices to interface with our bodies, offering unique opportunities for smart medical, biological and garment-integrated devices.
- they can be very light and can occupy a large volume (foam): these properties are extremely important for applications, such as aerospace devices, air force items and airplane components.

1.3. Shape Memory Polymers

As mentioned above, shape memory polymers (SMPs) have drawn increasing attention because of their scientific and technological significance. Shape memory polymers represent one of the most active areas in material science due to their easier processability, light weight and lower cost when they are compared with shape memory alloys or ceramics. Polymers offer extra advantages due to the fact that they may be biocompatible, nontoxic and biodegradable. SMPs are a promising class of smart materials which are able to change their shape in a predefined way under an appropriate external stimulus, such as heat, light, pressure, electrical field, magnetic field, pH, solvent, etc. [8,15,26,34,44]. The first shape memory polymer was developed by the CDF Chimie Company (France) in 1984 under the trade name of Polynorbornene [38,39] and was commercially available in the same year by Nippon Zeon Company of Japan under the trade name of Norsorex [45]. However, its application has been limited by its poor processibility. After that, lot of works have been done and various kinds of SMPs have been reported and developed.

A single polymer chain cannot present shape memory effect, because it is not a specific material property of the macromolecular chain. The shape memory effect (SME) results from a combination of the overall polymer structure and morphology, together with the applied processing technology. In a macroscopic sense, a thermally induced shape memory effect is due to the presence of networks of polymer chains. These networks determine the permanent shape. The network of polymer chains presents a thermal transition, either a glass transition or a crystallization point, within which the shape memory effect is triggered. The temporary shape can be stabilized

via the transition that is based on these switching segments. Both the deformability from the permanent to the temporary shape and the recovery of the permanent shape, can be attributed to entropy elasticity on the molecular scale [13,46–49].

As stated, shape memory polymers (SMPs) are a type of important stimuli-responsive polymers that have the ability to recover their (permanent) original shape after a deformation into a different one (temporary shape) upon exposure to external stimuli, such as temperature, pH, electric or magnetic fields, light intensity, etc. A stable network and a reversible switching transition of the polymer are the two pre-requisites for the shape memory effect [50–53].

The most common SMP is designed from a polymeric material, in which the polymer chains are able to fix a given deformation by cooling below a certain transition temperature (T_{trans}). The transition temperature (T_{trans}) can be the glass transition temperature (T_g) or the melting point (T_m) of the polymer. Upon reheating above T_{trans}, the oriented or crystalline chains in the network, restore the random conformation resulting in a macroscopic recovery of the original shape [54–57]. The typical process is shown schematically in *Figure 1.4*. Such polymer systems consist of two segments or phases; one of them is a fixed phase and the other one is a reversible or switching phase. *Figure 1.5* shows a schematic representation of the micromechanisms which describes the shape memory behavior.

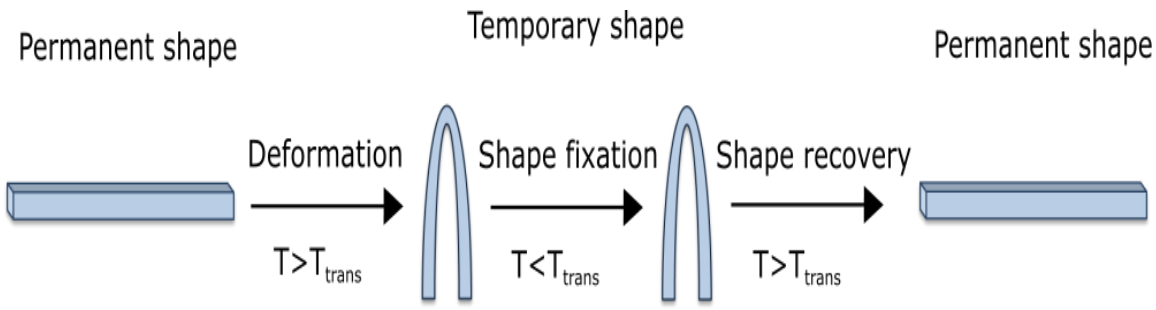

Figure 1.4. *Schematic representation of shape memory effect (SME)*

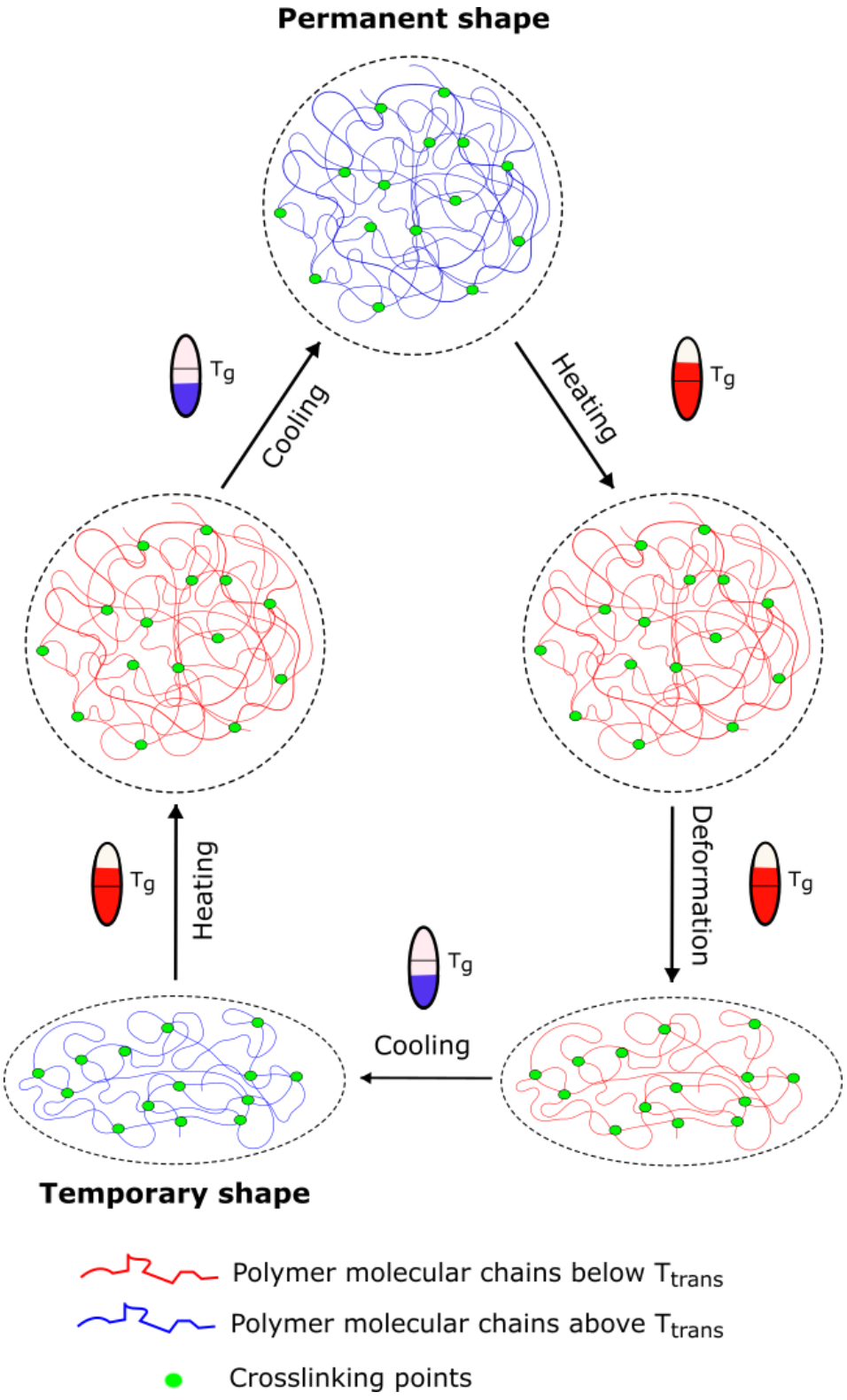

Figure 1.5. *Micromechanism of shape memory effect of polymers*

1.3.1. Classification of shape memory polymers

The classification of the SMPs have been widely discussed and several authors have proposed different models. One of the possible classification is associated to the architecture of SMPs. *Hu and Chen* [58] proposed an overall 3D SMP architecture based on the development of molecular mechanisms that can describe any SMP polymer. In this model, SMPs consist of both netpoints and switch units (*Figure 1.6*).

Relating to the nature of switching segments, the switch units are responsible for controlling the shape fixity and recovery upon a specific and predetermined external stimulus. SMPs are subdivided into different categories: SMPs with amorphous switching segments ($T_{trans} = T_g$) [59–61], SMPs with crystalline switching segments ($T_{trans} = T_m$) [62–65], SMPs with liquid crystallization [66–70], SMPs with supramolecular hydrogen bonding [71,72], SMPs with light reduced reversible network and percolating network in nanocomposites. In all of these systems, the entropic elastic force results from the polymer networks; thus, physical or chemical netpoints via intermolecular forces and/or covalent bonding are usually required.

On the basis of the nature of netpoints, the netpoints of the SMPs determine the permanent shape, which can be formed by physical crosslinking, chemical crosslinking, interpenetrating network and interlocking [62,73–76]. They can respond to a single stimulus or to multiple stimuli as a consequence of small environmental variations that induce macroscopic responses in the material. The driving force for strain recovery in SMPs is the entropic elasticity of the polymer network. The most common netpoints are physical and chemical crosslinking.

On the one hand, chemical crosslinking determines the macroscopic shape of the polymer, while a thermal transition of the polymer segments is used as the shape memory switch. In comparison with physically crosslinking, the polymer networks based on chemical crosslinking show practically no creep, thus any irreversible deformation during the programming or the release progress is greatly diminished.

Other possible classification of the shape memory polymers can be shown in *Figure 1.7*. This schematic figure presents an insight into SMPs based on structure, stimuli and functionality [48,77]. Thus, the structure and composition of SMPs can be block/segmented copolymer [64,78–80], supramolecular polymer [81], polymer blends [82–84], polymer composites [85–87], interpenetrating polymer networks (IPNs) [88], semi-IPNs [89,90] and even crosslinked homopolymer [91,92].

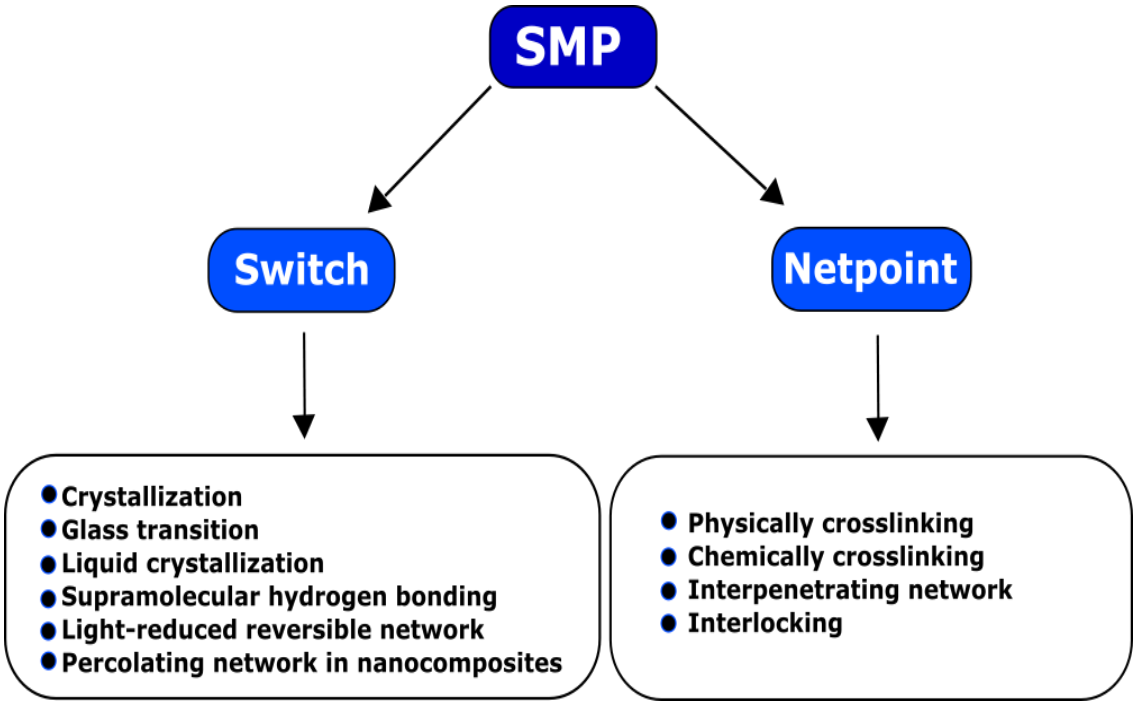

Figure 1.6. *Architecture of shape memory polymers*

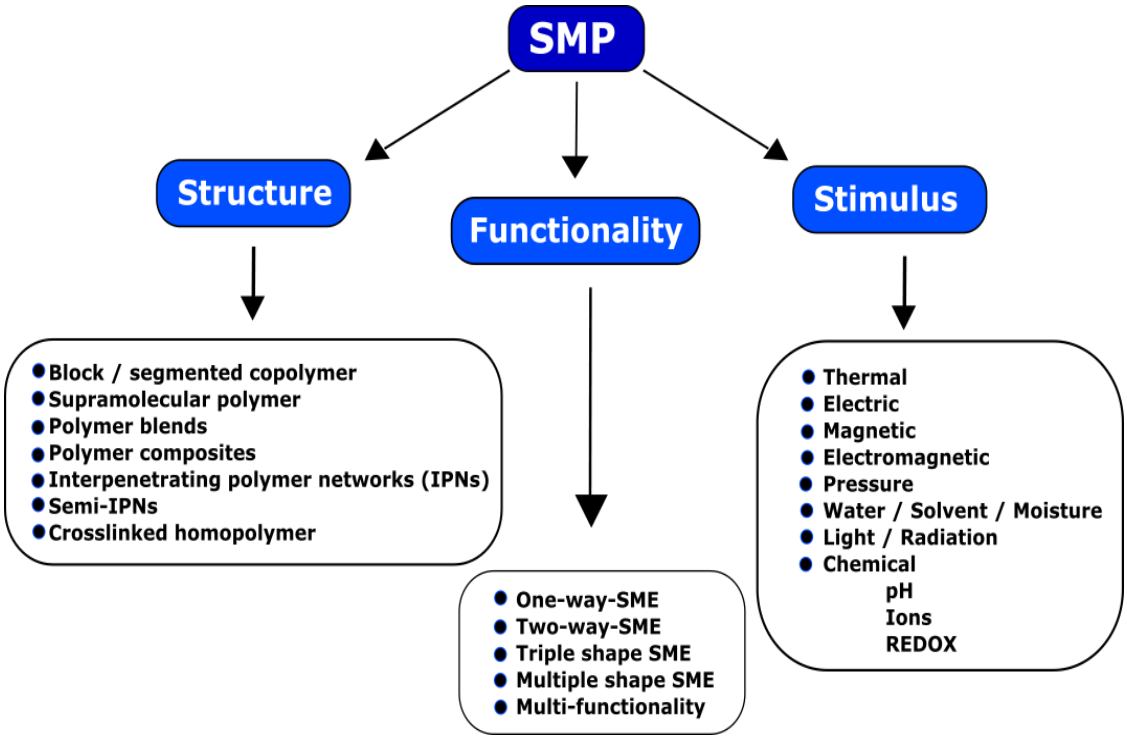

Figure 1.7. *Insight into SMPs based on structure, stimulus and functionality*

Relating to functionality, the shape memory effect (SME) of SMPs has been developed from different ways: the conventional one-way SME, two-way SME, triple shape SME and multiple shape SME. Additionally, multi-functionality can be achieved in SMPs, as discussed by *Behl et al.* [60].

Finally, an external stimulus is needed to achieve the SME, which is used to trigger the strain recovery after deformation. Thus, SMPs can be classified by their stimulus into the following groups: thermally induced [93,94], electrically induced [95,96], magnetically induced [97,98], electromagnetically induced [99], pressure induced [100], water/solvent/moisture induced [101,102], light/radiation sensitive [103,104], and chemical sensitive (pH, ions, oxidation-reduction [105,106]).

The most investigated shape memory polymers are the thermo-induced SMPs. They can convert the thermal energy directly into mechanical work. This work focuses on this kind of polymers because they may be very useful in textile industry applications. Therefore, the actuation must be triggered by heating at around body temperature (~37°C), e.g., the materials must change back to their permanent shape at approximately this temperature.

Moreover, relating to the final product, shape memory polymers can be easily fabricated in different forms *(Figure 1.8)*. Some examples are films, fibers or wires, yarns, powder, emulsion, chips, foams and plates. These application forms enable them feasibly to be incorporated with other materials to create hybrid composites.

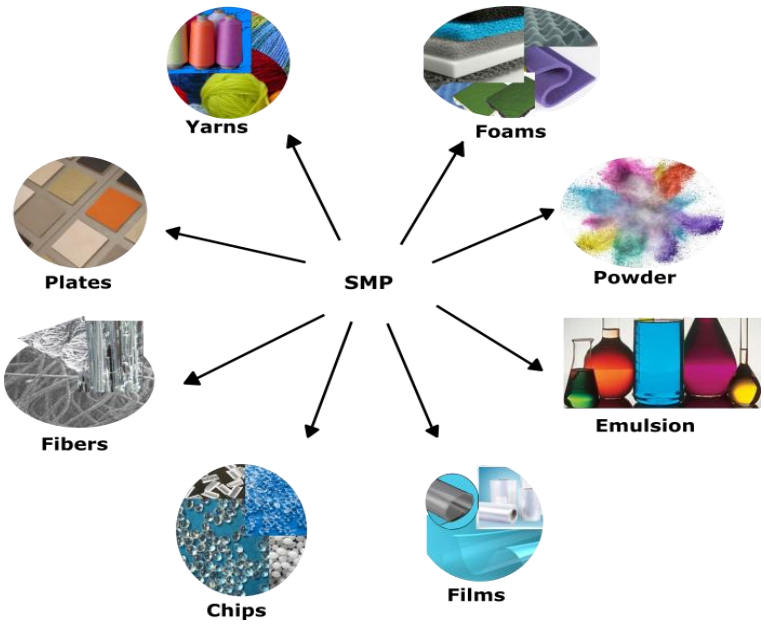

Figure 1.8. *Application forms of shape memory polymers*

1.4. Shape memory polyurethanes (SMPUs)

This thesis has been focus on a common shape memory polymer: the polyurethane (PU). Shape memory polyurethanes (SMPUs) have been chosen because of its wide variety of applications in the footwear and textile industry. General considerations of polyurethanes and some other important aspects of shape memory polyurethanes are presented in this section.

1.4.1. General considerations of polyurethanes

More than half a century ago, plastic industries were working with polymerization and polycondensation processes to produce plastics. In 1937 the German scientist Dr. Otto Bayer, also known as "father" of polyurethane, with IG Farbenindustrie developed the polyurethane technology: the polyaddition reaction. The polyaddition of a diisocyanate to a diol in the presence of a catalyst proceeds completely to a polyurethane under mild conditions without the formation of undesired products. During World War II polyurethanes were used in small scale for aircraft coating, but it was not until 1952 that polyisocyanates became available in the market. In 1954, a commercial production of flexible foam began, based on toluene diisocyanate (TDI) and polyester polyols. The invention of these foams was thanks to water accidentally introduced in the reaction mix. These materials were also used to produce rigid foams, gum rubbers and elastomers. Schollenberger (1958) introduced the crosslinked thermoplastic polyurethane elastomers [107,108]. Commercial use of polyurethanes in several technical areas were considered after 1960.

Polyurethanes (PUs) are the most versatile synthetic polymer materials that have been employed in diverse industrial applications for several decades. Their many uses range from flexible foams and rigid foams as insulation in walls and roofs, to thermoplastic polyurethanes used in medical devices and footwear, to coatings, adhesives, sealants and elastomers used on floors and automotive interiors [109–111]. Polyurethane is a unique material that offers the elasticity of rubber combined with the toughness and durability of metal. Because polyurethanes are available in a very broad hardness range, it allows the engineer to replace rubber, plastic and metal by these materials.

1.4.2. Polyurethane structure

Polyurethane is a multiblock copolymer having urethane bonds in its backbone. This polymer structure can vary its properties over a very wide range of strength and stiffness by modification of its three basic building blocks: the polyol, the diisocyanate and the chain extender. Polyurethanes are made up of hard and soft-segments. In other words, polyurethane is a multi-block copolymer that consists of alternating hard and soft-segments. A hard-segment (HS) usually consists of diisocyanate and a chain extender, and a soft-segment (SS) is usually made up of polyol (*Figure 1.9*). The hard and soft-segments are thermodynamically incompatible at low temperature resulting in the microphase separated structure (*Figure 1.10*). The properties of segmented polyurethanes depend on their structure [112].

The polyurethanes possess enhanced mechanical, thermal and optical properties. These properties are related to segmented flexibility, chain entanglement, interchain forces and crosslinking. Some relevant properties of polyurethanes are low density, excellent flexibility, shape memory, high abrasion resistance, corrosion resistance, high elongation at break, weathering durability, high elasticity, anti-aging, good processability, high impact strength, excellent gloss, transparency, controllable hardness, high biocompatibility and biostability, excellent blood compatibility and good low temperature flexibility [113–116]. The structure of polyurethanes can be modified according to the preferred application requirements. Therefore, choice of reactants, their ratio as well as the synthesis methods are important for PU design. In this way, PUs have been tailored to meet the highly diversified demands of modern technologies.

There are also some major disadvantages associated with PUs in terms of high temperature applications. PUs have some drawbacks, for example, insufficient tensile strength and thermal stability in a high temperature working environment with low anticorrosive properties [117]. PUs are highly flammable in these conditions and have poor adhesion to metal surfaces [118]. The poor heat resistance and the low tensile strength of PUs are the most known barriers for their application [119]. PUs also exhibit poor thermal and electrical conductivity [120]. The PUs limitations have led to the birth of nanocomposites to compensate them by addition of other materials [121].

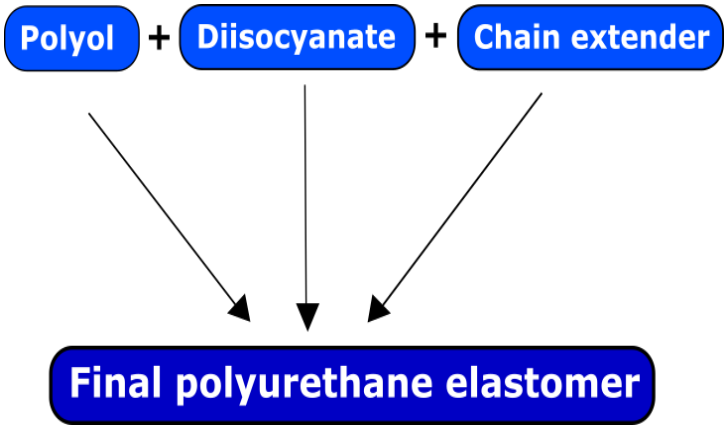

Figure 1.9. *Composition of polyurethane*

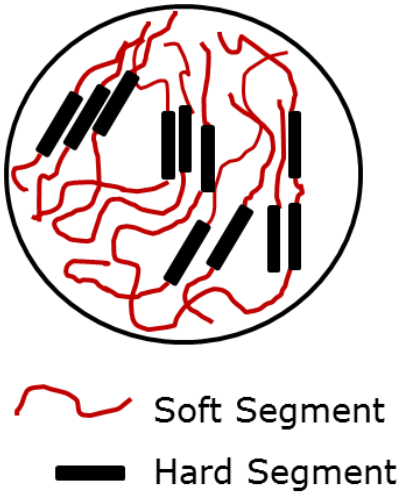

Figure 1.10. *Polyurethane structure*

As indicated earlier in this chapter, the main components of polyurethanes are a polyol (soft-segment), a diisocyanate and a diol (hard-segment). A brief description is reported below.

Polyols are the predominant reaction partners of diisocyanates. The two main classes of polyols are polyethers and polyesters, usually with molecular weights between 500 and 5000 $g \cdot mol^{-1}$. The most common polyethers are polypropylene glycols, polyethylene glycols, polybutadiene diols and polytetramethylene glycols. The polyesters include aliphatic and aromatic polyesters. Among them, the most used

are polyethylene adipate glycol, polyhexamethylene carbonate glycol and polytetramethylene adipate glycol. They are more expensive to produce and much more viscous than polyethers with comparable chain lengths. In both cases the manufacture involves the addition polymerization of the monomeric epoxide [122].

Relating to diisocyanates, isocyanates are characterized by the percentage of NCO content and their functionality, which indicates how many NCO groups a molecule contains. There are different types of diisocyantes: aromatic, aliphatic and cycloaliphatic isocyanates. Aromatic isocyanates account for the vast majority of global diisocyanate production. Aliphatic and cycloaliphatic isocyanates are also important building blocks for polyurethane materials, but in much smaller degree. This is because the aromatically linked isocyanate group is much more reactive than an aliphatic one. Another reason is that aromatic isocyanates are more economical than the aliphatic isocyanates. The most important ones used in elastomer manufacture are 2,4- and 2,6-toluene diisocyanates (TDI); 4,4'-diphenylmethane diisocyanate (MDI) and its aliphatic analogue 4,4'-dicyclohexylmethane diisocyanate (HMDI); 1,5- naphthalene diisocyanate (NDI); 1,6-hexamethylenediisocyanate (HDI); isophorone diisocyanate (IPDI); and 3- isocyanatomethyl-3,5,5-trimethylcyclohexyl isocyanate (TMDI) [123,124].

The last component to form polyurethanes is the chain extender. Typical chain extenders are low molecular weight (M_w<400 g·mol^{-1}) difunctional intermediates designed to react with the isocyanate groups to become part of the hard-segment. The chain extenders play a very important role. Without a chain extender, a PU formed by directly reacting a diisocyanate and a polyol generally has very poor physical properties and often does not exhibit microphase separation. The introduction of a chain extender may increase the HS length allowing its segregation, which results in good mechanical properties, such as an increase in the modulus and an increase in the HS glass transition temperature of the polymer. PUs chain extenders can be categorized into two classes: aromatic diols and diamines and the corresponding aliphatic ones. Examples of diol chain extenders include 1,6-hexanediol (HD), ethylene glycol (EG), 1,4-butanediol (BD) and diethylene glycol (DEG). Examples of diamine chain extenders include 2,5-bis-(4-aminophenylene-1,3,4-oxadiazole) (DAPO), 4,4’-diamino-dibenzyl (DAB), 2,6-diaminopyridine (DAPy) or 4,4’-methylene-diamine (MDA) [125,126].

Other important aspect to be taken into account in polyurethanes is the way to synthesize them. PUs microstructure and its mechanical behavior are strongly dependent on the employed synthesis method. There are two methods of reaction control: the components being allowed to react either simultaneously ("one shot process") or successively in two stages (prepolymer process) [127,128].

In the one shot polyaddition procedure all reagents (polyol, diisocyanate and chain extender) are added at once during the initial reaction. Although this is a commonly used industrial technique, this procedure does not have the control required to yield regular block sequences. However, the process is faster, easier and more reproducible and can be used to best advantage where the reaction rates of the diol components with the diisocyanate are comparable.

In contrast, in the prepolymer method, in the first step of the reaction a prepolymer is produced through the reaction of a polyol with an excess of diisocyanate, followed by a chain extension with a chain extender to form the HS and also to increase the overall molecular weight of the polymer. The PUs obtained via the prepolymer method are statistically more regular in the chain sequence of polyester-diisocyanate-glycol-diisocyanate-polyester, whereas PUs obtained by using the one shot process (assuming the polyester and the glycol are of equal activity) have a more random sequence [129].

1.4.3. Shape memory polyurethanes

Shape memory polyurethanes (SMPUs) are a class of polyurethanes that are different from conventional ones. SMPUs exhibit a hard-segment phase and a soft-segment phase, forming a two-phase heterogeneous structure and morphology. In order to show good shape memory properties, the hard segment content in the SMPUs must be high enough to inhibit the plastic flow of the chains by forming physical crosslinks that are responsible for memorizing the primary shape.

Since the discovery of the shape memory effect (SME) in polyurethanes by Mitsubishi Heavy Industry (MHI) in 1988 [130], extensive research on SMPUs has been carried out, resulting in the most systematic knowledge on SMPs. The advantage of the shape memory polyurethanes is the flexibility that the polyurethane chemistry provides in designing materials with a wide range of phase transition temperature.

In addition, these polyurethanes are thermoplastic polymers that provide a significant improvement to be processed [27].

Thus, a wide variety of polyurethanes can be synthesized with different types of molecular architectures just by manipulating their composition and choosing properly the chemical structure of their components, which in turn would be beneficial for their different applications [131,132]. Among them, the textile finishing, adhesives, coatings, automotive, furniture, construction, thermal insulation and footwear industries are the most important [133,134].

For example, shape memory polymers yield intelligent textiles that exhibit unique responses to environmental changes. In the history of humans, textiles have been the driving force to industrialization. Now it seems that smart textiles and intelligent clothing could play an important role again when developing smart materials for all round applications.

1.5. SMPs applications

Shape memory polymers can be widely used in many areas such as adaptive biomedical devices, cell growth, aerospace, functional textiles, footwear, energy, bionics engineering, electronic, civil engineering, toys, pipe joints, utensils, cosmetics, products for rest, adhesives, films for packaging, household products, etc. These examples cover only a small number of the possible applications of shape memory technology, which shows potential in numerous other applications. In fact, there is a need for a comprehensive review of SMPs to provide some guidance for people who initiate in this field and to stimulate more meaningful work for people in the area in the years ahead. *Figure 1.11* summarizes the most common applications of SMPs [135–141]. It is difficult to extensively explain all the applications. Therefore, as this work focuses on the textile and footwear applications of SMPUs, only some relevant examples about these applications are described in this section.

In recent years, significant progresses have been achieved in the area of technical textiles. Fibers, yarns, fabrics and other structures with added value functionality have been successfully developed for high performance end uses. Technical textiles have been promoted as alternative materials for a limitless range of applications, including engineering, automotive industry, aerospace and medical

industry. In textile industry, rapid progresses in high performance materials have attracted a lot of interest for the sports and protective clothing industry. The clothing industry can potentially be revolutionized with the commercialization of the latest 'smart' textiles research. Numerous SMPs have been commercialized in large scales such as polyurethanes (DiAPLEX, SMP Technologies Inc., originally from Mitsubishi Heavy Industries), polystyrene based SMPs (Veriflex, Verilyte, Veritex, Cornerstone Research Group, Inc.), aliphatic polyurethanes (Tecoflex, Lubrizol Advanced Materials), epoxy based SMPs (TEMBO, Composite Technology Development, Inc.), and UV curable polyurethanes (NOA-63, Norland Products Inc.) [142].

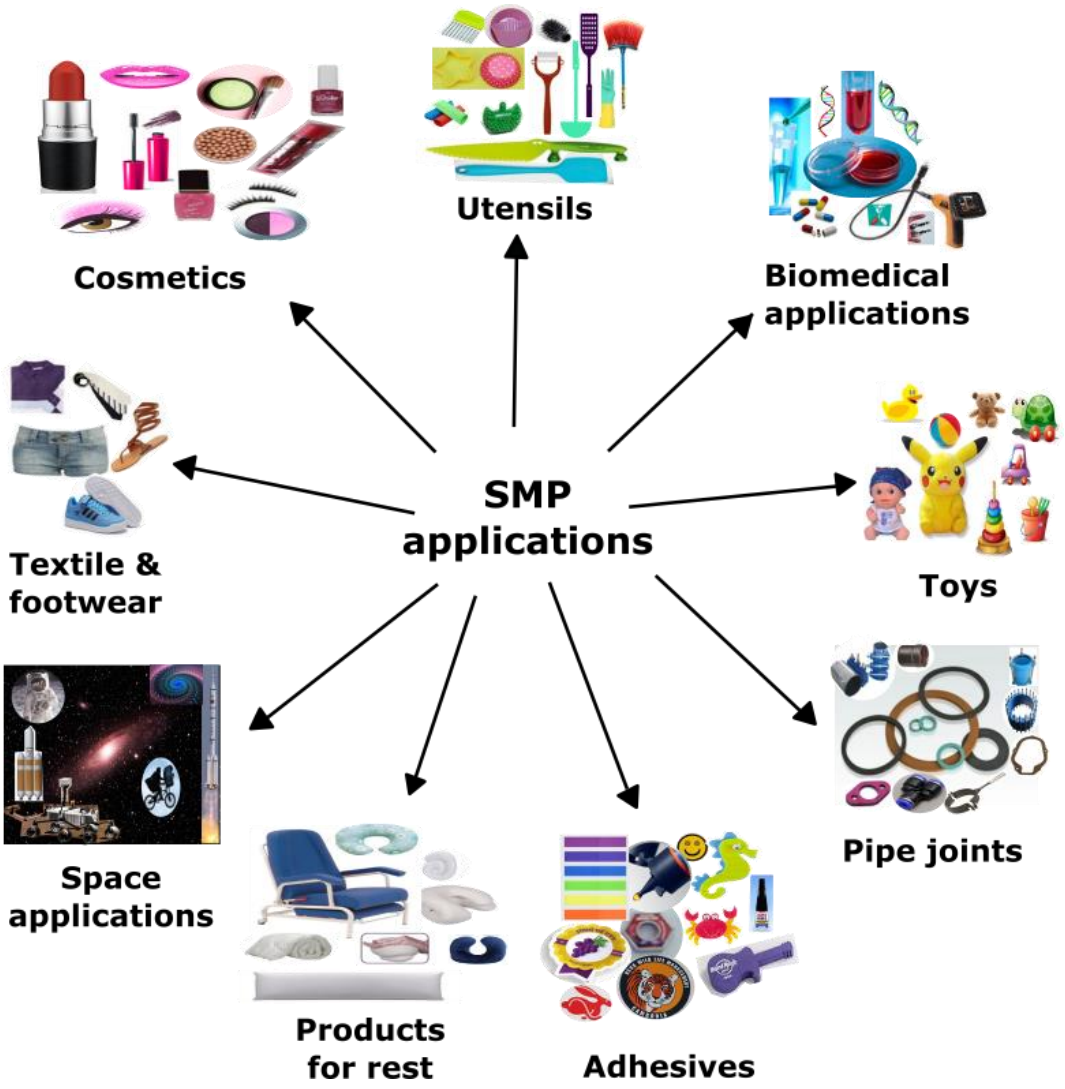

Figure 1.11. *Some applications of shape memory polymers*

For example, when a piece of fabric is sewn with a conductive yarn or the entire fabric piece is conductive itself, it allows the designer to integrate all sorts of electrical components onto it. These results can be used to create interactive fashion clothing that demonstrate the capabilities of textiles integrated with electronics (*Figure 1.12*).

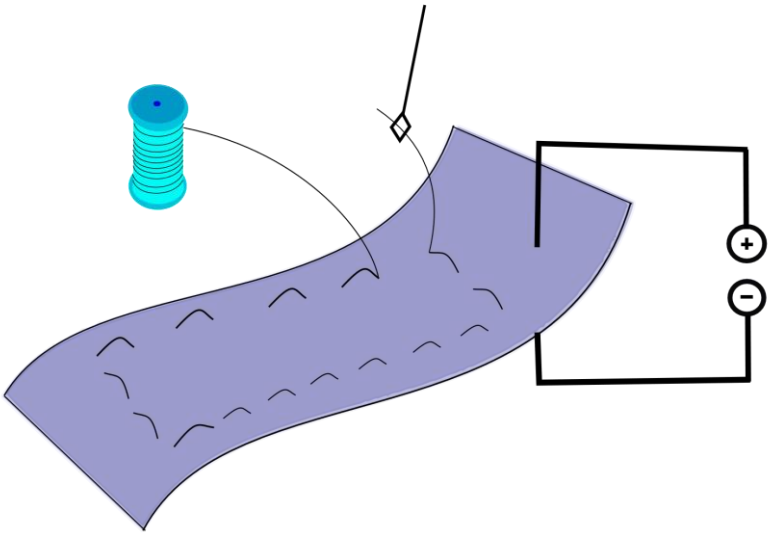

Figure 1.12. *Smart textiles*

As it is known, many materials are never further developed and remain in the prototype or research stage. This usually happens when the costs are very high, and causes a poor reception from the design world and commercial market. On the contrary, these smart material systems are adapted more easily because are not expensive materials since are composed by a simple base material and some integrated electronics. Examples range from smart products that make use of integrated sensors to a couple of products in which an actual intrinsic smart material is used. Thus, the shape memory textile created by *Mariëlle Leenders* [143], "Curious collections", is a piece of clothing that shrinks up its lower part when a temperature of around 45ºC is reached. Imagine a hot summer or an increasing body temperature due to perspiration and your shirt helping you to cool by opening up (*Figure 1.13*).

Figure 1.13. *Shape memory textile by Mariëlle Leenders.*

Linda Worbin [144] is a senior lecturer in Textile Design at the Swedish School of Textiles who exhibited a collection of smart textile samples. In the collection, *Worbin et al.* [145] created qualities such as color changing textiles (due to temperature or light conditions), lighting textiles (light transporting and emitting textiles, etc.), and conductive textiles (for example to be used as sensors, heat emitters or for transporting electricity). To begin with the collection, they met industrial requirements and limitations to spark a discussion and to make users see the actual textile material as a design tool. By creating a collection of smart textile samples, a possibility arose for other disciplines to work with smart textile materials. The goal was to collect feedback on how these new textile qualities can be used and to further develop textiles for different areas and for a variety of applications. They wanted to know if smart textile materials gain from being developed from a more craft based perspective in the next phase (*Figure 1.14*).

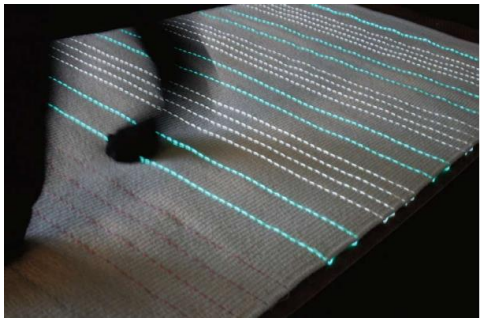

Figure 1.14. *Smart textiles. Photo: Linda Worbin*

Other example of the use of smart textiles is the black air dress. For the black air dress and its white counterpart, the white air dress, *Hertenberger et al.* [146] were inspired by inflatable life-jackets. By the release of gaseous carbon dioxide, the collar or back of the dress is inflated to form a pillow. This allows the wearer to lean against a wall or another person to rest while waiting for the train or the arrival of a friend. The white air dress also lights up to invite other people to use the pillow. The idea behind inflatables is philosophical but also very practical. Some people get very stressed in a crowded space. The concept of their inflatable garments helps create instant private space around you, said Marta Kisand (one member of the group). Strips of textile from the dress were displayed in the exhibition, allowing visitors to try out the various color combinations available (*Figure 1.15*).

Figure 1.15. *Exhibition footage: Photo: Jan Berg*

1.6. Objectives and outline of the report

Shape memory polymers are expected to have a prominent role in the future. Therefore, this research project tries to reach a wide understanding about shape memory polymers, specifically shape memory polyurethanes (SMPUs), to create new materials with novel functionalities involved in footwear and textile industry. For this reason, this doctoral Thesis was realized in collaboration between The Footwear Technology Center of La Rioja (CTCR) in Arnedo and the University of the Basque Country (UPV/EHU) in Leioa.

The overall objective of this work is the study, synthesis and characterization of new SMPUs in order to develop fabrics capable of modify their shape against an external stimulus: changes in temperature. Thus, it is necessary to acquire and generate novel significant knowledge in the polyurethane synthesis and finally, to create new shape memory fibers and fabrics from the developed SMPUs to be industrially applied in both textile and footwear fields. For this purpose two polyols (poly(ethylene glycol), PEG, and poly(oxytetramethylene) glycol, PTMG), two isocyanates (4,4'-methylene diphenyl diisocyanate, MDI, and 2,4-toluene diisocyanate, TDI) and a chain extender (1,4-butanediol, BD) were selected. As synthesis method, the prepolymer method was chosen. Moreover, relevant shape memory properties such as themogravimetric behavior, thermomechanical properties, permeability and shape memory effect were characterized.

Obviously, to achieve this overall objective it is essential to organize the work in clearly and defined specific technical objectives:

- To acquire and generate novel knowledge about the synthesis of shape memory polyurethanes and the technologies required to obtain them.

- Synthesis and characterization of different shape memory polyurethanes obtained from the chosen reagents: PEG, PTMG, MDI, TDI, BD and mixtures of them. To verify the mechanical and thermal properties and shape memory behavior of every developed SMPUs. To optimize the synthesis procedure to get SMPUs with a transition temperature near the body temperature (~ 37ºC).

- To develop fibers with the optimized shape memory polyurethanes and to characterize them. Finally, with these fibers, to make fabrics in order to be tested in textile industry.

The content of the chapters, their main objectives and hypotheses, are summarized as follows (*Figure 1.16*).

Chapter I presents a brief description of the state of art of smart materials, an overview on the most important research issues of shape memory polymers, their applications and the principal objectives of the doctoral Thesis. Specifically, in this chapter, conceptualization, antecedents and applications of shape memory materials are reviewed. This chapter is the starting point of the present guide research throughout the following chapters.

Chapter II introduces the materials, the synthesis mechanism performed in this work and the characterization techniques. Characterization techniques were firstly used to check the success of the SMPUs synthesis reaction, secondly to test the most relevant mechanical and thermal properties and, finally, to analyze the shape memory behavior of the developed polyurethanes.

In *Chapter III,* Attenuated Total Reflectance (ATR) was used to assess the extent of the reaction between the isocyanate and hydroxyl groups, i.e., to confirm that the isocyanate groups were completely reacted. Moreover, thermal properties as the glass transition temperature (T_g) and the initial temperature of the degradation were measured by Differential Scanning Calorimetry (DSC) and Thermogravimetric Analysis (TGA), respectively. Finally, the thermomechanical behavior of shape memory polyurethanes was analyzed by Dynamic Mechanical Analysis (DMA) and tensile stress-strain tests.

In *Chapter IV,* the shape memory behavior of all polyurethanes was evaluated by thermomechanical analysis (TMA). Shape fixity and shape recovery ratios were calculated from some parameters, defined in this chapter, such as the maximum strain, the strain fixed and the residual strain. Finally, in some selected samples, the repeatable shape recovery ability was tested by six subsequent shape recovery cycles.

Chapter V focuses on permeability behavior exclusively. In this chapter the water vapor transmission rate (WVTR), the oxygen permeability (PO_2) and the limonene vapor transmission rate (LVTR) are studied.

In *Chapter VI*, attention is paid to direct applications. Fibers and fabrics created (this work was performed at the University of Borås, Sweden) from some selected shape memory polyurethanes synthesized previously in the laboratory (those with glass transition temperatures near body temperature) were characterized by DSC, TGA, DMA, TMA, etc.

Finally, in the *Chapter VII*, general conclusions and the most significant results of each chapter are summarized. All results are integrated in order to move one step forward in the understanding of shape memory polyurethanes and their application in textile and footwear fields. At last, weakness, strengths and challenges for future research are also presented.

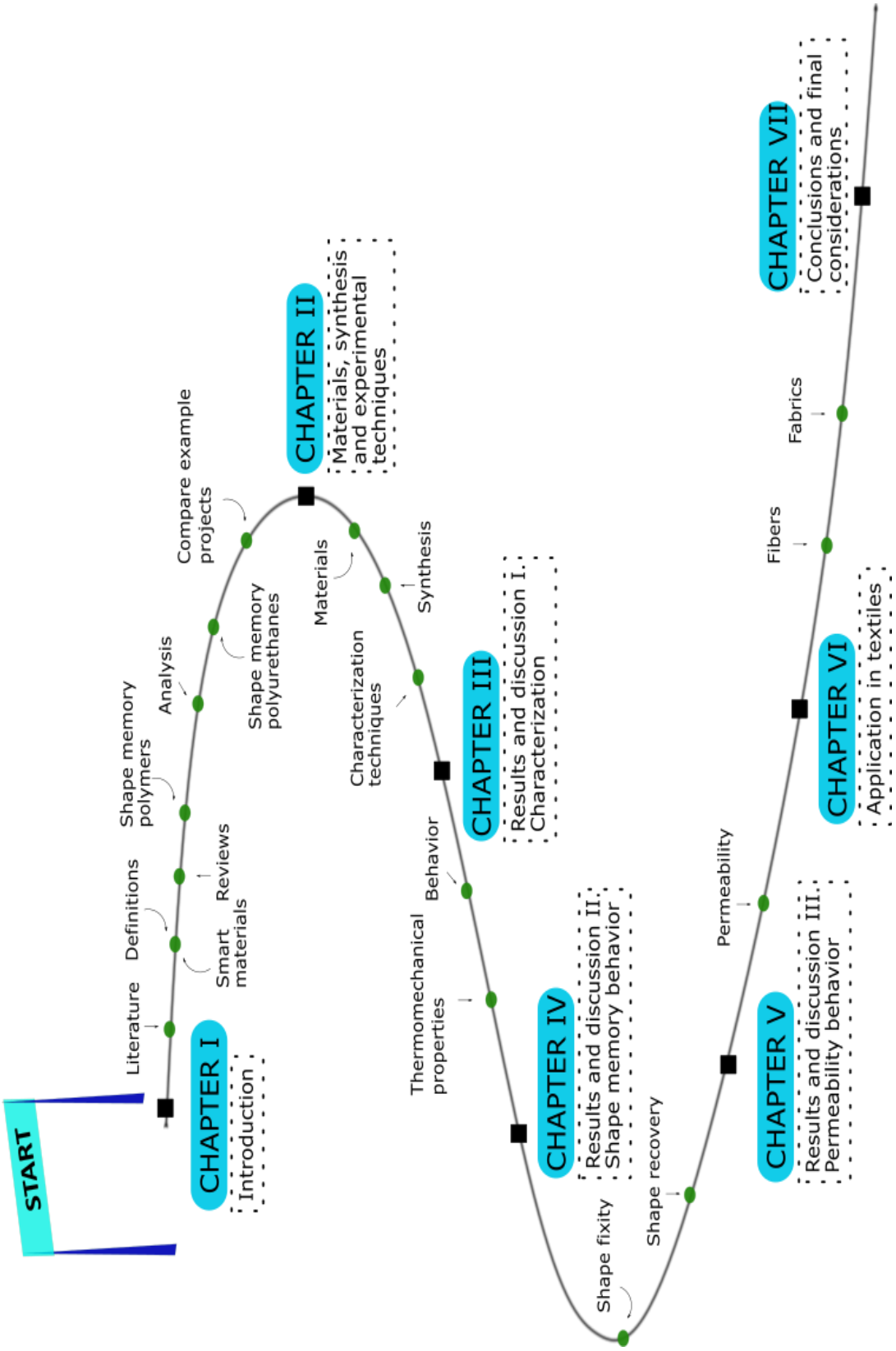

Figure 1.16. *Thesis overview goal*

1.7. References

1. Gordon JE, Mattis DC (1985) The New Science of Strong Materials, or, Why You Don't Fall Through the Floor. Am J Phys 53:508–509.
2. Bergström J, Clark B, Frigo A, et al (2010) Becoming materials: material forms and forms of practice. Digit Creat 21:155–172.
3. Coyle S, Diamond D (2010) Smart Nanotextiles: Materials and Their Application. In: Encycl. Mater. Sci. Technol. Elsevier, Oxford, pp 1–5
4. Rogers CA, Ahmad I (1989) US Army Research Office Workshop on Smart Materials, Structures and Mathematical Issues proceedings. In: Work. held Blacksburg, VA, 15-16 Sep. 1988. pp 15–16
5. Rogers, A. C (1989) Introduction to Smart Materials and Structures. Smart Mater Struct Math Issues 17–28.
6. Takagi T (1990) A Concept of Intelligent Materials. J Intell Mater Syst Struct 1:149–156.
7. Fairweather J (1999) Designing with active materials: An impedance based approach. UMI, New York.
8. Tao X (2001) Smart Fibres, Fabrics and Clothing. CRC Press, New York.
9. Karana E, Kandachar P (2006) Smart Surroundings: a New Era for Communication and Information Technologies. 1st Int CIB Endorsed METU Postgrad Conf Built Environ Inf Technol 35–44.
10. Kumar S (1991) Smart Materials for Acoustic or Vibration Control. Pennsylvania State University
11. Poelman W, - ET, Hungary U, et al (2014) Organic interfaces. Proc TMCE 1561–1572.
12. Aguilar MR, San Román J (2014) Smart Polymers and their Applications. Woodhead Publishing, Cambridge.
13. Leng J, Du S (2010) Shape-Memory Polymers and Multifunctional Composites. CRC Press, New York.

14. Leng J, Lan X, Liu Y, Du S (2011) Shape-memory polymers and their composites: Stimulus methods and applications. Prog Mater Sci 56:1077–1135.

15. Hu J, Zhu Y, Huang H, Lu J (2012) Recent advances in shape–memory polymers: Structure, mechanism, functionality, modeling and applications. Prog Polym Sci 37:1720–1763.

16. Li F, Zhu W, Zhang X, et al (1999) Shape memory effect of ethylene–vinyl acetate copolymers. J Appl Polym Sci 71:1063–1070.

17. Banks R (1975) Nitinol Heat Engines. Shape Mem Eff Alloy 537–545.

18. Bruno OP (1997) Energetics in martensites. Smart Struct Mater 1997 Math Control smart Struct (San Diego, CA) 14–24.

19. Patil D, Song G (2017) A review of shape memory material's applications in the offshore oil and gas industry. Smart Mater Struct 26:093002–093019.

20. Ölander A (1932) An electrochemical investigation of solid cadmium-gold alloys. J Am Chem Soc 54:3819–3833.

21. Buehler WJ, Gilfrich J V., Wiley RC (1963) Effect of Low-Temperature Phase Changes on the Mechanical Properties of Alloys near Composition TiNi. J Appl Phys 34:1475–1477.

22. Greninger and V.G. Mooradian AB (1938) Strain transformation in meta stable beta copper-zinc and beta copper-tin alloys. Trans AIME 128:338–339.

23. Kurdyumov G, Khandros L (1949) On the "Thermoelastic" Equilibrium on Martensitic Transformations. Dokl Akad Nauk SSSR 66:211–214.

24. Chang LC, Read TA (1951) Plastic Deformation and Diffusionless Phase Changes in Metals - The Gold-Cadmium Beta-Phase. Trans Am Inst Min Metall Eng 191:47–52.

25. Rodrigue H, Wang W, Han M-W, et al (2017) An Overview of Shape Memory Alloy-Coupled Actuators and Robots. Soft Robot 4:3–15.

26. Ratna D, Karger-Kocsis J (2008) Recent advances in shape memory polymers and composites: a review. J Mater Sci 43:254–269.

27. Wei ZG, Sandstroröm R, Miyazaki S (1998) Shape memory materials and hybrid composites for smart systems Part I Shape-memory materials. J Mater Sci 33:3743–3762.

28. Wei ZG, Sandstroröm R, Miyazaki S (1998) Shape memory materials and hybrid composites for smart systems Part II Shape-memory hybrid composites. J Mater Sci 33:3763–3783.

29. Swain M V. (1986) Shape memory behaviour in partially stabilized zirconia ceramics. Nature 322:234–236.

30. Steinbrech RW (1992) Toughening Mechanisms for Ceramic Materials. Rev Lit Arts Am 10:131–142.

31. Schurch KE, Ashbee KHG (1977) A near perfect shape-memory ceramic material. Nature 266:706–707.

32. Heuer AH, Ruhle M, Marshall DB (1990) On the Thermoelastic Martensitic Transformation in Tetragonal Zirconia. J Am Ceram Soc 73:1084–1093.

33. Gall K, Dunn ML, Liu Y, et al (2002) Shape memory polymer nanocomposites. Acta Mater 50:5115–5126.

34. Berg G, McBride M, Wang C, Bowman C (2014) New directions in the chemistry of shape memory polymers. Polymer (Guildf) 55:5849–5872.

35. Gould P (2007) Biodegradable thermoplastics stay strong: Polymers. Mater Today 10:10–17.

36. Liu C, Qin H, Mather PT (2007) Review of progress in shape-memory polymers. J Mater Chem 17:1543–1558.

37. Behl M, Lendlein A (2007) Shape-memory polymers. Mater Today 10:20–28.

38. Lendlein A, Kelch S (2002) Shape-Memory Polymers. Angew Chemie Int Ed 41:2034–2057.

39. Xie T (2011) Recent advances in polymer shape memory. Polymer (Guildf) 52:4985–5000.

40. Brennan M (2001) Suite of shape-memory polymers. Chem Eng 79:5–6.

41. Lendlein A, Shastri VP (2010) Stimuli-Sensitive Polymers. Adv Mater 22:3344–

3347.

42. Yu Y, Ikeda T (2005) Photodeformable polymers: A new kind of promising smart material for micro- and nano-applications. Macromol Chem Phys 206:1705–1708.

43. Kim BK, Lee SH, Furukawa M (2006) Shape Memory Effects of Multiblock Thermoplastic Elastomers. In: Handb. Condens. Thermoplast. Elastomers. Wiley-VCH Verlag GmbH & Co. KGaA, Weinheim, FRG, pp 521–566

44. Wang K, Strandman S, Zhu XX (2017) A mini review: Shape memory polymers for biomedical applications. Front Chem Sci Eng 11:143–153.

45. Liang C, Rogers CA, Malafeew E (1997) Investigation of Shape Memory Polymers and Their Hybrid Composites. J Intell Mater Syst Struct 8:380–386.

46. Meng H, Li G (2013) A review of stimuli-responsive shape memory polymer composites. Polymer (Guildf) 54:2199–2221.

47. Hu J, Meng H, Li G, et al (2012) A review of stimuli-responsive polymers for smart textile applications. Smart Mater Struct 21:53001–53024.

48. Hu J (2013) Advances in shape memory polymers. Woodhead in association with the Textile Institute, Cambridge.

49. Meng Q, Hu J (2009) A review of shape memory polymer composites and blends. Compos Part A Appl Sci Manuf 40:1661–1672.

50. Hardy JG, Palma M, Wind SJ, Biggs MJ (2016) Responsive Biomaterials: Advances in Materials Based on Shape-Memory Polymers. Adv Mater 28:5717–5724.

51. Kolesov I (2015) Shape-memory behavior of cross-linked semi-crystalline polymers and their blends. Express Polym Lett 9:255–276.

52. Löwenberg C, Balk M, Wischke C, et al (2017) Shape-Memory Hydrogels: Evolution of Structural Principles To Enable Shape Switching of Hydrophilic Polymer Networks. Acc Chem Res 50:723–732.

53. Li Y, Chen H, Liu D, et al (2015) pH-Responsive Shape Memory Poly(ethylene glycol)-Poly(ε-caprolactone)-based Polyurethane/Cellulose Nanocrystals Nanocomposite. ACS Appl Mater Interfaces 7:12988–12999.

54. Kaursoin J, Agrawal AK (2007) Melt spun thermoresponsive shape memory fibers based on polyurethanes: Effect of drawing and heat-setting on fiber morphology and properties. J Appl Polym Sci 103:2172–2182.

55. Ragin Ramdas M, Reghunadhan Nair CP, Santhosh Kumar KS (2017) H-bonded polytriazoles: Synthesis and thermoresponsive shape memory properties. Eur Polym J 91:176–186.

56. Chung SE, Park CH, Yu W-R, Kang TJ (2011) Thermoresponsive shape memory characteristics of polyurethane electrospun web. J Appl Polym Sci 120:492–500.

57. Tsai Y-C, Li S, Hu S-G, et al (2015) Synthesis of Thermoresponsive Amphiphilic Polyurethane Gel as a New Cell Printing Material near Body Temperature. ACS Appl Mater Interfaces 7:27613–27623.

58. Hu J, Chen S (2010) A review of actively moving polymers in textile applications. J Mater Chem 20:3346–3355.

59. Rousseau IA, Xie T (2010) Shape memory epoxy: Composition, structure, properties and shape memory performances. J Mater Chem 20:3431–3439.

60. Behl M, Razzaq M, Lendlein A (2010) Multifunctional Shape-Memory Polymers. Adv. Mater.

61. Leng J, Wu X, Liu Y (2009) Effect of a linear monomer on the thermomechanical properties of epoxy shape-memory polymer. Smart Mater Struct 18:095031–095043.

62. Liu C, Qin H, Mather PT (2007) Review of progress in shape-memory polymers. J Mater Chem 17:1543–1555.

63. Voit W, Ware T, Dasari RR, et al (2010) High-strain shape-memory polymers. Adv Funct Mater 20:162–171.

64. Ji FL, Hu JL, Li TC, Wong YW (2007) Morphology and shape memory effect of segmented polyurethanes. Part I: With crystalline reversible phase. Polymer (Guildf) 48:5133–5145.

65. Ji F, Zhu Y, Hu J, et al (2006) Smart polymer fibers with shape memory effect. Smart Mater Struct 15:1547–1554.

66. Rousseau IA, Mather PT (2003) Shape Memory Effect Exhibited by Smectic-C Liquid Crystalline Elastomers. J Am Chem Soc 125:15300–15301.

67. Rousseau IA, Qin H, Mather PT (2005) Tailored phase transitions via mixed-mesogen liquid crystalline polymers with silicon-based spacers. Macromolecules 38:4103–4113.

68. Ahn S, Deshmukh P, Kasi RM (2010) Shape Memory Behavior of Side-Chain Liquid Crystalline Polymer Networks Triggered by Dual Transition Temperatures. Macromolecules 43:7330–7340.

69. Deshmukh P, Ahn SK, Gopinadhan M, et al (2013) Hierarchically self-assembled photonic materials from liquid crystalline random brush copolymers. Macromolecules 46:4558–4566.

70. Lee KM, Wang DH, Koerner H, et al (2012) Enhancement of Photogenerated Mechanical Force in Azobenzene- Functionalized Polyimides. Angew Chemie 124:4193–4197.

71. Wu Y, Wang L, Zhao X, et al (2016) Self-healing supramolecular bioelastomers with shape memory property as a multifunctional platform for biomedical applications via modular assembly. Biomaterials 104:18–31.

72. Jiang Z-C, Xiao Y-Y, Kang Y, et al (2017) Shape Memory Polymers Based on Supramolecular Interactions. ACS Appl Mater Interfaces 9:20276–20293.

73. Mondal S, Hu JL (2006) Structural characterization and mass transfer properties of nonporous segmented polyurethane membrane: Influence of hydrophilic and carboxylic group. J Memb Sci 274:219–226.

74. Hu J, Yang Z, Yeung L, et al (2005) Crosslinked polyurethanes with shape memory properties. Polym Int 54:854–859.

75. Zhang W, Chen L, Zhang Y (2009) Surprising shape-memory effect of polylactide resulted from toughening by polyamide elastomer. Polymer (Guildf) 50:1311–1315.

76. Lu H, Yu K, Huang WM, Leng J (2016) On the Takayanagi principle for the shape memory effect and thermomechanical behaviors in polymers with multi-phases. Smart Mater Struct 25:125001–125012.

77. Hu J, Kumar B, Narayana H (2015) Stress memory polymers. J Polym Sci Part B Polym Phys 53:893–898.

78. Korley LSTJ, Pate BD, Thomas EL, Hammond PT (2006) Effect of the degree of soft and hard segment ordering on the morphology and mechanical behavior of semicrystalline segmented polyurethanes. Polymer (Guildf) 47:3073–3082.

79. Ji FL, Hu JL, Yu WMW, Chiu SSY (2011) Structure and shape memory properties of polyurethane copolymers having urethane chains as soft segments. J Macromol Sci Part B Phys 50:2290–2306.

80. Chen S, Hu J, Liu Y, et al (2007) Effect of SSL and HSC on morphology and properties of PHA based SMPU synthesized by bulk polymerization method. J Polym Sci Part B Polym Phys 45:444–454.

81. Li J, Viveros JA, Wrue MH, Anthamatten M (2007) Shape-memory effects in polymer networks containing reversibly associating side-groups. Adv Mater 19:2851–2855.

82. Zhang H, Wang H, Zhong W, Du Q (2009) A novel type of shape memory polymer blend and the shape memory mechanism. Polymer (Guildf) 50:1596–1601.

83. Kurahashi E, Sugimoto H, Nakanishi E, et al (2012) Shape memory properties of polyurethane/poly(oxyethylene) blends. Soft Matter 8:496–503.

84. Li SC, Tao L (2010) Melt rheological and thermoresponsive shape memory properties of HDPE/PA6/POE-g-MAH blends. Polym - Plast Technol Eng 49:218–222.

85. Zheng X, Ã SZ, Li X, Weng J (2006) Shape memory properties of poly (D , L -lactide)/ hydroxyapatite composites. Elsevier 27:4288–4295.

86. Jang MK, Hartwig A, Kim BK (2009) Shape memory polyurethanes cross-linked by surface modified silica particles. J Mater Chem 19:1166–1178.

87. Ivens J, Urbanus M, De Smet C (2011) Shape recovery in a thermoset shape memory polymer and its fabric-reinforced composites. Express Polym Lett 5:254–261.

88. Zhang S, Feng Y, Zhang L, et al (2007) Novel interpenetrating networks with

shape-memory properties. J Polym Sci Part A Polym Chem 45:768–775.

89. Liu G, Ding X, Cao Y, et al (2005) Novel shape-memory polymer with two transition temperatures. Macromol Rapid Commun 26:649–652.

90. Rodriguez ED, Luo X, Mather PT (2011) Linear/network poly(caprolactone) blends exhibiting shape memory assisted self-healing (SMASH). ACS Appl Mater Interfaces 3:152–161.

91. Liu C, Chun SB, Mather PT, et al (2002) Chemically cross-linked polycyclooctene: Synthesis, characterization, and shape memory behavior. Macromolecules 35:9868–9874.

92. Safranski DL, Gall K (2008) Effect of chemical structure and crosslinking density on the thermo-mechanical properties and toughness of (meth)acrylate shape memory polymer networks. Polymer (Guildf) 49:4446–4455.

93. Gu SY, Chang K, Jin SP (2018) A dual-induced self-expandable stent based on biodegradable shape memory polyurethane nanocomposites (PCLAU/Fe3O4) triggered around body temperature. J Appl Polym Sci 135:45686–45701.

94. Shao L, Dai J, Zhang Z, et al (2015) Thermal and electroactive shape memory behaviors of poly(l -lactide)/thermoplastic polyurethane blend induced by carbon nanotubes. RSC Adv 5:101455–101465.

95. Vaia R (2005) Nanocomposites: Remote-controlled actuators. Nat Mater 4:429–430.

96. Lu TJ, Evans a G (2002) Design of a high authority flexural actuator using an electro-strictive polymer. Sensors Actuators, A Phys 99:290–296.

97. Razzaq MY, Anhalt M, Frormann L, Weidenfeller B (2007) Thermal, electrical and magnetic studies of magnetite filled polyurethane shape memory polymers. Mater Sci Eng A 444:227–235.

98. Wang Y, Hu Y, Gong X, et al (2007) Preparation and properties of magnetorheological elastomers based on silicon rubber/polystyrene blend matrix. J Appl Polym Sci 103:3143–3149.

99. Maitland DJ, Metzger MF, Schumann D, et al (2002) Photothermal properties of shape memory polymer micro-actuators for treating stroke. Lasers Surg Med

30:1–11.

100. Kumar B, Hu J, Pan N, Narayana H (2016) A smart orthopedic compression device based on a polymeric stress memory actuator. Mater Des 97:222–229.

101. Song L, Li Y, Xiong Z, et al (2018) Water-Induced shape memory effect of nanocellulose papers from sisal cellulose nanofibers with graphene oxide. Carbohydr Polym 179:110–117.

102. Bai Y, Chen X (2017) A fast water-induced shape memory polymer based on hydroxyethyl cellulose/graphene oxide composites. Compos Part A Appl Sci Manuf 103:9–16.

103. Ahir S V, Terentjev EM (2005) Photomechanical actuation in polymer nanotube composites. Nat Mater 4:491–510.

104. Lendlein A, Jiang H, Jünger O, Langer R (2005) Light-induced shape-memory polymers. Nature 434:879–882.

105. Miguel Camacho-Lopez Peter Palffy-Muhoray and Michael Shelley HF (2004) Fast liquid crystal elastomer swims into the dark. Nat Mater Vol 3:307–310.

106. Harris KD, Bastiaansen CWM, Broer DJ (2007) Physical Properties of Anisotropically Swelling Polymer Actuators. J Microelectromechanical Syst 16:480–488.

107. Schollenber CS (2011) Thermoplastic polyurethane elastomers. In: Carl Hanser Verlag, Thermoplast. Elastomers a …. Marcel Dekker, New York, pp 1–44

108. Cateto CA, Barreiro MF, Rodrigues AE, Belgacem MN (2009) Optimization study of lignin oxypropylation in view of the preparation of polyurethane rigid foams. Ind Eng Chem Res 48:2583–2589.

109. Fridrihsone-Girone A, Stirna U (2014) Characterization of polyurethane networks based on rapeseed oil derived polyol. Polimery/Polymers 59:333–338.

110. Yang LT, Zhao CS, Dai CL, et al (2012) Thermal and Mechanical Properties of Polyurethane Rigid Foam Based on Epoxidized Soybean Oil. J Polym Environ 20:230–236.

111. Gnanasundaram S, Kannan S, Ranganathan M, et al (2015) Preparation and Characterization of Footwear Soling Materials Based on Biodegradable Polyurethane. Polym - Plast Technol Eng 54:1585–1595.

112. Lee JH, Ju YM, Kim DM (2000) Platelet adhesion onto segmented polyurethane " lm surfaces modi " ed by addition and crosslinking of PEO-containing block copolymers. Elsevier 21:683–691.

113. Kausar A, Anwar Z, Muhammad B (2016) Recent Developments in Epoxy/Graphite, Epoxy/Graphene, and Epoxy/Graphene Nanoplatelet Composites: A Comparative Review. Polym - Plast Technol Eng 55:1192–1210.

114. Khan DM, Kausar A, Salman SM (2016) Exploitation of nanobifiller in polymer/graphene oxide–carbon nanotube, polymer/graphene oxide–nanodiamond, and polymer/graphene oxide–montmorillonite composite: A review. Polym - Plast Technol Eng 55:744–768.

115. Zhu Y, Murali S, Cai W, et al (2010) Graphene and graphene oxide: Synthesis, properties, and applications. Adv Mater 22:3906–3924.

116. Huang X, Yin Z, Wu S, et al (2011) Graphene-based materials: Synthesis, characterization, properties, and applications. Small 7:1876–1902.

117. Jing Q, Liu W, Pan Y, et al (2015) Chemical functionalization of graphene oxide for improving mechanical and thermal properties of polyurethane composites. Mater Des 85:808–814.

118. Ciecierska E, Jurczyk-Kowalska M, Bazarnik P, et al (2016) Flammability, mechanical properties and structure of rigid polyurethane foams with different types of carbon reinforcing materials. Compos Struct 140:67–76.

119. Jiang S, Li Q, Zhao Y, et al (2015) Effect of surface silanization of carbon fiber on mechanical properties of carbon fiber reinforced polyurethane composites. Elsevier 110:87–94.

120. Tayfun U, Kanbur Y, Abaci U, et al (2015) Mechanical, flow and electrical properties of thermoplastic polyurethane/fullerene composites: Effect of surface modification of fullerene. Compos Part B Eng 80:101–107.

121. Lin J, Zhang P, Zheng C, et al (2014) Reduced silanized graphene oxide/epoxy-polyurethane composites with enhanced thermal and mechanical properties.

Appl Surf Sci 316:114–123.

122. Ionescu M (2007) Chemistry and technology of polyols for polyurethanes. . Rapra Technology, Shrewsbury.

123. Mo F, Zhou F, Chen S, Yang H (2015) Development of SMPU based on polyethylene glycol and liquefied 4, 4’-diphenylmethane diisocyanate using a bulk method for biomedical. Polym Int 64:477–485.

124. Lakatos C (2016) Segmented linear shape memory polyurethanes with thermoreversible Diels-Alder coupling: Effects of polycaprolactone molecular weight and diisocyanate type. Express Polym Lett 10:324–336.

125. Zhu Y, Hu J, Yeung K (2009) Effect of soft segment crystallization and hard segment physical crosslink on shape memory function in antibacterial segmented polyurethane ionomers. Acta Biomater 5:3346–3357.

126. Korley LSTJ, Pate BD, Thomas EL, Hammond PT (2006) Effect of the degree of soft and hard segment ordering on the morphology and mechanical behavior of semicrystalline segmented polyurethanes. Polymer (Guildf) 47:3073–3082.

127. Sun L, Huang WM, Ding Z, et al (2012) Stimulus-responsive shape memory materials: A review. Mater Des 33:577–640.

128. Król P (2008) Linear polyurethanes : synthesis methods, chemical structures, properties and applications. VSP, Boston.

129. Jing X, Mi H-Y, Huang H-X, Turng L-S (2016) Shape memory thermoplastic polyurethane (TPU)/poly(ε-caprolactone) (PCL) blends as self-knotting sutures. J Mech Behav Biomed Mater 64:94–103.

130. Shirai Y, Hayashi S (1988) Development of polymeric shape memory material.

131. Bothe M, Emmerling F, Pretsch T (2013) Poly(ester urethane) with Varying Polyester Chain Length: Polymorphism and Shape-Memory Behavior. Macromol Chem Phys 214:2683–2693.

132. Meng H, Mohamadian H, Stubblefield M, et al (2013) Various shape memory effects of stimuli-responsive shape memory polymers. Smart Mater Struct 22:93001–93023.

133. Ji F, Zhu Y, Hu J, et al (2006) Smart polymer fibers with shape memory effect.

Smart Mater Struct 15:1547–1554.

134. Hu J (2007) Shape memory polymers and textiles. Woodhead in association with the Textile Institute, Cambridge.

135. Le DM, Kulangara K, Adler AF, et al (2011) Dynamic topographical control of mesenchymal stem cells by culture on responsive poly(Ïµ-caprolactone) surfaces. Adv Mater 23:3278–3283.

136. Nan W, Wang W, Gao H, Liu W (2013) Fabrication of a shape memory hydrogel based on imidazole–zinc ion coordination for potential cell-encapsulating tubular scaffold application. Soft Matter 9:132–137.

137. Xue L, Dai S, Li Z (2010) Biodegradable shape-memory block co-polymers for fast self-expandable stents. Biomaterials 31:8132–8140.

138. Yakacki CM, Shandas R, Lanning C, et al (2007) Unconstrained recovery characterization of shape-memory polymer networks for cardiovascular applications. Biomaterials 28:2255–2263.

139. Yu Z, Niu X, Liu Z, Pei Q (2011) Intrinsically stretchable polymer light-emitting devices using carbon nanotube-polymer composite electrodes. Adv Mater 23:3989–3994.

140. Mondal S, Hu JL (2006) Temperature stimulating shape memory polyurethane for smart clothing. Indian J Fibre Text Res 31:66–71.

141. Jeong HM, Ahn BK, Kim BK (2001) Miscibility and shape memory effect of thermoplastic polyurethane blends with phenoxy resin. Eur Polym J 37:2245–2252.

142. Susmita Kamila (2013) Introduction, classification and application and applications of smart materials: an overview. Am J Appl Sci 10:876–880.

143. Stamhuis CT (2015) Designing with Smart Materials: A Case presenting a Tactile Interface Disc for Intuitive Control of Light and Sound in Domestic environments.

144. Worbin L (2006) Textile disobedience. Fabr Archit 18:68.

145. Cabral I, Silva C, Worbin L, Souto AP (2017) Exploring dynamic lighting, colour and form with smart textiles. In: IOP Conf. Ser. Mater. Sci. Eng. Institute of

Physics Publishing, p 72005

146. Hertenberger A, Stewart B, Calder L, et al (2014) 2013 e-textile swatchbook exchange. In: Proc. 2014 ACM Int. Symp. Wearable Comput. Adjun. Progr. - ISWC ’14 Adjun. ACM Press, New York, New York, USA, pp 77–81

Chapter II.

MATERIALS, SYNTHESIS AND EXPERIMENTAL TECHNIQUES

"Bere pentsamendua hondarrezkoa zen, eta bere pentsamendu horren eskukada bat biltzen saiatzen zenean, hondar ale gehienak irristatu egiten zitzaizkion behatz artean, eta betirako galdu".

"Su pensamiento era arena, y cuando intentaba recoger un puñado de ese pensamiento, la mayor parte de los gramos se le escurrían entre los dedos y se perdían para siempre".

Bernardo Atxaga

Chapter II

MATERIALS, SYNTHESIS AND EXPERIMENTAL TECHNIQUES

2.1. Materials

Polyurethane elastomers (PUs) are formed typically by reacting together three chemical constituents: a diisocyanate (aromatic or aliphatic), a long-chain diol (or "macrodiol"), and a small molecule called chain-extender that can be a diol or a diamine. The resulting polymer may be considered as a copolymer with macrodiol and diisocyanate-chain extender sequences, named soft-segment (SS) and hard-segment (HS), respectively (*Figure 2.1*) [1–5].

In this work, all the cured polyurethane elastomers were made from three main components that are detailed in *Table 2.1.* Thus, three polyols (PEG, PTMG-650, PTMG-1000), two isocyanates (MDI, TDI) and a chain extender (BD) were used.

Moreover, in some polyurethanes, titanium oxide (TiO_2) nanoparticles were used as fillers in order to check their influence in the properties of the polyurethanes.

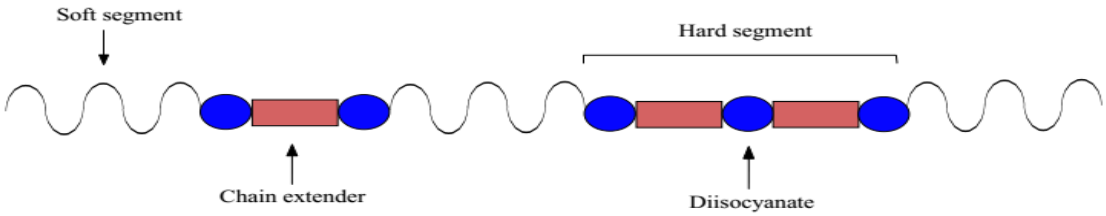

Figure 2.1.*Typical repetitive structure of the polyurethane elastomers*

Table 2.1. *Main polyurethane components*

Reagents	
Polyols	Poly(oxytetramethylene) glycol (PTMG-650) Poly(oxytetramethylene) glycol (PTMG-1000) Poly(etylene glycol) (PEG)
Diisocyanate	2,4-toluene diisocyanate (TDI) 4,4'-methylene diphenyl diisocyanate (MDI)
Chain extender	1,4-butanediol (BD)
Other chemicals	Nanoparticles (TiO_2)

2.1.1. Polyols

Flexibility in polyurethanes is provided by the backbone or "soft-segment." Polyols, the soft-segment of the polymer, are capped with a hydroxyl group. Unless there are special requirements, these polyols must be linear (i.e., no branching) and with a molecular weight between 400 and 7000 $g \cdot mol^{-1}$. The overall molecular weight of the soft-segment controls the frequency of the hard phase and hence the hardness, resilience, and stiffness of the final polyurethane. The lower the molecular weight of the polyol, the higher the occurrence of the hard phase. There are two main groups of polyols used to make polyurethanes: polyethers and polyesters [6,7]. Thus, in this work, two different polyols were used: poly(oxytetramethylene) glycol (PTMG) with

two different molecular weight (M_n = 650 g·mol^{-1} and M_n = 1000 g·mol^{-1}) and poly(ethylene glycol) (PEG, M_n = 1000 g·mol^{-1}) (*Figure 2.2*).

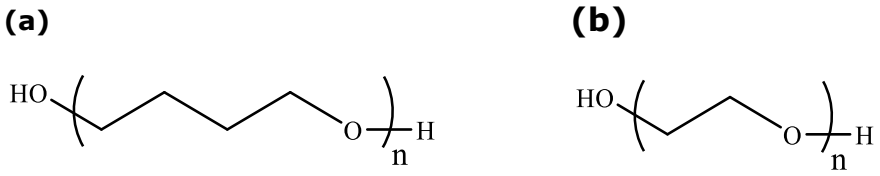

Figure 2.2. *Molecular structure of poly(oxytetramethylene) glycol (a) and poly(ethylene glycol) (b)*

All these raw materials were purchased from Sigma-Aldrich and were used as received. Properties of the three polyols are presented in *Table 2.2*.

Table 2.2. *Properties of polyols*

	PTMG (650)	**PTMG (1000)**	**PEG**
***Mn* (g·mol^{-1})**	650	1000	1000
Vapor Pressure	<0.01 mm Hg (25°C)	<0.01 mm Hg (25°C)	<0.075 mm Hg (20°C)
Melting point (°C)	11-19	25-33	33-40
Density (g·cm^{-3})	0.978 at 25°C	0.974 25°C	1.2 at 20°C

2.1.2. Diisocyanates

The major polyisocyanates usually employed for the synthesis of polyurethanes are 2,4-toluene diisocyanate (TDI) and 4,4'-methylene diphenyl diisocyanate (MDI) in oligomeric type. Their chemical structures are shown in *Figure 2.3*.

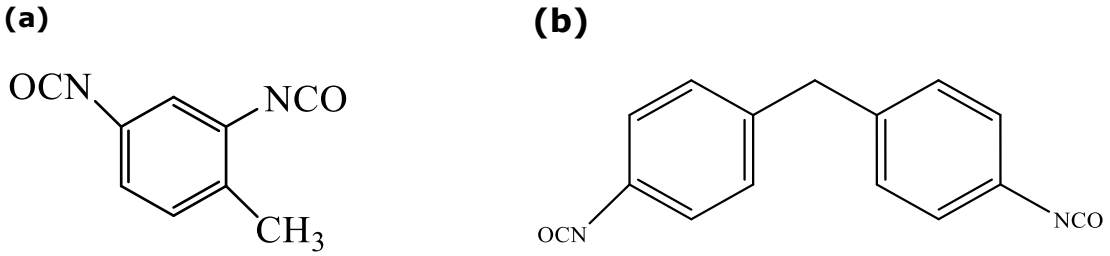

Figure 2.3. *Molecular structure of 2,4-toluene diisocyanate (a) and 4,4'-methylene diphenyl diisocyanate (b)*

On the one hand, TDI is manufactured by phosgenation of diaminotoluene, which is obtained by reduction of nitrotoluene. Commercial products of TDI are mixtures of 2,4- and 2,6-isomers in the weight ratio of 80/20 or 65/35. TDI with 80/20 isomer ratio was used in this work. On the other hand, MDI is obtained by the phosgenation of the condensation product of aniline with formaldehyde. MDI is mainly 4,4'-isomer based and has small quantities of the 2,2'-isomer and up to 10% of the 2,4-isomer. Its average functionality is in a range of 2.3 to 3.0 [8,9].

In this work, 2,4-toluene diisocyanate (TDI) and 4,4'-methylene diphenyl diisocyanate (MDI) were used as received from Sigma-Aldrich and kept in the refrigerator and freezer, respectively. Their physical properties are shown in *Table 2.3*.

Table 2.3. *Properties of diisocyanates*

	TDI	**MDI**
M_n (g·mol^{-1})	174.16	250.25
Melting point (ºC)	19.5-21.5	42-45
Density (g·cm^{-3})	1.21 at 20°C	1.18 at 25°C
Storage temperature (ºC)	2-8	-20

2.1.3. Chain extender

Low molecular weight diols such as ethylene glycol, diethylene glycol, 1,3-propylene glycol or 1,4-butanediol (*Figure 2.4*) are usually used as chain extenders. In this case, 1,4-butanediol (BD) was used to synthesize polyurethanes and was dried under vacuum for 3 h at 65ºC before using (see properties on *Table 2.4*) [6,10].

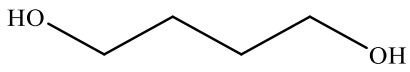

***Figure 2.4**. Structure molecular of 1,4-butanediol*

***Table 2.4.** Properties of diol*

	1,4-BD
M_n (g·mol^{-1})	90.12
Melting point (ºC)	16
Density (g·cm^{-3})	1.017

2.1.4. Nanoparticles

Some of the shape memory polyurethanes (SMPUs) were also synthesized with TiO_2 nanoparticles in order to provide them better and novel properties. These nanoparticles have been kindly purchased by L´Urederra Technological Centre (Spain). The morphology of these nanoparticles has been analyzed by Transmission Electron Microscopy (TEM), using an equipment PHILIPS EM208S with Morada digital camera and PHILIPS CM120 biofilter with STEM module and elemental mapping and filtering of images via EELS (*Figure 2.5*).

By TEM it is possible to obtain a quantitative measure about the grain size, the size distribution (*Figure 2.6*) and the morphology of these nanoparticles. Therefore, it can be observed that TiO_2 nanoparticles own a spherical structure, with a width of particle size distribution between 10-30 nm and a mean value of 16-17 nm.

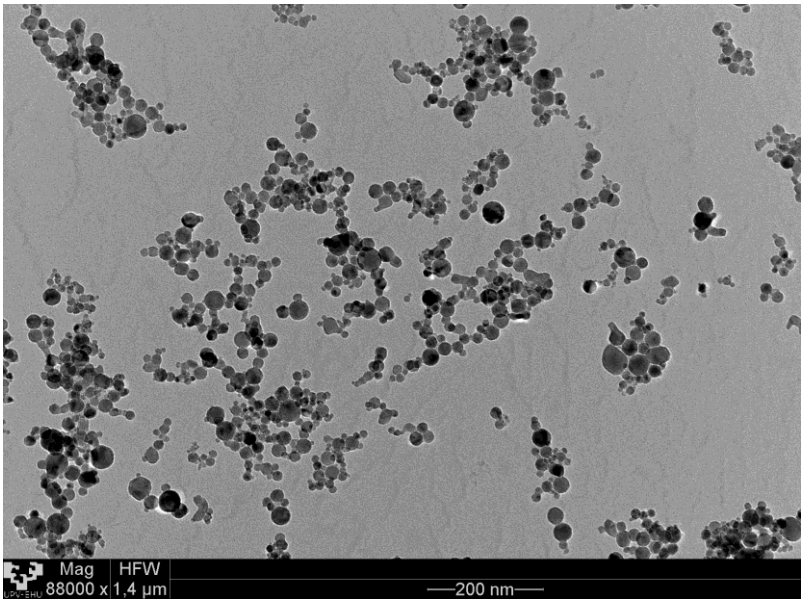

Figure 2.5. *TEM of TiO_2 nanoparticles*

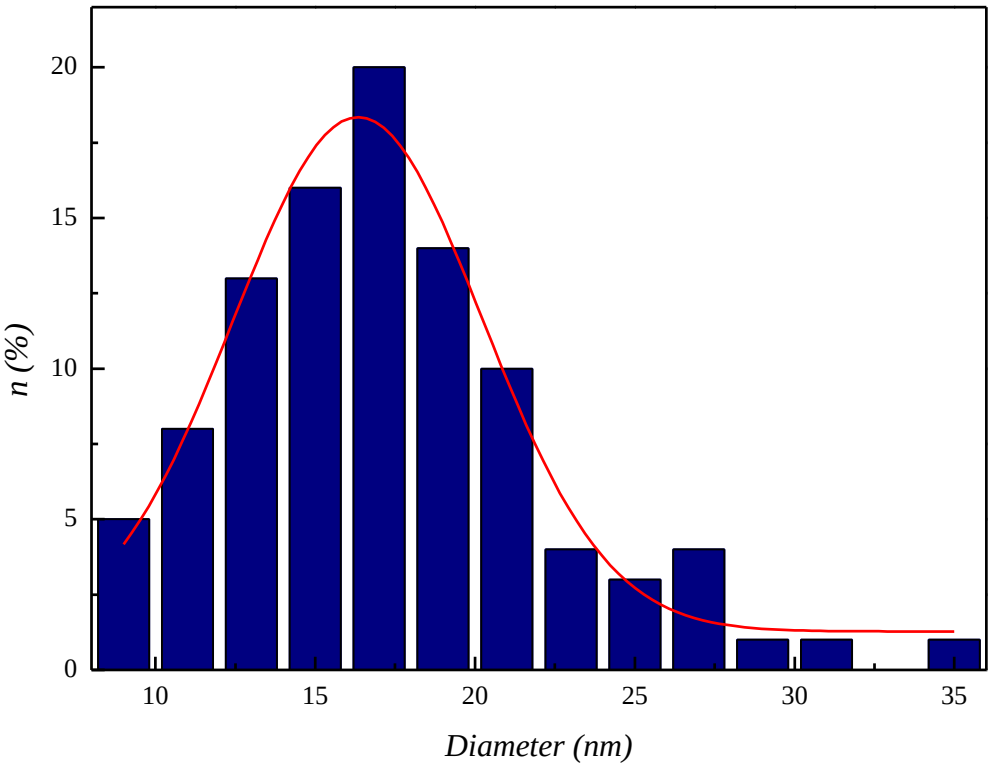

Figure 2.6. *Distribution of particle size of TiO_2 nanoparticles*

2.1.5. DIAPLEX

Diaplex is a commercial shape memory polyurethane, as mentioned in *Chapter I*, supplied by a Japanese Company called 'SMP Technologies'. Diaplex is the newly developed intelligent material which changes its features according to temperature. In this thesis, DIAPLEX MM4520 was used to compare with different polyurethanes synthesized in laboratory.

2.2. Synthesis of polyurethanes

All SMPUs were synthesized by a two-step method (prepolymerization method), as described in *Chapter I*, varying the relationship between the hard-segment / soft-segment content between approximately 25 and 75%. Briefly, SMPUs were prepared by the reaction of stoichiometric amounts of polyol / diisocyanate / chain extender with block ratios of 1:*n*+1:*n* (where *n*, the mole ratio of reactants, was kept between 0.5 and 6.5). Therefore, the hard-segments of the SMPUs were composed of MDI, TDI or a 50% weight mixture between MDI and TDI; the chain extender was 1,4-butanediol (BD); and the soft-segments were composed of PEG or PTMG with two different molecular weights (M_n): 650 g·mol^{-1} or 1000 g·mol^{-1}.

Once the reaction temperature and the reaction time were optimized, both the followed procedure and the experimental conditions were kept the same for all the polyurethane syntheses (view *Table 2.5*) [11]. The reaction scheme for the synthesis is shown according to the route outlined in *Figure 2.7* [12,13]*.Tables 2.6, 2.7, 2.8 and 2.9.* show the different shape memory polyurethanes that were synthesized in this thesis.

Table 2.5. *Experimental conditions for polyurethane syntheses*

Experimental conditions	
Nitrogen atmosphere	
Ratio → Polyol:Diisocyanate:diol → 1:n+1:n (*n*: 0.5-6.5)	
Reaction temperature	70ºC
Reaction time	2 h

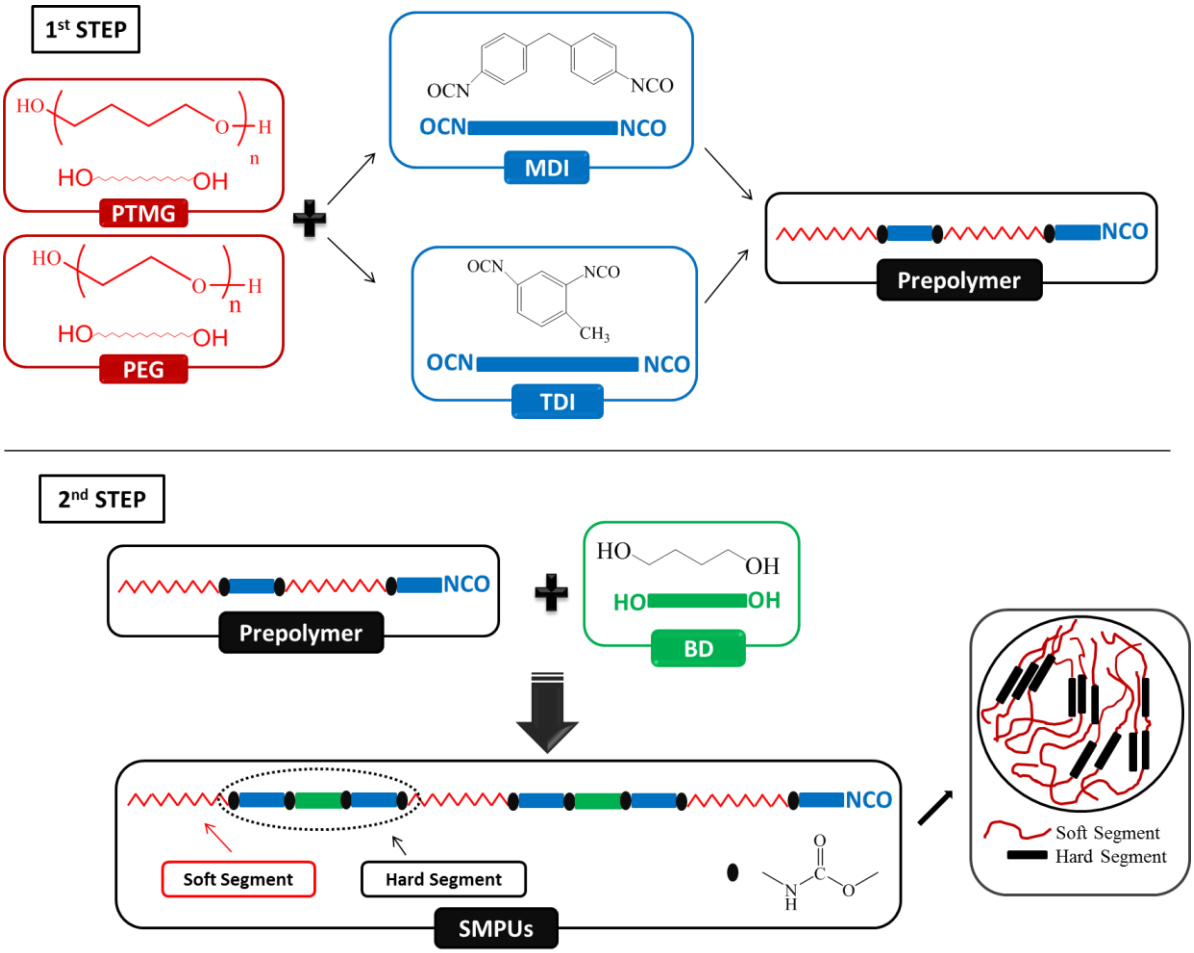

Figure 2.7. *Synthetic route for shape memory polyurethanes*

Table 2.6. *Summary of the SMPUs based on PEG (n represents the molar ratio)*

System & Sample		Composition of polyurethane (1:n+1:n)				%HS	%SS
		PEG	TDI	MDI	BD		
S1	PEGTDI_3.5	1	4.5	0	3.5	52.4	47.6
	PEGTDI_4.5	1	5.5	0	4.5	64.1	35.9
	PEGTDI_5.5	1	6.5	0	5.5	68.0	32.0
S2	PEGMDI_2	1	0	3	2	48.2	51.8
	PEGMDI_3	1	0	4	3	56.0	44.0
	PEGMDI_4	1	0	5	4	61.7	38.3

Table 2.7. *Summary of the SMPUs based on PTMG 650 (n represents the molar ratio)*

System & Sample		Composition of polyurethane (1:n+1:n)					%HS	%SS
		PTMG	**TDI**	**MDI**	**TDI/MDI***	**BD**		
S3	PTMG650TDI_2.5	1	3.5	0	0	2.5	62.9	37.1
	PTMG650TDI_3	1	4	0	0	3	66.2	33.8
	PTMG650TDI_3.5	1	4.5	0	0	3.5	68.9	31.1
	PTMG650TDI_4	1	5	0	0	4	71.3	28.7
	PTMG650TDI_4.5	1	5.5	0	0	4.5	73.3	26.7
	PTMG650TDI_5	1	6	0	0	5	75.0	25.0
	PTMG650TDI_5.5	1	6.5	0	0	5.5	76.6	23.4
S4	PTMG650MDI_0.5	1	0	1.5	0	0.5	39.3	60.7
	PTMG650MDI_1	1	0	2	0	1	47.6	52.4
	PTMG650MDI_1.5	1	0	2.5	0	1.5	53.9	46.1
	PTMG650MDI_2	1	0	3	0	2	58.9	41.1
	PTMG650MDI_2.5	1	0	3.5	0	2.5	62.9	37.1
	PTMG650MDI_3	1	0	4	0	3	66.2	33.8
	PTMG650MDI_3.5	1	0	4.5	0	3.5	68.9	31.1
	PTMG650MDI_4	1	0	5	0	4	71.3	28.7
	PTMG650MDI_4.5	1	0	5.5	0	4.5	73.3	26.7
S5	PTMG650MDITDI_1.5	1	-	-	2.5	1.5	50.6	49.4
	PTMG650MDITDI_2	1	-	-	3	2	55.7	44.3
	PTMG650MDITDI_2.5	1	-	-	3.5	2.5	59.8	40.2
	PTMG650MDITDI_3	1	-	-	4	3	63.3	36.7
	PTMG650MDITDI_3.5	1	-	-	4.5	3.5	66.2	33.8

*50% weight of TDI and 50% weight of MDI

Table 2.8. *Summary of the SMPUs based on PTMG 1000 (n represents the molar ratio)*

System & Sample		Composition of polyurethane (1:n+1:n)					%HS	%SS
		PTMG	**TDI**	**MDI**	**TDI/MDI***	**BD**		
S6	PTMG1000TDI_2.5	1	3.5	0	0	2.5	52.4	47.6
	PTMG1000TDI_3	1	4	0	0	3	56.0	44.0
	PTMG1000TDI_3.5	1	4.5	0	0	3.5	59.0	41.0
	PTMG1000TDI_4	1	5	0	0	4	61.7	38.3
	PTMG1000TDI_4.5	1	5.5	0	0	4.5	64.1	35.9
	PTMG1000TDI_5	1	6	0	0	5	66.1	33.9
	PTMG1000TDI_5.5	1	6.5	0	0	5.5	68.0	32.0
	PTMG1000TDI_6.5	1	7.5	0	0	6.5	71.1	28.9
S7	PTMG1000MDI_0.5	1	0	1.5	0	0.5	29.6	70.4
	PTMG1000MDI_1	1	0	2	0	1	37.1	62.9
	PTMG1000MDI_1.5	1	0	2.5	0	1.5	43.2	56.8
	PTMG1000MDI_2	1	0	3	0	2	48.2	51.8
	PTMG1000MDI_2.5	1	0	3.5	0	2.5	52.4	47.6
	PTMG1000MDI_3	1	0	4	0	3	56.0	44.0
	PTMG1000MDI_3.5	1	0	4.5	0	3.5	59.0	41.0
	PTMG1000MDI_4	1	0	5	0	4	61.7	38.3
	PTMG1000MDI_4.5	1	0	5.5	0	4.5	64.1	35.9
S8	PTMG1000MDITDI_3.5	1	-	-	4.5	3.5	44.0	56.0
	PTMG1000MDITDI_4	1	-	-	5	4	41.3	58.7
	PTMG1000MDITDI_4.5	1	-	-	5.5	4.5	38.9	61.1
	PTMG1000MDITDI_5	1	-	-	6	5	36.7	63.3
	PTMG1000MDITDI_5.5	1	-	-	6.5	5.5	34.8	65.2
	PTMG1000MDITDI_6	1	-	-	7	6	33.0	67.0

*50% weight of TDI and 50% weight of MDI

Table 2.9. *Summary of the SMPUs synthesized with nanoparticles (n represents the molar ratio)*

System & Sample		Composition of polyurethane (1:n+1:n)				%HS	%SS
		PTMG	TDI/MDI*	BD	TiO_2		
S9	PTMG650MDITDI_1.5_1	1	2.5	1.5	1	50.6	49.4
	PTMG650MDITDI_2_1	1	3	2	1	55.7	44.3
	PTMG650MDITDI_2.5_1	1	3.5	2.5	1	59.8	40.2
	PTMG650MDITDI_3_1	1	4	3	1	63.3	36.7
	PTMG650MDITDI_3.5_1	1	4.5	3.5	1	66.2	33.8
S10	PTMG1000MDITDI_3.5_1	1	4.5	3.5	1	44.0	56.0
	PTMG1000MDITDI_4_1	1	5	4	1	41.3	58.7
	PTMG1000MDITDI_4.5_1	1	5.5	4.5	1	38.9	61.1
	PTMG1000MDITDI_5_1	1	6	5	1	36.7	63.3
	PTMG1000MDITDI_5.5_1	1	6.5	5.5	1	34.8	65.2
	PTMG1000MDITDI_6_1	1	7	6	1	33.0	67.0
S11	PTMG1000MDITDI_3.5_3	1	4.5	3.5	3	44.0	56.0
	PTMG1000MDITDI_4_3	1	5	4	3	41.3	58.7
	PTMG1000MDITDI_4.5_3	1	5.5	4.5	3	38.9	61.1
	PTMG1000MDITDI_5_3	1	6	5	3	36.7	63.3
	PTMG1000MDITDI_5.5_3	1	6.5	5.5	3	34.8	65.2
	PTMG1000MDITDI_6_3	1	7	6	3	33.0	67.0

*50% weight of TDI and 50% weight of MDI

The synthesis was carried out in a 150 mL 5-neck round-bottom flask heated at 70ºC in an oil bath, equipped with a mechanical stirrer and a nitrogen inlet (*Figure 2.8*). In the first step, the polyol (PEG or PTMG) was added into the dried reactor, and after 30 min under nitrogen atmosphere, MDI and/or TDI was added dropwise. The reaction continued at 70ºC for 2 hours to obtain a –NCO terminated prepolymer. In the case of polyurethanes with nanoparticles, TiO_2 was put into the reactor 1 hour

after adding the diisocyanates. Moreover, a vigorous nitrogen flow has been used to prevent the reaction of the isocyanate groups with air moisture [14,15].

Figure 2.8. *Equipment for synthesis of shape memory polyurethanes*

In the second step, the BD chain extender was added dropwise into the reaction system. The reaction mixture was continuously stirred between 2 or 5 minutes (depending on the reagents) until a significant increase in viscosity was detected. Then, the viscous mixture was poured into a preheated stainless steel mold at 100ºC, and put into a hydraulic press overnight (*Figure 2.9)* to obtain the final polymer. Thus, SMPUs sheets were manufactured by compression molding under a pressure of 150 bar. Two teflon sheets were placed on both sides of the mold to reduce the surface roughness of the obtained SMPUs. After curing, the obtained specimens were cooled to room temperature in the mold under constant pressure (*Figure 2.10*). The specific routes of synthesis are drawn in *Figures 2.11, 2.12* and *2.13*, for the polyurethanes with TDI, with MDI and with a mixture of MDI and TDI, respectively [16,17].

Figure 2.9. *Hydraulic press*

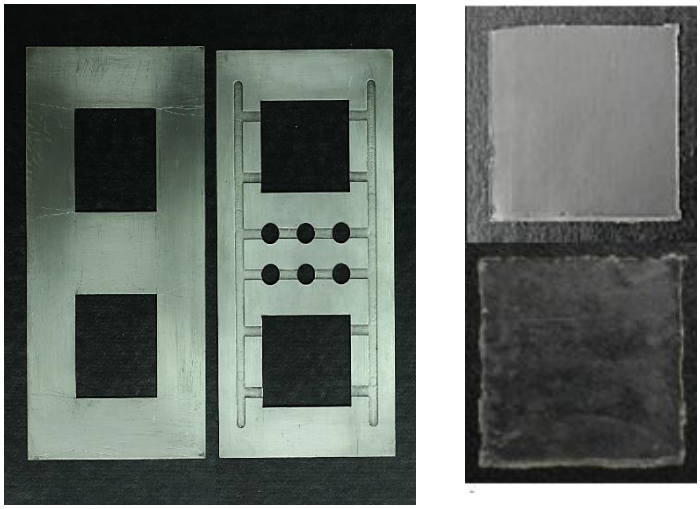

Figure 2.10. *Steel molds and final polyurethanes*

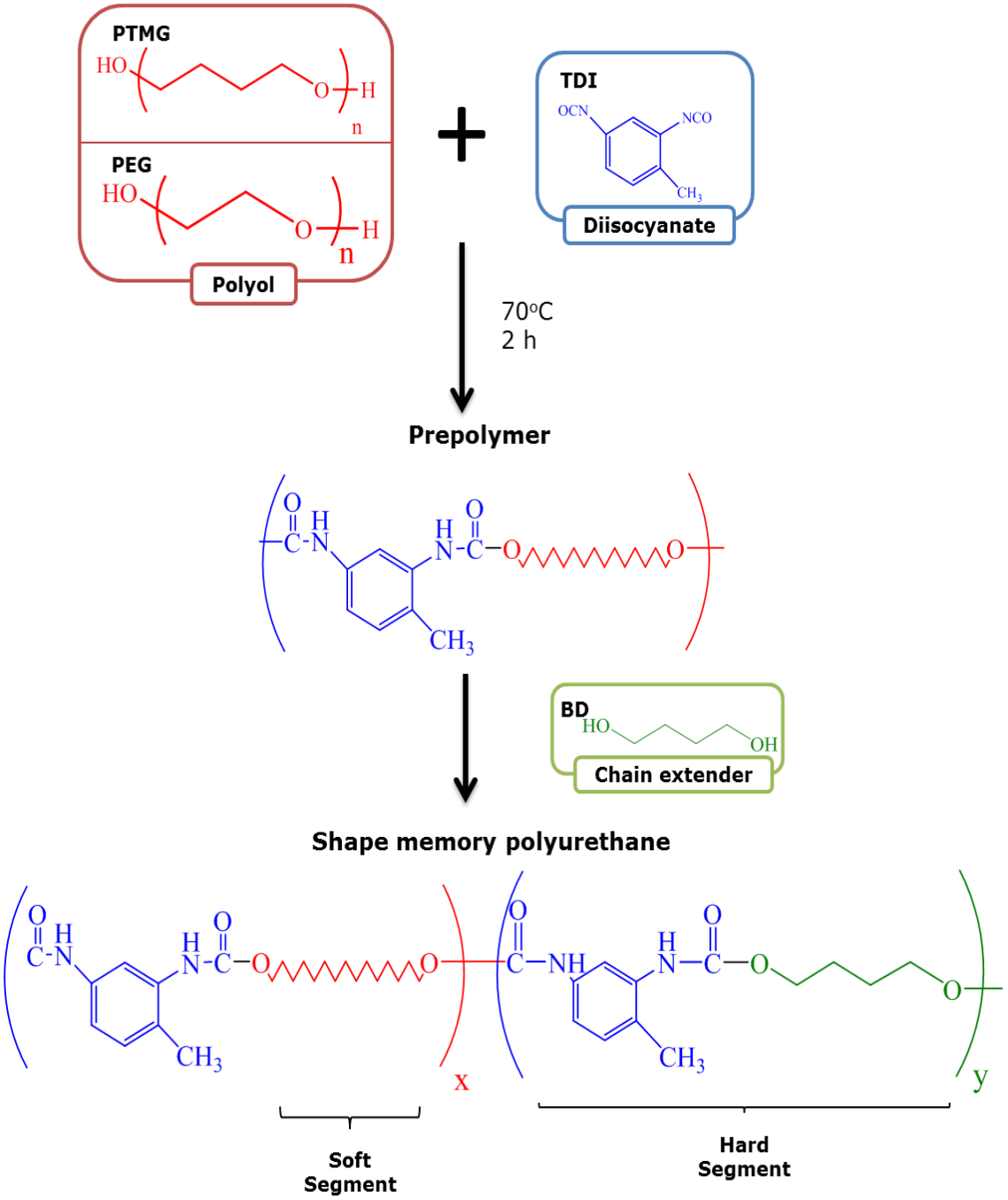

Figure 2.11. *Specific route of SMPU synthesis with TDI as diisocyanate*

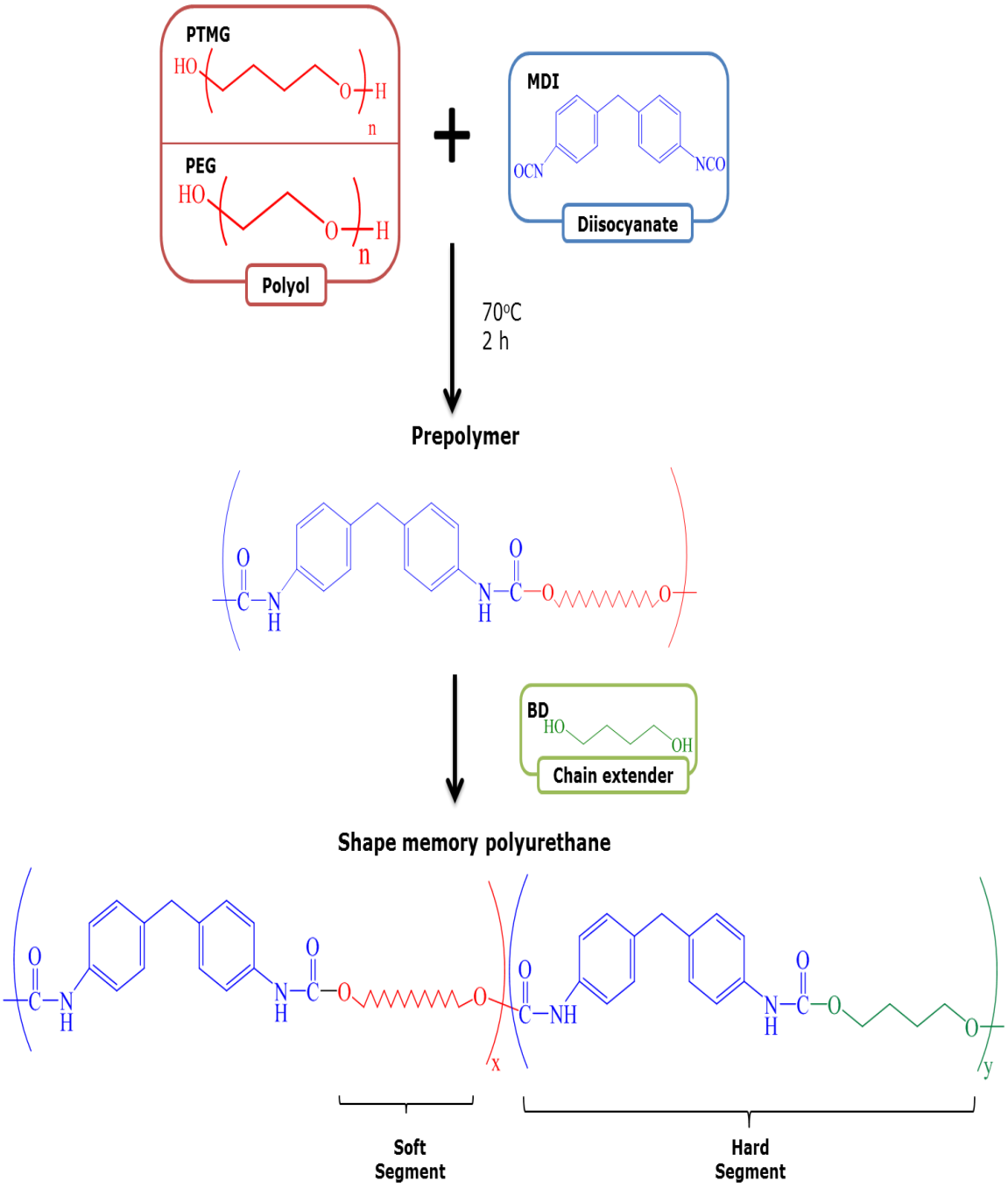

Figure 2.12. *Specific route of SMPU synthesis with MDI as diisocyanate*

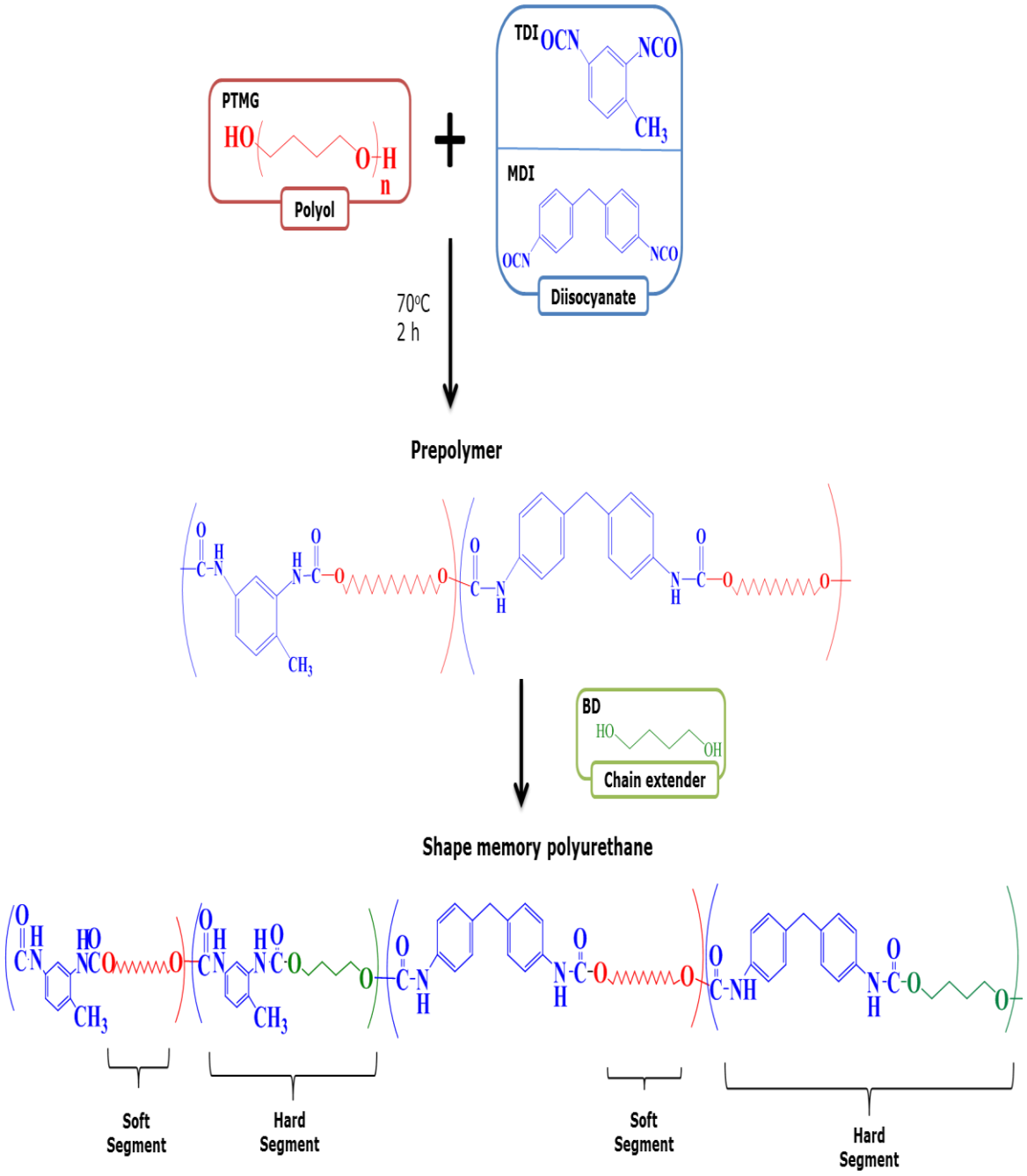

Figure 2.13. *Specific route of SMPU synthesis with a mixture of TDI and MDI as diisocyanate*

2.3. Characterization techniques

The most important characterization techniques are presented in this section such as attenuated total reflectance (ATR), thermogravimetric analysis (TGA), differential scanning calorimetry (DSC), dynamical mechanical analysis (DMA) or thermomechanical analysis (TMA). All of these techniques were used to analyze the shape memory polyurethanes (SMPUs).

2.3.1. Attenuated total reflectance (ATR)

ATR is an infrared (IR) sampling technique that provides excellent quality data in conjunction with the best possible reproducibility of any IR sampling technique. It has revolutionized IR solid and liquid sampling, eliminating in many cases the need for sample preparation or at least simplifies the procedures, improving sample-to-sample reproducibility and minimizing user to user spectral variation. An attenuated total reflection accessory operates by measuring the changes that occur in a total internal reflected infrared beam when the beam comes into contact with a sample. An infrared beam is directed onto an optically dense crystal with a high refractive index at a certain angle. This internal reflectance creates an evanescent wave that extends beyond the surface of the crystal into the sample held in contact with the crystal.

In this work, ATR was used to assess the extent of the reaction between the isocyanate and hydroxyl groups so that, it could be confirmed that the isocyanate groups were completely reacted. It should be noted that not all the polyurethanes were characterized through ATR due to their unsuitable mechanical properties. This impediment comes from the procedure of synthesis. Thus, some MDI-based polyurethanes were too rigid and solid to be measured and some TDI-based polyurethanes were too liquid to be put into a press under pressure.

Infrared measurements (FTIR) were performed at room temperature on a Nicolet Nexus FTIR spectrophotometer (Thermo Electron Corporation). The spectrums were obtained using an ATR tool in the range from 500 to 4000 cm^{-1} at a resolution of 4 cm^{-1} and 64 scans per spectrum (*Figure 2.14*) [18].

Figure 2.14. *Photography of a Nicolet Nexus FTIR spectrophotometer*

2.3.2. Thermogravimetric analysis (TGA)

Thermogravimetric Analysis (TGA) is a technique in which the mass of a substance is monitored as a function of temperature or time as the sample specimen is subjected to a controlled temperature program in a controlled atmosphere. Thermogravimetric and Derivative Thermogravimetric (DTG) analysis gives information about the weight loss process as well as the degradation rate (*%/ºC*) of the sample, respectively. The temperatures at the maximum degradation rate (*dw/dt*) were obtained from DTG curves. In a typical thermogram, several characteristics of the degradation process can be observed (*Figure 2.15*) [19] such as:

-Initial temperature of the degradation process ($T_{5\%}$): temperature when the mass change reaches a value that can be detected by the thermobalance (5%). This temperature is the one used to establish the thermal stability of the materials.

-Degradation process temperature (T_d): it reflects the temperature when the maximum rate of degradation takes place. It is determined from the minimum of the first derivative of the thermogravimetric curve.

-Final temperature (T_f): temperature when the mass change reaches a maximum value, corresponding to the complete reaction.

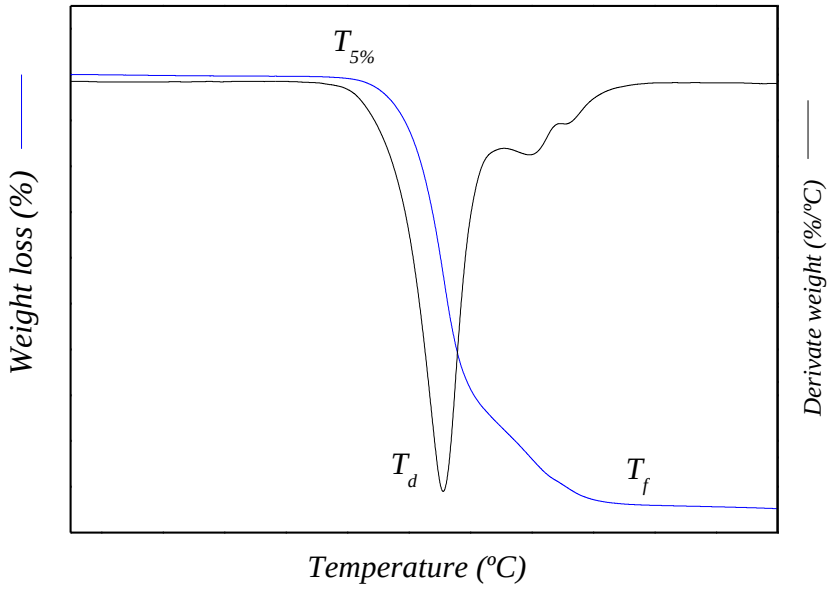

Figure 2.15. *Thermogravimetric curve where the different characteristic temperatures can be observed*

Thermal stability of shape memory polyurethanes was evaluated by Thermogravimetric Analysis on a TGA Mettler Toledo 822^e (view *Figure 2.16)* in alumina pans by heating the samples (10-15 mg) from room temperature to 800°C at 10°C·min^{-1}. A nitrogen atmosphere was used to drag the gases produced in the measuring cell with a carrier flow rate of 50 cm^3·min^{-1}, and also another purge gas to protect the balance, with a flow rate of 100 cm^3·min^{-1}.

Figure 2.16. *Photography of a TGA Mettler Toledo 822^e module*

2.3.3. Differential scanning calorimetry (DSC)

Differential Scanning Calorimetry (DSC) is one of the most effective analytical techniques to characterize the physical properties of polymers. DSC allows to determine heat capacities in both solid and liquid states, phase transition temperatures and the corresponding enthalpy and entropy changes as well as changes in heat capacity.

Differential scanning calorimetry (DSC) is an instrument that measures the rate of heat evolution of absorption of a specimen while it is undergoing a programmed temperature rise. DSC maintains the sample and the reference at the same temperature through varying the heat flow linearly as a function of time. Thus, the reference sample should have a well-defined heat capacity over the range of temperatures to be scanned.

When the differential heat flow supplied is plotted as a function of temperature, it is possible, after normalizing the sample mass, to obtain enthalpic information, such as the heat of fusion. The glass transition temperature can be defined in different ways. In the literature, both the onset temperature (T_{onset}) and the inflection point temperature are used to report relevant information about the polymer. These parameters are obtained from the thermogram from points A and B, respectively, as shown in *Figure 2.17*. One of the advantages of DSC is that samples are very easily encapsulated, usually with little or no preparation, ready to be placed in the DSC, so that measurements can be quickly and easily made [20].

Thermal properties of all samples were measured by differential scanning calorimetry (DSC 822^e from Mettler Toledo) (*Figure 2.18*) to identify the thermal transitions of the obtained materials. The transition temperature of shape memory effect (T_{trans}) was defined from glass transition temperature measured in the second heating cycle (T_g). In all the experiments, the glass transition temperatures were determined by the onset method. Samples containing 10-15 mg were sealed in aluminum pans and were characterized under constant nitrogen flow (50 $cm^3 \cdot min^{-1}$). First, samples were equilibrated at -100°C, and then heated at a rate of 10ºC·min^{-1} from -100 to 250ºC. In this first cycle, the thermal history of the sample was erased. It was then cooled down to -100ºC at a cooling rate of 10ºC·min^{-1}. Subsequently, a second heating scan to 250ºC was conducted at the same heating rate [21,22]. As in the TGA, this analysis was performed for all the synthesized polyurethanes and also for the commercial sample (DIAPLEX MM4520).

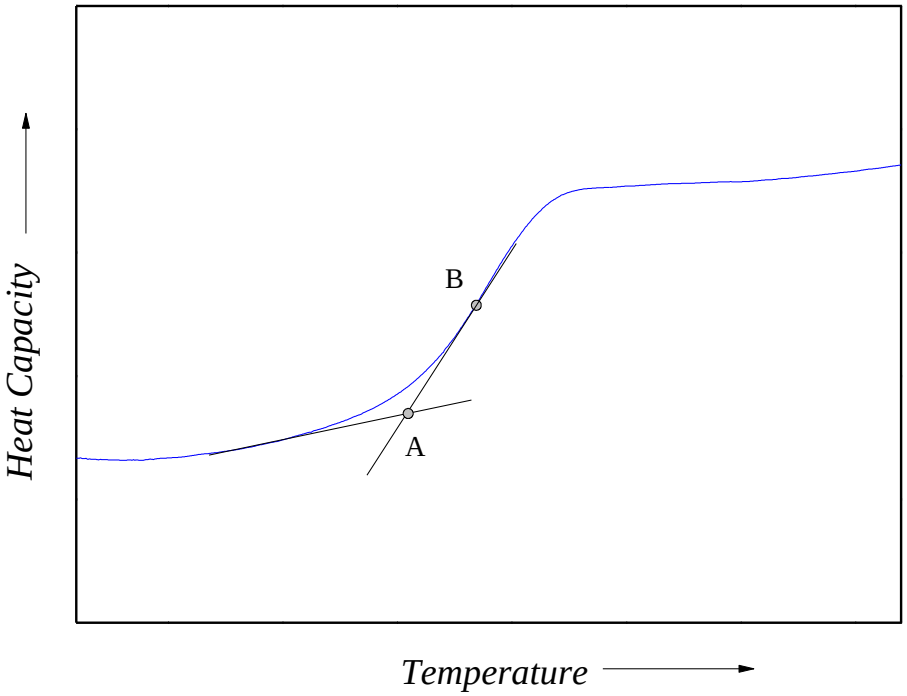

Figure 2.17. *The onset temperature (A) and the inflection point (B) of a glass transition in a DSC curve*

Figure 2.18. *Photography of a DSC 822^e module*

2.3.4. Dynamical Mechanical Analysis (DMA)

Dynamic Mechanical Analysis (DMA) is a technique that is widely used to characterize material's properties as a function of temperature, time, frequency, stress, atmosphere or a combination of these parameters.

Dynamic mechanical analysis allows to obtain characteristic temperatures of polymers such as glass transition temperature (T_g) and melting temperature (T_m). Analyses of polyurethanes were performed on a MettlerToledo DMA1 analyzer (*Figure 2.19.a*). A rectangular sample with a cross-section area of 6 mm x 1.5 mm and initial clamps distance of 10 mm was directly cut from the polyurethane sheet and measured in tensile mode. Curves displaying the storage modulus (*E'*) and the loss factor (*tanδ*) were recorded in the range of -100 to 150ºC at a heating rate of 3ºC·min^{-1}. Glass transition temperature ($T_{g,DMA}$) was determined from the maximum of the loss factor of the thermomechanical diagram (*Figure 2.20*).

Deformation frequency of 1 Hz and displacement of 20 µm were used, which are found within the linear viscoelastic region (LVR) of the synthesized SMPUs [15]. Test of polyurethane fibers were carried out in the same way on a TA-Instruments DMA Q800 at the University of Borås (*Figure 2.19.b*), but in a temperature range from -40 to 150ºC.

(a) **(b)**

Figure 2.19. *Photography of Mettler Toledo DMA1 (a) and TA-Instruments DMA Q800 (b)*

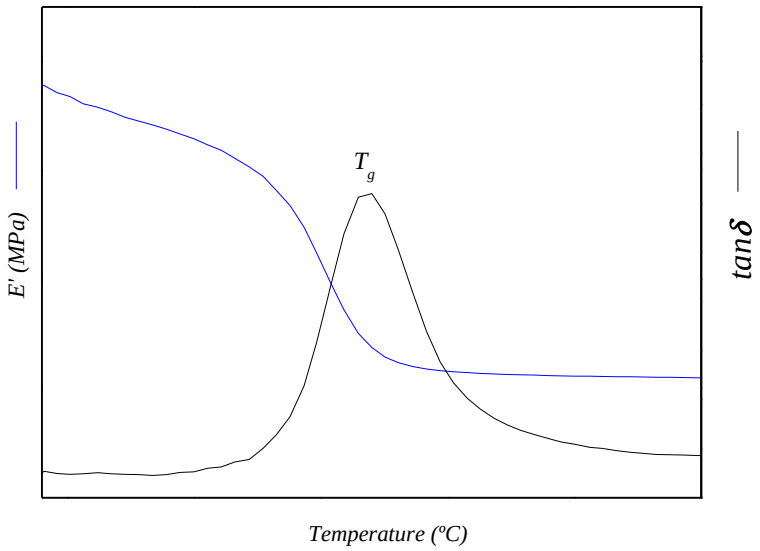

Figure 2.20. *An example of a thermomechanical curve*

2.3.5. Thermomechanical analysis (TMA)

Thermomechanical Analysis (TMA) is the study of the relationships between the length and the temperature of a sample. A technique in which a deformation of the sample under non-oscillating stress was monitored against time or temperature while the temperature of the sample was programmed. The sample is inserted into a furnace and a thermocouple for temperature measurements is located near the sample. The sample deformation, such as thermal expansion and softening, with changing temperature was measured as the probe displacement by the length detector.

Polyurethane is a thermally induced shape memory polymer, where the transition temperature corresponds with the glass transition temperature (T_g), so that cyclic thermomechanical experiment was designed in the stress-controlled mode in order to evaluate quantitatively its shape memory behavior. Schematic representation of thermomechanical experiment is shown in *Figure 2.21*.

For thermomechanical analysis (TMA), samples were conducted in tension mode on the same Mettler Toledo DMA1 at a cooling rate of -20ºC·min^{-1} and at a heating rate of 4°C·min^{-1}, in different temperature ranges depending on the system analyzed. This temperature range was selected according to the transition

temperature of shape memory effect (T_{trans}) defined from the glass transition temperature of the sample measured by DMA. The different performed experiments can be appreciated in *Table 2.10*, where T_{high}, T_{low} and deformation force were modified in order to study how these parameters affect the fixation of the temporary shape [23,24].

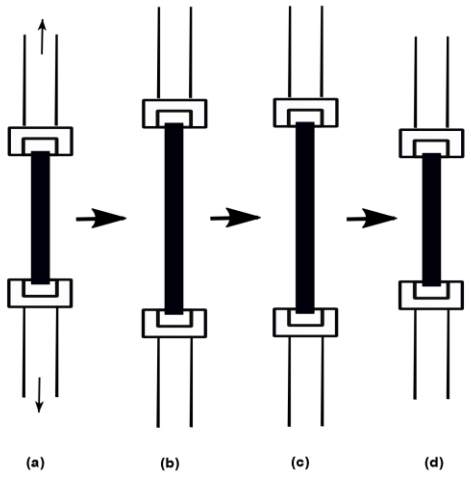

Figure 2.21. *Description of thermomechanical experiment. (a) Tension at T_{high}. (b) Cooling to T_{low} at constant strain (temporary shape). (c) Unloading at T_{low}. (d) Heating to T_{high} at zero stress (shape recovery)*

Table 2.10. *Experimental conditions to perform shape memory experiments in polyurethanes*

System	Experiment	T_{low} (ºC)	T_{high} (ºC)	F (N)
S1 and S2	PEG	-20	80	2
S3	PTMG(650)TDI	-20	80	2
S4	PTMG(650)MDI	-100	40	5, 10
S5	PTMG650MDITDI	-20	80	2
S6	PTMG(1000)TDI	-20	80	2
S7	PTMG(1000)MDI	-100	30	5, 10
S8	PTMG1000MDITDI	-20	80	2
S9-S11	TiO_2	-20	80	2
	DIAPLEX MM4520	-20	80	1

Rectangular samples of about 10 mm x 6 mm x 1.5 mm were used in shape memory tests. TMA measurements were made following the procedure depicted in *Figure* 2.*22*, where the increase of the sample length is recorded as a function of temperature. First, the sample is heated to a desired programming temperature (T_{high}), at least 20ºC above the glass transition temperature in order to allow relaxation of the polymer chains, and deformed applying a determined force, which depends on the system used as mentioned above. Once the sample is stretched, ε_m, the next stage consists of a cooling below transition temperature (T_{low}, temperature under 20ºC to T_g) in order to fix the temporary shape. When the sample is unloaded (F = 0 N), the deformation of the sample is ε_u. The shape memory effect is triggered by heating the sample to a temperature above the transition temperature. The amount of non-recoverable deformation at the end of programming is ε_p. The fixing (R_f) and recovery (R_r) ratios were calculated for each sample using equations *2.1* and *2.2*.

$$R_f(\%) = \frac{\varepsilon_u}{\varepsilon_m} \cdot 100 \qquad (2.1)$$

$$R_r(\%) = \frac{\varepsilon_m - \varepsilon_p}{\varepsilon_m} \cdot 100 \qquad (2.2)$$

Where, R_f is strain fixity ratio

R_r is strain recovery ratio

ε_m is the maximum strain applied to the material

ε_u is the strain of the material at T_{low} after the external stress has been removed

ε_p is the residual strain at T_{high}

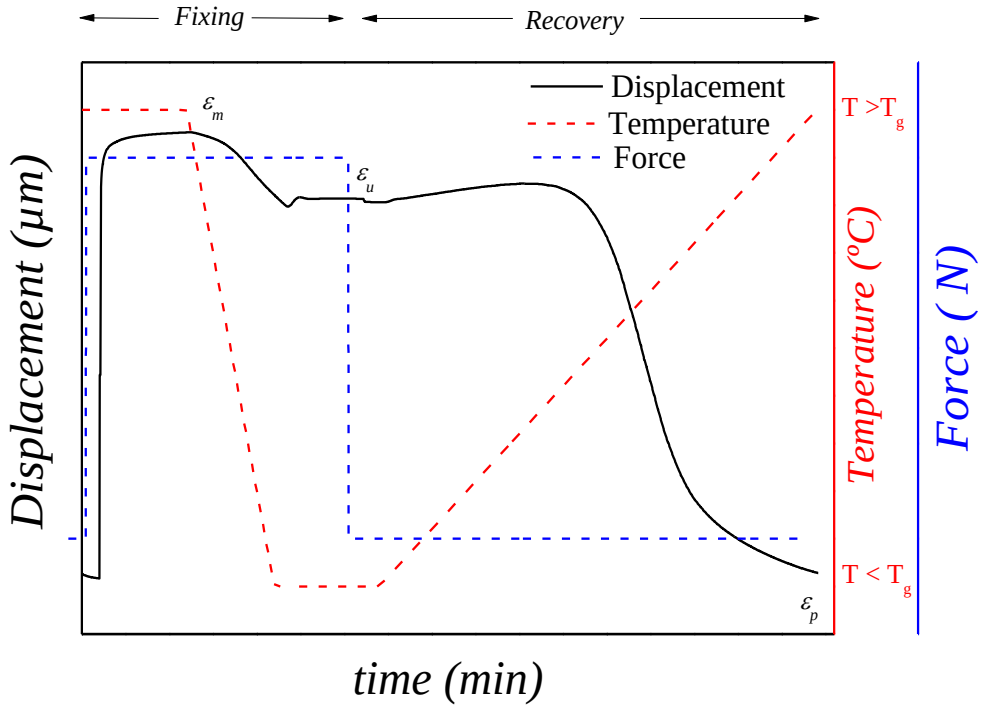

Figure 2.22. *Description of the method used in thermomechanical analysis*

2.3.6. Scanning Electron Microscopy (SEM)

A scanning electron microscope (SEM) is a type of electron microscope that produces images of a sample by scanning it with a focused beam of electrons instead of light to form an image. A beam of electrons is produced at the top of the microscope by an electron gun. The electron beam follows a vertical path through the microscope, which is held within a vacuum. The beam travels through electromagnetic fields and lenses, which focus the beam down toward the sample. The electrons in the beam interact with the sample, producing various signals that can be used to obtain information.

The morphology of SMPUs have been analyzed in a Hitachi S-4800 field emission scanning electron microscope (FE-SEM), an equipment located in the general services of the University of the Basque Country (SGIKER), *Figure 2.23*, at an acceleration voltage of 15 kV. Prior to SEM, the samples were coated with copper in a Quorum Q150T ES turbo-pumped sputter coater (5 nm thick coating). However, fibers produced by melt spinning were analyzed using an optical microscopic, a Nikon SMZ800.

Figure 2.23. *Photography of Hitachi S-4800 field emission scanning electron microscope (FE-SEM)*

2.3.7. Permeability test

In this work, permeability has been measured in different SMPUs in order to know the performance of this kind of polyurethanes at different temperatures. Thus, three different tests of permeability were realized at the Polymer Science and Technology Department of the University of Basque Country (UPV/EHU) in Donostia-San Sebastian:

- Water Vapor Transmission Rate (WVTR)
- Permeability Oxygen Measurements (PO_2)
- Limonene Vapor Transmission Rate (LVTR)

All samples of systems S4 and S7 were tested, as well as some samples of system S8 (PTMG1000MDITDI_4 and PTMG1000MDITDI_5) and system S10 (PTMG1000MDITDI_4_1 and PTMG1000MDITDI_5_1). In all cases, the required thickness of the films was measured by a Duo Check gauge with an accuracy of 1 μm. The procedure is illustrated in *Figure 2.24.*

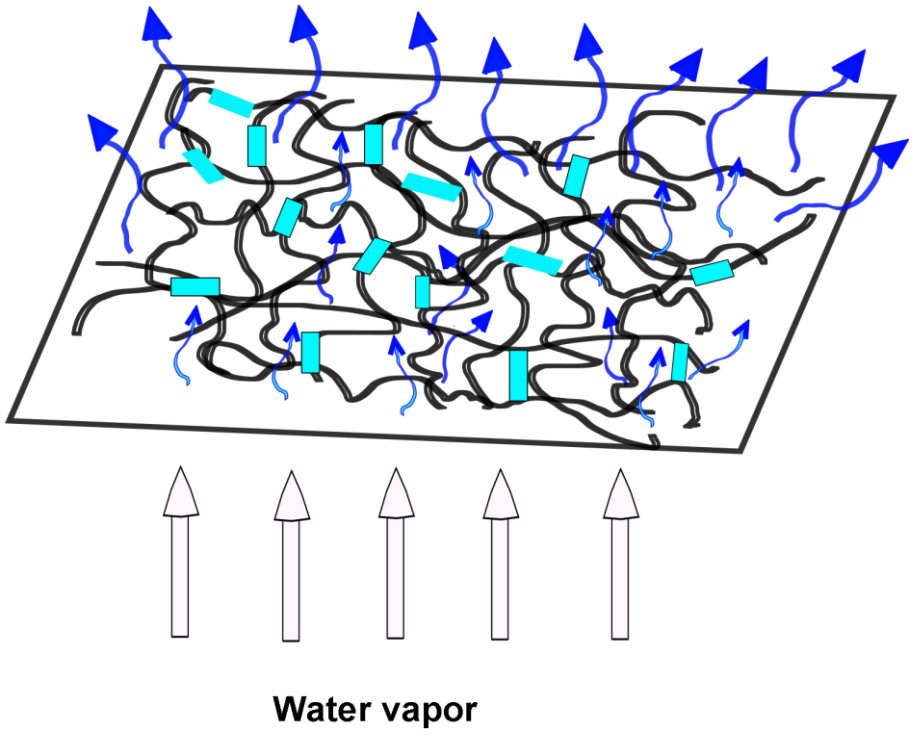

Figure 2.24. *Representation of permeability through a film of shape memory polyurethane*

Water Vapor Transmission Rate

The analysis of water vapor permeability was carried out with a Sartorius gravimetric cell. Taking into account the results obtained of time and weight gain, due to the water vapor that crosses the film, water vapor transmission rate (WVTR) values could be calculated. These data are directly related with the water vapor permeability. Permeability is measured in 'g mm/m^2 day' [25].

Permeability Oxygen Measurements

The measurements were carried out using a MOCON OX-TRAN Model 2/21 gas permeability tester (USA) in accordance with ASTM standard D3985 and ISO 15105-1,2. The permeability of O_2 through the polyurethanes was tested at 760 mm Hg, 0% of relative humidity and 23ºC. The permeability of oxygen is measured in 'barrer' units [26].

Limonene Vapor Transmission Rate

The analysis of limonene vapor permeability was carried out with a Sartorius gravimetric cell, following the same procedure as water vapor transmission rate. Taking into account the results obtained of time and weight gain, due to the limonene vapor that crosses the film, limonene vapor transmission rate (LVTR) values could be calculated. These data are directly related with the limonene vapor permeability. Permeability is measured in 'g mm/m^2 day'.

2.3.8. Tensile testing

Tensile test is the application of uniaxial force to measure the performance of a sample up to the point of yield or breaking. In simple terms, it consists in pulling the sample out in a straight line and analyzing how it behaves. Even where performance to ultimate failure is not required, characteristics of elongation, deformation and relaxation can be accurately recorded, as in elastomers and springs.

Some dog-bone shaped specimens (25 mm x 4 mm x 1 mm) of shape memory polyurethanes (*Figure 2.25*) were tested on a Shimadzu Autograph at the Basque Center for Materials, Applications and Nanostructures in Derio (*Figure 2.26.a*) using a 500 N load cell at a stretching speed of 2.5 mm·min^{-1} and at room temperature, over 5 specimens per SMPU [27]. Different parameters have been calculated for all samples such as Young's modulus (*E'*), stress and strain at yield (σ_y, ε_y) or stress and strain at break (σ_b, ε_b).

Figure 2.25. *Example of a dog-bone shaped specimen*

Moreover, fibers of shape memory polyurethanes were also measured by a tensile machine. The tensile tests were carried out according to ISO 527 standard in a Tinius Olsen H10KT testing machine at the University of Borås (*Figure 2.26.b*) with an extensometer to measure the strain. Five dumbbell-shaped specimens were

examined for each sample in the machine direction of the fibers at room temperature. The gauge length was 100 mm while the test speed was 10 mm·min^{-1}. The capacity of used load cell was 10 N.

(a) **(b)**

Figure 2.26. *Photography of Shimadzu Autograph (a) and Tinius Olsen H10KT (b)*

2.4. References

1. Król P (2008) Linear polyurethanes : synthesis methods, chemical structures, properties and applications. VSP, Boston.
2. Prisacariu C (2011) Polyurethane Elastomers: From Morphology to Mechanical Aspects. Springer, Wien.
3. Yildirim E, Yurtsever M, Wilkes GL, Yilgör I (2016) Effect of intersegmental interactions on the morphology of segmented polyurethanes with mixed soft segments: A coarse-grained simulation study. Polymer (Guildf) 90:204–214.
4. Rafiemanzelat F, Fathollahi Zonouz A, Emtiazi G (2012) Synthesis and characterization of poly(ether-urethane)s derived from 3,6-diisobutyl-2,5-diketopiperazine and PTMG and study of their degradability in environment. Polym Degrad Stab 97:72–80.
5. Liu N, Zhao Y, Kang M, et al (2015) The effects of the molecular weight and structure of polycarbonatediols on the properties of waterborne polyurethanes. Prog Org Coatings 82:46–56.
6. Ionescu M (2007) Chemistry and technology of polyols for polyurethanes. . Rapra Technology, Shrewsbury.
7. Mondal S, Hu JL (2006) Structural characterization and mass transfer properties of nonporous segmented polyurethane membrane: Influence of hydrophilic and carboxylic group. J Memb Sci 274:219–226.
8. Lligadas G, Ronda JC, Galià M, Cádiz V (2006) Novel silicon-containing polyurethanes from vegetable oils as renewable resources. Synthesis and properties. Biomacromolecules 7:2420–2426.
9. Senthilkumar N, Narasimhaswamy T, Kim I-J (2012) Novel metallomesogenic polyurethanes: Synthesis, characterization and properties. Mater Sci Eng C 32:2258–2266.
10. Kim JT, Kim BK, Kim EY, et al (2013) Synthesis and properties of near IR induced self-healable polyurethane/graphene nanocomposites. Eur Polym J 49:3889–3896.
11. Cristina Rodríguez Álvarez (2008) Elastómeros magnetostrictivos de poliuretano y terfenol-D: síntesis y propiedades. University of the Basque

Country (UPV/EHU).

12. Alishiri M, Shojaei A, Abdekhodaie MJ, Yeganeh H (2014) Synthesis and characterization of biodegradable acrylated polyurethane based on poly(ε-caprolactone) and 1,6-hexamethylene diisocyanate. Mater Sci Eng C Mater Biol Appl 42:763–773.

13. Eyvazzadeh Kalajahi A, Rezaei M, Abbasi F (2016) Preparation, characterization, and thermo-mechanical properties of poly (??-caprolactone)-piperazine-based polyurethane-urea shape memory polymers. J Mater Sci 51:4379–4389.

14. Charlon M, Heinrich B, Matter Y, et al (2014) Synthesis, structure and properties of fully biobased thermoplastic polyurethanes, obtained from a diisocyanate based on modified dimer fatty acids, and different renewable diols. Eur Polym J 61:197–205.

15. Chang Z, Zhang M, Hudson AG, et al (2013) Synthesis and properties of segmented polyurethanes with triptycene units in the hard segment. Polymer (Guildf) 54:6910–6917.

16. Sáenz-Pérez M, Lizundia E, Laza JM, et al (2016) Methylene diphenyl diisocyanate (MDI) and toluene diisocyanate (TDI) based polyurethanes: thermal, shape-memory and mechanical behavior. RSC Adv 6:69094–69102.

17. Sáenz-Pérez M, Laza JM, García-Barrasa J, et al (2017) Influence of the soft segment nature on the thermomechanical behavior of shape memory polyurethanes. Polym Eng Sci 1–7.

18. Arshanitsa A, Krumina L, Telysheva G, Dizhbite T (2016) Exploring the application potential of incompletely soluble organosolv lignin as a macromonomer for polyurethane synthesis. Ind Crops Prod 92:1–12.

19. Clemitson I (2015) Castable polyurethane elastomers. CRC Press, New York.

20. Gooch JW (2011) Encyclopedic dictionary of polymers. Vol. 1, A-0. Springer, New York.

21. Jeong H, Lee S, Kim B (2000) Shape memory polyurethane containing amorphous reversible phase. J Mater Sci 35:1579–1583.

22. Kausar A, Zulfiqar S, Sarwar MI (2013) High performance segmented polyurethanes derived from a new aromatic diisocyanate and polyol. Polym

Degrad Stab 98:368–376.

23. Xu X, Li Y, Xiong Z, et al (2016) Preparation and model of high-performance shape-memory polyurethane with hydroxylated perylene bisimide. RSC Adv 6:110329–110336.

24. García-Huete N, Laza JM, Cuevas JM, et al (2014) Shape memory effect for recovering surface damages on polymer substrates. J Polym Res 21:481–490.

25. Algar I, Garcia-Astrain C, Gonzalez A, et al (2016) Improved Permeability Properties for Bacterial Cellulose/Montmorillonite Hybrid Bionanocomposite Membranes by *In-Situ* Assembling. J Renew Mater 4:57–65.

26. Sardon H, González A, Fernández-Berridi MJ, Irusta L (2015) Oxygen Barrier Properties of Waterborne Polyurethane/Silica Hybrids. J Macromol Sci Part B 54:711–721.

27. Wei W, Shi A, Wu T, et al (2016) Thermo-responsive shape and optical memories of photonic composite films enabled by glassy liquid crystalline polymer networks. Soft Matter 12:8534–8541.

Chapter III.

RESULTS AND DISCUSSION. I. CHARACTERIZATION

"Cada día sabemos más y entendemos menos"

Albert Einstein

Chapter III.

RESULTS AND DISCUSSION. I. CHARACTERIZATION

3.1. Introduction

All shape memory polyurethanes synthesized in this work were characterized by multiple different techniques in order to define their properties properly. In this chapter, the physico-mechanical characterization is studied. In next chapters, *Chapter IV* and *Chapter V*, the shape memory behavior and the permeability behavior will be studied, respectively. Thus, attenuated total reflectance Fourier transform infrared spectroscopy (ATR-FTIR) was used in order to follow and control the reaction for the formation of polyurethanes. Moreover, thermal stability was studied by thermogravimetric analysis (TGA), whereas transition temperatures, which correspond with the glass transition temperatures, were determined by differential scanning calorimetry (DSC) and dynamic mechanical analysis (DMA). Finally,

mechanical properties were analyzed by tensile tests and scanning electron microscopy (SEM) was used to study the morphology of the polyurethanes.

3.2. Attenuated total reflectance (ATR)

All shape memory polyurethanes were analyzed by attenuated total reflectance (ATR). ATR-FTIR was used to assess the extent of the reaction between the isocyanate and the hydroxyl groups [1–3]. The major benefit of ATR is the ability to measure a wide variety of solid and liquid samples without requiring complex preparations. This technique consists of a beam of infrared light passing through an ATR crystal, which comprises an IR transparent material with a high refractive index and polished surfaces [4]. In this work, infrared spectra were collected on a Nicolet Nexus FTIR spectrophotometer. The spectra were obtained using an ATR tool in the range from 500 to 4000 cm^{-1} at a resolution of 4 cm^{-1} and 64 scans per spectrum, as mentioned in *Chapter II*.

In *Table 3.1*, the typical band assignment for all the polyurethanes synthesized in the laboratory is presented. Moreover, *Figure 3.1* shows the typical spectrum for this kind of polyurethanes, specifically, for the sample PTMG1000MDI_2.5. Chemical structure of all the resultant SMPUs was fully confirmed [5–7].

The stretching band corresponding to the isocyanate group was not found at 2270 cm^{-1}, indicating that the initial isocyanate groups have reacted completely during the synthesis [8–12]. Furthermore, in *Figure 3.1* it can be observed, for the isocyanate segments, the symmetric and asymmetric stretching vibrations of N-H corresponding to the broad absorption bands near 3320 cm^{-1}; the medium-strong peak at 1590 cm^{-1} which confirms the in-plane bending vibration of N-H; the sharp absorption peaks around 1730-1700 cm^{-1} which are typical for the stretching vibration of esters C=O (NHCOO stretching combined with ester COO stretching); the 1220 cm^{-1} absorption peak caused by the vibration of C=C in benzene ring; and several weak peaks near 900-700 cm^{-1} that belong to out-of-plane bending vibration of C-H in multisubstituted benzene ring. On the other hand, *Figure 3.1* shows, for the soft-segment polyether polyols, the peak groups near 2940 to 2850 cm^{-1} caused by the stretching vibration of C-H_2, and the broad and strong peak at 1100 cm^{-1} from the ether bond C-O-C stretch. Furthermore, the peaks observed at around 1530 and

1450 cm^{-1} corresponding to C-N and CH_2 bond, respectively, support the formation of the urethane group [13–15].

Table 3.1. *Summary of typical band assignment for polyurethanes*

Nº	Band assignment	Wavenumber (cm^{-1})
1	ν (NH)	3320
2	ν_s (CH_2)	2940
3	ν_{as} (CH_2)	2850
4	ν (C=O) Non-bonded urethane stretching	1730
5	ν (C=O) Associated urethane and isocyanurate ring stretch	1700
6	δ (NH)	1590
7	δ (C-N)	1530
8	δ_s (CH_2)	1446
9	δ_{as} (CH_2)	1414
10	ν (C=C)	1220
11	ν_s (C-O-C)	1100

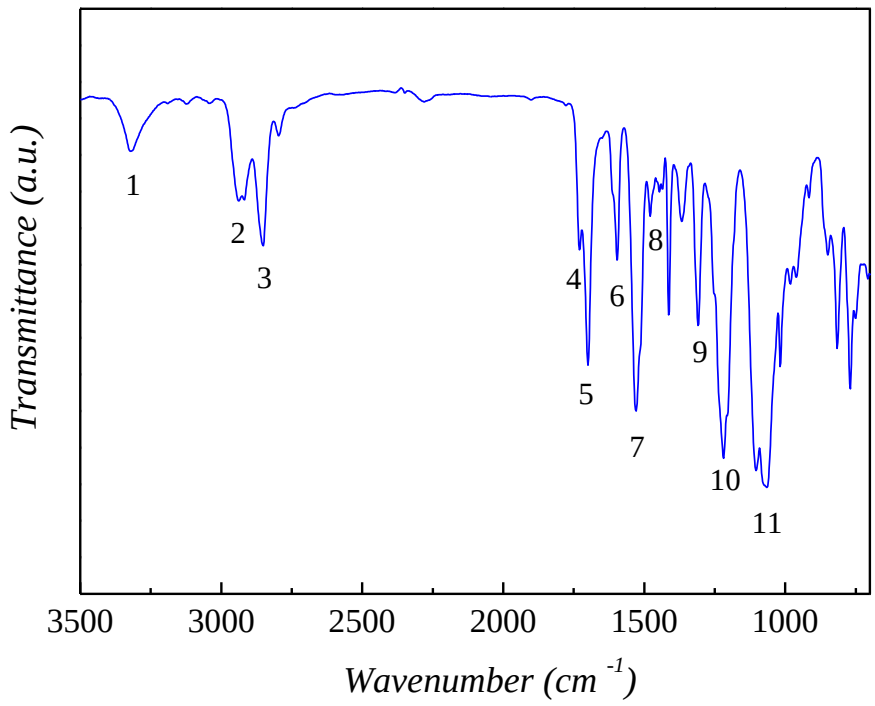

Figure 3.1. *Example of an ATR spectrum for polyurethanes*

Furthermore, as an example, in *Figure 3.2* and *Figure 3.3* the ATR spectra for the PTMG1000MDI samples are divided in two parts, from 4000 to 2500 cm^{-1} and from 2100 to 700 cm^{-1}, respectively. All samples of system 7 (PTMG1000MDI) were shown in these figures, except PTMG1000MDI_0.5 and PTMG1000MDI_1 samples because they were too liquid to be measured by ATR.

In these figures, it can be observed that the intensity of all signals related to the urethane links (1730 cm^{-1}, 1530 cm^{-1}…) decreases from PTMG1000MDI_1.5 to PTMG1000MDI_4.5, that is, decreases when the amount in moles of 1,4-butanediol (*n*) rises. In other words, these peaks became lower indicating a higher concentration of hard-segment content which is composed, as mentioned in *Chapter II*, of diisocyanate (n+1) and diol (n) [16,17].

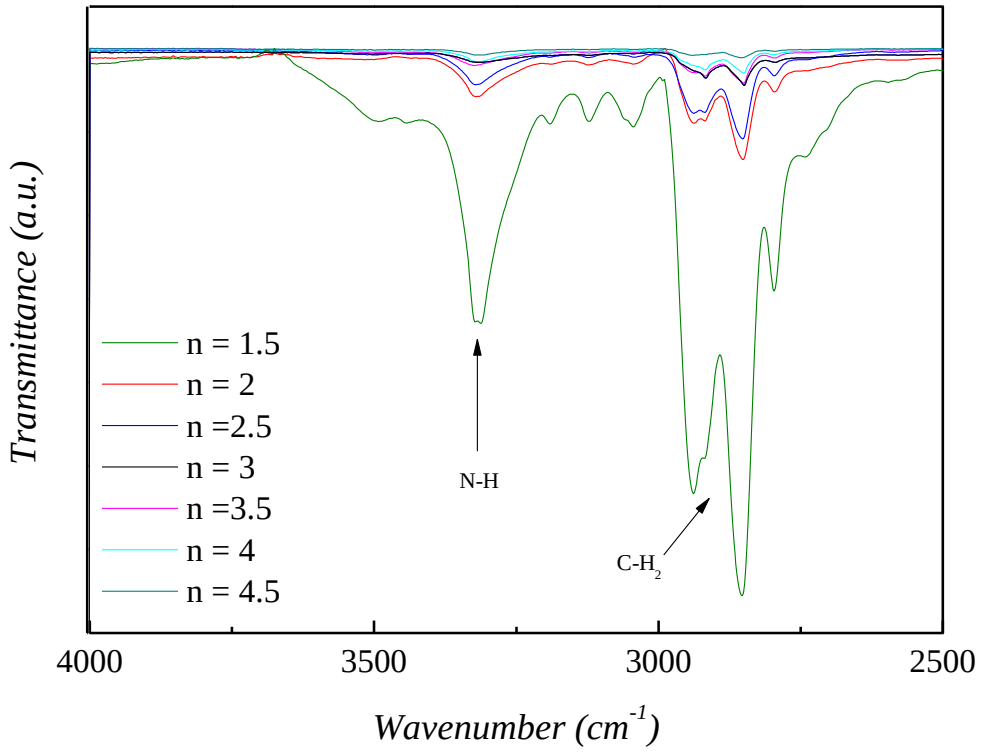

Figure 3.2. *ATR spectra for system 7, PTMG1000MDI, from 4000 to 2500 cm^{-1}*

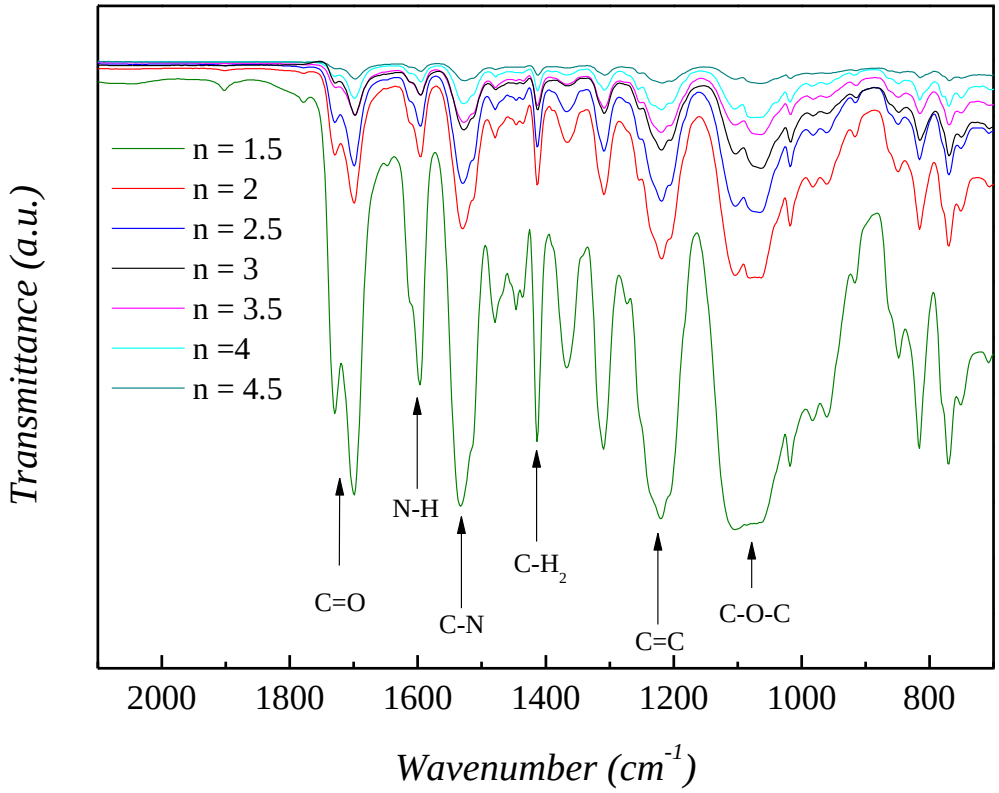

Figure 3.3. *ATR spectra for system 7, PTMG1000MDI, from 2100 to 700 cm^{-1}*

3.3. Thermogravimetric behavior of shape memory polyurethanes

In a thermogravimetric analysis (TGA), the weight loss of a sample is continuously monitored as the temperature is raised. Therefore, TGA was used to evaluate the thermal stability of all synthesized polyurethanes. Thermal stability of polyurethanes is related to the structure, the chemical composition and, of course, the hard-segment/soft-segment molar ratio [18]. For example, the initial degradation temperature of the polyurethanes is a relevant parameter because it is dependent on the thermal history of the weakest points within the PU macromolecule, which are the urethane and the ester bonds [19].

All the TGA and DTG curves obtained from PTMG-based and PEG-based SMPUs with different molar ratio are shown in the *Appendix A.* Here, the most representative ones are presented in the following figures. Thus, *Figure 3.4* represents the TGA and

DTG curves for the polyurethanes based on PEG and TDI; *Figure 3.5* for the polyurethanes based on PTMG650 and TDI; *Figure 3.6* for the polyurethanes based on PTMG1000 and MDI; and *Figure 3.7* for the polyurethanes based on PTMG1000, a mixture of TDI and MDI and 1 wt% TiO_2.

The initial decomposition temperatures (T_i), defined as the temperature at 5% weight loss; the temperatures at the maximum degradation rate ($T_{max,1}$, $T_{max,2}$ and $T_{max,3}$) for each degradation step, obtained from the minimum in DTG curves; and the weight percentages of residue remaining at the end of the degradation (*wt% residue*) [20,21], are listed in the following tables. Thus, the thermal properties for PEG-based polyurethanes are tabulated in *Table 3.2*; whereas *Table 3.3, Table 3.4* and *Table 3.5* show the results of PTMG-based polyurethanes (PTMG650, PTMG1000 and polyurethanes synthesized with TiO_2 nanoparticles, respectively).

PUs thermal decomposition is a multi-stage process, generally accepted a two-stage or three-stage decomposition, which depends on the presence of the hard-segment. The first stage of degradation is fast, although its rate decreases as the soft-segment content increases [22–25]. The chemical structure of the samples allows to relate the observed regions of decomposition to following processes: first region is related to decomposition of urethane groups; second region can be connected to destruction of ether groups and third region is related to destruction of carbon chains and rings. The PEG-based SMPUs (*Table 3.2* and *Figure 3.4*) display a typical two-stage degradation process: the first one, attributed to the PU hard-segments, occurs between 275-370ºC; whereas the second degradation step, caused by the soft-segments, takes place between 340-440ºC. *Table 3.2* also shows that the initial decomposition temperatures are slightly higher in MDI-based SMPUs than in TDI-based SMPUs; and that the weight percentages of residue remaining at the end of the degradation, which rises with the hard-segment content, is also higher for the PUs based on MDI.

The TGA and DTG analyses were also made for the PTMG-based polyurethanes, PTMG650 and PTMG1000. In both cases, three different types of diisocyanates (TDI, MDI or TDI+MDI) were used. *Table 3.3* shows the thermal properties for all SMPUs based on PTMG650, whereas in *Figure 3.5* are depicted, as an example, the TGA and DTG curves for system 3 (PTMG650-TDI based PUs). From this curves, it can be noted that PTMG-based polyurethanes show the same tendencies that PEG-based SMPUs, that is, higher initial decomposition temperatures and higher *wt% residue*

when MDI is used as diisocyanate instead of TDI. As expected, when mixtures of both TDI and MDI are used, PUs present intermediate values. Moreover, while MDI-based and TDI-based PUs present just two decomposition stages (250-375ºC and 375-500ºC), these last SMPUs show a three-stage decomposition process as a consequence of using a mixture of isocyanates.

Table 3.4 shows the thermal properties for all SMPUs based on PTMG1000, whereas in *Figure 3.6* are depicted as an example the TGA and DTG curves for system 7 (PTMG1000-MDI based PUs). For these systems, the thermal stability shows a similar behavior to that described above for the SMPUs based on PTMG650.

In the case of the PUs synthesized with nanoparticles (*Table 3.5*), all samples present a three-stage decomposition process because a mixture of isocyanates (MDI+TDI) was used. Moreover, it could be observed that these PUs are less stable than the ones synthesized without nanoparticles. Thus, the initial decomposition temperatures for PUs of system 10 (PMTG1000/MDI+TDI/1 wt% TiO_2) are 10-15ºC smaller than the T_is for the same PUs without TiO_2 nanoparticles (system 8). Moreover, as the nanoparticles content increases, less stable is the polyurethane [26–28]. *Table 3.5* shows that T_i*s* are 10-20ºC smaller for system 11 (3wt% TiO_2) than for system 10 (1wt% TiO_2).

Therefore, it can be concluded that MDI-based PUs are more stable than TDI+MDI-based PUs which are, at the same time, more stable than TDI-based PUs due to the chemical structure of the diisocyanates. This fact can be explained because MDI owns two aromatic rings (TDI only owns one aromatic ring) that provide a higher thermal stability to polyurethanes. Moreover, in general, polyurethanes made from PTMG650 have a higher thermal stability than the equivalent ones achieved from PTMG1000. This fact can be related to the length of the soft-segment, which is smaller when the molecular weight of the polyol decreases [25].

It can also be observed that the presence of TiO_2 nanoparticles decreases the thermal stability of the polyurethanes, considering that T_i decreases. Moreover, as the wt% TiO_2 increases, thermal stability decreases. This loss of thermal stability can be explained because TiO_2 nanoparticles act as impurities or breaking points in the PUs macromolecular network.

Furthermore, as indicated above, all the polyurethanes synthesized in this work display a typical two-stage degradation, except for those synthesized with a mixture of diisocyanates (TDI+MDI), where three stages are observed.

Finally, the obtained results show good thermal stability for all samples, indicating that the choice of both the hard-segment component and the soft-segment component influence on the thermal decomposition of the polyurethanes.

Table 3.2. *Thermal properties of the SMPUs based on PEG*

System & Sample		$T_{5\%}$	wt% residue	$T_{max,1}$	$T_{max,2}$
S1	PEGTDI_3.5	275.7	1.9	330.2	410.1
	PEGTDI_4.5	293.7	3.1	328.9	411.8
	PEGTDI_5.5	299.7	4.3	334.9	413.7
S2	PEGMDI_2	296.6	10.7	322.1	411.4
	PEGMDI_3	289.4	11.5	310.7	409.4
	PEGMDI_4	298.1	13.4	326.1	408.3

Table 3.3. *Thermal properties of the SMPUs based on PTMG 650*

System & Sample		$T_{5\%}$	wt% residue	$T_{max,1}$	$T_{max,2}$	$T_{max,3}$
S3	PTMG650TDI_2.5	273.8	0.2	324.3	415.7	
	PTMG650TDI_3	285.9	1.1	328.7	418.7	
	PTMG650TDI_3.5	279.6	2.1	321.8	418.9	
	PTMG650TDI_4	276.1	2.5	326.0	411.2	
	PTMG650TDI_4.5	275.7	2.7	320.2	421.0	
	PTMG650TDI_5	290.3	3.5	328.9	405.0	
	PTMG650TDI_5.5	283.0	6.1	331.1	421.0	
S4	PTMG650MDI_0.5	314.6	1.1	353.3	414.1	
	PTMG650MDI_1	308.3	4.7	353.5	421.9	
	PTMG650MDI_1.5	295.9	6.9	335.9	423.8	
	PTMG650MDI_2	304.3	8.4	327.0	423.4	
	PTMG650MDI_2.5	292.5	8.9	311.5	421.6	
	PTMG650MDI_3	303.3	9.9	317.9	421.4	
	PTMG650MDI_3.5	302.9	9.5	324.7	425.2	
	PTMG650MDI_4	325.2	13.2	325.2	425.2	
	PTMG650MDI_4.5	323.3	12.4	323.3	425.6	
S5	PTMG650MDITDI_1.5	294.2	0.5	320.2	353.8	418.2
	PTMG650MDITDI_2	287.3	3.8	321.2	361.5	419.7
	PTMG650MDITDI_2.5	296.1	4.4	332.7	360.4	425.7
	PTMG650MDITDI_3	291.8	4.7	329.8	358.4	423.8
	PTMG650MDITDI_3.5	295.8	5.9	326.2	340.5	422.8

Table 3.4. *Thermal properties of the SMPUs based on PTMG 1000*

System & Sample		$T_{5\%}$	wt% residue	$T_{max,1}$	$T_{max,2}$	$T_{max,3}$
S6	PTMG1000TDI_2.5	285.3	1.5	323.3	416.5	
	PTMG1000TDI_3	281.6	1.7	315.9	411.2	
	PTMG1000TDI_3.5	293.5	1.7	307.9	421.4	
	PTMG1000TDI_4	285.1	2.2	328.8	416.7	
	PTMG1000TDI_4.5	284.6	2.5	322.4	414.9	
	PTMG1000TDI_5	279.7	3.2	328.9	418.9	
	PTMG1000TDI_5.5	280.9	4.9	321.1	417.1	
	PTMG1000TDI_6.5	277.6	7.3	323.3	419.9	
S7	PTMG1000MDI_0.5	311.2	1.9	354.4	417.4	
	PTMG1000MDI_1	306.6	2.5	352.8	416.9	
	PTMG1000MDI_1.5	303.8	3.8	350.3	418.8	
	PTMG1000MDI_2	300.4	6.4	322.0	419.9	
	PTMG1000MDI_2.5	301.8	9.4	317.5	423.2	
	PTMG1000MDI_3	289.1	9.7	298.7	419.4	
	PTMG1000MDI_3.5	307.6	9.7	323.8	417.1	
	PTMG1000MDI_4	299.7	13.1	329.2	421.8	
	PTMG1000MDI_4.5	304.4	18.0	331.9	426.4	
S8	PTMG1000MDITDI_3.5	293.7	2.4	332.8	361.1	417.9
	PTMG1000MDITDI_4	292.6	3.2	332.3	361.2	417.7
	PTMG1000MDITDI_4.5	288.9	3.2	334.2	362.3	420.6
	PTMG1000MDITDI_5	294.2	3.7	330.8	358.3	422.3
	PTMG1000MDITDI_5.5	286.1	3.9	335.7	361.4	421.4
	PTMG1000MDITDI_6	294.6	6.1	335.2	354.8	423.2

Table 3.5. *Thermal properties of the SMPUs synthesized with nanoparticles*

System & Sample		$T_{5\%}$	wt% residue	$T_{max,1}$	$T_{max,2}$	$T_{max,3}$
S9	PTMG650MDITDI_1.5_1	295.8	4.4	320.2	353.3	418.8
	PTMG650MDITDI_2_1	287.7	4.6	320.4	360.2	404.9
	PTMG650MDITDI_2.5_1	290.3	4.7	326.7	359.5	414.1
	PTMG650MDITDI_3_1	289.7	5.0	328.9	360.2	418.8
	PTMG650MDITDI_3.5_1	289.8	5.2	326.0	358.2	422.7
S10	PTMG1000MDITDI_3.5_1	285.0	4.0	313.6	351.1	404.4
	PTMG1000MDITDI_4_1	289.8	4.1	323.5	351.1	418.1
	PTMG1000MDITDI_4.5_1	284.2	4.6	320.9	354.8	415.9
	PTMG1000MDITDI_5_1	289.2	4.6	322.0	358.8	416.2
	PTMG1000MDITDI_5.5_1	291.3	5.1	329.0	359.9	419.9
	PTMG1000MDITDI_6_1	287.3	5.5	321.7	358.8	421.0
S11	PTMG1000MDITDI_3.5_3	263.1	5.5	314.8	350.9	405.2
	PTMG1000MDITDI_4_3	274.5	5.7	308.7	349.6	387.1
	PTMG1000MDITDI_4.5_3	282.9	6.1	316.8	352.9	389.1
	PTMG1000MDITDI_5_3	279.1	6.7	316.8	355.6	413.2
	PTMG1000MDITDI_5.5_3	277.3	7.4	279.2	351.6	404.5
	PTMG1000MDITDI_6_3	276.2	8.7	308.7	344.8	408.5

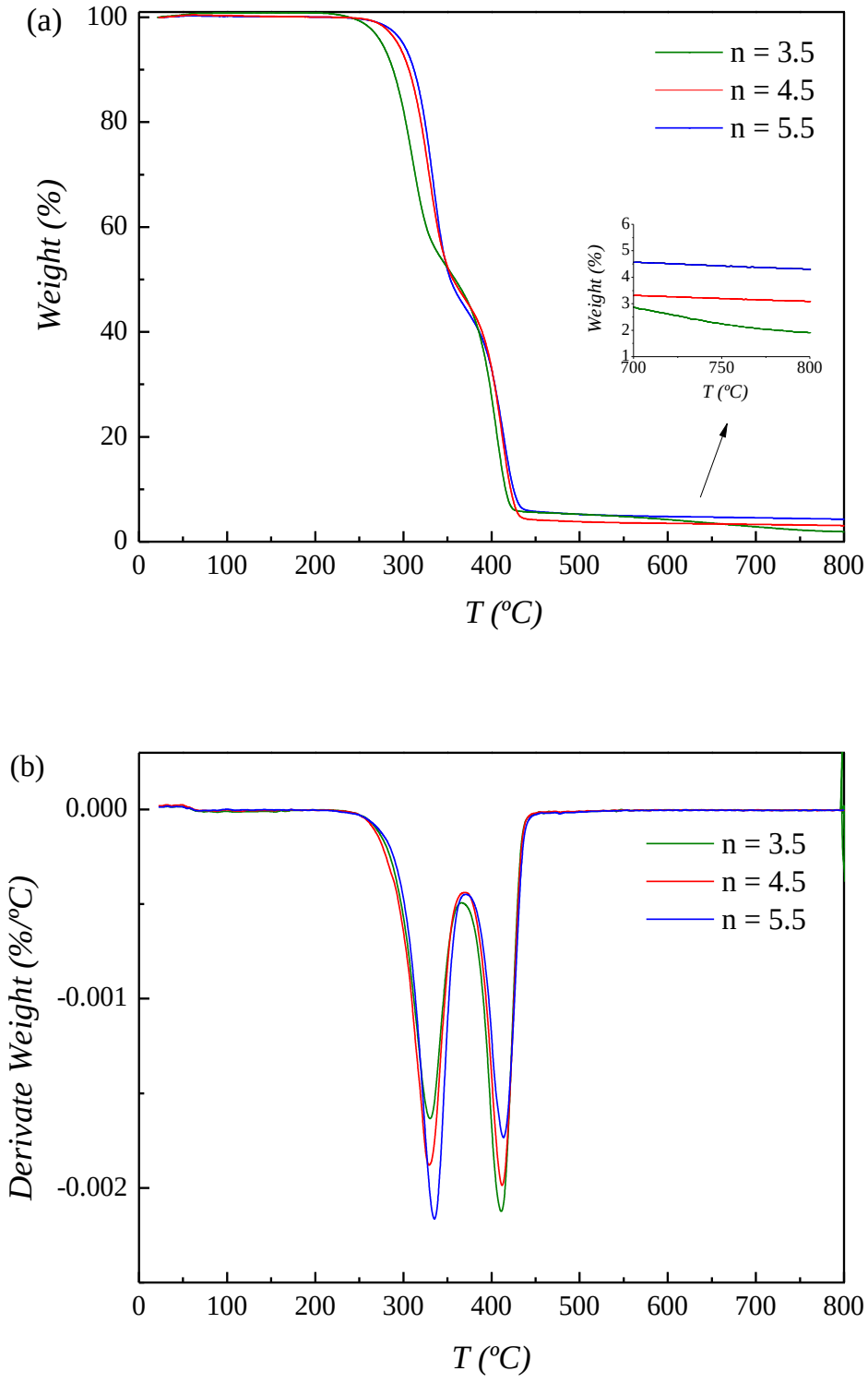

Figure 3.4. *TGA (a) and DTG (b) curves for system 1, PEG1000TDI*

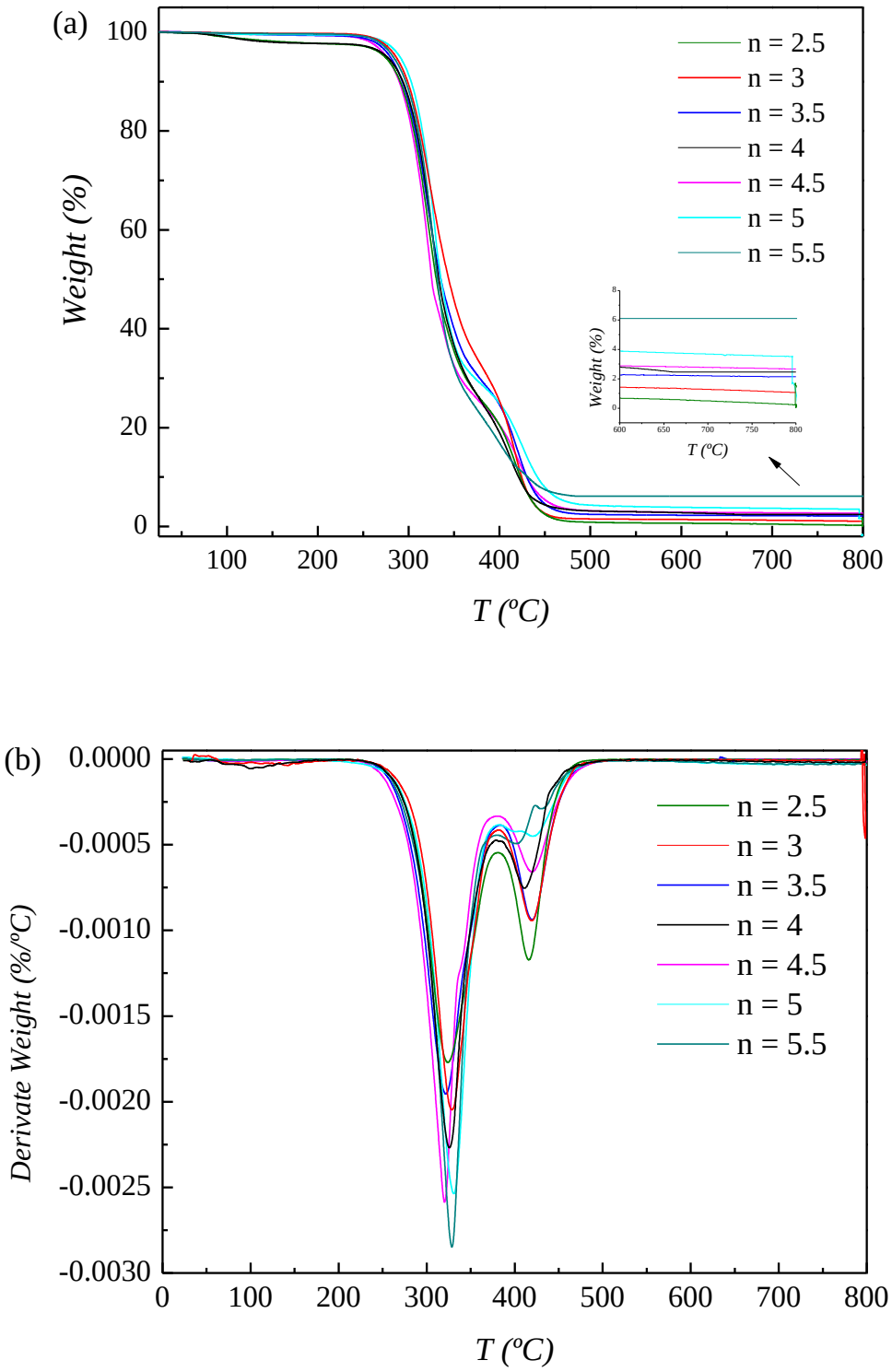

Figure 3.5. *TGA (a) and DTG (b) curves for system 3, PTMG650TDI*

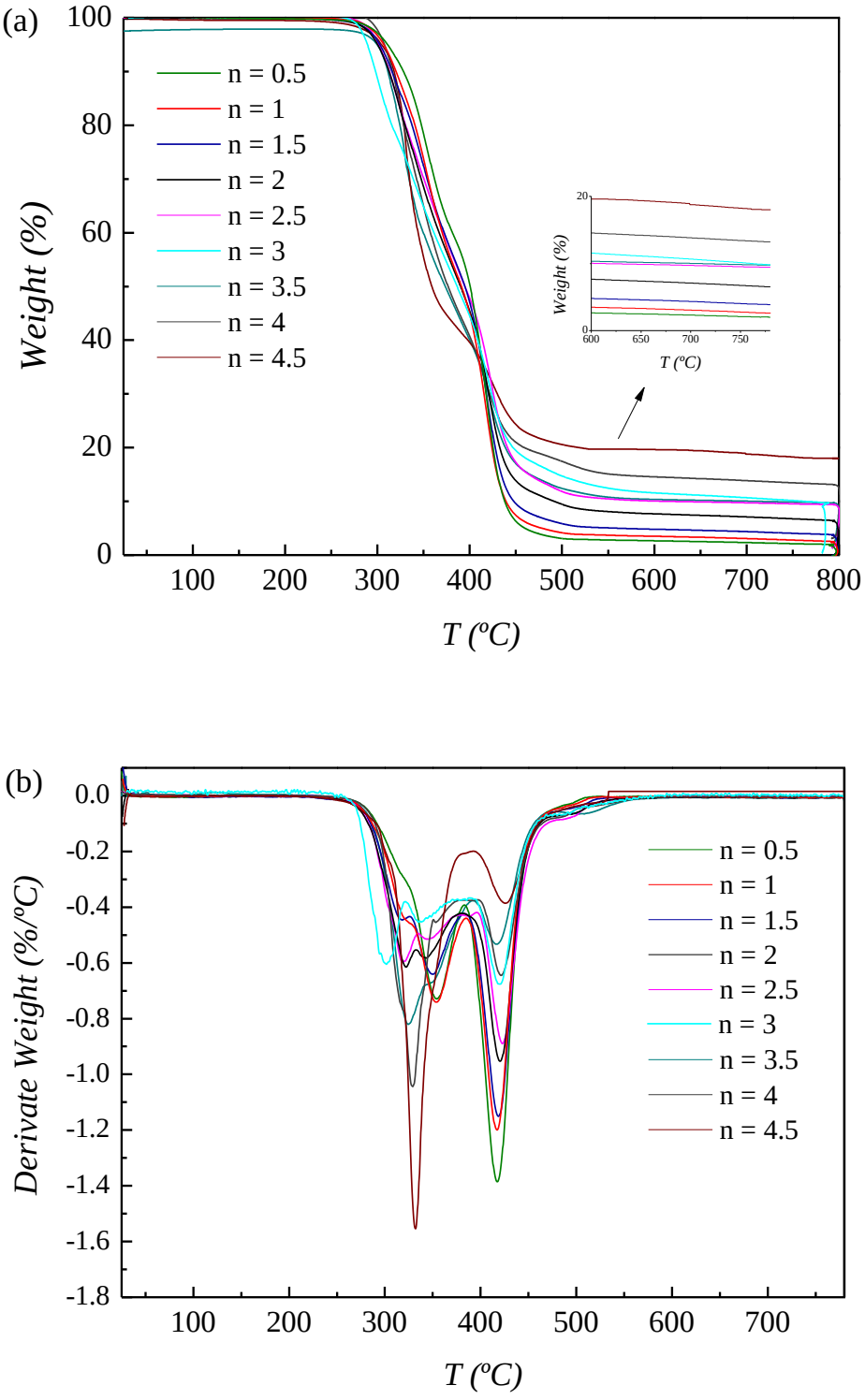

Figure 3.6. *TGA (a) and DTG (b) curves for system 7, PTMG1000MDI*

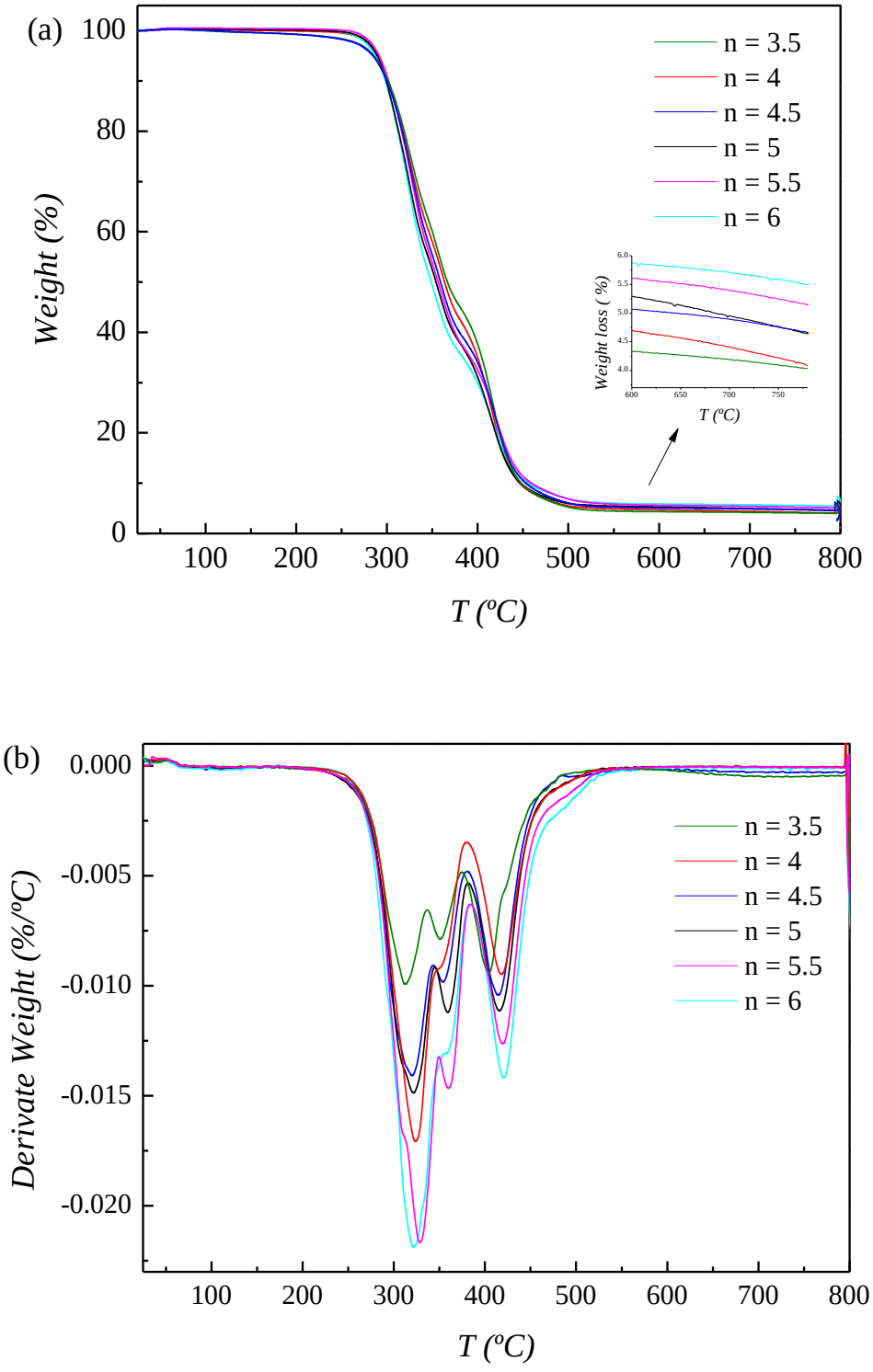

Figure 3.7. *TGA (a) and DTG (b) curves for system 10, PTMG1000/MDI+TDI/1%TiO_2*

3.4. DSC behavior of shape memory polyurethanes

As it was already mentioned, PU chains are composed of hard and soft-segments arranged alternately. This structure results from the spatial arrangement of polymer chains in the condensed phase. MDI-based PUs form zigzag chains in which benzene rings of MDI are arranged at the right angle against each other. On the other hand, the TDI-based PU chains are arranged in one plane because of the coplanar arrangement of both TDI-derived benzene rings and urethane groups attached to those rings [19,29].

Moreover, it is well known that SMPUs have an amorphous reversible phase due to their microstructure composed by hard and soft-segments. Therefore, for these SMPUs, T_g represents both the glass transition temperature and also the shape recovery temperature at which the shape memory effect (SME) is activated for this thermo-responsive SMP. On the one hand, at a temperature below T_g, this SMP is in the glassy state and is too stiff and hard to be deformed (with high modulus). In this state, the soft-segment in the SMP is frozen. It may be able to vibrate slightly, but no significant segmental motion occurs. When the SMPU is gradually heated, it enters in the glass transition region. This glass transition does not start or finish instantaneously, but takes place gradually over a temperature range [30]. On the other hand, at a temperature above T_g, this SMP is in the rubber phase and it can be able to be deformed without any difficulty and sometimes it even changes from solid to liquid state.

In this section, the glass transition temperatures ($T_{g,DSC}$) of the SMPUs were obtained with DSC. *Table 3.6*, *Table 3.7*, *Table 3.8* and *Table 3.9* summarize the measured glass transition temperatures corresponding to the second DSC heating scan for PEG-based PUs, PTMG650-based PUs, PTMG1000-based PUs and polyurethanes synthesized with TiO_2 nanoparticles, respectively. Furthermore, *Figure 3.8*, *Figure 3.9*, *Figure 3.10* and *Figure 3.11* show the DSC curves corresponding to the first heating, the cooling cycle and the second heating for system 1, system 3, system 7 and system 10, respectively. All DSC curves are in *Appendix B*.

DSC results show that, for all systems, the glass transition temperature of polyurethanes increases with the hard-segment content (higher *n*). For example, the T_gs of PEG-based polyurethanes in system 1 appear between -2.1—10.9ºC, T_gs of TDI-based polyurethanes in system 3 appear between -4.3—24.6ºC whilst for MDI-

based polyurethanes in system 7 T_gs are observed between -52.5—23.7ºC. This suggests that high contents in hard-segments can achieve a more well-oriented position within the polymeric structure [31,32]. In addition, $T_{g,DSC}$ increases with the rise in NCO/OH molar ratio. This fact might be due to the increase in the H-bonding as well as the crosslinking density as NCO/OH molar ratio increases [33]. The $T_{g,DSC}$ values of polyurethanes based on PEG and TDI can be assigned to the amorphous structure of polyol because of the lack of crystalline structure in this kind of polyurethanes, as reported in literature [34].

Additionally, it was found that for a given *n* the T_g values of TDI-based polyurethanes are lower than those of MDI-based polyurethanes, whereas the T_g values of the polyurethanes made from a mixture of diisocyanates (TDI+MDI) are found in the middle of them. For example, for PTMG650-based polyurethanes and *n* = 3.5, T_g in system 3 (TDI) is 10ºC, in system 4 (MDI) is 33.4ºC, and in system 5 (TDI+MDI) is 27.7ºC. On the contrary, there is no a clear trend for polyurethanes made from PTMG1000.

Moreover, in the heating scans, a melting peak can be observed for MDI-based SMPUs, which can be attributed to the crystallization of the soft domains. As a result, PTMG650-based polyurethanes present melting temperatures (T_m) between 130-180ºC, and PTMG1000-based polyurethanes between 130-220ºC. In addition, the melting enthalpy (ΔH_m) measured by DSC becomes higher, from 6.7 to 22.1 $J \cdot g^{-1}$ for PTMG650-based PUs and from 2.7 to 22.9 $J \cdot g^{-1}$ for PTMG1000-based PUs, as the hard-segment content increases [35–37].

As shown in *Table 3.7* and *Table 3.8*, the glass transition temperatures of PTMG650-based PUs are higher than the glass transition temperatures of PTMG1000-based PUs. Thus, at a determined temperature, PTMG650-based polyurethanes have less mobility than PTMG1000-based polyurethanes. The main difference between both polyurethanes, with the same molar ratio, is their soft-segment: PTMG650 or PTMG1000.

Finally, it can be observed in *Table 3.9* for the SMPUs synthetized with TiO_2 nanoparticles, that these polyurethanes own similar T_gs than polyurethanes without nanoparticles [38,39]. Furthermore, in the same way as for the other SMPUs, as the hard-segment content increases the glass transition temperature becomes higher.

Table 3.6. *Glass transition temperature of the SMPUs based on PEG*

System & Sample		$T_{g,DSC}$ (ºC)
S1	PEGTDI_3.5	-2.1
	PEGTDI_4.5	5.8
	PEGTDI_5.5	10.9
S2	PEGMDI_2	-7.9
	PEGMDI_3	10.5
	PEGMDI_4	22.3

Table 3.7. *Glass transition temperature of the SMPUs based on PTMG 650*

System & Sample		$T_{g,DSC}$ (ºC)	ΔH_m ($J \cdot g^{-1}$)
S3	PTMG650TDI_2.5	-4.3	
	PTMG650TDI_3	6.6	
	PTMG650TDI_3.5	10.0	
	PTMG650TDI_4	12.7	
	PTMG650TDI_4.5	14.4	
	PTMG650TDI_5	18.6	
	PTMG650TDI_5.5	24.6	
S4	PTMG650MDI_0.5	-35.5	6.7
	PTMG650MDI_1	-29.4	10.3
	PTMG650MDI_1.5	-24.7	14.4
	PTMG650MDI_2	-22.9	14.7
	PTMG650MDI_2.5	-12.0	16.5
	PTMG650MDI_3	30.3	19.2
	PTMG650MDI_3.5	33.4	20.7
	PTMG650MDI_4	42.6	21.3
	PTMG650MDI_4.5	48.2	22.1
S5	PTMG650MDITDI_1.5	-6.2	
	PTMG650MDITDI_2	3.5	
	PTMG650MDITDI_2.5	9.2	
	PTMG650MDITDI_3	15.9	
	PTMG650MDITDI_3.5	27.7	

Table 3.8. *Glass transition temperature of the SMPUs based on PTMG 1000*

System & Sample		$T_{g,DSC}$ (ºC)	ΔH_m (J·g^{-1})
S6	PTMG1000TDI_2.5	-61.2	
	PTMG1000TDI_3	-55.7	
	PTMG1000TDI_3.5	-30.2	
	PTMG1000TDI_4	-28.3	
	PTMG1000TDI_4.5	-27.4	
	PTMG1000TDI_5	-19.2	
	PTMG1000TDI_5.5	3.9	
	PTMG1000TDI_6.5	8.7	
S7	PTMG1000MDI_0.5	-52.5	2.7
	PTMG1000MDI_1	-50.8	5.2
	PTMG1000MDI_1.5	-42.7	5.3
	PTMG1000MDI_2	-40.7	8.1
	PTMG1000MDI_2.5	-38.3	8.8
	PTMG1000MDI_3	-35.6	9.9
	PTMG1000MDI_3.5	-29.9	11.9
	PTMG1000MDI_4	-27.4	14.8
	PTMG1000MDI_4.5	-23.7	22.9
S8	PTMG1000MDITDI_3.5	-12.9	
	PTMG1000MDITDI_4	7.7	
	PTMG1000MDITDI_4.5	14.8	
	PTMG1000MDITDI_5	16.4	
	PTMG1000MDITDI_5.5	20.4	
	PTMG1000MDITDI_6	25.9	

Table 3.9. *Glass transition temperature of the SMPUs synthesized with nanoparticles*

System & Sample		$T_{g,DSC}$ (ºC)
S9	PTMG650MDITDI_1.5_1	-7.6
	PTMG650MDITDI_2_1	3.4
	PTMG650MDITDI_2.5_1	12.1
	PTMG650MDITDI_3_1	15.0
	PTMG650MDITDI_3.5_1	23.6
S10	PTMG1000MDITDI_3.5_1	-17.7
	PTMG1000MDITDI_4_1	5.5
	PTMG1000MDITDI_4.5_1	7.3
	PTMG1000MDITDI_5_1	16.8
	PTMG1000MDITDI_5.5_1	21.8
	PTMG1000MDITDI_6_1	25.8
S11	PTMG1000MDITDI_3.5_3	-34.9
	PTMG1000MDITDI_4_3	-6.0
	PTMG1000MDITDI_4.5_3	12.3
	PTMG1000MDITDI_5_3	21.3
	PTMG1000MDITDI_5.5_3	24.9
	PTMG1000MDITDI_6_3	26.8

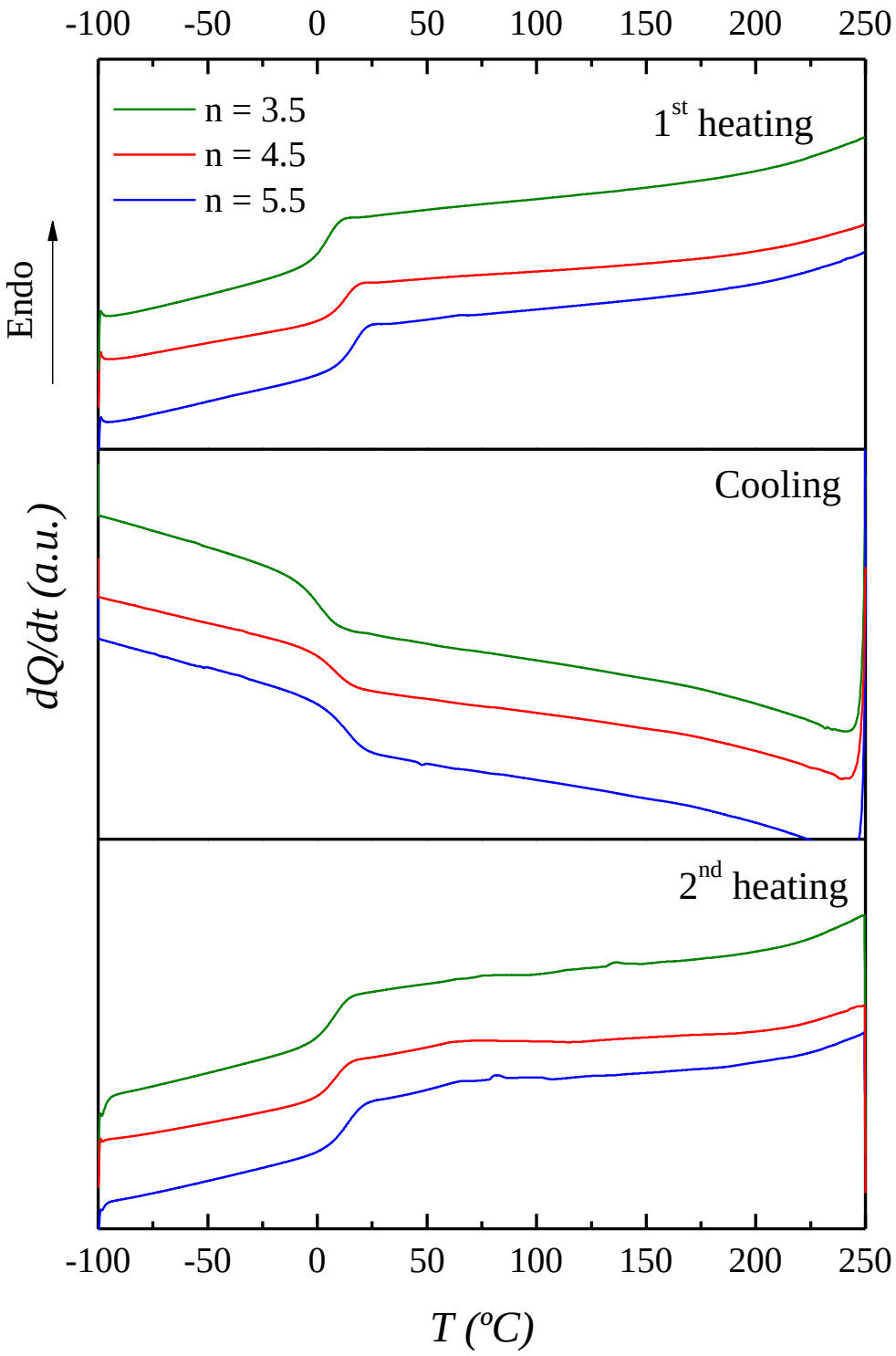

Figure 3.8. *DSC curves for system 1, PEG1000TDI*

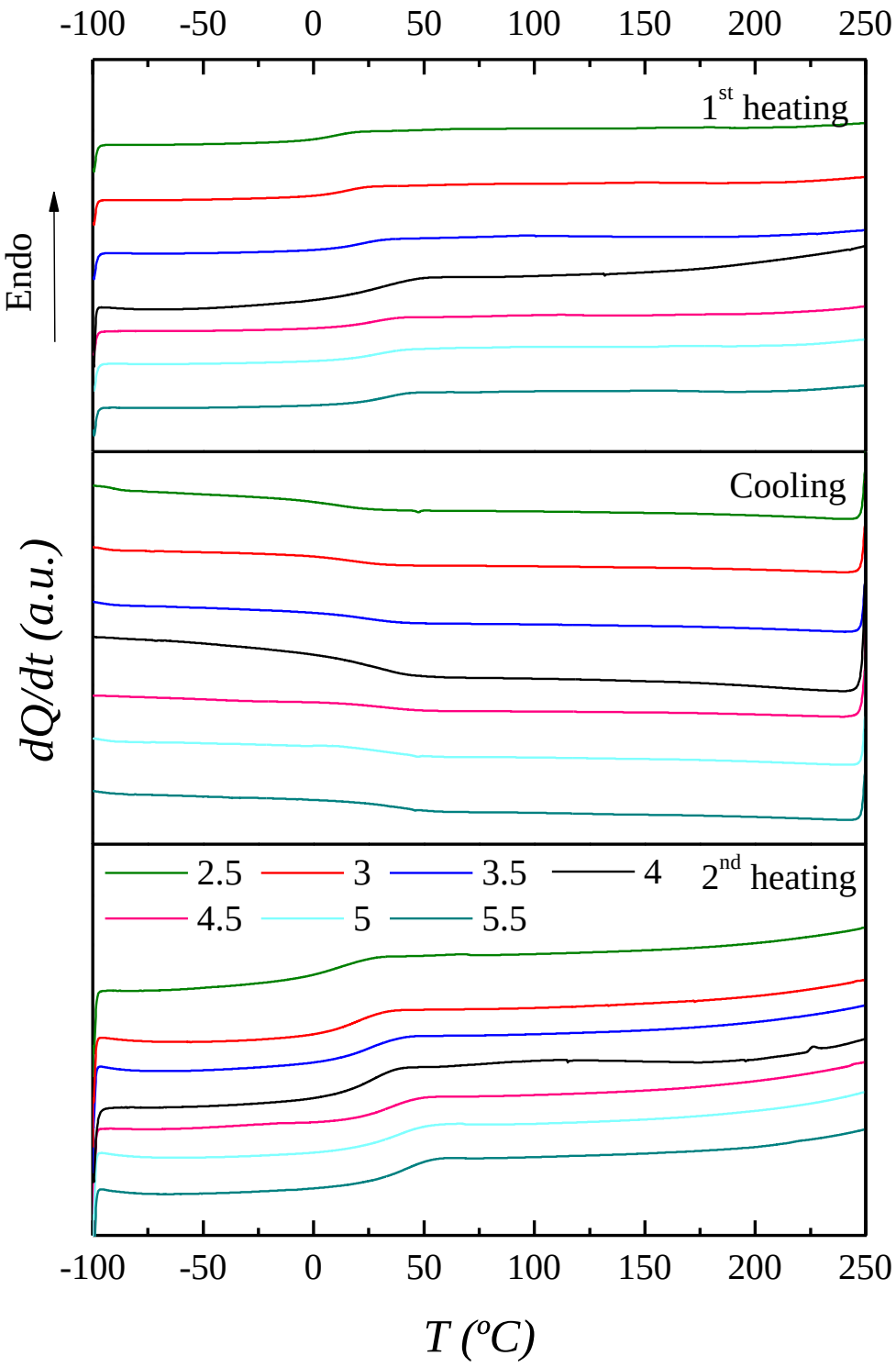

Figure 3.9. *DSC curves for system 3, PTMG650TDI*

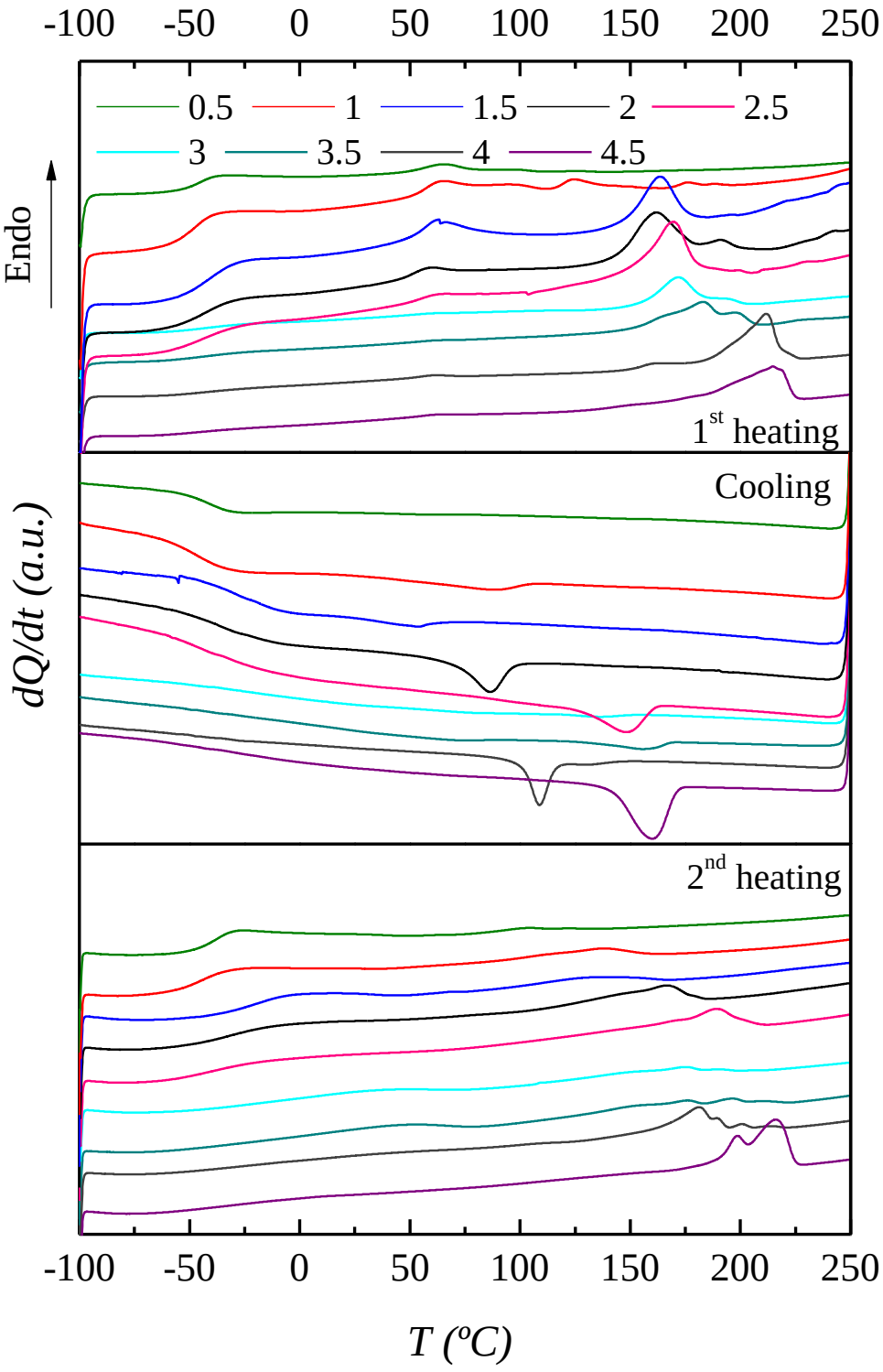

Figure 3.10. *DSC curves for system 7, PTMG1000MDI*

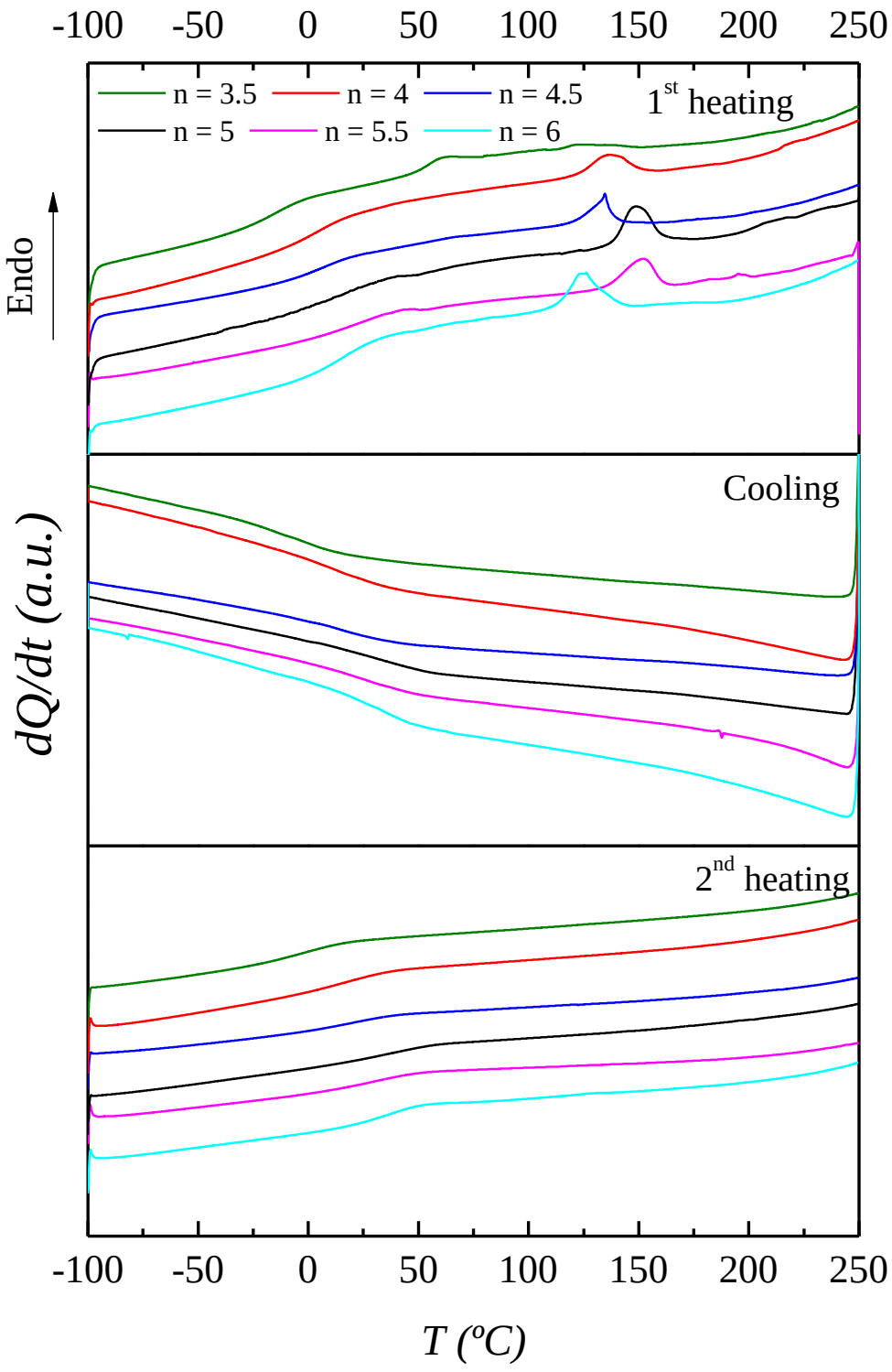

Figure 3.11. *DSC curves for system 10, PTMG1000/MDI+TDI/1%TiO_2*

3.5. Thermomechanical behavior of shape memory polyurethanes

In addition to differential scanning calorimetry (DSC), dynamic mechanical analysis (DMA) was used to know the viscoelastic behavior of the synthesized polyurethanes. DMA is a sensitive method to study the thermomechanical behavior of polymers, which provides methods for testing the microphase separation characteristics through changes in the glass transitions of the components. DMA experiments measure the ability of a viscoelastic material to store and dissipate mechanical energy, and are based on the differences in the load response of the viscous and elastic components to a small sinusoidal applied strain. The resulting stress, that is measured using an appropriate sensor, lags behind the applied strain by a phase angle δ [19]. The storage modulus (*E'*) quantifies the energy stored elastically by the material upon deformation, and provides information regarding the stiffness of the material. The loss factor (*tanδ)* is a measurement of the ratio of the energy absorbed by the sample as heat to the energy used by the sample to return to its original shape, and measures the degree of molecular motion. The major peak in the loss factor, tanδ, is usually used to designate the glass transition temperature ($T_{g,DMA}$). This peak corresponds with a sharp drop in the storage modulus (*E'*), so this is also an important parameter in order to evaluate the structure-property relationship of these materials. The glass transition temperature (T_g) is defined as the α transition in the *tanδ* curve [40]. DMA technique is sensitive to the various transitions which polymer undergoes as a function of the temperature changing [41].

Significant features of a *tanδ* plot include the location of the low temperature maximum, where smaller areas are associated with better phase separation of PUs hard and soft phases, as well as less of the hard phase being involved in the glass transition. Very low temperature β peaks are associated with reordering of hard-segment domains. The degree of phase mixing can be estimated from the shift of the glass transition temperature (as with DSC), and also from the storage modulus *E'*, which has an intermediate value between the moduli of the two phases and depends on the relative amount of each phase. Phase separation in PUs is based on the presence of two thermal transitions in the dynamical mechanical data that were assigned to the glass transition temperature (T_g) of the hard and soft-segments softening point. Two transitions are a sign of incompatibility whereas only one transition is expected for compatible polymers [42–44].

From the experimental point of view, several differences exist between DSC and DMA. Although the DSC technique is less sensitive to molecular transitions than DMA, it generally supports results regarding the thermodynamical changes which the material undergoes upon heating or cooling. As does DSC, DMA allows the estimation of the PUs characteristics of microphase separation or phase mixing. In a standard DSC, the T_g is defined in relation to the measured heat flow, preferably in cooling experiments. Thus, DSC is sensitive to specific heat capacity (C_p)changes associated with the glass transition, while DMA is sensitive to mechanical relaxation, also associated with the glass transition, but the expression of which depends on the mechanical frequency imposed by the test [45]. The glass transition temperature could be determined by both techniques, but it has been demonstrated in macromolecular systems that methods such as DSC are less sensitive to the glass transition phenomenon than the DMA employed in this study [46] due to DMA is a method with great sensitivity in detecting changes in internal molecular mobility. Furthermore, the predominant heat transfer mechanism in DSC is conduction while in DMA is convection [46]. Therefore, it should be noted that dynamic experiments (DMA) exhibit higher glass transition temperatures than static experiment (DSC), i.e. $T_{g,\,DMA} > T_{g\,DSC}$.

Thus, in this work, the viscoelastic behavior of the synthesized polyurethanes was investigated using DMA. *Tables 3.10, 3.11, 3.12* and *3.13* show the storage modulus (*E'*) at -100ºC, β temperatures (T_β) and glass transition temperatures (T_α) for PEG-based PUs, PTMG650-based PUs, PTMG1000-based PUs and polyurethanes synthesized with TiO_2 nanoparticles, respectively. *Figures 3.12, 3.13, 3.14 and 3.15* depict the temperature dependence of the storage modulus, *E´*, and *tanδ* as a function of *n* for system 1, system 3, system 7 and system 10, respectively. All DMA graphics are in *Appendix C*. Two of the samples (PTMG650TDI_2.5 and PTMG1000TDI_2.5) were too liquid to be measured.

Therefore, to compare the values of glass transition temperature of the obtained SMPUs, the values measured by DMA ($T_{g,\,DMA}$) are taken into account. As it can be seen from the following tables, the symmetry/asymmetry of the diisocyanate strongly influences the dynamic mechanical properties. As a result, symmetric diisocyanates (MDI) have more phase mixing (lower T_g) than asymmetric diisocyanates (TDI). In the asymmetric diisocyanates, the broad transition above T_g was ascribed to the domain boundary mixing. From DMA results, it could be observed

that MDI-based SMPUs present lower T_g values than TDI-based polyurethanes (40.4ºC for PTMG650MDI_3.5 vs. 44.7ºC for PMG650TDI_3.5). Despite this, MDI-based polyurethanes present higher flow temperatures, which is attributed to the stronger hydrogen bonding interactions and partially crystallized hard-segments [7]. In fact, while the flow zone is located at temperatures above 70ºC for all MDI-based polyurethanes (90ºC above their T_g), glass transition is closely followed (almost overlapping) by the flow region in TDI-based SMPUs. Thereby, MDI-based SMPUs have a wider range of temperatures where its mechanical properties are maintained (*E'*), (higher temperature) and therefore, these polyurethanes provide higher stability and are more suitable for commercial applications.

Moreover, results reveal a well-defined single α-relaxation associated with the glass transition ($T_{g,DMA}$ values are determined as the maximum in *tanδ*) for all the obtained polyurethanes, which gradually increases with *n*. The transition around this temperature was ascribed to the glass transition of the hard-segment phase. Therefore, as the hard-segment content increases, the corresponding glass transition temperature is higher, which is in agreement with the DSC results. This increase in T_g, from 15.3 to 30.4ºC for system 1 (PEGTDI), from 37.5 to 62.9ºC for system 3 (PTMG650TDI) and from 24.1 to 48.9ºC for system 10 (PTMG1000MDITDI), may be ascribed to the reduction in chain-segment mobility induced by the increased presence of hard-segments. Similar T_g behavior has been found in semicrystalline thermoplastics via the development of further rigid crystalline domains. For example, in system 7, which consists of MDI-based polyurethanes, the T_g varies from -30.9 to 52.5ºC when *n* increases [47]. Moreover, as the temperature rises, the polyurethanes are transformed from glassy to rubbery state, and polymer chains start to move with a high internal friction resistance. As a result, the storage modulus falls quickly, as it can be observed in DMA graphics (*Figures 3.12*, *3.13*, *3.14* and *3.15*, and *Appendix C*).

As denoted by the intensity and the area of the smaller loss factor peak, the energy dissipation of synthesized polyurethanes through the studied temperature range decreases upon the addition of hard-segment content. This decrease in damping is due to the restriction of the hard diisocyanates in the viscous component of soft poly(tetrahydrofuran) segment [48]. In fact, it has been reported that the constraints introduced by the hydrogen bonding between the hard-segments provide an increased rigidity to the whole system [49–51]. It should be pointed out that the range

of *tanδ* values obtained here through the introduction of different amount of MDI and TDI is notably larger than those previously reported by *Tan et al.* [37] for TPU/TPS blends using a polyolefin elastomer as compatibilizer. This would be useful to develop polyurethanes with rather different damping behavior simply by tuning the soft/hard-segment ratio.

In summary, the following general remarks can be made with regard to the PUs thermal behavior as revealed by the DMA experiments: the increase of the hard-segment content results in an increase of T_g of the polymer; the increase of the molecular weight of polyol increases the PUs degree of phase separation caused by the increase of mobility; leading to a decrease in the T_g, as less energy is needed for motion.

Table 3.10. *Thermomechanical properties of the SMPUs based on PEG*

System & Sample		E' (MPa)	T_β (°C)	T_α (°C)
S1	PEGTDI_3.5	2826.1	-69.7	15.3
	PEGTDI_4.5	950.4	-71.8	24.7
	PEGTDI_5.5	3092.8	-69.8	30.4
S2	PEGMDI_2	2956.6	-63.2	-17.7
	PEGMDI_3	3177.5	-68.9	-14.9
	PEGMDI_4	3584.4	-65.5	-12.1

Table 3.11. *Thermomechanical properties of the SMPUs based on PTMG 650*

System & Sample		E' (MPa)	T_β (°C)	T_α (°C)
S3	PTMG650TDI_2.5	-	-	-
	PTMG650TDI_3	2176.8	-76.2	37.5
	PTMG650TDI_3.5	2768.3	-71.7	44.7
	PTMG650TDI_4	1832.6	-72.1	55.2
	PTMG650TDI_4.5	2599.0	-66.4	58.1
	PTMG650TDI_5	2414.8	-66.9	60.6
	PTMG650TDI_5.5	3119.7	-72.3	62.9
S4	PTMG650MDI_0.5	2434.0	-70.8	-10.2
	PTMG650MDI_1	2359.5	-76.4	-3.0
	PTMG650MDI_1.5	2140.4	-70.9	6.3
	PTMG650MDI_2	2339.8	-70.9	10.9
	PTMG650MDI_2.5	2176.9	-73.7	15.7
	PTMG650MDI_3	1997.6	-70.1	23.1
	PTMG650MDI_3.5	2036.6	-68.5	40.4
	PTMG650MDI_4	2203.0	-71.7	46.6
	PTMG650MDI_4.5	1458.0	-63.3	62.4
S5	PTMG650MDITDI_1.5	987.4	-64.3	23.3
	PTMG650MDITDI_2	2374.3	-62.7	32.1
	PTMG650MDITDI_2.5	2793.9	-70.6	37.2
	PTMG650MDITDI_3	1971.5	-68.2	46.2
	PTMG650MDITDI_3.5	2675.7	-66.9	52.0

Table 3.12. *Thermomechanical properties of the SMPUs based on PTMG 1000*

System & Sample		E' (MPa)	T_β (°C)	T_α (°C)
S6	PTMG1000TDI_2.5	-	-	-
	PTMG1000TDI_3	1989.4	-74.2	22.1
	PTMG1000TDI_3.5	2562.6	-74.7	25.3
	PTMG1000TDI_4	2725.4	-75.6	35.4
	PTMG1000TDI_4.5	2068.6	-66.4	37.9
	PTMG1000TDI_5	1650.1	-69.4	41.9
	PTMG1000TDI_5.5	2622.7	-74.9	49.4
	PTMG1000TDI_6.5	1948.9	-76.5	56.1
S7	PTMG1000MDI_0.5	812.6	-67.2	-30.9
	PTMG1000MDI_1	1985.1	-65.9	-30.5
	PTMG1000MDI_1.5	2110.9	-72.1	-20.0
	PTMG1000MDI_2	2301.5	-71.5	-18.4
	PTMG1000MDI_2.5	2138.9	-69.6	-16.2
	PTMG1000MDI_3	2449.0	-74.4	-12.5
	PTMG1000MDI_3.5	2313.4	-64.9	-7.6
	PTMG1000MDI_4	2100.0	-67.1	-3.9
	PTMG1000MDI_4.5	2200.0	-71.5	52.5
S8	PTMG1000MDITDI_3.5	2965.4	-66.1	9.9
	PTMG1000MDITDI_4	1046.5	-68.9	23.8
	PTMG1000MDITDI_4.5	2155.2	-67.8	34.7
	PTMG1000MDITDI_5	2212.4	-65.1	40.2
	PTMG1000MDITDI_5.5	1715.7	-62.1	42.7
	PTMG1000MDITDI_6	2782.7	-67.4	51.7

Table 3.13. *Thermomechanical properties of the SMPUs synthesized with nanoparticles*

System & Sample		E' (MPa)	T_β (ºC)	T_α (ºC)
S9	PTMG650MDITDI_1.5_1	2141.4	-64.3	26.8
	PTMG650MDITDI_2_1	2119.9	-52.3	36.3
	PTMG650MDITDI_2.5_1	2306.2	-65.7	44.3
	PTMG650MDITDI_3_1	2334.0	-65.2	46.9
	PTMG650MDITDI_3.5_1	2149.0	-54.3	50.7
S10	PTMG1000MDITDI_3.5_1	2650.7	-82.9	24.1
	PTMG1000MDITDI_4_1	2277.0	-62.8	30.8
	PTMG1000MDITDI_4.5_1	2093.2	-61.5	32.7
	PTMG1000MDITDI_5_1	2052.1	-62.4	40.6
	PTMG1000MDITDI_5.5_1	2374.6	-57.5	47.5
	PTMG1000MDITDI_6_1	2216.9	-68.6	48.9
S11	PTMG1000MDITDI_3.5_3	1330.0	-74.1	14.5
	PTMG1000MDITDI_4_3	1940.9	-79.0	19.5
	PTMG1000MDITDI_4.5_3	2736.1	-78.4	22.2
	PTMG1000MDITDI_5_3	1916.8	-75.4	28.5
	PTMG1000MDITDI_5.5_3	1998.1	-75.8	29.9
	PTMG1000MDITDI_6_3	2522.7	-76.0	41.7

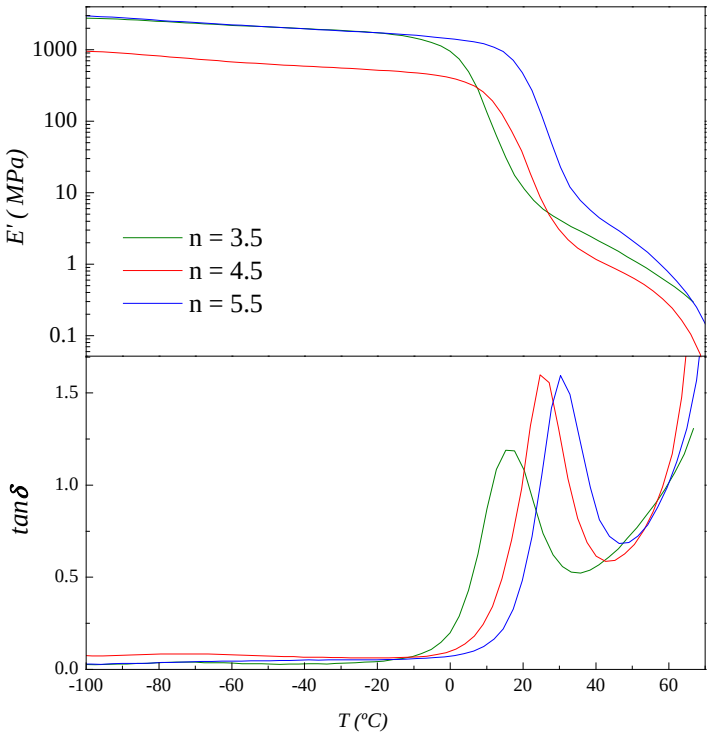

Figure 3.12. *DMA curves for system 1, PEG1000TDI*

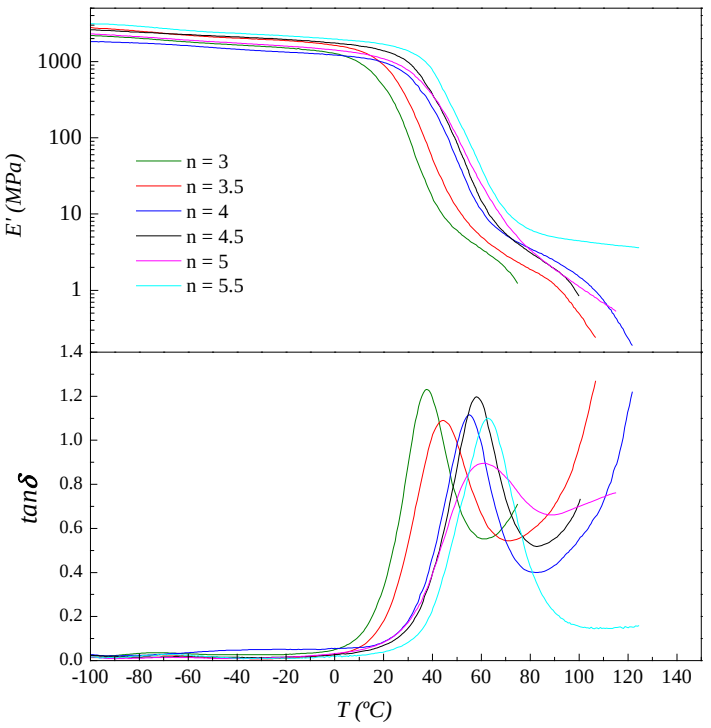

Figure 3.13. *DMA curves for system 3, PTMG650TDI*

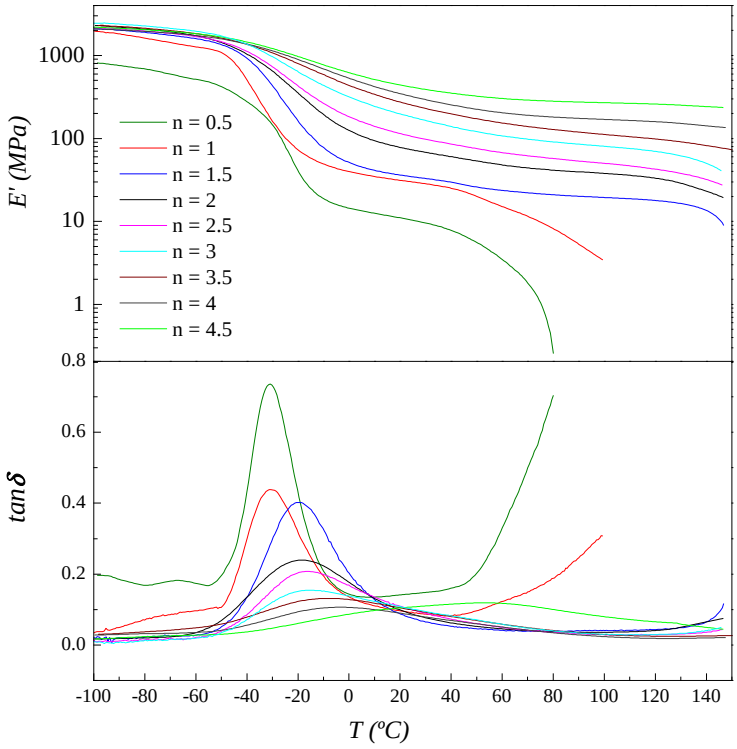

Figure 3.14. *DMA curves for system 7, PTMG1000MDI*

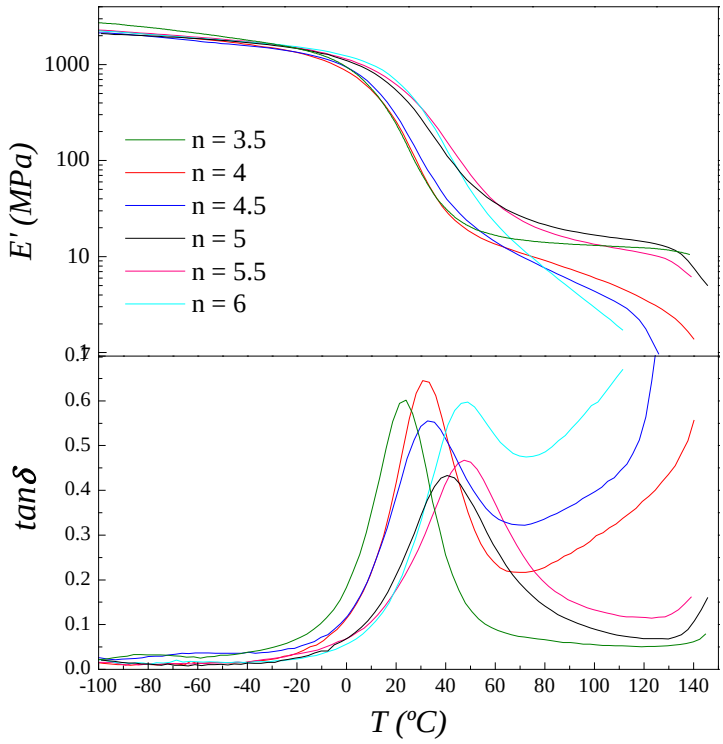

Figure 3.15. *DMA curves for system 10, PTMG1000/MDI+TDI/1%TiO_2*

3.6. Tensile Stress-Strain

Tensile tests are generally used to control product quality and for determining the effect of chemical or thermal exposure on an elastomer. Tensile strength is defined as the maximum amount of tensile stress that a material can be subjected to before failure. It is known variously as "breaking load", "breaking stress" and "ultimate tensile strength". Tensile stress, and tensile strength are both measured in units of force divided by units of area, usually $N \cdot cm^{-2}$, or MPa. Moreover, the tensile modulus or elastic modulus (E) is the force per unit of original cross-sectional area required to stretch the specimen to a stated elongation. Elongation is the percentage increase from the original length of an elastomer as a result of a tensile force being applied to a PU specimen. Ultimate elongation or elongation at break (ε_b) is the elongation at the point where sample breaks. Fracture toughness (U_T) is a quantitative way of expressing a material's resistance to brittle fracture when a crack is present.

In this work, the tests were performed on dumbbell-shaped specimens. In PUs, the stress is not linear with strain. Therefore, the modulus is neither a ratio nor a constant slope, but rather denotes a point on the stress-strain curve [25,52].

The statistic values of elastic modulus (E), secant modulus at 2% (E^*), elongation at break (ε_b) and fracture toughness (U_T) are summarized in *Table 3.14*, while *Figures 3.16* and *3.17* show the stress-strain curves of some samples from systems 6 and 7. In this case, for tensile test experiments, only some of the samples were tested in order to know how the polyurethanes behave. While all the polyurethanes present ductile or elastomeric behavior, results reveal a similar effect of n on the mechanical response of synthesized materials. As the hard phase content (n) is increased the elastomeric behavior of specimens is shifted towards a less ductile behavior. More precisely, as shown in *Figures 3.16* and *3.17*, the elongation at break is reduced from 945% to 408% and from 291% to 182% for systems 6 and 7, respectively, upon the increase of n. This behavior is usually found in polyurethanes and it is ascribed to the formation of a densely crosslinked structure when the presence of hard-segment increases. The increased ε_b of TDI-based SMPUs in regard to MDI-based ones for a given n is associated with a reduced molecular mobility of chains in the last ones [48,53,54]. This is in concordance with DMA results where MDI-based polyurethanes exhibit fairly lower glass transition temperatures when comparing with TDI-based polyurethanes.

It is interesting to note that intermediate *n* values result in a concurrent increase of strength and elongation at break, yielding fracture toughness values up to 77.9 (*n* = 5) and 91.2 (*n* = 2) MJ·m^{-3} for TDI-based and MDI-based SMPUs, respectively. This 34-fold and 23-fold increase in fracture toughness arises from the synergetic effect obtained when both rigid and soft-segments are found at an appropriate ratio. Indeed, hard phase is responsible of holding together the rubbery soft phase by intermolecular hydrogen bonding and crosslinked network, whereas the soft-segments are able to extend with no rupture upon stretching [55]. The proper combination of both segments imparts combined ductility and strength. When the soft phase is very large (low *n*) the material cannot withstand applied stress and is easily deformed. On the contrary, at high *n* values, hard-segments prevent macromolecules moving too far out of position, yielding lower ε_b values but increased elastic modulus.

Table 3.14. *Main mechanical parameters for some of the samples of system 6 and 7*

n	Elastic Modulus *E* (MPa)	Secant Modulus *E** (MPa)	Elongation at break ε_b (%)	Fracture toughness U_T (MJ·m^{-3})
PTMG1000TDI_3	1.6 ± 0.1	1.6	945	2.3
PTMG1000TDI_3.5	1.9 ± 0.1	2.0	1167	11.1
PTMG1000TDI_4.5	2.5 ± 0.1	2.5	622	20.9
PTMG1000TDI_5	78.6 ± 0.7	75.3	408	77.9
PTMG1000MDI_0.5	8.2 ± 0.1	8.1	291	4.0
PTMG1000MDI_1	22.8 ± 0.1	22.6	404	16.5
PTMG1000MDI_2	37.5 ± 0.7	37.2	463	91.2
PTMG1000MDI_3	124.4 ± 0.8	121.8	212	36.3
PTMG1000MDI_4	239.0 ± 1.9	232.3	182	42.3

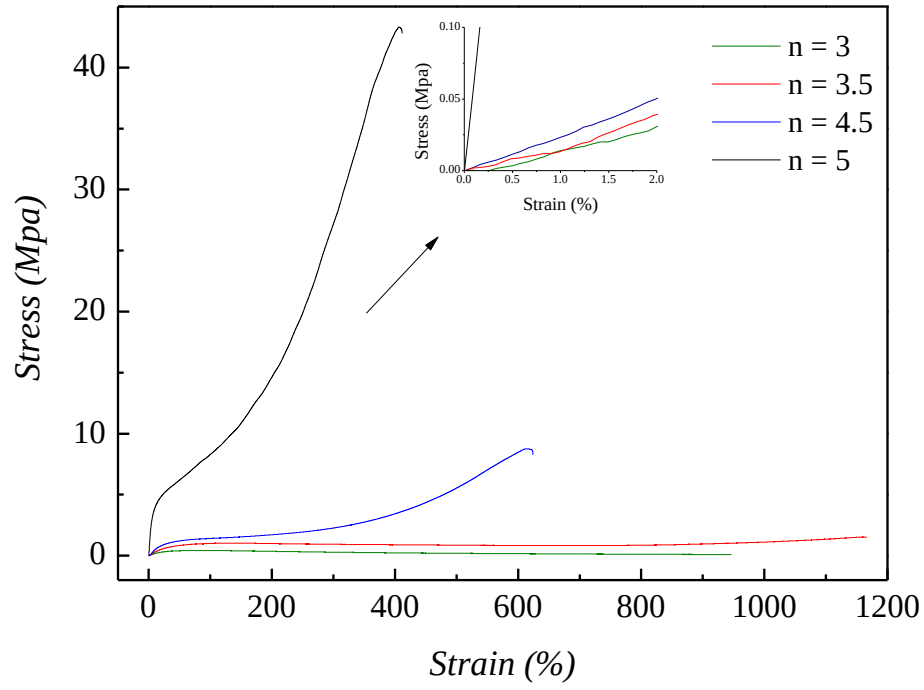

Figure 3.16. *Stress-strain curves for system 6, PTMG1000TDI. Note that stress–strain curves are partially enlarged in the inset*

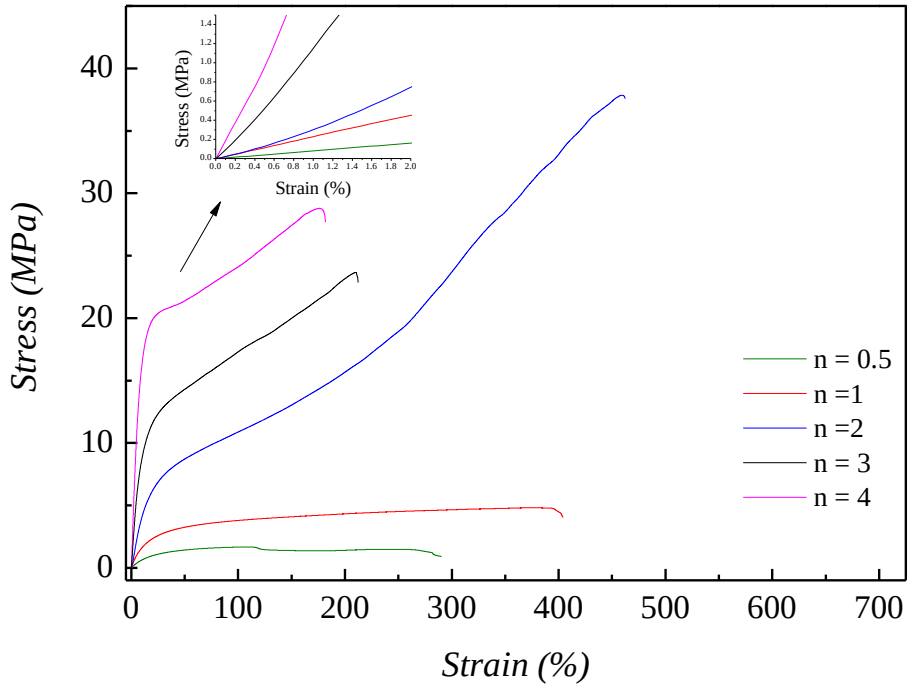

Figure 3.17. *Stress-strain curves for system 7, PTMG1000MDI. Note that stress–strain curves are partially enlarged in the inset*

3.7. Scanning Electron Microscopy (SEM)

The morphology of almost all synthesized polyurethanes has been studied by FE-SEM. *Figure 3.18* shows some pictures of two different samples, one of them corresponds to system 6 (PTMG1000TDI_4 (a)) and the other sample to system 7 (PTMG1000MDI_4 (b)).

As it can be observed from the pictures, no phase separation is produced in the synthesized SMPUs indicating that homogeneous materials were obtained during the synthesis. Although all the samples were cryogenically fractured, according to their morphological features, they show different fracture modes. Thus, it could be seen that specimens containing large fractions of hard-segment present a rather smooth surface. More interestingly, at medium *n* values, where higher fracture toughness are achieved (*Table 3.14*), surfaces present more zones with shear and fibrils, indicating that a higher amount of energy was dissipated by the material during the plastic deformation. *Korley et al.* [41] mentioned that as the hard-segment composition increases, mechanical data are consistent with a shift in continuous domain morphology, producing materials with inter-connected hard domains, exhibit limited extensibility, but increased initial modulus, as shown in *Table 3.14.*

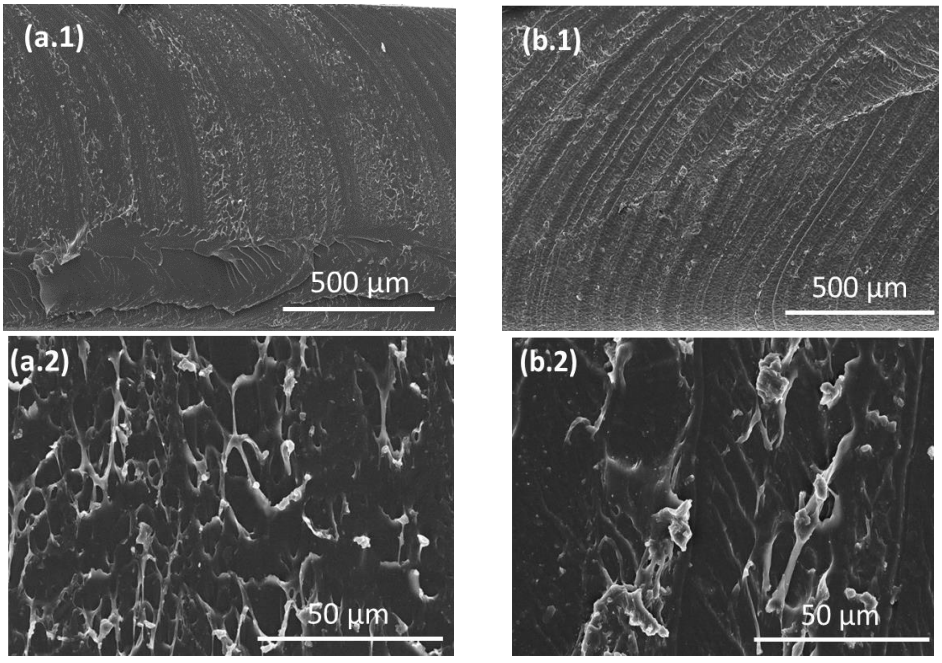

Figure 3.18. *Representative FE-SEM images showing the morphology of cryogenically fractured SMPU surfaces: PTMG1000TDI_4 (a) and PTMG1000MDI_4 (b).*

3.8. Conclusions

Shape memory polyurethanes (SMPUs), synthesized by a two-step polymerization method in a solvent-free process as mentioned in *Chapter II*, have been characterized in this chapter by different techniques such as attenuated total reflectance Fourier transform infrared spectroscopy (ATR-FTIR), thermogravimetric analysis (TGA), differential scanning calorimetry (DSC), dynamic-mechanical analysis (DMA), tensile tests, and scanning electron microscopy (SEM).

ATR-FTIR was used to assess the formation of polyurethanes, showing that the reaction procedure was appropriate and the initial isocyanate groups reacted completely during the synthesis.

Regarding the thermogravimetric analysis, it could be concluded that all the polyurethanes synthesized in this work display a typical two-stage degradation, except those synthesized with a mixture of diisocyanates (TDI+MDI) which present three stages. Anyway, all synthetized SMPUs show good thermal stability with initial decomposition temperatures higher than 275°C. Moreover, TGA analysis shows, on the one hand, that MDI-based PUs are more stable than TDI-based PUs, observing an intermediate stability for TDI+MDI-based PUs. On the other hand, all systems synthesized from PTMG650 are more stable than the synthesized from PTMG1000.

Furthermore, both DSC and DMA show that glass transition temperature of polyurethanes increases with the hard-segment content (higher *n*). Both methods indicate that PEG-based SMPUs own glass transition temperatures lower than PTMG-based SMPUs. In addition, it could be concluded that the glass transition temperatures of the polyurethanes synthetized with PTMG650 are higher than the polyurethanes synthetized with PTMG1000, that is, an increase in the molecular weight of the polyol provokes a decrease in T_g.

Regarding the mechanical properties, both types of polyurethanes show a huge versatility. When the soft phase is very large (low *n*), the material cannot withstand applied stress and is easily deformed. On the contrary, at high *n* values, hard-segments prevent macromolecules moving too far out of position, yielding lower ε_b values but increasing the elastic modulus.

In conclusion, polyurethanes with tunable thermal and mechanical properties were obtained just by varying the hard to soft-segment content. Overall, the obtained experimental findings through this work highlight the potential of both MDI and TDI-

based SMPUs for applications in which a vibration isolation in needed over a wide range of temperatures. These may include manufacturing of soles for footwear, isolators for large industrial equipment and isolation systems for vibration-sensitive instruments such as scanning electron microscopes among others.

3.9. References

1. Kuo M-C, Shau S-M, Su J-M, et al (2012) Preparation of Supramolecular Extenders with Precise Chain Lengths via Iterative Synthesis and Their Applications in Polyurethane Elastomers. Macromolecules 45:5358–5370.
2. Kim JT, Kim BK, Kim EY, et al (2013) Synthesis and properties of near IR induced self-healable polyurethane/graphene nanocomposites. Eur Polym J 49:3889–3896.
3. Jiao L, Xiao H, Wang Q, Sun J (2013) Thermal degradation characteristics of rigid polyurethane foam and the volatile products analysis with TG-FTIR-MS. Polym Degrad Stab 98:2687–2696.
4. Mirabella FM (2002) Principles, Theory and Practice of Internal Reflection Spectroscopy. Handb Vib Spectrosc 21–61.
5. Cateto CA, Barreiro MF, Rodrigues AE (2008) Monitoring of lignin-based polyurethane synthesis by FTIR-ATR. Ind Crops Prod 27:168–174.
6. Cervantes-Uc JM, Espinosa JIM, Cauich-Rodríguez JV, et al (2009) TGA/FTIR studies of segmented aliphatic polyurethanes and their nanocomposites prepared with commercial montmorillonites. Polym Degrad Stab 94:1666–1677.
7. Chang Z, Zhang M, Hudson AG, et al (2013) Synthesis and properties of segmented polyurethanes with triptycene units in the hard segment. Polymer (Guildf) 54:6910–6917.
8. Wu C-H, Shau S-M, Liu S-C, et al (2015) Enhanced shape memory performance of polyurethanes via the incorporation of organic or inorganic networks. RSC Adv 5:16897–16910.
9. Raja M, Ryu SH, Shanmugharaj AM (2013) Thermal, mechanical and

electroactive shape memory properties of polyurethane (PU)/poly (lactic acid) (PLA)/CNT nanocomposites. Eur Polym J 49:3492–3500.

10. Palimi MJ, Rostami M, Mahdavian M, Ramezanzadeh B (2014) Surface modification of Fe2O3 nanoparticles with 3-aminopropyltrimethoxysilane (APTMS): An attempt to investigate surface treatment on surface chemistry and mechanical properties of polyurethane/Fe2O3 nanocomposites. Appl Surf Sci 320:60–72.

11. Saeed A, Shabir G (2013) Synthesis of thermally stable high gloss water dispersible polyurethane/polyacrylate resins. Prog Org Coatings 76:1135–1143.

12. Trovati G, Sanches EA, Neto SC, et al (2010) Characterization of polyurethane resins by FTIR, TGA, and XRD. J Appl Polym Sci 115:263–268.

13. Sun L, Huang WM, Ding Z, et al (2012) Stimulus-responsive shape memory materials: A review. Mater Des 33:577–640.

14. Petrović ZS, Javni I, Waddon A, Bánhegyi G (2000) Structure and properties of polyurethane-silica nanocomposites. J Appl Polym Sci 76:133–151.

15. Zhang L, Zhang M, Hu L, Zhou Y (2014) Synthesis of rigid polyurethane foams with castor oil-based flame retardant polyols. Ind Crops Prod 52:380–388.

16. Charlon M, Heinrich B, Matter Y, et al (2014) Synthesis, structure and properties of fully biobased thermoplastic polyurethanes, obtained from a diisocyanate based on modified dimer fatty acids, and different renewable diols. Eur Polym J 61:197–205.

17. Yilgor I, Yilgor E, Guler IG, et al (2006) FTIR investigation of the influence of diisocyanate symmetry on the morphology development in model segmented polyurethanes. Polymer (Guildf) 47:4105–4114.

18. Corcuera MA, Rueda L, Fernandez d'Arlas B, et al (2010) Microstructure and properties of polyurethanes derived from castor oil. Polym Degrad Stab 95:2175–2184.

19. Prisacariu C (2011) Polyurethane Elastomers: From Morphology to Mechanical Aspects. Springer, Wien.

20. Saad GR, Salama HE, Mohamed NA, Sabaa MW (2014) Crystallization and thermal properties of biodegradable polyurethanes based on poly[(R)-3-

hydroxybutyrate] and their composites with chitin whiskers. J Appl Polym Sci 131:40784–40797.

21. Guo J, Lv H, Wang Z, et al (2015) Thermo-mechanical property of shape memory polymer/carbon fibre composites. Mater Res Innov 19:566–572.
22. Arshanitsa A, Krumina L, Telysheva G, Dizhbite T (2016) Exploring the application potential of incompletely soluble organosolv lignin as a macromonomer for polyurethane synthesis. Ind Crops Prod 92:1–12.
23. Gao H, Lan X, Liu L, et al (2017) Study on performances of colorless and transparent shape memory polyimide film in space thermal cycling, atomic oxygen and ultraviolet irradiation environments. Smart Mater Struct 26:095001–095014.
24. Król P (2007) Synthesis methods, chemical structures and phase structures of linear polyurethanes. Properties and applications of linear polyurethanes in polyurethane elastomers, copolymers and ionomers. Prog Mater Sci 52:915–1015.
25. Prisacariu C, Scortanu E, Coseri S, Agapie B (2013) Effect of Soft Segment Polydispersity on the Elasticity of Polyurethane Elastomers. Ind Eng Chem Res 52:2316–2322.
26. Strankowski M, Piszczyk Ł, Kosmela P, Korzeniewski P (2015) Morphology and the physical and thermal properties of thermoplastic polyurethane reinforced with thermally reduced graphene oxide. Polish J Chem Technol 17:88–94.
27. Joseph PV, Joseph K, Thomas S, et al (2003) The thermal and crystallisation studies of short sisal fibre reinforced polypropylene composites. Compos Part A Appl Sci Manuf 34:253–266.
28. Liu N, Zhao Y, Kang M, et al (2015) The effects of the molecular weight and structure of polycarbonatediols on the properties of waterborne polyurethanes. Prog Org Coatings 82:46–56.
29. Clemitson I (2015) Castable polyurethane elastomers. CRC Press, New York.
30. Huang WM, Yang B, Fu YQ (2012) Polyurethane shape memory polymers. Taylor & Francis, New York.
31. Yang JH, Chun BC, Chung Y-C, Cho JH (2003) Comparison of thermal/mechanical properties and shape memory effect of polyurethane

block-copolymers with planar or bent shape of hard segment. Polymer (Guildf) 44:3251–3258.

32. Lin JR, Chen LW (1998) Study on shape-memory behavior of polyether-based polyurethanes. II. Influence of soft-segment molecular weight. J Appl Polym Sci 69:1575–1586.

33. Lakatos C (2016) Segmented linear shape memory polyurethanes with thermoreversible Diels-Alder coupling: Effects of polycaprolactone molecular weight and diisocyanate type. Express Polym Lett 10:324–336.

34. Alishiri M, Shojaei A, Abdekhodaie MJ, Yeganeh H (2014) Synthesis and characterization of biodegradable acrylated polyurethane based on poly(ε-caprolactone) and 1,6-hexamethylene diisocyanate. Mater Sci Eng C Mater Biol Appl 42:763–773.

35. Panwiriyarat W, Tanrattanakul V, Pilard J-F, et al (2016) Elaboration and properties of renewable polyurethanes based on natural rubber and biodegradable poly(butylene succinate) soft segments. J Appl Polym Sci 133:42943–42951.

36. Lu H, Lu C, Huang W, Leng J (2015) Chemo-responsive shape memory effect in shape memory polyurethane triggered by inductive release of mechanical energy storage undergoing copper (II) chloride. Smart Mater Struct 24:035018–035025.

37. Tan L, Su Q, Zhang S, Huang H (2015) Preparing thermoplastic polyurethane/thermoplastic starch with high mechanical and biodegradable properties. RSC Adv 5:80884–80892.

38. Wolcott MP, Yin S, Rials TG (2000) Using dynamic mechanical spectroscopy to monitor the crystallization of PP/MAPP blends in the presence of wood. Compos Interfaces 7:3–12.

39. Pielichowska K, Król P, Król B, Pagacz J (2012) TOPEM DSC study of glass transition region of polyurethane cationomers. Thermochim Acta 545:187–193.

40. Ashida K (Kaneyoshi) (2007) Polyurethane and related foams : chemistry and technology. CRC/Taylor & Francis, New York.

41. Korley LTJ, Pate BD, Thomas EL, Hammond PT (2006) Effect of the degree of

soft and hard segment ordering on the morphology and mechanical behavior of semicrystalline segmented polyurethanes. Polymer (Guildf) 47:3073–3082.

42. Fritzsche N, Pretsch T (2014) Programming of Temperature-Memory Onsets in a Semicrystalline Polyurethane Elastomer. Macromolecules 47:5952–5959.

43. Pieczyska EA, Maj M, Kowalczyk-Gajewska K, et al (2015) Thermomechanical properties of polyurethane shape memory polymer–experiment and modelling. Smart Mater Struct 24:045043–045066.

44. Cooper SL, Tobolsky A V. (1966) Properties of linear elastomeric polyurethanes. J Appl Polym Sci 10:1837–1844.

45. Gracia-Fernández CA, Gómez-Barreiro S, López-Beceiro J, et al (2010) Comparative study of the dynamic glass transition temperature by DMA and TMDSC. Polym Test 29:1002–1006.

46. Rimdusit S, Ishida H (2000) Synergism and multiple mechanical relaxations observed in ternary systems based on benzoxazine, epoxy, and phenolic resins. J Polym Sci Part B Polym Phys 38:1687–1698.

47. Lizundia E, Petisco S, Sarasua J-R (2013) Phase-structure and mechanical properties of isothermally melt-and cold-crystallized poly (L-lactide). J Mech Behav Biomed Mater 17:242–251.

48. Shao L, Dai J, Zhang Z, et al (2015) Thermal and electroactive shape memory behaviors of poly(l -lactide)/thermoplastic polyurethane blend induced by carbon nanotubes. RSC Adv 5:101455–101465.

49. KROL P (2007) Synthesis methods, chemical structures and phase structures of linear polyurethanes. Properties and applications of linear polyurethanes in polyurethane elastomers, copolymers and ionomers. Prog Mater Sci 52:915–1015.

50. Petrović ZS, Ferguson J (1991) Polyurethane elastomers. Prog Polym Sci 16:695–836.

51. Chattopadhyay DK, Webster DC (2009) Thermal stability and flame retardancy of polyurethanes. Prog Polym Sci 34:1068–1133.

52. Prisacariu C, Scortanu E (2010) Structural Studies and the Correlation with the Stress-Strain Response in Polyurethanes. John Wiley & Sons, Ltd, Chichester, UK.

53. He Y-S, Zeng J-B, Liu G-C, et al (2014) Super-tough poly(l-lactide)/crosslinked polyurethane blends with tunable impact toughness. RSC Adv 4:12857–12866.

54. Zhou Y, Xiu H, Dai J, et al (2015) Largely reinforced polyurethane via simultaneous incorporation of poly(lactic acid) and multiwalled carbon nanotubes. RSC Adv 5:30912–30919.

55. Ionita D, Gaina C, Cristea M, Banabic D (2015) Tailoring the hard domain cohesiveness in polyurethanes by interplay between the functionality and the content of chain extender. RSC Adv 5:76852–76861.

Chapter IV.

RESULTS AND DISCUSSION. II. SHAPE MEMORY BEHAVIOR

"Nuestra felicidad más grande no está en no caer nunca, sino en levantarnos siempre después de cada caída"

Confucio

Chapter IV.

RESULTS AND DISCUSSION. II. SHAPE MEMORY BEHAVIOR

4.1. Introduction

Smart materials are one of the exciting new frontier technologies in engineering and manufacturing. As mentioned, smart materials are those materials capable of recognizing appropriate environmental stimuli, processing the information arising from the stimuli, and responding to it in an appropriate manner and time frame [1–5]. The ability of smart polymers to respond to external stimuli is of great scientific and technological significance and enables such materials to change on demand certain macroscopic properties such as shape, color or refractive index. Because of that, in the last few years, research activities in the field of shape memory polymers have been intensified substantially. A shape memory polymer (SMP) can be processed into

a pre-determined (original) shape by molding, casting or coating, etc. The shape memory effect (SME) of a thermo-responsive SMP is illustrated in *Figure 4.1* and includes the following steps:

1) SMPs are easily deformed at a temperature above their transition temperature, T_{trans}.
2) The constraint is removed after cooling below $T_{trans,}$ resulting in a very small elastic shape recovery; deformation is largely maintained. This is the temporary shape.
3) This temporary shape holds permanently unless the material is heated above its T_{trans}, which triggers full recovery to its original shape.
4) The SME cycle may be repeated again and again.

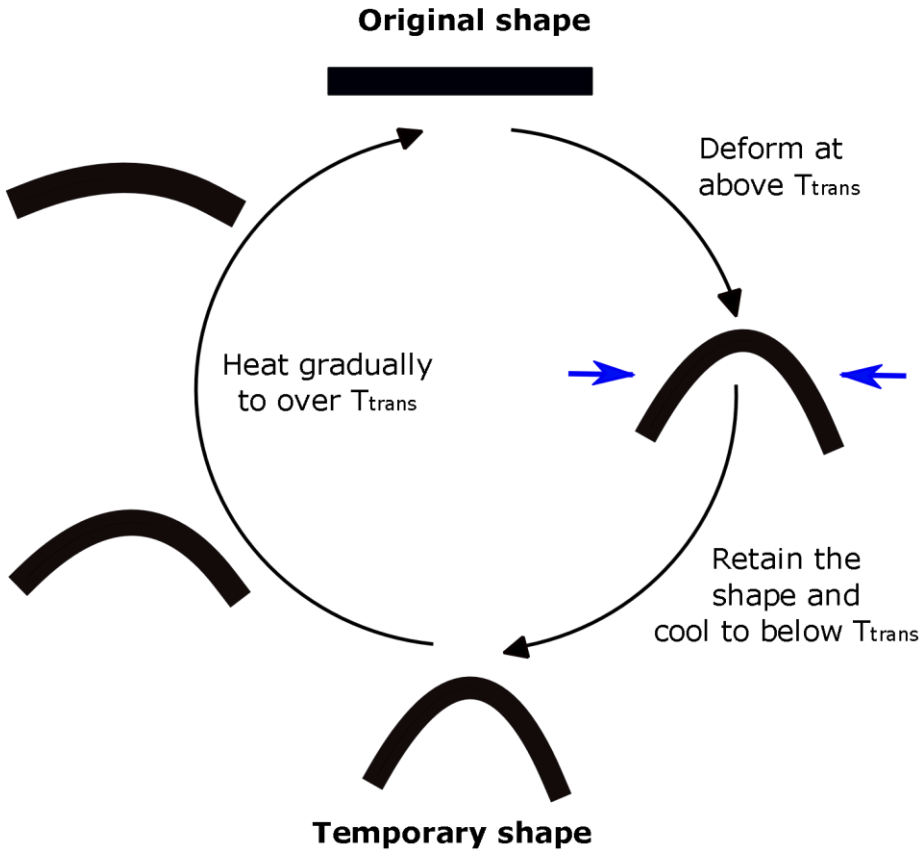

Figure 4.1. *Thermo-responsive shape memory effect*

4.2. Characterization of shape memory properties

In this chapter, all polyurethanes synthesized in the laboratory have been characterized to test the shape memory effect, not only in one cycle, but also in six cycles. The results show that all the developed polyurethanes have both the capacity to fix the temporary shape and to recover the original shape.

4.2.1. Shape fixity and shape recovery ratios

The shape memory effect of the synthesized polyurethanes has been measured qualitatively and quantitatively.

- **Qualitative**

A first approach to evaluate qualitatively the thermally-induced shape memory behavior of SMPUs was performed by digital monitoring of the shape recovery process. A rectangular strip (10 mm x 6 mm x 1.5 mm) of the polyurethane samples was deformed in an elbow-shaped strip at a temperature 20ºC above its transition temperature of shape memory effect ($T_{g,\ DMA}$) (immersed in a water bath at 40ºC). Then, the temporary shape was fixed cooling down the sample with liquid nitrogen to a temperature below T_{trans}. Finally, this new geometry was heated again above T_g (T = 40ºC), and the shape recovery process was registered by a digital camera [6,7]. Four samples were analysed, all with T_{gs} approximately 20ºC lower than the temperature of water bath (40ºC): PTMG650MDI_2 (T_g = 10.9ºC), PTMG650MDI_2.5 (T_g = 15.7ºC), PEGTDI_3.5 (T_g = 15.3ºC) and PTMG1000TDI_3 (T_g = 22.1ºC).

As example, *Figure 4.2* demonstrates qualitatively the shape memory capacity of a synthesized polyurethane (sample PTMG1000TDI_3). The sample was deformed at 40ºC to adopt a temporary shape (*Figure 4.2.a*). After cooling into liquid nitrogen (*Figure 4.2.b*), the temporary shape was retained as a result of the restriction of the domains and the glassy polymer network. The permanent shape was recovered by heating the material to 40ºC to remove the restriction [8–10] (*Figures 4.2.c-d*). Because of the original sample at room temperature is transparent, the sample was green painted in order to see the changes in its shape [11–13].

Regarding thermally-activated shapememory properties, soft-segments are responsible for shape fixity, acting as the switching segments, while hard-segments are responsible for shape recovery, determining the permanent shape of the polymer [14–21].

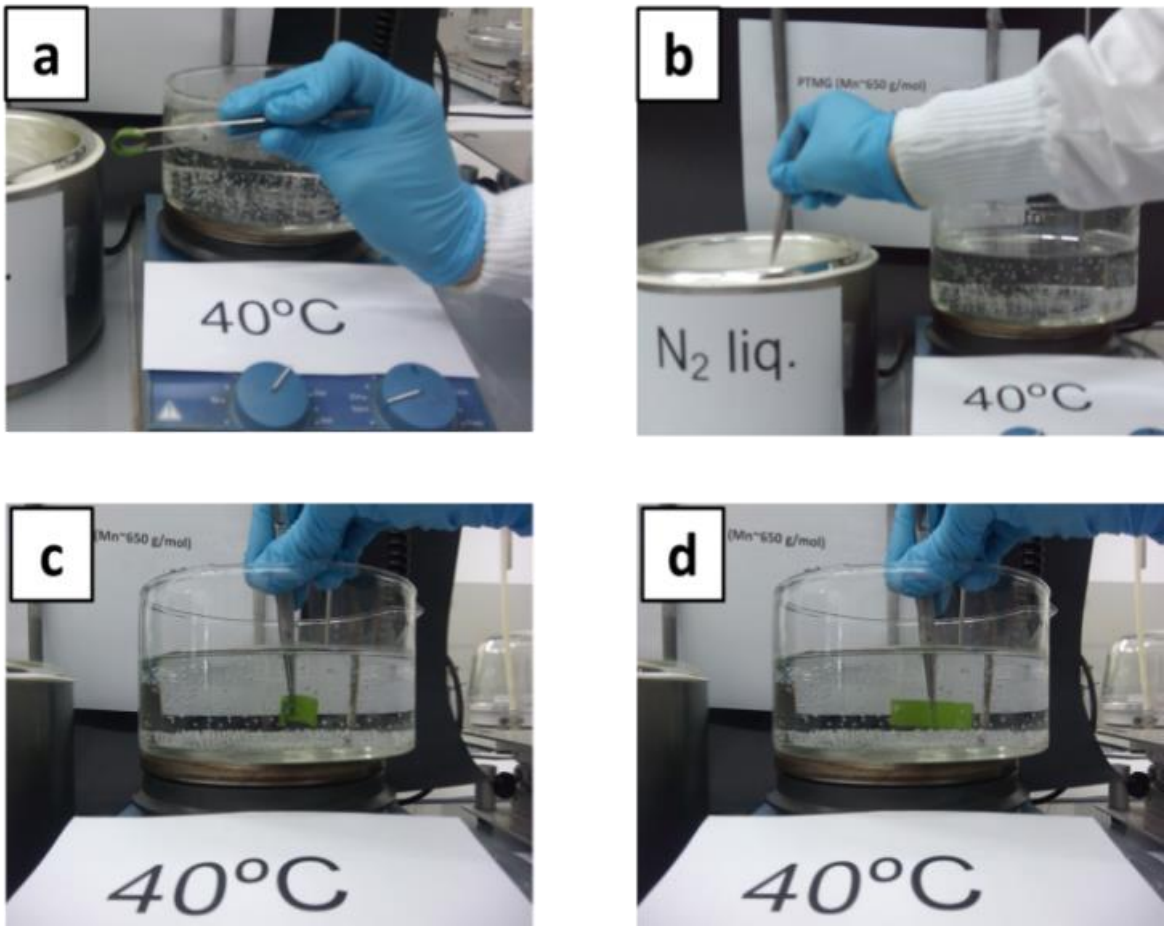

Figure 4.2. *Qualitative shape memory behavior of sample PTMG1000TDI_3. a) Deformation, b) Shape Fixation, c) Recovery, d) Original shape*

- **Quantitative**

The thermally activated shape memory behavior of the synthesized SMPUs can be also studied quantitatively by means of thermomechanical cycles according to Thermomechanical Analysis (TMA), employing a Mettler Toledo DMA-1 in different ranges of temperatures, at a heating rate of 4ºC min^{-1} and at a cooling rate

of -20ºC·min^{-1}. The cross-section area of the samples was 6 mm × 1.5 mm, and the experiment was performed using an initial clamp distances of 10 mm. The conditions of all performed tests are described in the *Table 4.1*. First, the sample was heated until T_{high} (a temperature at least 20ºC higher than the transition temperatures of all samples involved in the specified system) with the minimum force (F = 0.001 N) in order to allow relaxation of the polymer chains, so initial conditions are fixed (sample dimensions and temperature). Then, the sample was stretched applying a determined force (2, 5 or 10 N), cooled at -20ºC·min^{-1} until T_{low} (a temperature at least 20ºC lower than the transition temperatures of all samples involved in the specified system) and maintained at this temperature during 5 minutes. After this, the applied stress was reduced to the preload value (0.001 N) in order to fix the temporary shape. In the final step, the sample was heated again at 4ºC·min^{-1} and original shape was recovered. This study aims to show the shape memory effect of SMPUs in just one cycle (*Figure 4.3)*.

***Table 4.1**. Experimental conditions to perform shape memory experiments for all systems*

System	T_{high} (ºC)	T_{low} (ºC)	Cooling rate (ºC·min^{-1})	Heating rate (ºC·min^{-1})	F (N)
1	80	-20	-20	4	2
2	80	-20	-20	4	2
3	80	-20	-20	4	2
4	40	-100	-20	4	5 and 10
5	80	-20	-20	4	2
6	80	-20	-20	4	2
7	30	-100	-20	4	5 and 10
8	80	-20	-20	4	2
9	80	-20	-20	4	2
10	80	-20	-20	4	2
11	80	-20	-20	4	2

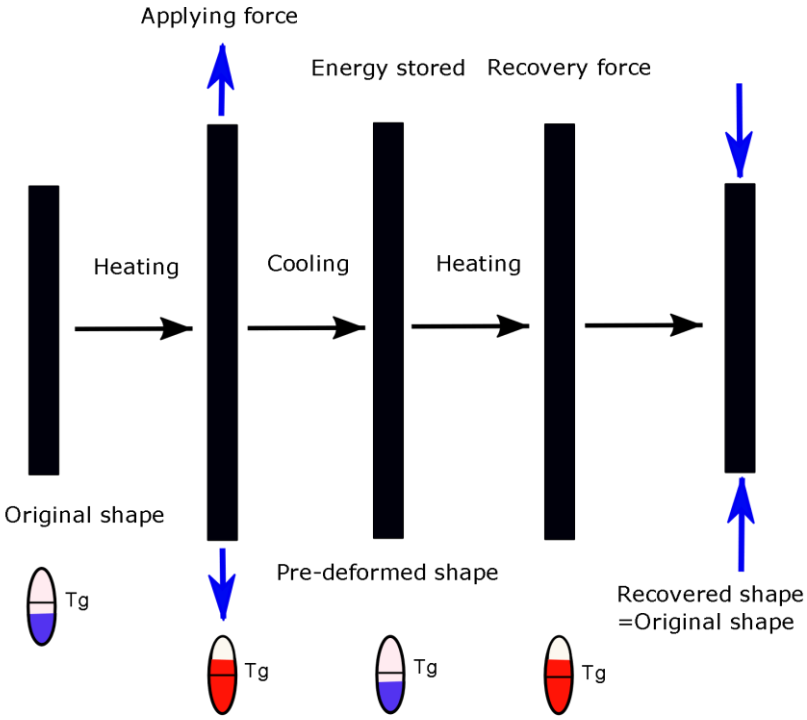

Figure 4.3. *Shape memory effect – one cycle*

The shape memory performance was quantified in terms of two parameters: the shape fixity ratio (R_f) and the shape recovery ratio (R_r), calculated through *eqs. 4.1* and *4.2*, respectively. On the one hand, the shape fixity ratio represents the effectiveness of the temporary shape in maintaining its dimensions. On the other hand, the shape recovery ratio represents how close are the dimensions of the recovered sample to the dimensions at the start of the experiment. For an ideal shape memory material, $R_f = R_r = 100\%$, where all the applied strain energy is stored by the temporary shape, being later recovered during the recovery step so that the sample returns to its original dimensions [22].

$$R_f(\%) = \frac{\varepsilon_u}{\varepsilon_m} \cdot 100 \qquad (4.1)$$

$$R_r(\%) = \frac{\varepsilon_m - \varepsilon_p}{\varepsilon_m} \cdot 100 \qquad (4.2)$$

In the performed mechanical tests, ε_u is the strain obtained after releasing the applied load, ε_m is the maximum strain before the load is released, and ε_p is the final strain after heating and without load, i.e., after maximum recovery of the deformation (*Figure 4.4*).

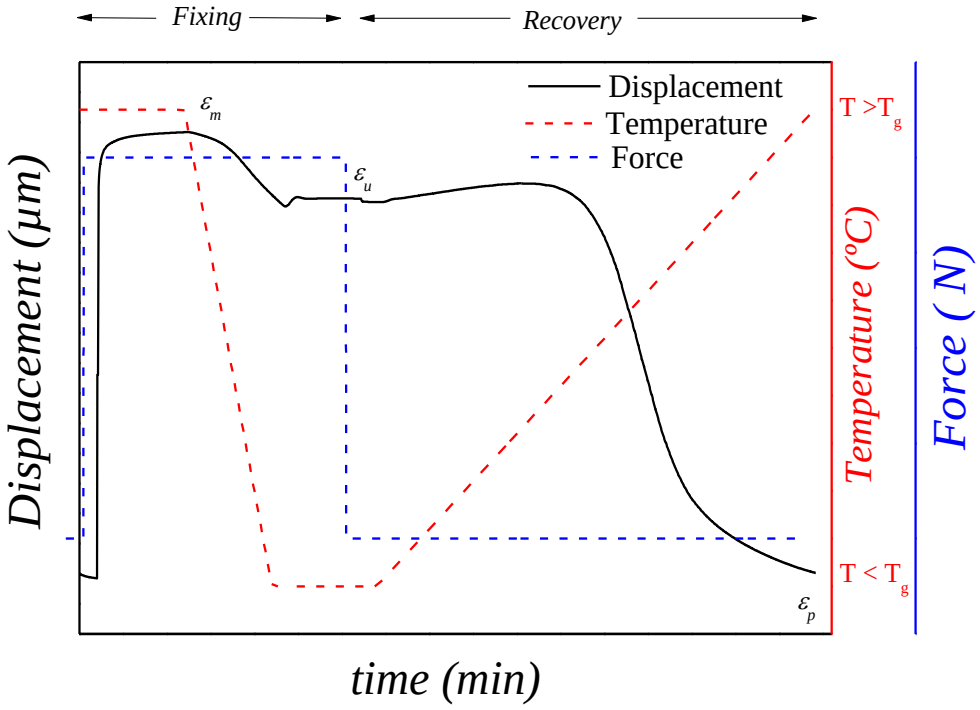

Figure 4.4. *Description of the method used in thermomechanical analysis*

Tables 4.2, 4.3, 4.4 and *4.5* summarize the values of shape fixity ratios (R_f) and shape recovery ratios (R_r) obtained for SMPUs based on PEG, PTMG650, PTMG1000 and SMPUS with nanoparticles, respectively, at F = 2N except for systems 4 and 7, where F = 5 and 10 N were applied. In these systems, a different force was used due to the properties of MDI-based SMPUs. For some samples, it was not possible to calculate these parameters, for example in system 2, because the effect of contraction and expansion is higher than the shape memory effect. This inconvenience is due to the limitations in the equipment. All the results showed in the tables are based on the average of three measurements.

The thermally activated shape memory behavior for systems 1, 3, 7 and 10 are shown in *Figures 4.5, 4.6, 4.7* and *4.8*, respectively. All graphs are in *Appendix D*.

Table 4.2. *Shape memory parameters for the SMPUs based on PEG*

System & Sample		R_f (%)	R_r (%)
S1	PEGTDI_3.5	90.3	99.7
	PEGTDI_4.5	90.9	99.8
	PEGTDI_5.5	92.1	99.8
S2	PEGMDI_2	-	-
	PEGMDI_3	-	-
	PEGMDI_4	-	-

Table 4.3. Shape memory parameters for SMPUs based on PTMG 650

System & Sample		R_f (%)		R_r (%)	
S3	PTMG650TDI_2.5				
	PTMG650TDI_3	93.3		99.9	
	PTMG650TDI_3.5	89.9		99.8	
	PTMG650TDI_4	89.7		99.6	
	PTMG650TDI_4.5	98.9		99.8	
	PTMG650TDI_5	91.4		99.7	
	PTMG650TDI_5.5	87.2		100	
		F = 5 N	**F = 10 N**	**F = 5 N**	**F = 10 N**
S4	PTMG650MDI_0.5	84.1	-	88.6	
	PTMG650MDI_1	49.6	73.7	73.8	79.5
	PTMG650MDI_1.5	-	48.9	-	69.6
	PTMG650MDI_2	-	-	-	
	PTMG650MDI_2.5	-	-	-	
	PTMG650MDI_3	-	-	-	
	PTMG650MDI_3.5	-	-	-	
	PTMG650MDI_4	-	-	-	
	PTMG650MDI_4.5	-	-	-	
S5	PTMG650MDITDI_1.5	87.1		98.4	
	PTMG650MDITDI_2	97.4		96.5	
	PTMG650MDITDI_2.5	75.9		92.8	
	PTMG650MDITDI_3	66.9		98.1	
	PTMG650MDITDI_3.5	72.4		99.2	

Table 4.4. *Shape memory parameters for SMPUs based on PTMG 1000*

System & Sample		R_f (%)		R_r (%)	
S6	PTMG1000TDI_2.5				
	PTMG1000TDI_3	95.8		99.7	
	PTMG1000TDI_3.5	89.8		100	
	PTMG1000TDI_4	89.7		99.7	
	PTMG1000TDI_4.5	89.6		99.9	
	PTMG1000TDI_5	84.9		99.8	
	PTMG1000TDI_5.5	94.2		99.9	
	PTMG1000TDI_6.5	60.4		91.9	
S7		**F = 5 N**	**F = 10 N**	**F = 5 N**	**F = 10 N**
	PTMG1000MDI_0.5	89.3	-	89.9	-
	PTMG1000MDI_1	69.3	-	80.4	-
	PTMG1000MDI_1.5	64.4	-	63.9	-
	PTMG1000MDI_2	-	45.3	-	84.7
	PTMG1000MDI_2.5	-	27.4	-	74.4
	PTMG1000MDI_3	-	30.1	-	60.4
	PTMG1000MDI_3.5	-	-	-	-
	PTMG1000MDI_4	-	-	-	-
	PTMG1000MDI_4.5	-	-	-	-
S8	PTMG1000MDITDI_3.5	91.2		99.5	
	PTMG1000MDITDI_4	92.5		99.9	
	PTMG1000MDITDI_4.5	91.8		100	
	PTMG1000MDITDI_5	76.5		96.7	
	PTMG1000MDITDI_5.5	72.1		94.0	
	PTMG1000MDITDI_6	63.1		80.9	

Table 4.5. *Shape memory parameters for SMPUs synthesized with nanoparticles*

System & Sample		R_f (%)	R_r (%)
S9	PTMG650MDITDI_1.5_1	93.9	99.9
	PTMG650MDITDI_2_1	96.6	99.9
	PTMG650MDITDI_2.5_1	91.9	99.9
	PTMG650MDITDI_3_1	99.4	98.0
	PTMG650MDITDI_3.5_1	96.2	99.4
S10	PTMG1000MDITDI_3.5_1	92.7	100.0
	PTMG1000MDITDI_4_1	99.7	99.4
	PTMG1000MDITDI_4.5_1	80.3	97.6
	PTMG1000MDITDI_5_1	74.1	88.6
	PTMG1000MDITDI_5.5_1	-	-
	PTMG1000MDITDI_6_1	-	-
S11	PTMG1000MDITDI_3.5_3	89.7	99.5
	PTMG1000MDITDI_4_3	89.0	99.7
	PTMG1000MDITDI_4.5_3	91.1	99.8
	PTMG1000MDITDI_5_3	100.0	99.8
	PTMG1000MDITDI_5.5_3	99.8	100.0
	PTMG1000MDITDI_6_3	99.7	99.6

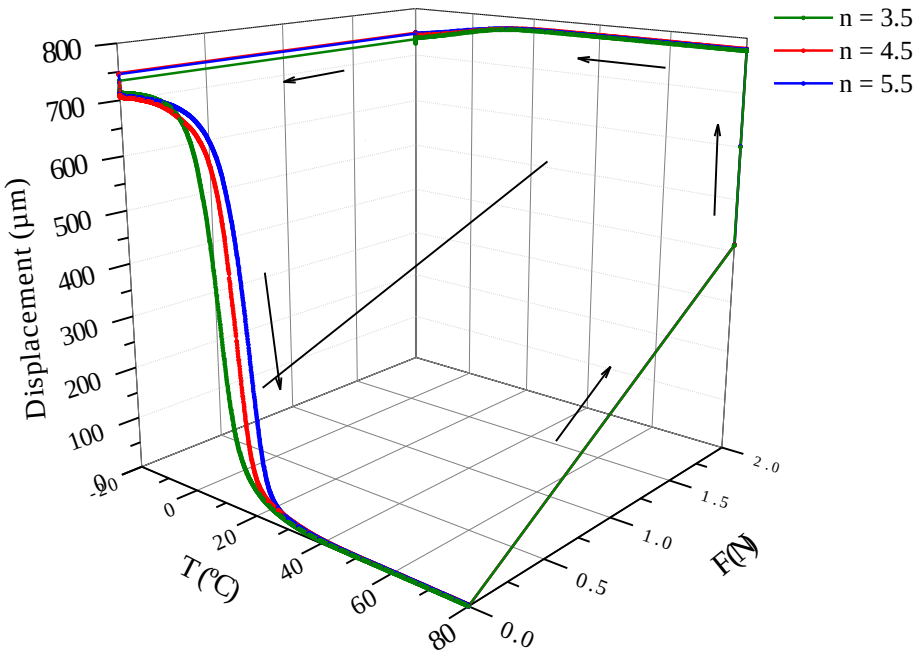

Figure 4.5. *Three-dimensional thermomechanical response for system 1, PEG1000TDI*

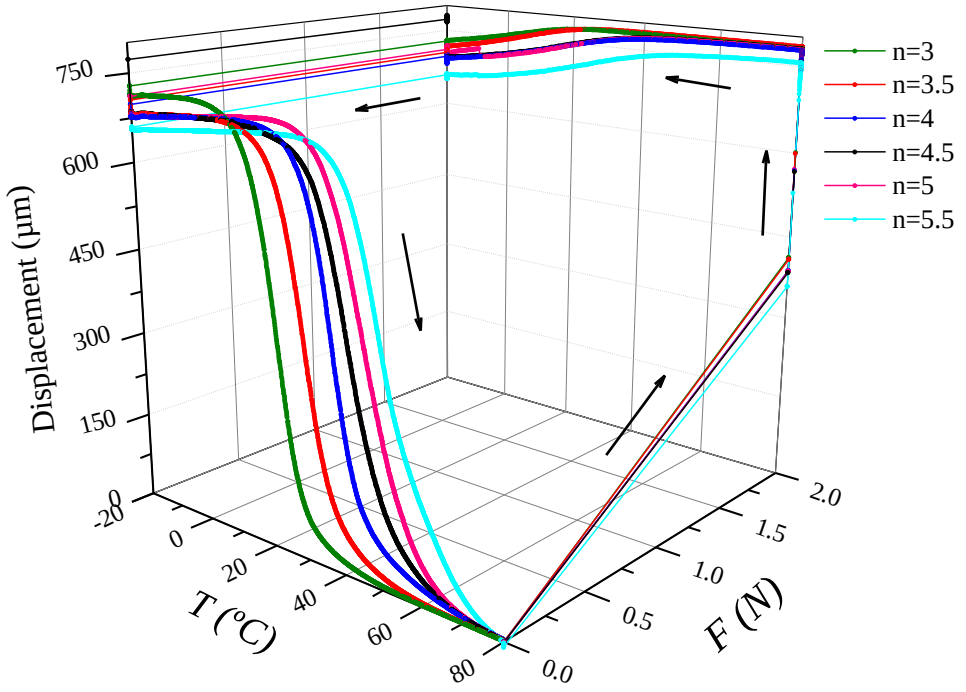

Figure 4.6. *Three-dimensional thermomechanical response for system 3, PTMG650TDI*

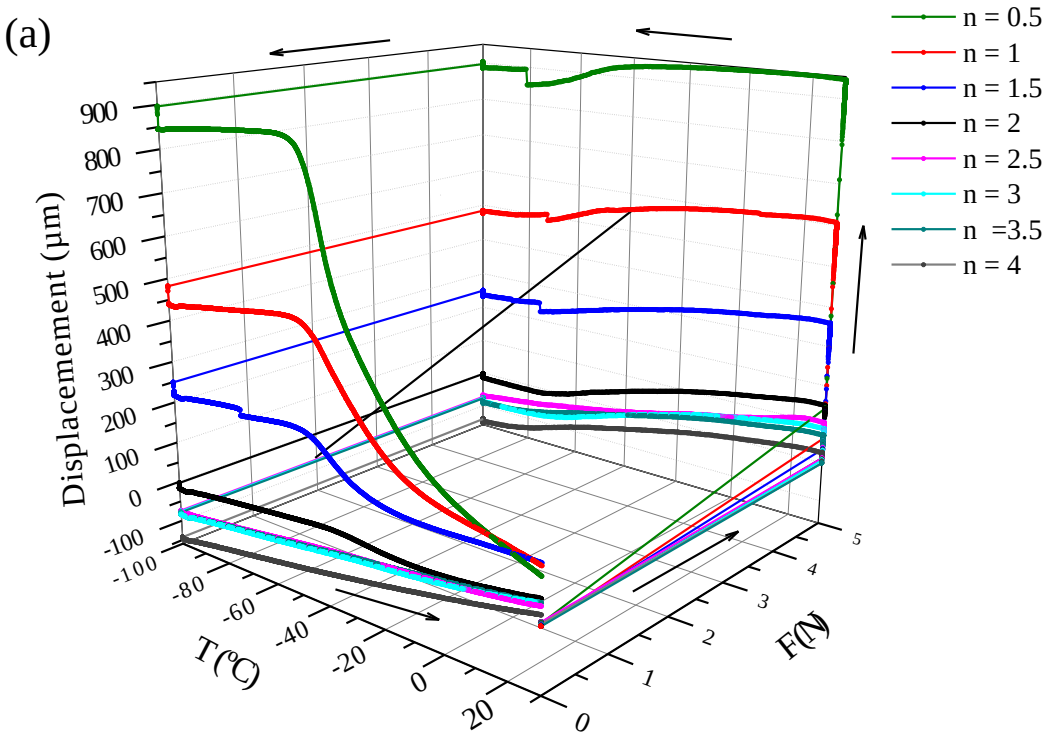

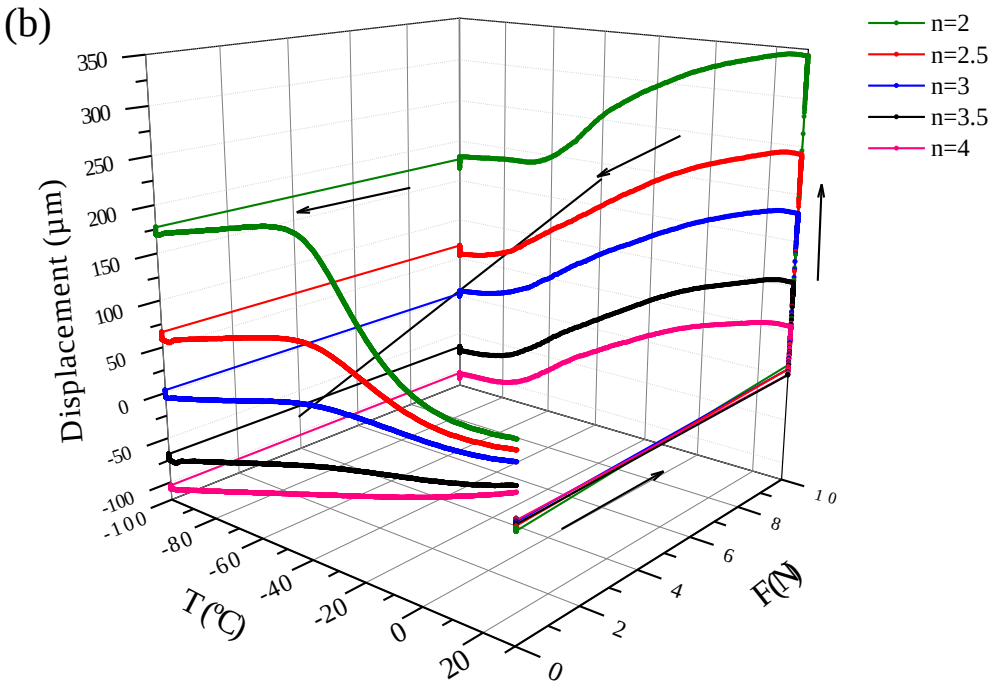

Figure 4.7. *Three-dimensional thermomechanical response for system 7, PTMG1000MDI, F = 5 N (a) and F = 10 N (b)*

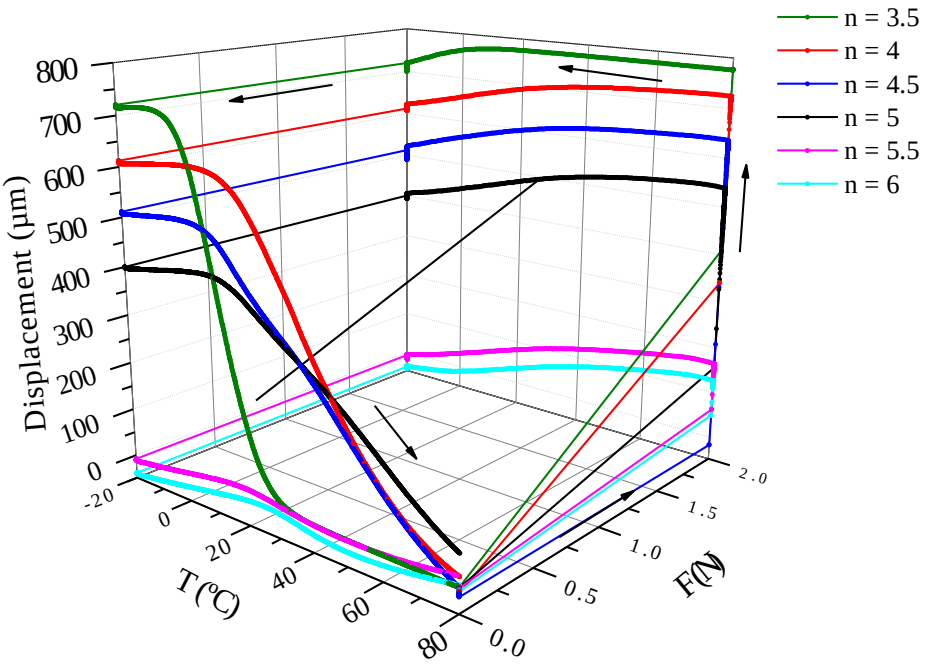

Figure 4.8. *Three-dimensional thermomechanical response for system 10, PTMG1000/MDI+TDI/1%TiO_2*

As previously indicated, the value of the fixity ratio is attributed to the soft-segment of the polyurethane while the hard-segment of the polyurethane is responsible for the shape recovery.

Relating to soft-segment, it is evident that both the PTMG-based and PEG-based SMPUs show a similar shape memory effect [7,23]. When PEG1000TDI and PTMG1000TDI with the same molecular weight and the same molar ratio (e.g. n=4.5) are compared, the shape memory behavior of PEG1000TDI presents almost complete strain fixing (90.9%) and strain recovery (99.8%), as PTMG100TDI does (R_f = 89.6% and R_r = 99.9%). These values are practically equal because the hard-segment, which controls the recovery, is the same. It could be concluded that these two polyols (PEG and PTMG), combined with TDI to synthetize a polyurethane, provide not only almost complete shape recovery but also similar and favorable results relating to shape fixity.

Furthermore, *Figure 4.9* shows the bi-dimensional representation of the thermomechanical cycles corresponding to PTMG650TDI_5.5 (R_f = 87.2% and R_r = 100%) and PEG1000TDI_5.5 (R_f = 92.1% and R_r = 99.8%) samples, which have same hard-segment, same molar ratio and a different polyol. Since the hard-segment is the same, R_r is very similar in both polyurethanes. However, this time the polyol is different both in nature and in molecular weight, so the difference in R_f becomes higher than in the case of PTMG1000TDI_4.5 and PEG1000TDI_4.5 where the polyol differs just in nature. Moreover, it is observed that PEG1000TDI_5.5 sample recovers its permanent shape (original shape) in a shorter time than PTMG650TDI_5.5 (30 minutes versus 42 minutes). In the thermo-mechanical cycle developed in order to study the shape memory behavior, the last stage consists in heating the sample to a temperature above the transition temperature. Therefore, as the glass transition temperature of PEG1000TDI_5.5 ($T_{g,DMA}$ = 30.4ºC) is lower than the one of PTMG650TDI_5.5 ($T_{g,DMA}$ = 62.9ºC), the recovery process takes place at a shorter time, although shape recovery is close to 100% in both cases.

Finally, it is concluded that PEG1000TDI, PTMG650TDI and PTMG1000TDI were completely recovered with recovery ratios higher than 99.7%.

Relating to hard-segment, in this work, TDI, MDI and a mixture 50% weight of TDI and 50% weight of MDI were used to synthesize polyurethanes with different compositions. The soft-segments in the polyurethanes act as reversible phases, while physical entanglement of the amorphous polyurethanes act as the fixed phase, such as physical netpoints. Polyurethanes synthesized with MDI showed remarkable lower shape recovery ratios than TDI-based SMPUs. This is because the chain entanglements in the stretched sample were not sufficiently high to provide enough physical netpoints and elasticity required to restore the original shape [24–26].

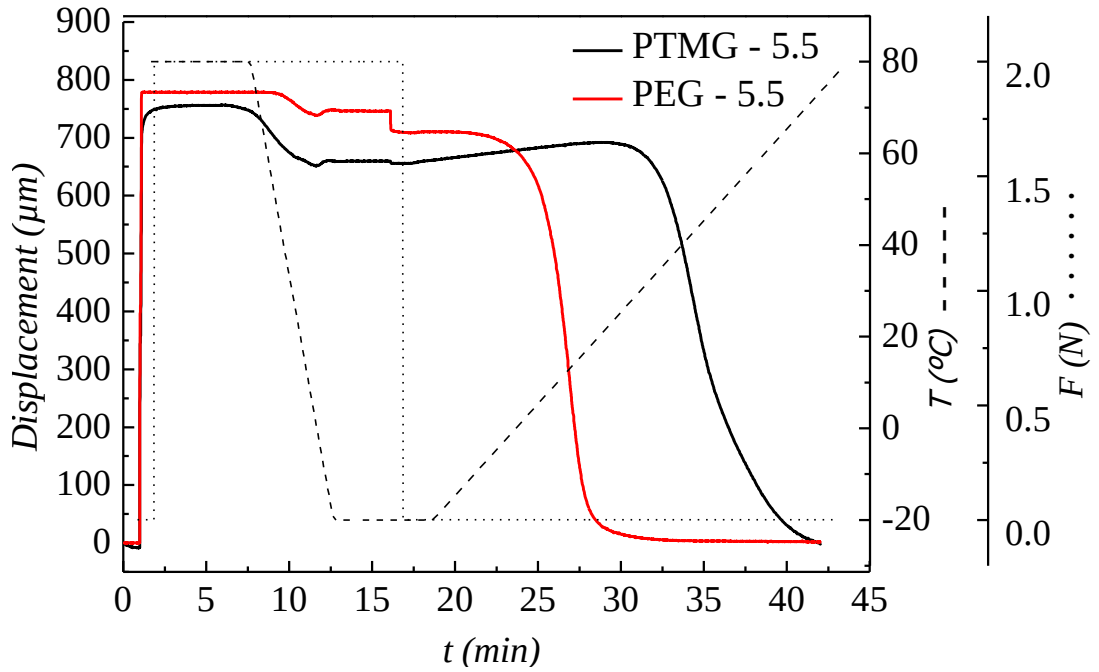

Figure 4.9. *Bi-dimensional thermomechanical cycles to compare PTMG650TDI_5.5 and PEG1000TDI_5.5 samples*

It can be seen that the shape fixity values (R_f) obtained for the TDI-based SMPUs are larger than those previously showed by *Gu et al.* [27] for PEG-based SMPUs, which obtained a maximum of 75%. Moreover, the hard-segment domain formed by TDI and BD provides stable physical netpoints to achieve good shape recovery, approximately near 100%. For MDI-based SMPUs, shape fixity and shape recovery ratios decrease with the increase in hard-segment content in almost all samples. The shape fixity values for MDI-based SMPUs with molar ratio higher than 1.5 for F = 5 N and higher than n = 3 for F = 10 N, were not possible to calculate because of the

limitations in the equipment. These negative values are directly related to the TMA test procedure developed in order to measure the shape memory behavior, as mentioned above. It should be noted that the maximum displacement that the Mettler Toledo DMA1 can register is 1 mm (1000 μm) and the maximum force is 10 N. Thus, on the one hand, when forces higher than 5 N were applied this limit can be overcome in some samples and, on the other hand, the applied force (5 N) is not enough to fix the temporary shape due to a thermal process contraction which decreases values used in *eq. 4.1* to calculate R_f.

It is worth noting that a certain fraction of the stretched polymer is unlocked even at a temperature below T_g, hence there is an instantaneous retractive force upon loading removal, which causes incomplete shape fixing in MDI-based SMPUs and in some TDI-based SMPUS [22].

It can be concluded that the shape memory properties for the TDI-based SMPUs (R_r (%)) are superior to MDI-based SMPUs. One possible reason is that their physical netpoints formed by molecular interactions are weak in the MDI–based SMPUs, whereas TDI-based SMPUs show higher hydrogen bonded molecular interaction as mentioned above.

In contrast to MDI-based SMPUs, SMPUs with nanoparticles show better recovery ratios, as in almost all samples R_r higher than 99.5% were achieved. Hence, the added TiO_2 nanoparticles can be considered as secondary physical netpoints in conjunctions with the main physical netpoints of the matrix. Thus, it can be noted here that the observed improvement in R_r with the incorporation of nanoparticles is originated from the high physical crosslink density and large stored elastic strain energy in the polyurethane, which provide a high driving force for the subsequent complete shape recovery [22,28,29].

In addition, it can be seen from *Table 4.3* and *Table 4.5* that PTMG650TDIMDI without nanoparticles presents moderate R_f values, while with the incorporation of 1% TiO_2 into the polyurethane, the shape fixing of nanocomposites is noticeably improved [30]. As an example, R_f of PTMG650TDIMDI_3.5 without nanoparticles is 72.4% and adding 1% TiO_2 is 96.2%. In the case of PTMG1000TDIMDI (*Table 4.4* and *Table 4.5*), results are not as remarkable as it happens with PTM650TDIMDI but R_f values are higher with nanoparticles than without them, in almost all cases [31,32].

To sum up, all shape memory polyurethanes show good shape recovery, being the MDI-based SMPUs which show the worst shape recovery. This could be attributed to the presence of more physical crosslinking in the other samples due to the highest frequency of urethane bonds, which cause the storage of more deformed energy in the system. In addition, some samples with lower T_g values show higher shape recovery. This could be explained because of the restricted mobility of long chains and highly crosslinked polymer networks [33].

4.2.2. Cycles

Once demonstrated the shape memory ability of shape memory polyurethanes over a thermomechanical cycle, shape memory behavior during several cycles was studied. All the samples were tested performing the same described TMA procedure in order to check the reproducibility of the shape memory behavior for repetitive cycles [3,34,35]. As explained in *section 4.2.1*, in these cyclic thermomechanical tests, shape memory behavior is usually quantified by parameters such as the strain fixity ratio, R_f, and the strain recovery ratio, R_r. The experimental conditions to perform the cyclic experiments were the same as in *Table 4.1*. These cyclic experiments were realized only for one specific polyurethane in each system, so that, 11 cyclic tests were carried out. The shape fixity ratios and the shape recovery ratios corresponding to each cycle (N = 1-6) are shown in *Tables 4.6, 4.7, 4.8* and *4.9* for the SMPUs based on PEG, PTMG650, PTMG1000 and SMPUs with nanoparticles, respectively.

Moreover, the procedure was the same as in one cycle. First, the sample is heated without force at a temperature above T_{trans} with a heating rate of 4°C·min^{-1} in order to allow relaxation of the polymer chain. Then, the force is applied and the sample is deformed. The stress is then maintained during 5 min. The temporary shape was fixed cooling below its transition temperature of shape memory effect, T_{low} at a rate of -20°C·min^{-1}. Finally, the samples were heated-up above the transition temperature at a rate of 4°C·min^{-1}, so the thermal-induced recovery process was observed [36–39]. This cycle was then conducted consecutively five more times on the same sample (*Figure 4.10*) [40,41]. Therefore, the number of cycles (N) was 6.

For each cycle (N = 1-6), R_f quantifies the ability of the polymer to fix a mechanical deformation, ε_m, resulting in a temporary shape, $\varepsilon_u(N)$; whereas R_r quantifies the ability to restore the permanent shape $\varepsilon_p(N)$ after the application of a

certain deformation, ε_m, so it builds the ratio between the change in strain recorded during the shape memory effect $\varepsilon_m(N) - \varepsilon_p(N)$ and the change in strain in the course of programming given by $\varepsilon_m(N) - \varepsilon_p(N-1)$ [42,43]. The shape fixing ratio, $R_f(N)$, and the shape recovery ratio, $R_r(N)$, were calculated using the equations *4.3* and *4.4*, respectively [44,45]. From these equations, it is observed that ideally R_f and R_r should be 100%.

$$R_f(\%) = \frac{\varepsilon_u\,(N)}{\varepsilon_m\,(N)} \cdot 100 \qquad (4.3)$$

$$R_r(\%) = \frac{\varepsilon_m\,(N) - \varepsilon_p\,(N)}{\varepsilon_m(N) - \varepsilon_p(N-1)} \cdot 100 \qquad (4.4)$$

Where N is the cycle number, ε_m is the maximum compressive strain, $\varepsilon_p\,(N)$ and $\varepsilon_p\,(N-1)$ are the final strains of the sample in two successive cycles in the recovering process (*Figure 4.11*).

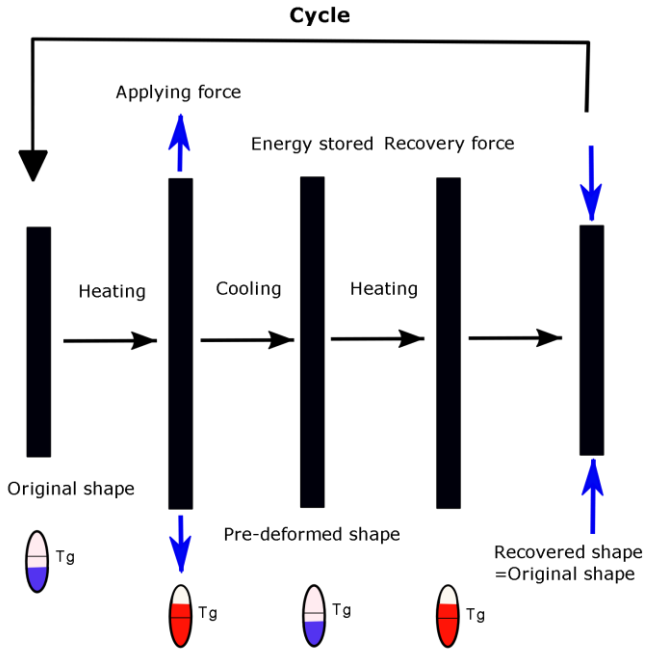

Figure 4.10. *Shape memory effect - cyclic*

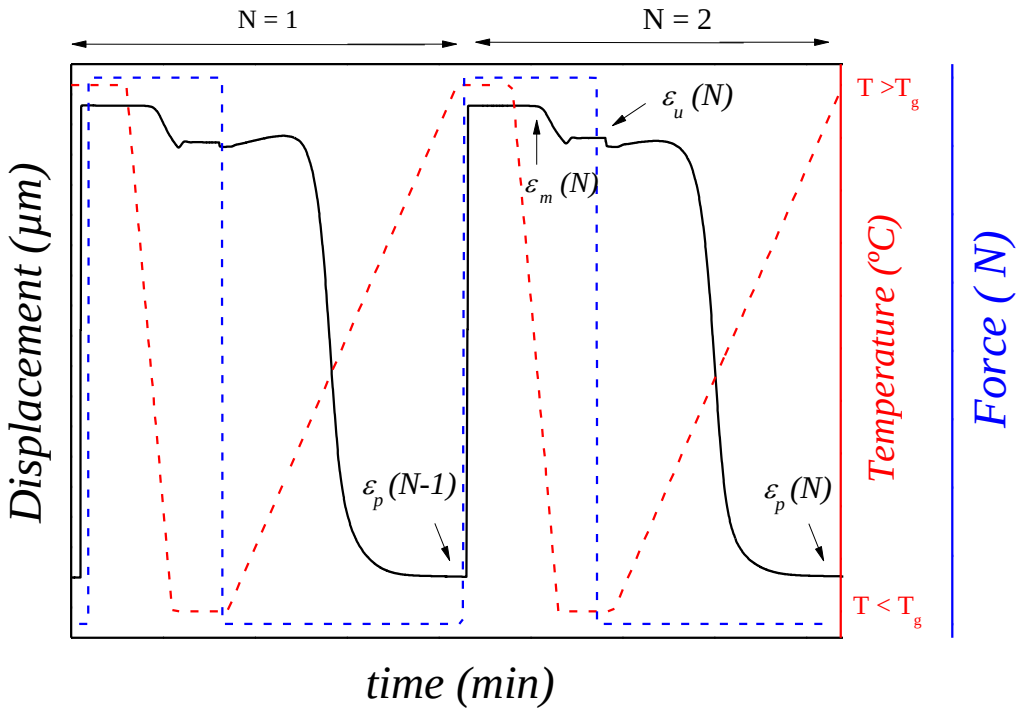

Figure 4.11. *Description of the method used in thermomechanical analysis – two consecutive cycles*

Table 4.6. *Shape memory parameters after six cycles for one SMPU in each system for the SMPUs based on PEG*

System & Sample		Cycle	R_f (%)	R_r (%)
S1	PEGTDI_4.5	N = 1	93.6	99.9
		N = 2	93.5	100
		N = 3	88.2	100
		N = 4	74.3	100
		N = 5	53.0	100
		N = 6	53.0	99.9
S2	PEGMDI_3	N = 1-6	-	

Table 4.7. *Shape memory parameters after six cycles for one SMPU in each system for the SMPUs based on PTMG 650*

System & Sample		Cycle	R_f (%)	R_r (%)
S3	PTMG650TDI_3	N = 1	91.9	99.8
		N = 2	91.9	100
		N = 3	91.5	100
		N = 4	91.4	99.9
		N = 5	94.2	100
		N = 6	94.4	100
S4	PTMG650MDI_1.5	N = 1	34.0	76.4
		N = 2	37.3	86.7
		N = 3	42.3	89.3
		N = 4	45.7	90.2
		N = 5	49.0	91.3
		N = 6	51.1	92.3
S5	PTMG650MDITDI_1.5	N = 1	89.6	100
		N = 2	89.4	99.6
		N = 3	89.1	100
		N = 4	89.2	99.9
		N = 5	89.9	99.9
		N = 6	89.5	100

Table 4.8. *Shape memory parameters after six cycles for one SMPU in each system for the SMPUs based on PTMG 1000*

System & Sample		Cycle	R_f (%)	R_r (%)
S6	PTMG1000TDI_4.5	N = 1	88.0	99.9
		N = 2	87.7	99.9
		N = 3	87.5	100
		N = 4	87.7	100
		N = 5	87.9	99.9
		N = 6	88.0	100
S7	PTMG1000MDI_1.5	N = 1	52.3	73.1
		N = 2	57.2	88.9
		N = 3	57.4	89.9
		N = 4	59.2	89.5
		N = 5	64.7	89.8
		N = 6	63.6	90.8
S8	PTMG1000MDITDI_3.5	N = 1	91.0	99.8
		N = 2	90.8	99.9
		N = 3	90.3	99.8
		N = 4	90.2	100
		N = 5	90.1	99.9
		N = 6	90.0	100

Table 4.9. *Shape memory parameters after six cycles for one SMPU in each system for SMPUs synthesized with nanoparticles*

System & Sample		Cycle	R_f (%)	R_r (%)
S9	PTMG650MDITDI_1.5_1	N = 1	90.9	100
		N = 2	90.4	99.9
		N = 3	90.3	99.9
		N = 4	89.8	99.9
		N = 5	90.3	99.9
		N = 6	90.9	99.7
S10	PTMG1000MDITDI_3.5_1	N = 1	93.0	99.9
		N = 2	92.7	99.9
		N = 3	92.5	99.9
		N = 4	92.5	100
		N = 5	92.8	100
		N = 6	92.5	99.9
S11	PTMG1000MDITDI_3.5_3	N = 1	90.5	99.9
		N = 2	90.3	99.9
		N = 3	90.1	100
		N = 4	90.2	99.9
		N = 5	90.6	99.9
		N = 6	90.5	100

In *Figure 4.12,* the thermomechanical behavior in 2D during 6 cycles for the sample PTMG650TDI_3 can be observed. Furthermore, *Figure 4.13*, *4.14*, *4.15* and *4.16* show the obtained results about shape memory behavior during 6 cycles for the samples corresponding to system 1, system 3, system 7 and system 10, respectively. All the graphics corresponding to this section can be found in *Appendix D*.

These figures provide the 3D shape memory cycles for the samples, showing the variation of the sample deformation with the applied force and temperature, where an outstanding reproducibility is observed in almost all samples [25]. Generally, regarding thermally activated shape memory properties, soft-segments are responsible for shape fixity, acting as the switching segments; while hard-segments are responsible for shape recovery, determining the permanent shape [20,21,46].

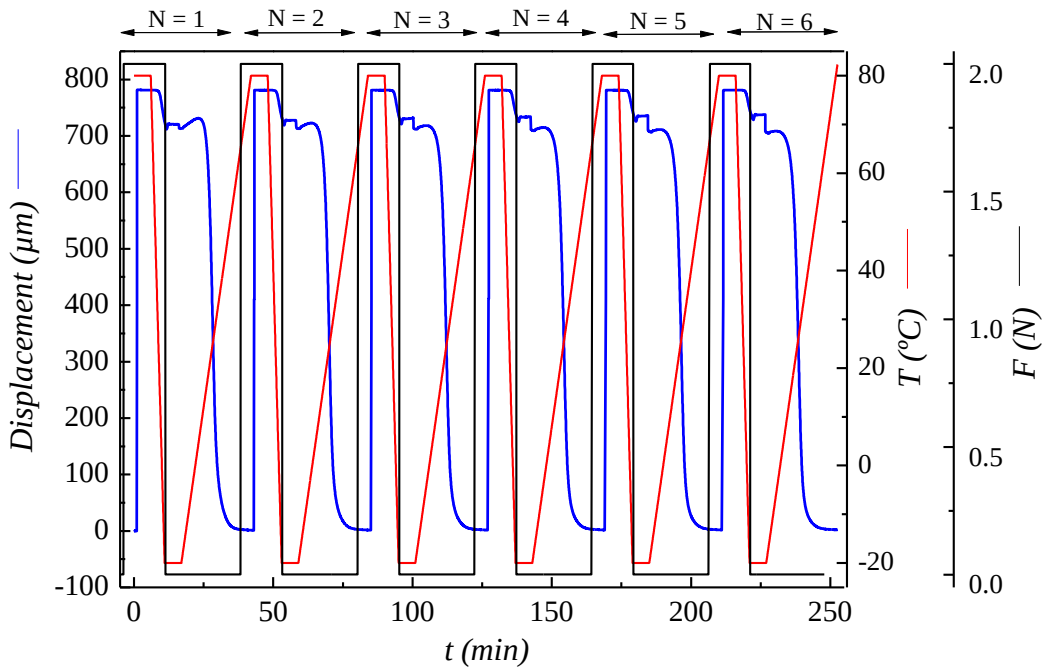

Figure 4.12. *Bi-dimensional thermomechanical response for PTMG650TDI_3 sample during 6 cycles.*

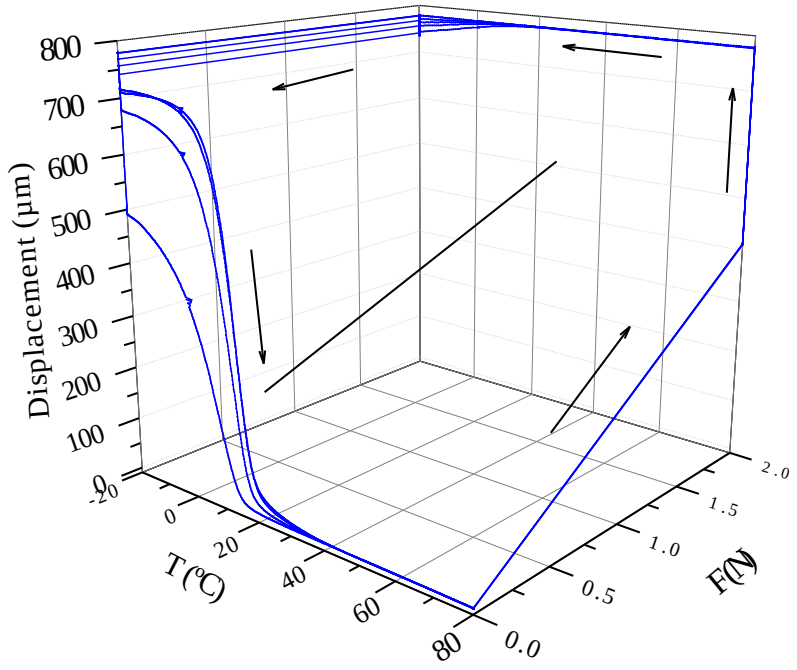

Figure 4.13. *Three-dimensional thermomechanical response for system 1, PEG1000TDI_4.5 – 6 cycles*

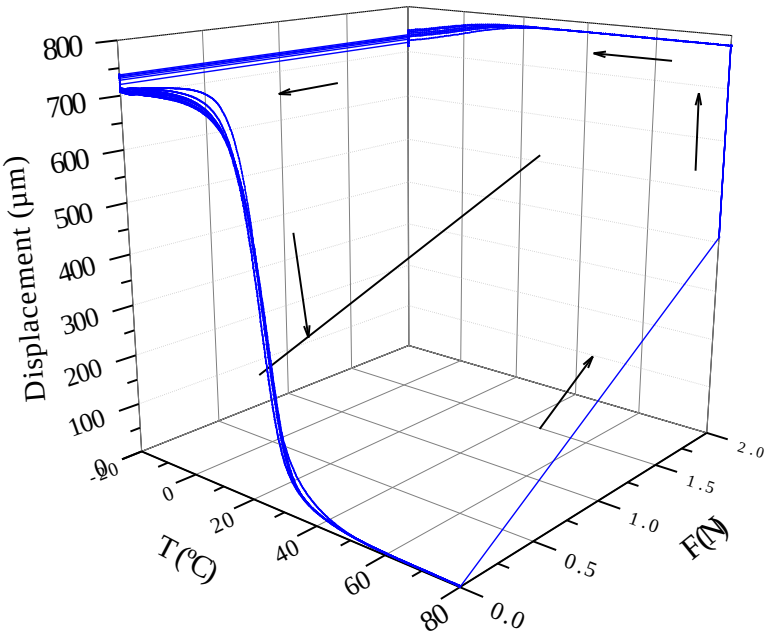

Figure 4.14. *Three-dimensional thermomechanical response for system 3, PTMG650TDI_3 – 6 cycles*

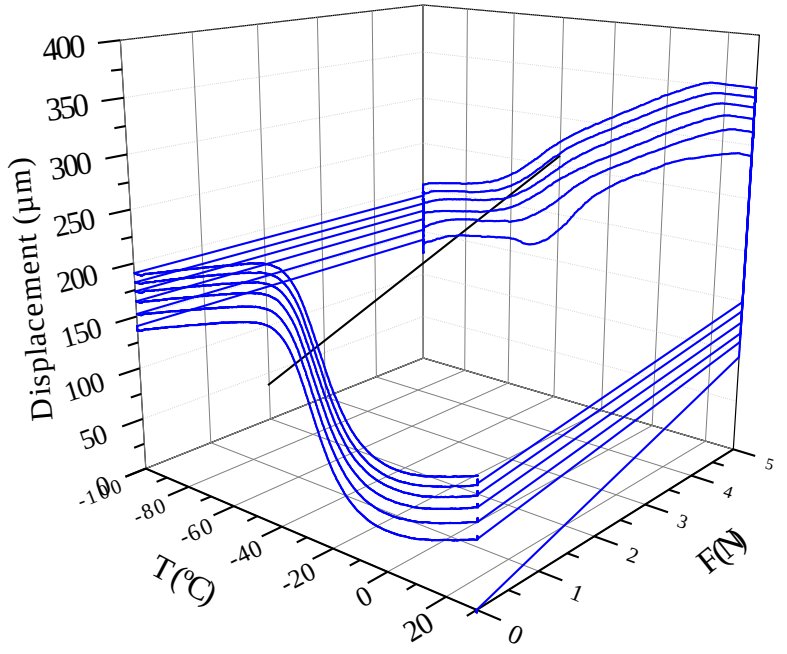

Figure 4.15. *Three-dimensional thermomechanical response for system 7, PTMG1000MDI_1.5 – 6 cycles*

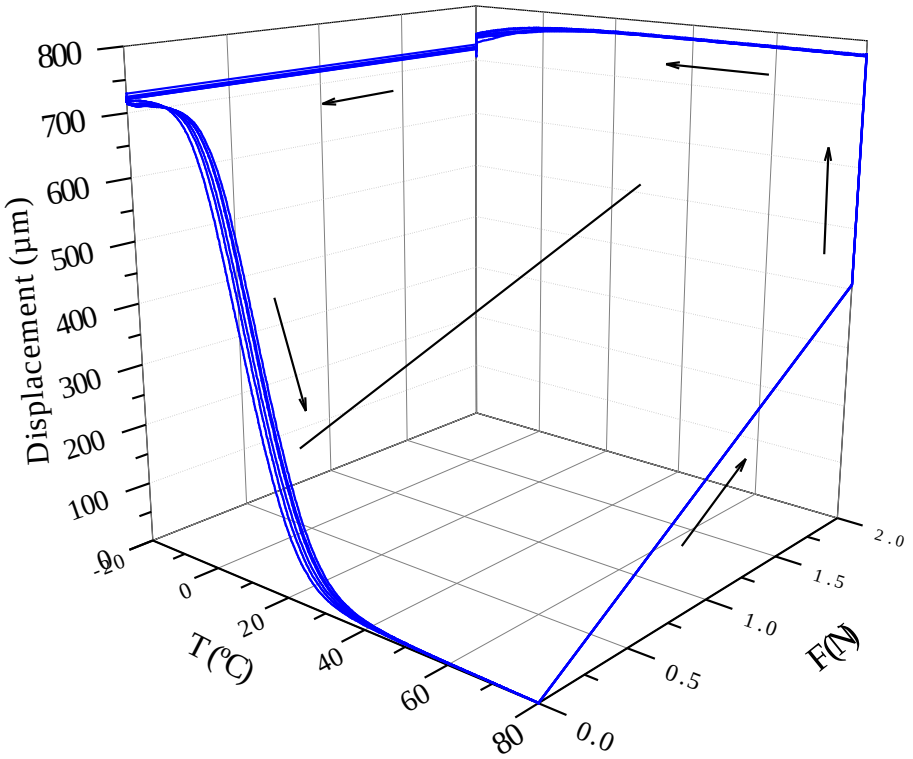

Figure 4.16. *Three-dimensional thermomechanical response for system 10, PTMG1000MDITDI_3.5_1– 6 cycles*

The shape fixity ratios for each sample are higher than 85% in almost all samples. It is clear that, in the same way that the observed results for one TMA cycle, the MDI-based SMPUs show the worst shape fixity and shape recovery properties among the polyurethanes studied in this work. In the case of PEG-based SMPUs, the shape fixity ratio decreases as N increases. This could be explained because the used soft-segment, PEG, fix the temporary shape worse than PTMG. In the rest of the cases, TDI and the mixture of MDI and TDI based SMPUS, the shape fixity and shape recovery ratios are similar regardless of the number of the cycle.

Relating to SMPUS with nanoparticles, the results demonstrate that the addition of nanoparticles enhances slightly the shape fixity and shape recovery ratios of SMPUs. The shape recovery ratios are higher than 99.5% in all cases and in all cycles from N = 1 to N = 6.

Finally, it could be concluded that TDI-based SMPUs and TDI+MDI based SMPUs have better shape fixity and shape recovery than MDI-based SMPUs in both cases, in one cycle and in more than one cycle.

4.3. Conclusions

Shape memory behavior of the synthesized polyurethanes was qualitatively and quantitatively evaluated. The qualitative evaluation demonstrates promoted shape memory response for all samples. At the same time, the quantitative analysis using TMA shows that almost all SMPUs samples are characterized by shape fixity ratios higher than 85% and shape recovery ratios near 99%.

Besides, depending on the hard-segment, the shape memory effect varies between MDI-based SMPUs and TDI-based SMPUs, finding TDI shape memory properties superior to MDI-based SMPUs.

In conclusion, considering the foregoing, PTMG-based SMPUs could be more promising thermal-induced shape memory polymers than PEG-based SMPUs. These polyurethanes could be able to provide promising applications in several fields as textile, footwear, biomedicine, automotive, aerospace, etc [42,47].

4.4. References

1. Petrović ZS, Milić J, Zhang F, Ilavsky J (2017) Fast-responding bio-based shape memory thermoplastic polyurethanes. Polymer (Guildf) 121:26–37.
2. Calvo-Correas T, Gabilondo N, Alonso-Varona A, et al (2016) Shape-memory properties of crosslinked biobased polyurethanes. Eur Polym J 78:253–263.
3. Xiao R, Zhang C, Gou X, et al (2017) Tunable shape-memory behaviors in amorphous polymers through bound solvent. Elsevier 209:131–133.
4. Odent J, Raquez J-M, Samuel C, et al (2017) Shape-Memory Behavior of Polylactide/Silica Ionic Hybrids. Macromolecules 50:2896–2905.
5. Chatterjee T, Dey P, Nando GB, Naskar K (2015) Thermo-Responsive Shape

Memory Polymer Blends Based on Alpha Olefin and Ethylene Propylene Diene Rubber. Polymer (Guildf) 78:180–192.

6. Meng H, Mohamadian H, Stubblefield M, et al (2013) Various shape memory effects of stimuli-responsive shape memory polymers. Smart Mater Struct 22:93001–93023.

7. Hu JL, Ji FL, Wong YW (2005) Dependency of the shape memory properties of a polyurethane upon thermomechanical cyclic conditions. Polym Int 54:600–605.

8. Li Y, Zhang Y, Rios O, et al (2017) Photo-responsive liquid crystalline epoxy networks with exchangeable disulfide bonds. RSC Adv 7:37248–37254.

9. Berlanga Duarte ML, Aranda Guevara F, Reyna Medina LA (2017) Preparation and Study of Shape Memory in Epoxy Resins. Macromol Symp 374:1600132–1600137.

10. Chen S, Zhang Q, Feng J, et al (2017) 3D printing of tunable shape memory polymer blends. J Mater Chem C 5:8361–8365.

11. Jing Z, Shi X, Zhang G, Gu J (2017) Synthesis and properties of poly(lactide)/poly(ε-caprolactone) multiblock supramolecular polymers bonded by the self-complementary quadruple hydrogen bonding. Polymer (Guildf) 121:124–136.

12. Teoh JEM, Zhao Y, An J, et al (2017) Multi-stage responsive 4D printed smart structure through varying geometric thickness of shape memory polymer. Smart Mater Struct 26:125001–125011.

13. Yao Y, Zhou T, Wang J, et al (2016) "Two way" shape memory composites based on electroactive polymer and thermoplastic membrane. Compos Part A Appl Sci Manuf 90:502–509.

14. Saralegi A, Gonzalez ML, Valea A, et al (2014) The role of cellulose nanocrystals in the improvement of the shape-memory properties of castor oil-based segmented thermoplastic polyurethanes. Compos Sci Technol 92:27–33.

15. Sun L, Huang WM, Lu H, et al (2014) Heating-Responsive Shape-Memory Effect in Thermoplastic Polyurethanes with Low Melt-Flow Index. Macromol Chem Phys 215:2430–2436.

16. Azra C, Ding Y, Plummer CJG, Månson J-AE (2013) Influence of molecular

architecture on the isothermal time-dependent response of amorphous shape memory polyurethanes. Eur Polym J 49:184–193.

17. Chen S, Hu J, Liu Y, et al (2007) Effect of SSL and HSC on morphology and properties of PHA based SMPU synthesized by bulk polymerization method. J Polym Sci Part B Polym Phys 45:444–454.

18. Sáenz-Pérez M, Lizundia E, Laza JM, et al (2016) Methylene diphenyl diisocyanate (MDI) and toluene diisocyanate (TDI) based polyurethanes: thermal, shape-memory and mechanical behavior. RSC Adv 6:69094–69102.

19. Li H, Luo Y, Gao X, et al (2017) Core–shell nano-latex blending method to prepare multi-shape memory polymers. Soft Matter 13:5324–5331.

20. Gu L, Cui B, Wu Q-Y, et al (2016) Bio-based polyurethanes with shape memory behavior at body temperature: effect of different chain extenders. RSC Adv 6:17888–17895.

21. Ge Z, Ren H, Fu S, et al (2017) Synergistic effects of zwitterionic segments and a silane coupling agent on zwitterionic shape memory polyurethanes. RSC Adv 7:42320–42328.

22. Sabzi M, Babaahmadi M, Rahnama M (2017) Thermally and Electrically Triggered Triple-Shape Memory Behavior of Poly(vinyl acetate)/Poly(lactic acid) Due to Graphene-Induced Phase Separation. ACS Appl Mater Interfaces 9:24061–24070.

23. Ji F, Zhu Y, Hu J, et al (2006) Smart polymer fibers with shape memory effect. Smart Mater Struct 15:1547–1554.

24. Wu S, Xu W, Balamurugan GP, et al (2017) Recovery behaviour of shape memory polyurethane based laminates after thermoforming. Smart Mater Struct 26:115002–115015.

25. Yu J, Xia H, Teramoto A, Ni Q-Q (2018) The effect of hydroxyapatite nanoparticles on mechanical behavior and biological performance of porous shape memory polyurethane scaffolds. J Biomed Mater Res Part A 106:244–254.

26. Lakatos C (2016) Segmented linear shape memory polyurethanes with thermoreversible Diels-Alder coupling: Effects of polycaprolactone molecular weight and diisocyanate type. Express Polym Lett 10:324–336.

27. Gu X, Mather PT (2012) Entanglement-based shape memory polyurethanes: Synthesis and characterization. Polymer (Guildf) 53:5924–5934.

28. Gao Y, Zhu G, Xu S, et al (2018) Biodegradable magnetic-sensitive shape memory poly(ε-caprolactone)/Fe3 O4 nanocomposites. J Appl Polym Sci 135:45652–45661.

29. Molavi, Fatemeh Khademeh, Ghasemi, Ismaeil, Massimo Messori ME (2017) Nanocomposites based on poly(l-lactide)/poly(ε-caprolactone) blends with triple-shape memory behavior: Effect of the incorporation of graphene nanoplatelets (GNps). Compos Sci Technol 151:219–227.

30. Qian C, Zhu Y, Dong Y, Fu Y (2017) Vapor-grown carbon nanofiber/poly(ethylene-co-vinyl acetate) composites with electrical-active two-way shape memory behavior. J Intell Mater Syst Struct 28:2749–2756.

31. Cai S, Sun Y-C, Ren J, Naguib HE (2017) Toward the low actuation temperature of flexible shape memory polymer composites with room temperature deformability *via* induced plasticizing effect. J Mater Chem B 5:8845–8853.

32. Alberto N, Fonseca MA, Neto V, et al (2017) Incorporation of fiber bragg sensors for shape memory polyurethanes characterization. Sensors (Switzerland) 17:2600–2611.

33. Mora-Murillo, LD, Orozco-Gutierrez, F, Vega-Baudrit, J, González-Paz R (2017) Thermal-Mechanical Characterization of Polyurethane Rigid Foams: Effect of Modifying Bio-Polyol Content in Isocyanate Prepolymers. J Renew Mater 5:220–230.

34. Parameswaranpillai J, Ramanan SP, Jose S, et al (2017) Shape Memory Properties of Epoxy/PPO–PEO–PPO Triblock Copolymer Blends with Tunable Thermal Transitions and Mechanical Characteristics. Ind Eng Chem Res 56:14069–14077.

35. Zhao X, Dong R, Guo B, Ma PX (2017) Dopamine-Incorporated Dual Bioactive Electroactive Shape Memory Polyurethane Elastomers with Physiological Shape Recovery Temperature, High Stretchability, and Enhanced C2C12 Myogenic Differentiation. ACS Appl Mater Interfaces 9:29595–29611.

36. Jeong HM, Ahn BK, Kim BK (2001) Miscibility and shape memory effect of thermoplastic polyurethane blends with phenoxy resin. Eur Polym J 37:2245–

2252.

37. Kim Y, Park H, Kim B (2015) Triple shape-memory effect by silanized polyurethane/silane-functionalized graphene oxide nanocomposites bilayer. High Perform Polym 27:886–897.

38. Xu W, Wu S, Balamurugan GP, et al (2017) Evaluating shape memory behavior of polymer under deep-drawing conditions. Polym Test 62:295–301.

39. Bayan R, Karak N, Pokhrel K, et al (2017) Renewable resource derived aliphatic hyperbranched polyurethane/aluminium hydroxide–reduced graphene oxide nanocomposites as robust, thermostable material with multi-stimuli responsive shape memory features. New J Chem 41:8781–8790.

40. Ban J, Mu L, Yang J, et al (2017) New stimulus-responsive shape-memory polyurethanes capable of UV light-triggered deformation, hydrogen bond-mediated fixation, and thermal-induced recovery. J Mater Chem A 5:14514–14518.

41. Zhang Z, Qi X, Li S, et al (2018) Water-actuated shape-memory and mechanically-adaptive poly(ethylene vinyl acetate) achieved by adding hydrophilic poly (vinyl alcohol). Eur Polym J 98:237–245.

42. Zhao Z, Peng F, Cavicchi KA, et al (2017) Three-Dimensional Printed Shape Memory Objects Based on an Olefin Ionomer of Zinc-Neutralized Poly(ethylene- *co* -methacrylic acid). ACS Appl Mater Interfaces 9:27239–27249.

43. Chai Q, Huang Y, Kirley TL, et al (2017) Shape memory polymer foams prepared from a heparin-inspired polyurethane/urea. Polym Chem 8:5039–5048.

44. Saleeb AF, Natsheh SH, Owusu-Danquah JS (2017) A multi-mechanism model for large-strain thermomechanical behavior of polyurethane shape memory polymer. Polymer (Guildf) 130:230–241.

45. Sonseca Á, Camarero-Espinosa S, Peponi L, et al (2014) Mechanical and shape-memory properties of poly(mannitol sebacate)/cellulose nanocrystal nanocomposites. J Polym Sci Part A Polym Chem 52:3123–3133.

46. Li H, Luo Y, Gao X, et al (2017) Core–shell nano-latex blending method to prepare multi-shape memory polymers. Soft Matter 13:5324–5331.

47. Uto K, Ebara M (2017) Magnetic-Responsive Microparticles that Switch Shape at 37 °C. Appl Sci 7:1203–1211.

Chapter V.

RESULTS AND DISCUSSION. III. PERMEABILITY BEHAVIOR

"¿Qué sería de la vida si no tuviésemos el coraje de intentarlo?"

Vincent van Gogh

Chapter V

RESULTS AND DISCUSSION. III. PERMEABILITY BEHAVIOR

5.1. Introduction

Permeability behavior of the shape memory polyurethanes is described in the following chapter. Barrier materials owns the ability to restrict the passage of gases, vapors, and organic liquids through their boundaries [1–3]. Polymeric materials dominate the barrier materials used in textile industry, being also found in other applications ranging from packaging industry to window films, because of their superior properties and low cost. The permeability or gas (vapor) transmission rate through any polymeric material is dependent upon two factors: the gas (or vapor) solubility and the rate of diffusion through the barrier. The solubility is dependent upon the chemical relationship between the permeant molecule (gas or vapor) and the polymer (barrier material); whilst the rate of diffusion is dependent upon the size of the permeant

molecule and the amorphous configuration of the barrier polymer. The permeability coefficient measures the relative permeation behavior, and it is used to compare the permeability of different polymers. Permeability coefficient, in general, is defined as the amount of permeant molecule transported through a membrane, per unit area and time, under the action of a driving force gradient unit. This driving force gradient must be expressed in terms of a variable which is measured outside the membrane, such as pressure or concentration [4,5]. The gases and vapors most often studied are water vapor, oxygen, carbon dioxide, and nitrogen. In this work, to measure permeability water vapor, oxygen and limonene vapor were used.

Water vapor permeability is defined as fabric's ability to transport water vapor from skin surface through fabric to external environment [6,7]. This water vapor can be transferred by diffusion of water vapors through layers; by absorption, transmission and desorption of water vapor by fibers; by adsorption and migration of water vapor along fiber surface; and by transmission of water vapor by forced convection. Water vapor transmission rate (WVTR) of shape memory polyurethanes (SMPUs) is of great importance when these SMPUs are going to be used in the textile sector, e.g., for the manufacture of shoes and garments [8–11]. In order to keep the human body warm and comfortable, shoes and garments should have high WVTR values, which allows perspiration to evaporate promptly, especially when human bodies are in hot environments. Thus, relative humidity inside the shoes and garments will decrease when water vapor transfers through the SMPUs into the environment. In this way, the water vapor transport properties of textile fabrics are of considerable importance to determine the thermal comfort properties of clothing systems. During heavy work or in hot environments, a high degree of water vapor permeability (high WVTR) of the clothing materials supports the moisture transfer from the wearer skin through the textile layers into the environment. Human body produces heat in the form of sweat during its activity, and permeability is used to evaporate sweat, resulting in the dissipation of heat and cooling of the body. However, if water vapor cannot escape to atmosphere then relative humidity (RH) inside clothing increases, causing discomfort. Hence, knowledge of water vapor transmission is necessary [12,13].

There are various test methods available for measuring water vapor permeability of the fabrics. They differ in the construction mechanisms, test conditions, measurement parameters, and units [8]. Water vapor transmission rate, WVTR, is reported as the grams of water that will pass through a given area of

material in a specified time. Therefore, the usual units are grams per square meter per day at a specified temperature and relative humidity ($g \cdot mm \cdot m^{-2} \cdot day^{-1}$).

Other gas analyzed to test how shape memory polyurethanes behave was oxygen. Permeability of oxygen, P_{O2}, is a very important parameter which must be controlled, not only in textile applications, but also in package applications. In the case of packaging, if oxygen is allowed to go into a package, it will break down organic compounds initiating or accelerating the decay process. Uncontrolled, this will promote food staleness and loss of nutritive value. In the case of fresh meat, a high rate of oxygen transmission is required to maintain the bright red color of meat. To meet this special requirement, special grades of cellophane, polyethylenes, and nitriles have been developed to provide the low water vapor transmission needed to avoid drying the meat while providing high oxygen transmission to maintain the color. This phenomenon of high transmission for oxygen combined with low transmission of water seems paradoxical but is very critical to these specialized needs [14,15]. Permeability oxygen transmission is usually reported in cubic centimeters of gas that pass through a square meter of film in 24 h when the gas pressure differential on one side of the film, at a specified temperature, is one atmosphere greater than on the other side ($cm^3(STP) \cdot cm \cdot cm^{-2} \cdot s^{-1} \cdot cm\ Hg^{-1}$).

Finally, limonene vapor transmission rate (LVTR) was measured. LVTR measurements were only performed with some shape memory polyurethanes. Limonene is a natural cyclic monoterpene, a clear colorless liquid at room temperature. Limonene, the naturally occurring chemical which is the major component in oil of oranges, is widely used as a flavor and fragrance. As it is known, odor is a relevant problem in footwear field, so that, it was considered that limonene would be an interesting molecule to analyze its permeability [16,17]. The units of limonene vapor transmission rate are the same as the water vapor transmission rate because the procedure of analysis is the same ($g \cdot mm \cdot m^{-2} \cdot day^{-1}$).

5.2. Characterization of permeability behavior of shape memory polyurethanes

There are different test methods for measuring the permeability of the shape memory polyurethanes performed in this work. The following measurements were

carried out at the Polymer Science and Technology Department of the University of the Basque Country (UPV/EHU) in Donostia – San Sebastian. As mentioned above, water vapor, oxygen and limonene vapor were used to know the permeability of the shape memory polyurethanes. This study was carried out in the systems S4 (PTMG650MDI) and S7 (PTMG1000MDI), as well as in some samples of system S8 (PTMG1000MDITDI_4 and PTMG1000MDITDI_5) and system S10 (PTMG1000MDITDI_4_1 and PTMG1000MDITDI_5_1).

5.2.1. Water vapor transmission rate

The analysis of water vapor permeability was carried out by the gravimetric method. This gravimetric method allows to measure permeability of vapors and liquids. The used cell was made of Teflon, chemically inert (*Figure 5.1*). The schematic diagram of the permeability cell used to evaluate water permeability is shown in *Figure 5.2*. The weighing scale used was a Sartorius BP 210 D with a resolution of 10^{-5} g, and it was connected to a computer where time and weight loss were registered. The relative humidity (RH) was measured by a hygrometer, model HD 2017 TV.

In the gravimetric method, the only requirement is to maintain constant the water vapor pressure difference between both sides of the sample during the test, under specified temperature conditions (*Figure 5.2*). However, it does not regulate which side should be the high humidity side [18,19]. The cell was sealed to prevent vapor loss except through the test sample. An initial weight was measured in the weighing scale and then, the weight variation of the permeable cell was periodically weighed over time until results become linear. The weight loss was measured after 8 h. Attention should be paid in ensuring that all weight losses were due to water vapor transmission through the specimen. In summary, water vapor passes through the test film in determined conditions whilst weight loss was measured. At last, the water vapor permeability parameters were measured taking into account the sample area and thickness, the weighing interval, and the humidity difference on two sides of the sample. In these tests, the cell was placed in a chamber where the temperature was constant at 25 or 40ºC, depending on the experiment. Some of the samples were measured at both temperatures, 25 and 40ºC, because their glass transition temperatures were close to body temperature (T = 38ºC, horizontal line in some

figures), and it is important to evaluate WVTR below and above glass transition temperature. For each WVTR measurement, an average of three different readings was used. The result of WVTR was calculated using the equation *5.1* [17]*:*

$$\mathrm{WVTR} = \frac{\mathrm{m} \cdot \mathrm{l}}{\mathrm{A} \cdot (\mathrm{a_{int}} - \mathrm{a_{ext}})} \qquad (5.1)$$

Where *WVTR* is the water vapor transmission rate (g mm·m^{-2} day^{-1})

m is the slope of the straight line obtained representing weight loss versus time (g·day^{-1})

l is thickness of the film (mm)

A is the area of the film (2.54 10^{-4} m^2)

a_{int} is the humidity inside the cell, which is equal to 1 because water is in balance with its own vapor at working temperature

a_{ext} is the humidity outside the cell, relative humidity (RH = 0.5)

Figure 5.1. *Teflon cell*

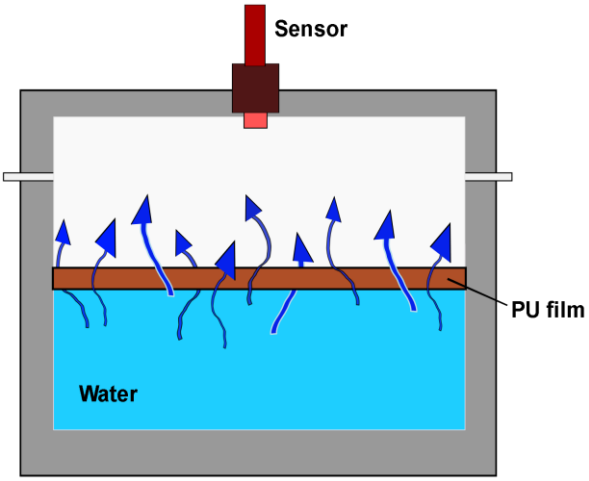

Figure 5.2. *Schematic diagram of permeability cell used to evaluate water permeation through films*

As mentioned above, WVTR was analyzed for system 4, system 7 (except for *n* = 1, 3.5), and also two samples of systems 8 and 10 in order to analyze and compare the effect of nanoparticles in the WVTR of SMPUs. All of them in the form of films (*Table 5.1).*

Table 5.1. *Composition of all the analyzed systems*

System	Polyol	Diisoyanate	Diol	n-TiO_2
4	PTMG (M_n = 650 g·mol^{-1})	MDI	1,4-BD	-
7	PTMG (M_n = 1000 g·mol^{-1})	MDI	1,4-BD	-
8	PTMG (M_n = 1000 g·mol^{-1})	TDI/MDI	1,4-BD	-
10	PTMG (M_n = 1000 g·mol^{-1})	TDI/MDI	1,4-BD	1 wt%

In *Table 5.2,* the WVTR values for system 4 are tabulated whereas *Figure 5.3* shows the representation of the WVTR values versus *n* at 25ºC and 40ºC. *Table 5.3* exhibits the WVTR values for system 7 and in *Figure 5.4* are shown WVTR at 25ºC and 40ºC. Moreover, in *Table 5.4* are tabulated the WVTR values for some samples of systems 8-10. Finally, in *Figure 5.5* is shown the comparative between system 4 and system 7 at 25ºC.

Table 5.2. *Results of WVTR for system 4 at 25ºC and 40ºC*

System 4	WVTR (g·mm·m^{-2} day^{-1}) at 25ºC	WVTR (g·mm·m^{-2} day^{-1}) at 40ºC	T_g (ºC)
PTMG650MDI_0.5	25.0±6.2	-	-10.2
PTMG650MDI_1	12.8±4.5	-	-3.0
PTMG650MDI_1.5	11.1±2.8	-	6.3
PTMG650MDI_2	12.0±1.8	-	10.9
PTMG650MDI_2.5	6.7±1.2	-	15.7
PTMG650MDI_3	4.0±1.2	-	23.1
PTMG650MDI_3.5	9.9 ±1.0	18.4±6.0	40.4
PTMG650MDI_4	9.4±0.9	10.1±4.2	46.6
PTMG650MDI_4.5	Films too brittle	-	62.4

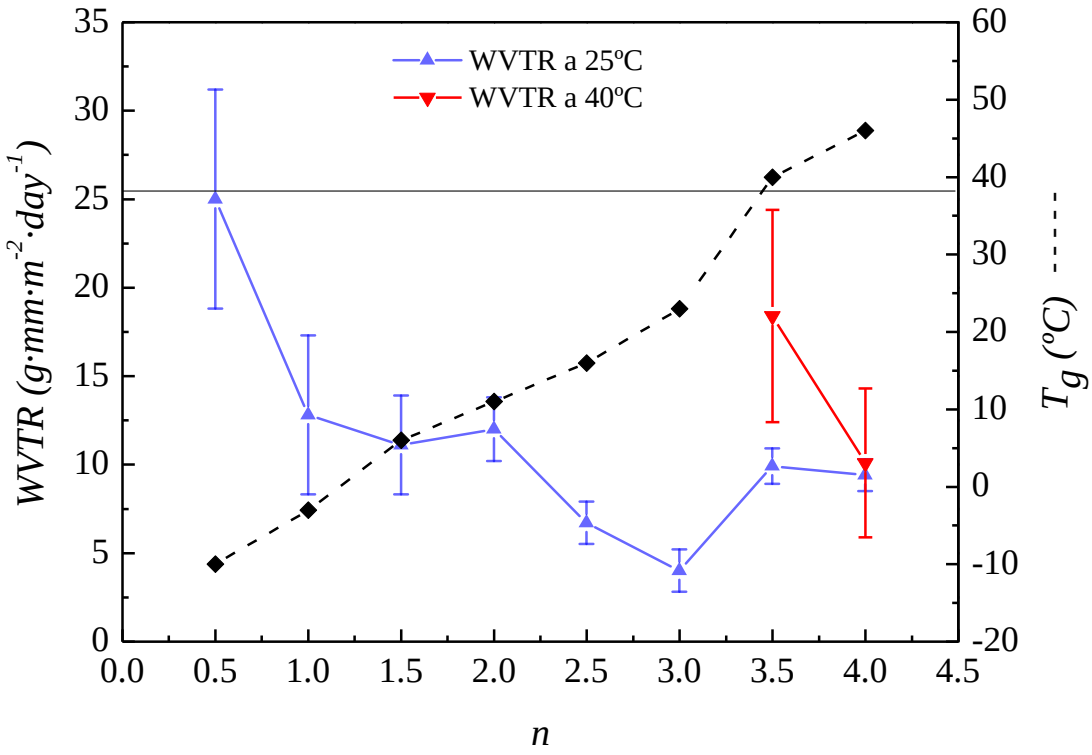

Figure 5.3. *WVTR at 25ºC and 40ºC for system 4*

Table 5.3. *Results of WVTR for system 7 at 25ºC and 40ºC*

System 7	**WVTR (g mm·m^{-2} day^{-1}) at 25ºC**	**WVTR (g mm·m^{-2} day^{-1}) at 40ºC**	**T_g (ºC)**
PTMG1000MDI_0.5	60.3±2.7	-	-30.9
PTMG1000MDI_1.5	37.9±0.6	-	-20.0
PTMG1000MDI_2	22.8±2.8	-	-18.4
PTMG1000MDI_2.5	28.1±0.5	-	-16.2
PTMG1000MDI_3	18.2±4.4	-	-12.5
PTMG1000MDI_4	15.2±3.1	-	-3.9
PTMG1000MDI_4.5	16.4±3.9	17.0±3.5	52.5

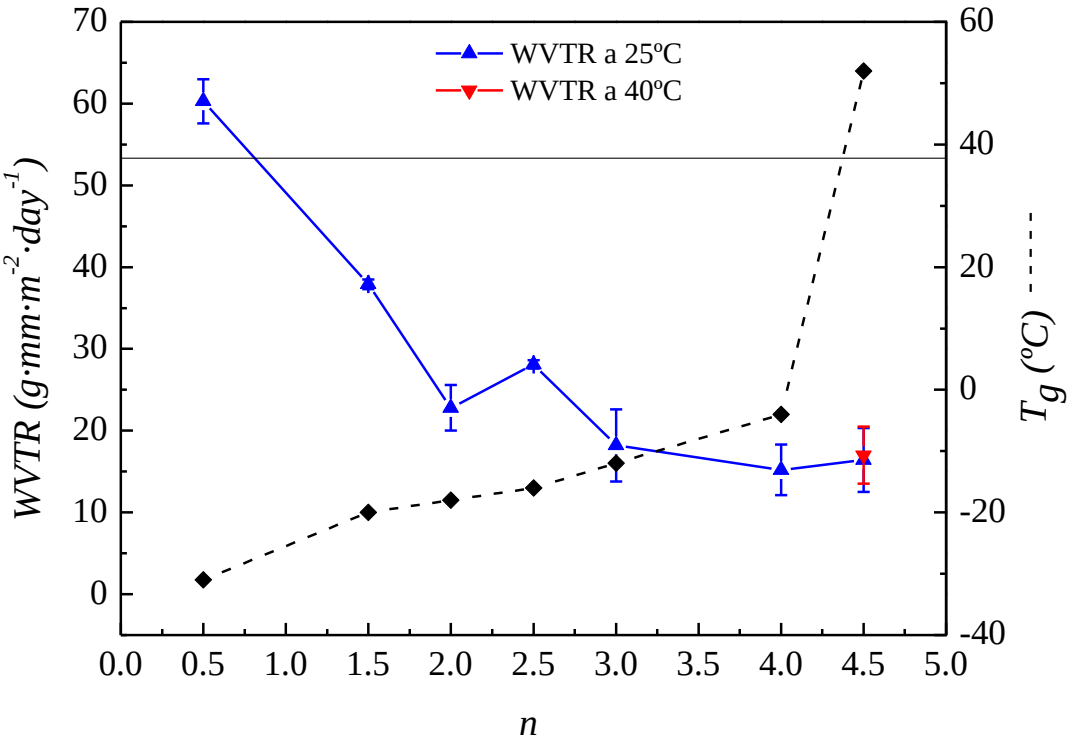

Figure 5.4. *WVTR at 25ºC and 40ºC for system 7*

Water vapor transmission rate of system 4 at 25ºC is represented in *Figure 5.3*. It can be seen that WVTR decreases from 25.0 to 9.4 g·mm·m^{-2}·day^{-1} while hard-segment content increases (n goes from 0.5 to 4). In system 7, a similar trend was observed (*Figure 5.4*). WVTR decreases from 60.3 to 16.4 g·mm·m^{-2}·day^{-1} when *n* increases from 0.5 to 4.5. All these samples from systems 4 and 7 are composed of PTMG, with M_n= 650 or 1000 g·mol^{-1}, respectively, MDI and BD. Therefore, in both systems, just varying *n* the NCO/OH relationship was modified. Once the NCO/OH ratio increases (i.e., the hard-segment/soft-segment ratio increases), WVTR decreases. This can be due to the fact that the presence of a high number of hard-segments surrounding the soft-segments difficult the water vapor transmission [8]. Moreover, when polyurethanes are slightly crosslinked the polymeric chains are positioned close to each other. Then, the free space for water vapor passage is limited, resulting in a reduction of WVTR. Therefore, WVTR was reduced because the water vapor pathway was restricted, not only due to the hard-segment/soft-segment ratio increasing, but also to the crosslinking caused by the reaction of the hardener

NCO group with the urethane/urea [20]. Actually, polyurethanes with higher hard-segment exhibited the greatest reduction in WVTR.

Furthermore, it is obvious that, in all analyzed samples, the WVTR of these films increases when temperature increases (from 25 to 40ºC), although in some of the cases this effect is not significant. Higher temperatures cause the soft-segments to become more flexible, so the water vapor molecule can pass through more readily [21]. Indeed, with the increase in the temperature, the motion of soft-segment molecular chains results in a significant increase in the free volume. Such increase in free volume can provide more paths for water vapor to pass through the films. Thus, WVTR increases with the increase of temperature (e.g. for PTMG1000MDI_4.5 sample in system 7, WVTR increases from 16.4 to 17.0 $g \cdot mm \cdot m^{-2} \cdot day^{-1}$ when temperature rises from 25 to 40ºC). Therefore, it is evident that as these polyurethane films are temperature-sensitive in the measured temperature range from 25 to 40ºC (its glass transition temperature is within or near these values), the smart water vapor permeability of the SMPU films mainly depends on the increase in the free volume, that is, depends on the microstructure and morphology of the materials.

Finally, water vapor transmission rate was analyzed for polyurethane films with nanoparticles (1 wt% TiO_2) to test the effect of adding this component. *Table 5.4* shows the WVTR results obtained for two samples without (PTMG1000MDITDI_4, PTMG1000MDITDI_5) and with TiO_2 nanoparticles (PTMG1000MDITDI_4_1, PTMG1000MDITDI_5_1).

Table 5.4. *Results of WVTR for system 8 and 10*

Systems 8 and 10	**WVTR (g mm·m^{-2} day^{-1}) at 25ºC**	**T_g (ºC)**
PTMG1000MDITDI_4	9.8±0.9	23.8
PTMG1000MDITDI_5	5.3 ±0.8	40.2
PTMG1000MDITDI_4_1	6.4±0.3	30.8
PTMG1000MDITDI_5_1	8.4±0.1	40.6

Theoretically, the PU film should become less permeable to water vapor with the increase of TiO_2 nanoparticles content because the water vapor path is restricted. However, the WVTR results obtained were not conclusive. PTMG1000MDITDI_4

sample decreases its WVTR when nanoparticles were added, whereas PTMG1000MDITDI_5 sample behaves in the opposite way. This disparity in the WVTR results may be due to the synthesis procedure. If during the synthesis procedure the nanoparticles dispersion is not uniform, not homogenous films are obtained, causing errors in WVTR measurements. Therefore, no conclusions can be drawn from this study, although it seems that the presence of TiO_2 nanoparticles (1 wt%) do not have at important influence on the water vapor permeability of this kind of SMPUs [22].

Figure 5.5 shows the WVTR comparative study between system 4 (PTMG650) and system 7 (PTMG1000). In both systems, as mentioned above, it can be observed that WVTR decreases severely while hard-segment content increases (*n* increases). Moreover, it seems that the PTMG molecular weight affects the WVTR. In fact, WVTR values are higher when the PTMG molecular weight is larger (system 7) for all *n* values. Therefore, the soft-segment of polyurethane can be used as a water vapor channel for the development of breathable fabric and adhesives.

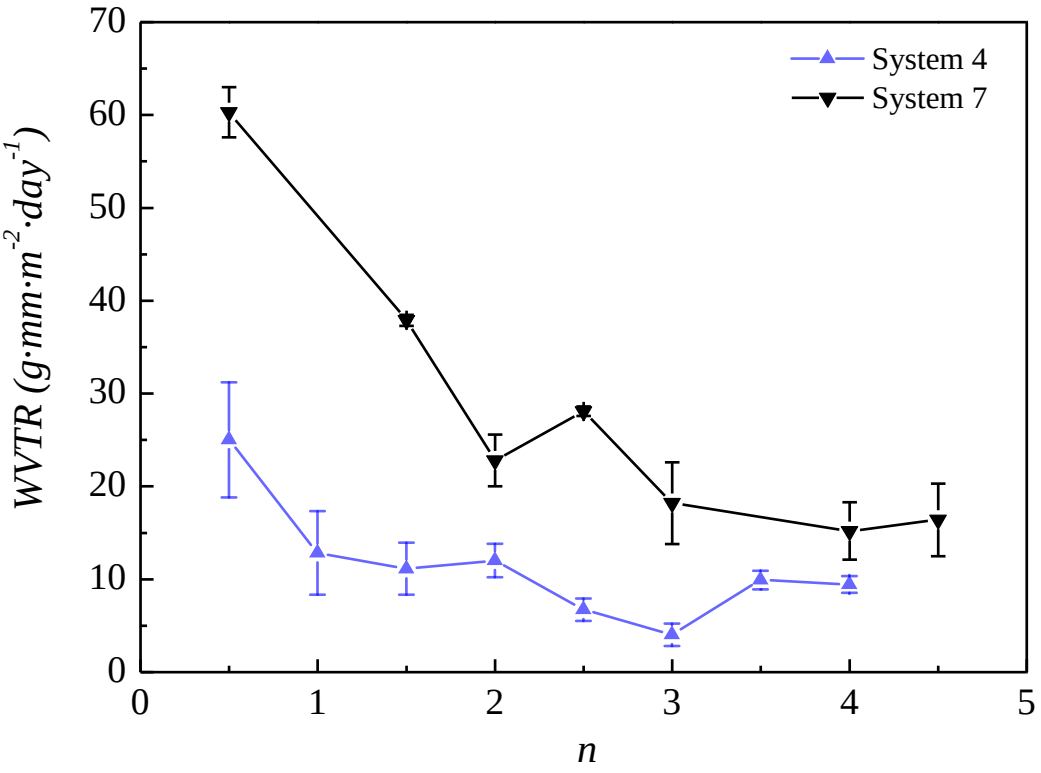

Figure 5.5. *Comparison between WVTR of system 4 and system 7 at 25ºC*

5.2.2. Oxygen Permeability

Oxygen transmission rate (*OTR)* is the steady state rate at which oxygen gas permeates through a film at specified conditions of temperature and relative humidity. Values are expressed in (cm^3(STP)·cm·cm^{-2}·s^{-1}·cm Hg^{-1}) [23,24].

The measurements of the oxygen permeability were done using a MOCON OX-TRAN Model 2/21 gas permeability tester (USA) in accordance with ASTM standard D3985 and ISO 15105-1,2. The oxygen permeability through the polyurethane films was tested at 760 mm Hg, 0% of relative humidity and 23ºC. The duration of the experiment was 24 h, and each OTR measurement was made twice. The result of OTR was calculated in Barrer (a non-SI unit of gas permeability used in the membrane technology):

$$1\ Barrer = 10^{-10} \cdot \frac{cm^3(STP) \cdot cm}{cm^2 \cdot s \cdot cm\ Hg}$$

ASTM Standard D3985 Test Method for OTR covers a procedure for determine the oxygen transmission steady state rate through plastics in different forms, including films. For homogeneous materials, it provides the determination of the oxygen gas transmission rate (OTR) and the oxygen gas permeability (P_{O2}). The oxygen gas transmission rate is determined after the sample has been equilibrated in a dry test environment. In this context, "dry" environment is considered to be one in which the relative humidity is RH < 1%. The equipment has two testing cells in order to realize two measurements at the same time. Each testing cell is divided into two chambers (*Figure 5.6*). The sample is mounted as a sealed semi-barrier between these two chambers at ambient atmospheric pressure. One chamber (the inside chamber) is slowly purged by a stream of a mixture of nitrogen and hydrogen, whereas the other (the outside chamber) contains oxygen. As the oxygen gas permeates through the polyurethane film, the nitrogen/hydrogen carrier gas transports it to the detector called Coulox. Then, it produces an electrical current that is converted by the computer into a magnitude proportional to the amount of oxygen flowing into the detector per unit time [25].

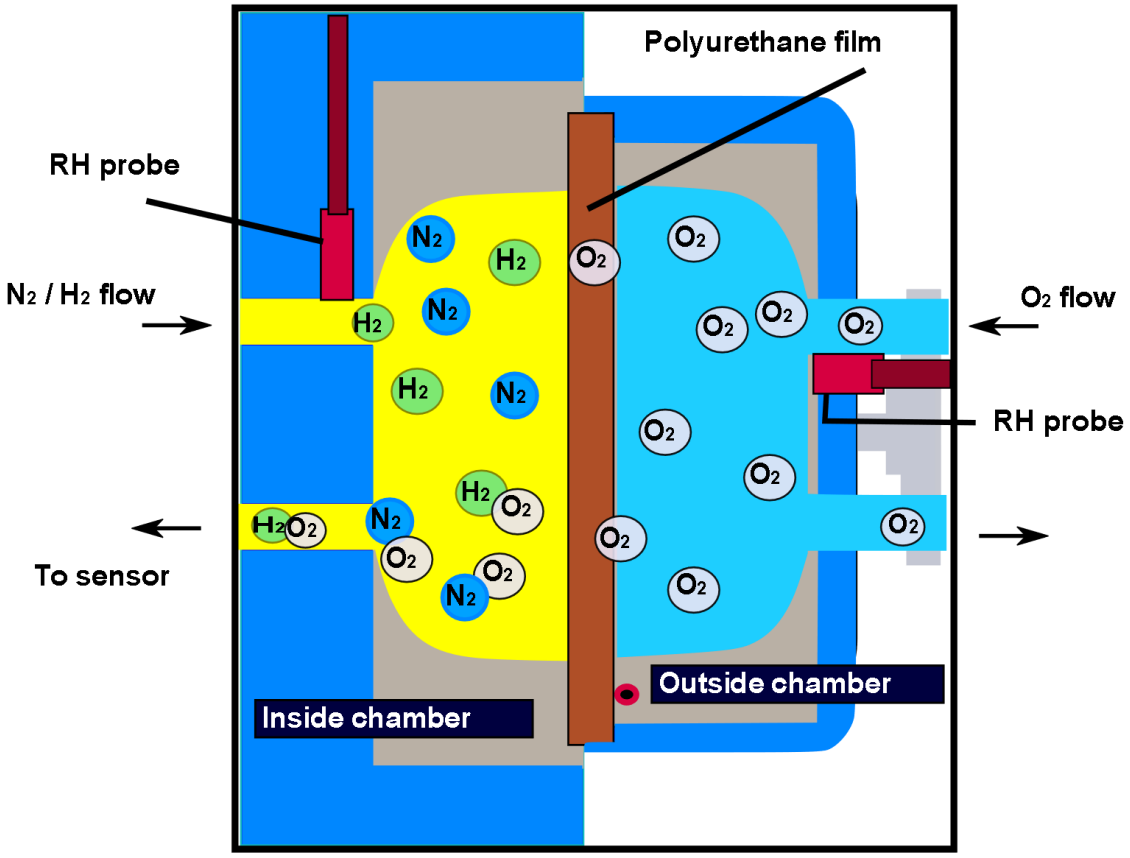

Figure 5.6. *Side view of test cell diagram (copyright MOCON)*

Table 5.5 and *Table 5.6* show the values of oxygen permeability (P_{O2}) for systems 4 and 7, respectively. Moreover, *Figure 5.7* and *Figure 5.8* represent the oxygen permeability for those systems at two different temperatures, 25ºC and 40ºC. As it can be seen, results for P_{O2} show a behavior similar to that of WVTR, previously reported. Thus, the oxygen permeability decreases when hard-segment content increases. For example, P_{O2} at 25ºC for systems 4 and 7 varied from 4.20 to 0.39 barrer and from 8.55 to 1.10 barrer, respectively, when *n* increases (hard-segment content rises). In addition, when the temperature increases up to 40ºC, the oxygen permeability increases in both systems. For example, from 0.46 to 0.7 barrer in system 4 (PTMG650MDI_3.5 sample), and from 1.1 to 1.6 barrer in system 7 (PTMG1000MDI_4.5 sample). This effect is due to a higher temperature causes the soft-segments to become more flexible such that the oxygen can pass through more readily [21,26].

Table 5.5. *Results of oxygen permeability for system 4 at 25ºC and 40ºC*

System 4	P_{O2} (barrer) at 25ºC	P_{O2} (barrer) at 40ºC	T_g (ºC)
PTMG650MDI_0.5	4.20±0.20	-	-10.2
PTMG650MDI_1	2.86±0.00	-	-3.0
PTMG650MDI_1.5	3.30±0.10	-	6.3
PTMG650MDI_2	1.19±0.00	-	10.9
PTMG650MDI_2.5	1.05±0.00	-	15.7
PTMG650MDI_3	0.50±0.00	-	23.1
PTMG650MDI_3.5	0.46±0.05	0.70±0.00	40.4
PTMG650MDI_4	0.39±0.05	0.53±0.02	46.6
PTMG650MDI_4.5	Films too brittle	-	62.4

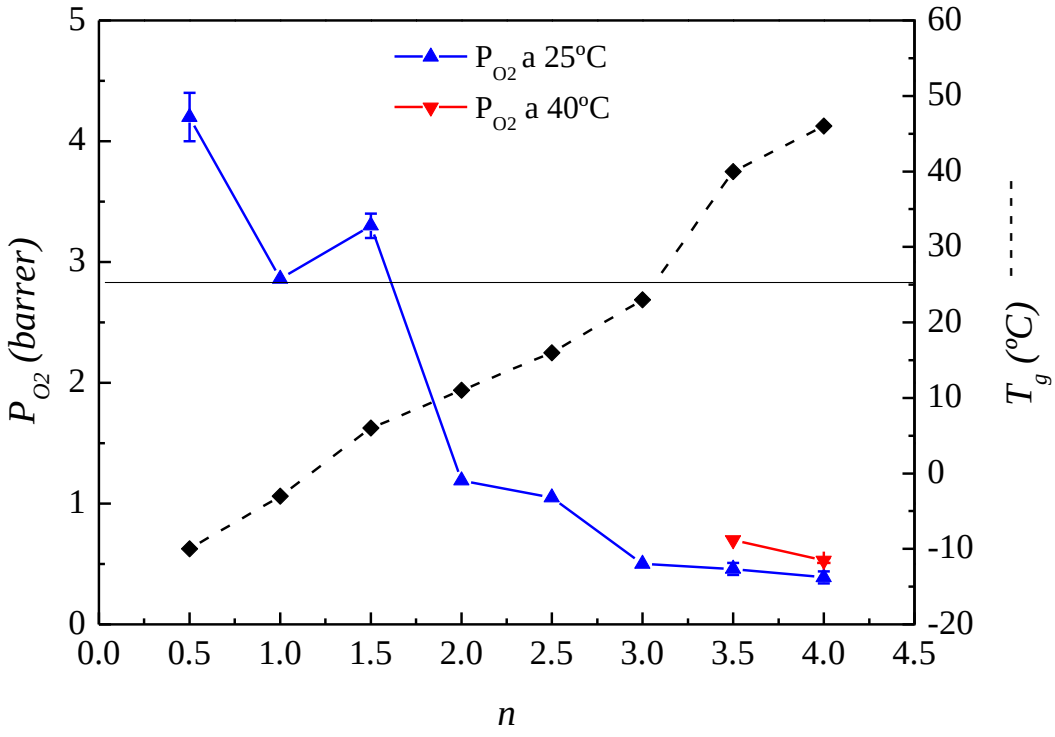

Figure 5.7. *Permeability of oxygen at 25ºC and 40ºC for system 4*

Table 5.6. *Results of oxygen permeability for system 7 at 25ºC and 40ºC*

System 7	P_{O2} (barrer) at 25ºC	P_{O2} (barrer) at 40ºC	T_g (ºC)
PTMG1000MDI_0.5	8.55±0.28	-	-30.9
PTMG1000MDI_1.5	6.31±0.33	-	-20.0
PTMG1000MDI_2	4.93±0.24	-	-18.4
PTMG1000MDI_2.5	4.30±0.15	-	-16.2
PTMG1000MDI_3	4.05±0.20	-	-12.5
PTMG1000MDI_3.5	3.09±0.25		-7.6
PTMG1000MDI_4	2.49±0.00	-	-3.9
PTMG1000MDI_4.5	1.10±0.02	1.6±0.80	52.5

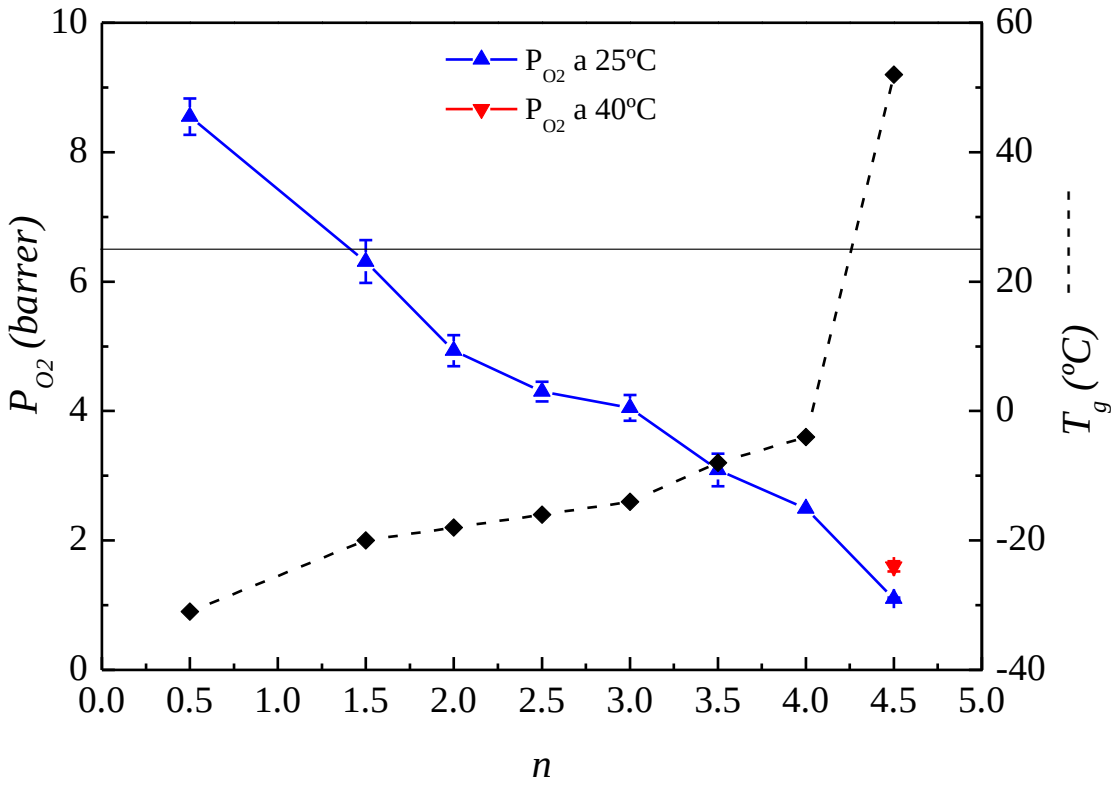

Figure 5.8. *Permeability of oxygen at 25ºC and 40ºC for system 7*

Table 5.7 presents the measurements of oxygen permeability for some samples of systems 8 and 10 in order to test the behavior of the material with and without nanoparticles. As it can be seen, oxygen permeability almost does not change when polyurethane films with TiO_2 nanoparticles were analyzed. This behavior is similar to that already reported for the water vapor transmission rate. At this point, it should be taken into account that, as mentioned in the section *5.2.1*, the synthesized films were heterogeneous and nanoparticles were not well dispersed [27].

Table 5.7. *Results of oxygen permeability for system 8 and 10*

Systems 8 and 10	**P_{O2} (barrer) at 25ºC**	**T_g (ºC)**
PTMG1000MDITDI_4	1.8±0.10	23.8
PTMG1000MDITDI_5	0.8±0.00	40.2
PTMG1000MDITDI_4_1	1.6±0.00	30.8
PTMG1000MDITDI_5_1	1.5±0.07	40.6

Oxygen permeability at 25ºC for systems 4 and 7 is shown in *Figure 5.9.* The only difference between these two systems is the soft-segment content. In both systems the soft-segment was PTMG, but M_n = 650 g·mol^{-1} for system 4 whilst M_n = 1000 g·mol^{-1} for system 7. It can be seen that the oxygen permeability of the polyurethane films was affected dramatically by the soft-segment content, which it is related to the PTMG molecular weight. In this way, the soft-segment content increases with the increase of molecular weight. Thus, for n = 0.5, values of oxygen permeability double, from 4.20 to 8.55 barrer for M_n = 650 g·mol^{-1} and M_n = 1000 g·mol^{-1}, respectively. This is because when molecular weight increases, the motion of soft-segment molecular chain results in a significant increase in paths for oxygen to pass through the films.

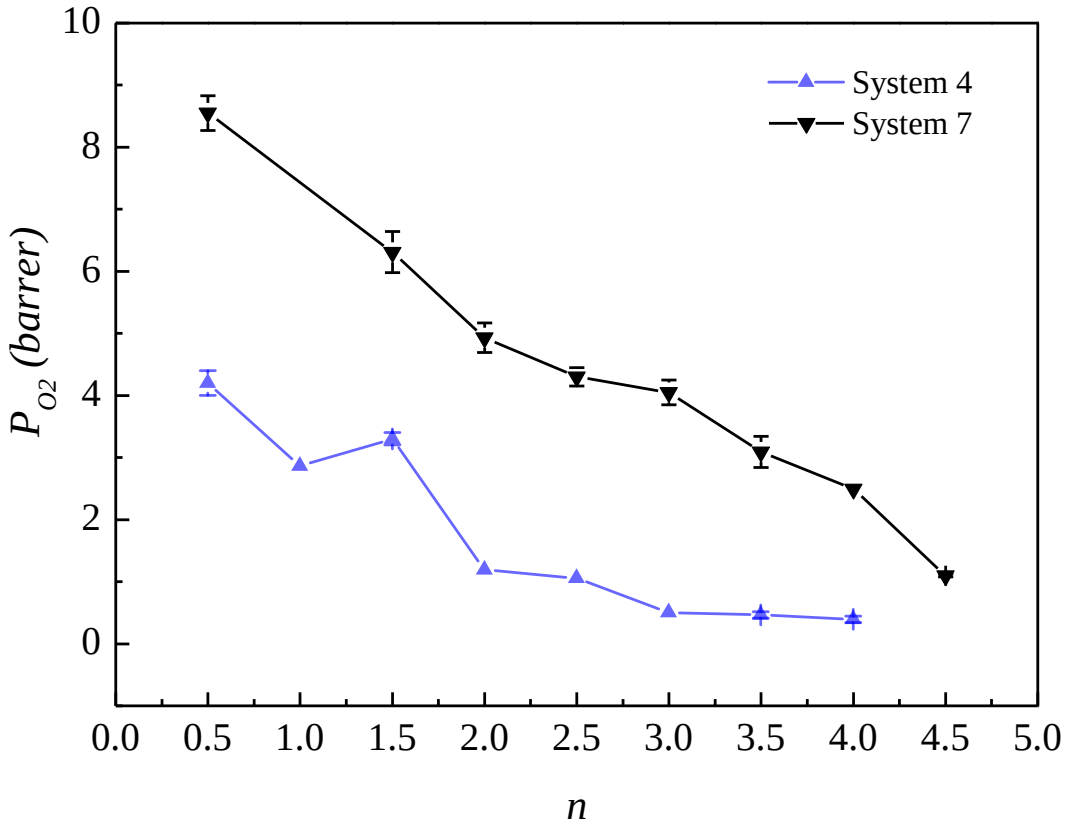

Figure 5.9. *Comparison between oxygen permeability for system 4 and system 7 at 25ºC*

5.2.3. Limonene vapor transmission rate

One of the main objectives in footwear sector is to improve the properties of shoes regarding the aroma, due to the problems generated for the odor inside shoes [28]. Therefore, it was thought that permeability of other gas which owns aroma, like limonene vapor, could be measured. Thus, limonene vapor transmission rate (LVTR) was also measured. The monoterpene is a naturally occurring chemical which is the major component in oil of orange. Currently, d-limonene is widely used as a flavor and fragrance (*Figure 5.10*) [29,30].

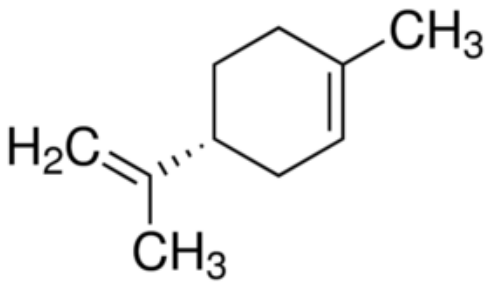

Figure 5.10. *Molecular structure of limonene*

The analysis of limonene vapor permeability was carried out by a gravimetric method in the same way as for water vapor permeability, already explained in section *5.2.1.* In these tests, the cell was placed in a chamber where the temperature was kept constant at 25ºC, as it is shown in *Figure 5.11.* The weight loss was measured after 8 h. LVTR measurement was only realized once in all samples and some of them were repeated twice. This was because this new procedure was realized for the first time in laboratories of Donostia-San Sebastian and the behavior of limonene in this method to calculate the permeability was unknown. The result of LVTR was calculated using the following equation:

$$\mathrm{LVTR} = \frac{\mathrm{m} \cdot \mathrm{l}}{\mathrm{A} \cdot (\mathrm{a_{int}} - \mathrm{a_{ext}})} \qquad (5.1)$$

Where *LVTR* is limonene vapor transmission rate (g mm·m^{-2} day^{-1})

m is the slope of the straight line obtained representing weight loss versus time (g·day^{-1})

l is thickness of the film (mm)

A is the area of the film (2.54 10^{-4} m^2)

a_{int} is the humidity inside the cell, the wet side of the specimen, RH = 1 because limonene is in balance with its own vapor at working temperature.

a_{ext} is the humidity outside the cell, the dry side of the specimen. Relative humidity (RH) ≅ 0 because in this area, the concentration of limonene is practically 0.

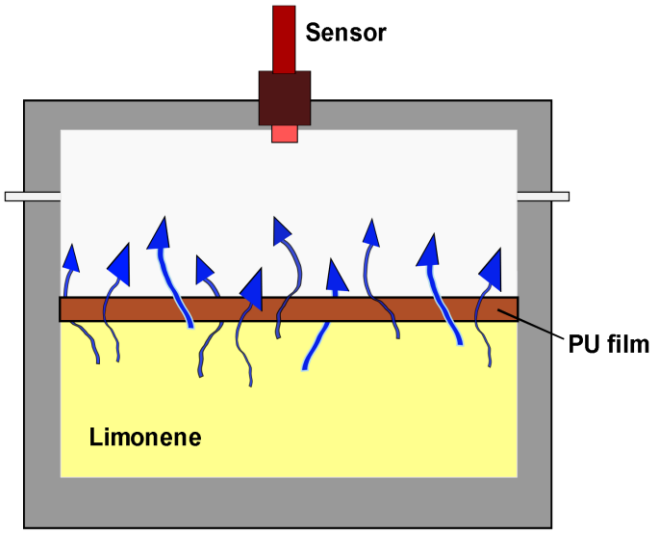

Figure 5.11. *Schematic diagram of permeability cell used to evaluate limonene permeation through films*

In *Table 5.8* and *Table 5.9* are tabulated the results of the experiments of limonene vapor transmission rate for systems 4 and 7, respectively. *Figure 5.12* and *Figure 5.13* show the trends of LVTR for those systems. It can be seen that in system 4, the LVRT values do not seem to follow a clear trend because LVTR increases and decreases, whereas in system 7 LVTR decreases as hard-segment contents increases (*n* rises). Thus, a clear tendency is not appreciated. Theoretically, LVTR should decrease when hard-segment content increases just as it happens in system 7 and in the other permeabilities (water vapor and oxygen) calculated for these systems. This could be explained because in this method, vapor pressure at room temperature was not high enough to pass through the polyurethane films, so that the LVTR values were not reliable [31].

Limonene vapor permeability is relevant because this component is often used as a standard system to test aroma barrier. However, it has been checked that this method is not effective to measure limonene permeability of the SMPU films. Therefore, it seems necessary to optimize the method before repeating the measurements.

Table 5.8. *Results of LVTR for system 4 at 25ºC*

System 4	LVTR (g mm·m^{-2} day^{-1}) at 25ºC	T_g (ºC)
PTMG650MDI_0.5	2.0	-10.2
PTMG650MDI_1	1.0	-3.0
PTMG650MDI_1.5	1.1	6.3
PTMG650MDI_2	8.3	10.9
PTMG650MDI_2.5	15	15.7
PTMG650MDI_3	93	23.1
PTMG650MDI_3.5	103	40.4
PTMG650MDI_4	16	46.6
PTMG650MDI_4.5	Films too brittle	62.4

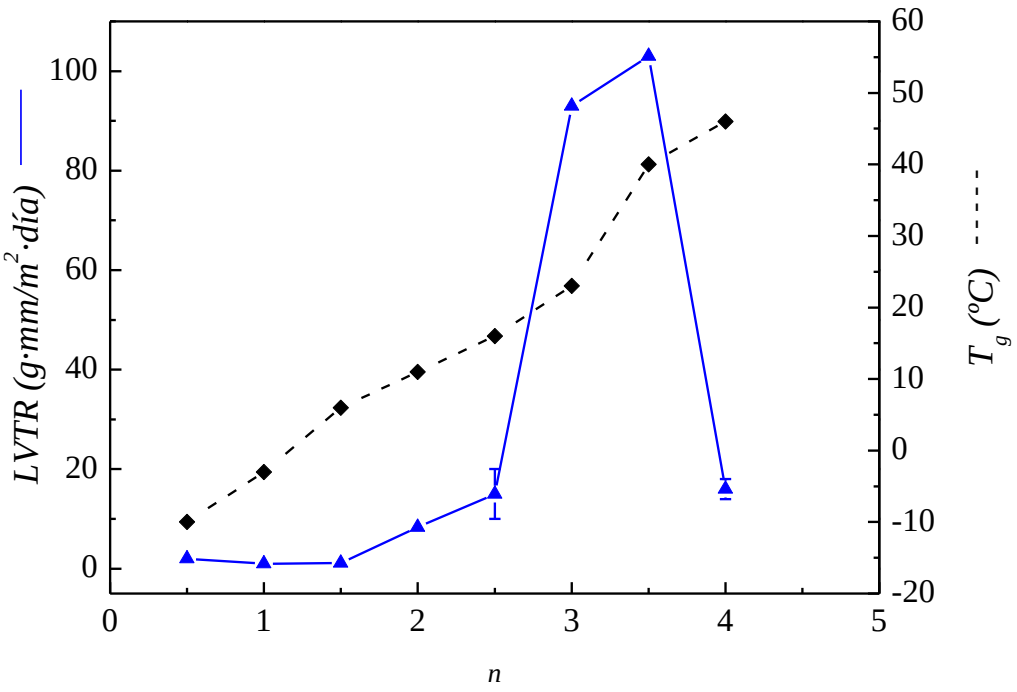

Figure 5.12. *LVTR at 25ºC for system 4*

Table 5.9. *Results of LVTR for system 7 at 25ºC*

System 7	LVTR (g mm·m^{-2} day^{-1}) at 25ºC	T_g (ºC)
PTMG1000MDI_0.5	52	-30.9
PTMG1000MDI_1.5	21	-20.0
PTMG1000MDI_2	23	-18.4
PTMG1000MDI_2.5	6	-16.2
PTMG1000MDI_3	2	-12.5
PTMG1000MDI_3.5	15	-7.6
PTMG1000MDI_4	12	-3.9
PTMG1000MDI_4.5	9	52.5

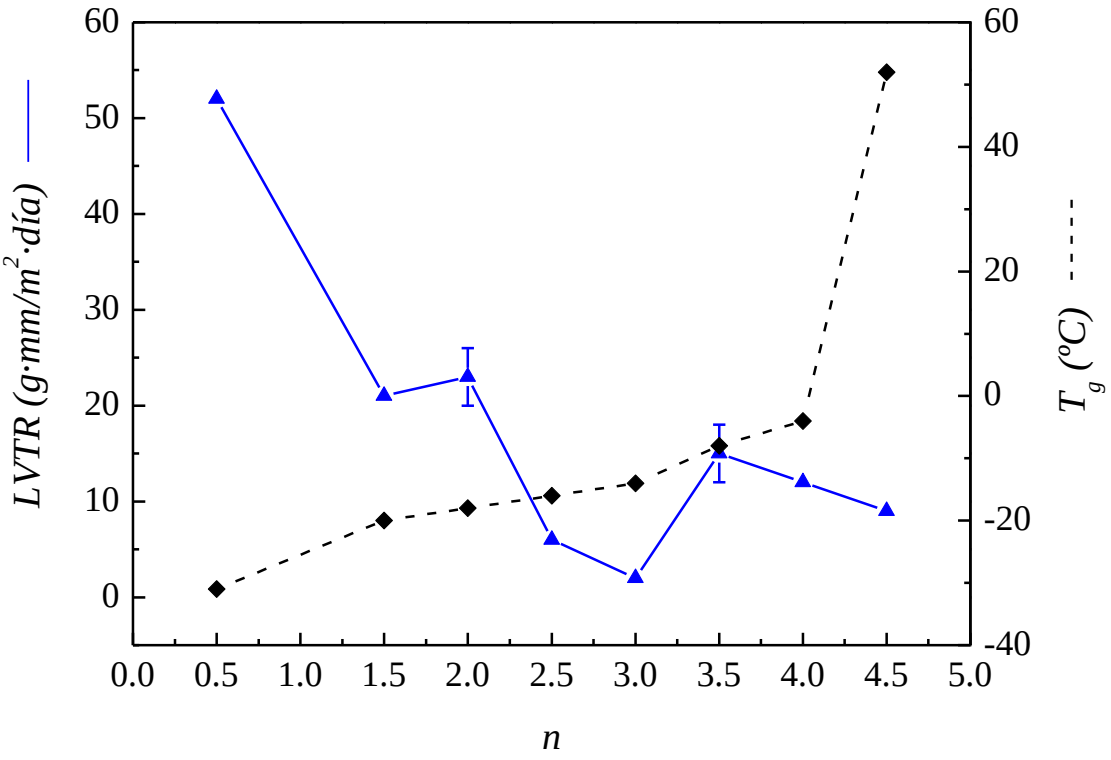

Figure 5.13. *LVTR at 25ºC for system 7*

Table 5.10 presents the results of limonene vapor transmission rate (LVTR) for some samples of systems 8 and 10. As mentioned in *sections 5.2.1* and *5.2.2*, LVRT values for the system 10 (samples with 1 wt% TiO_2 nanoparticles) should also decrease, not increase, when hard-segment content increases (*n* rises). However, the experimental results show just the opposite trend. Thus, for system 10, LVTR value increases from 17 to 63 barrer indicating that the measurement procedure was not correct and it is necessary to improve it.

Table 5.10. *Results of LVTR for system 8 and 10*

Systems 8 and 10	**LVTR (g mm·m^{-2} day^{-1}) at 25ºC**	**T_g (ºC)**
PTMG1000MDITDI_4	28±3	23.8
PTMG1000MDITDI_5	9 ±2	40.2
PTMG1000MDITDI_4_1	17±7	30.8
PTMG1000MDITDI_5_1	63±9	40.6

5.3. Conclusions

In this chapter, water vapor transmission rate (WVTR), oxygen transmission rate (OTR) and limonene vapor transmission rate (LVTR) were measured and analyzed in some polyurethane films. Used methods for water vapor and oxygen permeability have provided satisfactory results. On the contrary, LVTR measurements have not been completely correct due to a non-optimized procedure.

It can be concluded that water vapor transmission rate and oxygen permeability decrease when the hard-segment content in polyurethane increases. This may be due to a higher difficulty with the motion of the vapor molecules when they go through the film as the hard-segment content increases in the polyurethane matrix. This causes a lack of molecular mobility which makes the pass of gases through the film more difficult.

Besides, WVTR and OTR of polyurethane films increase as temperature increases (from 25 to 40ºC) in all analyzed samples, although in some cases this effect is not significant. It could be related to the flexibility of polymers, considering that an increase in the temperature leads to more movement in the soft-segment chains and thus, gases may pass through the polyurethane film more easily because of a significant increase in the free volume.

It is worth remarking that an increase in the molecular weight of the polyol (from 650 to 1000 $g \cdot mol^{-1}$), permeability rises too. Increasing the molecular weight, the length of the soft-segments increases, that is, the hard-segment/soft-segment ratio decreases. This behavior can be important for the development of breathable fabrics and adhesives, where the soft-segment of the polyurethanes may be used as channels to improve its permeability.

Furthermore, the variations of WVTR and oxygen permeability, when nanoparticles of TiO_2 were added, were not relevant. The problem seems to be the synthesis procedure because the obtained films with nanoparticles were not homogenous, presumably because of the mode of dispersion of small domains within the PU film so that, the values of permeability are not reliable.

Finally, the conclusion is that these shape memory polyurethane films have potential applications in different fields such as in textile sector that could promote sweat evaporation and humidity control. Moreover, barrier properties of polyurethane films make them promising candidates for food and pharmaceutical packaging applications. However, further studies are needed to improve the synthesis and processing method, for example, in order to increase the dispersion of the nanoparticles in the polyurethanes.

5.4. References

1. Hu J, Lu J (2015) Shape memory fibers. In: Handb. Smart Text. Springer Singapore, Singapore, pp 183–207

2. Hu J (2007) Shape memory polymers and textiles. Woodhead in association with the Textile Institute, Cambridge.

3. Ho WSW, Sirkar KK (1992) Membrane Handbook. Springer US, New York.

4. Yasuda H (1967) Basic consideration of permeability of polymer membrane to dissolved oxygen. J Polym Sci Part A-1 Polym Chem 5:2952–2956.

5. Freeman BD (1999) Basis of Permeability/Selectivity Tradeoff Relations in Polymeric Gas Separation Membranes. Macromolecules 32:375–380.

6. Hatch KL, Woo SS, Barker RL, et al (1990) In Vivo Cutaneous and Perceived Comfort Response to Fabric. Text Res J 60:405–412.

7. Onofrei E, Rocha AM, Catarino A (2011) The Influence of Knitted Fabrics' Structure on the Thermal and Moisture Management Properties. J Eng Fiber Fabr 6:10–23.

8. Jianhua Huang J, Xiaoming Qian X (2008) Comparison of Test Methods for Measuring Water Vapor Permeability of Fabrics. Text Res J 78:342–352.

9. Amini G, Samiee S, Gharehaghaji AA, Hajiani F (2015) Fabrication of Polyurethane and Nylon 66 Hybrid Electrospun Nanofiber Layer for Waterproof Clothing Applications. Adv Polym Technol 35:419–427.

10. Wan T, Stylios GK (2007) Shape Memory Training for Intelligent Fabrics. RJTA 11:11–17.

11. Smith WC (2010) Smart textile coatings and laminates. Woodhead Publishing Ltd, Cambridge.

12. Chung Y-C, Khiem ND, Choi JW, Chun BC (2014) Covalent Incorporation of Cellulose Derivative into Polyurethane Copolymers and the Effect on Crosslinking and Water Vapor Permeability. J Macromol Sci Part A 51:339–349.

13. Kim Y-J, Matsunaga YT, Nothdurft K, et al (2017) Thermo-responsive polymers and their application as smart biomaterials. J Mater Chem B 5:4307–4321.

14. Kalia S, Kaith BS, Kaur I (2011) Cellulose Fibers: Bio- and Nano-Polymer Composites: Green Chemistry and Technology. Springer, Berlin, Heidelberg.

15. Narayana H, Hu J, Kumar B, et al (2017) Stress-memory polymeric filaments for advanced compression therapy. J Mater Chem B 5:1905–1916.

16. Wu Y, Wang AH, Zheng RR, et al (2014) Laser-drilled micro-hole arrays on polyurethane synthetic leather for improvement of water vapor permeability. Appl Surf Sci 305:1–8.

17. Kasaai MR, Moosavi A (2017) Treatment of Kraft paper with citrus wastes for food packaging applications: Water and oxygen barrier properties improvement. Food Packag Shelf Life 12:59–65.

18. Sanchez-Garcia M, Lagaron J (2010) On the use of plant cellulose nanowhiskers to enhance the barrier properties of polylactic acid. Cellulose 17:987–1004.

19. Athimoolam M, Moorthy T V (2012) Polymer Nanocomposite Materials and Shape Memory Applications-A Review. Procedia Eng 38:3399–3408.

20. Kim E-Y, Lee J-H, Lee D-J, et al (2013) Synthesis and properties of highly hydrophilic waterborne polyurethane-ureas containing various hardener content for waterproof breathable fabrics. J Appl Polym Sci 129:1745–1751.

21. Lin C-Y, Liao K-H, Su C-F, et al (2007) Smart temperature-controlled water vapor permeable polyurethane film. J Memb Sci 299:91–96.

22. Ding XM, Hu JL, Tao XM, et al (2008) Morphology and water vapor permeability of temperature-sensitive polyurethanes. J Appl Polym Sci 107:4061–4069.

23. Fendler A, Villanueva MP, Gimenez E, Lagarón JM (2007) Characterization of the barrier properties of composites of HDPE and purified cellulose fibers. Cellulose 14:427–438.

24. Rubino M, Tung MA, Yada S, Britt IJ (2001) Permeation of Oxygen, Water Vapor, and Limonene through Printed and Unprinted Biaxially Oriented Polypropylene Films. J Agric Food Chem 49:3041–3045.

25. Sardon H, González A, Fernández-Berridi MJ, Irusta L (2015) Oxygen Barrier Properties of Waterborne Polyurethane/Silica Hybrids. J Macromol Sci Part B 54:711–721.

26. Ulubayram K, Hasirci N (1992) Polyurethanes: effect of chemical composition on mechanical properties and oxygen permeability. Polymer (Guildf) 33:2084–2088.

27. Kim D, Lim M, Kim I, et al (2014) Preparation and properties of hydrophobic layered silicate-reinforced UV-curable poly(urethane acrylate) nanocomposite films for packaging applications. Prog Org Coatings 77:1045–1052.

28. Sanchez-Garcia MD, Lopez-Rubio A, Lagaron JM (2010) Natural micro and nanobiocomposites with enhanced barrier properties and novel functionalities for food biopackaging applications. Trends Food Sci Technol 21:528–536.

29. Cava D, Catala R, Gavara R, Lagaron JM (2005) Testing limonene diffusion through food contact polyethylene by FT-IR spectroscopy: Film thickness, permeant concentration and outer medium effects. Polym Test 24:483–489.

30. Arrieta MP, López J, Hernández A, Rayón E (2014) Ternary PLA-PHB-Limonene blends intended for biodegradable food packaging applications. Eur Polym J 50:255–270.

31. Chung Y-C, Khiem ND, Choi JW, Chun BC (2015) Polyurethane membrane functionalization with the grafted cellulose derivatives to control water vapor permeability. Fibers Polym 16:492–502.

Chapter VI.

APPLICATION IN TEXTILES

"En ekvation jämställer två välkända ting och ger oss förståelsen av det tredje, det outsägbara"

"An equation equals two well-known things and gives us an understanding of the third, the unexplainable"

Faig Ahmed

Chapter VI

APPLICATION IN TEXTILES

6.1. Introduction

Shape memory polymers (SMPs), which can be stimulated by different external stimuli such as temperature, pH, chemicals or light [1,2], are defined as polymeric materials with the ability to sense and respond to these stimuli in a predetermined way (for example, changing their shape), as mentioned in *Chapter I* [3–6]. Thermoresponsive shape memory polymers can be designed taking polymer networks in which its polymer chains are able to fix a given deformation by cooling below a certain transition temperature. This transition temperature can be a glass transition or a melting point. Therefore, thermoresponsive SMPs can be triggered for promising applications in biomedicine, automotive, aerospace and also in the textile sector [7]. Different types of smart polymers have applications in textile technology. Among them, there are a variety of shape memory polymers that can be used in the textile sector with specific processing techniques, such as finishing,

spinning, weaving or laminating. In fact, in the textile sector, the use of SMPs is relatively new due to it is too hard to meet the stringent requirements on mechanical strength and thermal stability of fibers. This makes the majority of commercially available SMPs unsuitable for textile fibers [8,9]. Moreover, to make shape memory polymer fabrics, SMPs need to have a high molecular weight, suitable viscosity and melting point. Smart polymers used in textiles usually appear in various forms such as film, fiber, solution, microcapsules, nonwoven or gel to meet different processing requirements in textiles [10–13]. Functionalities, in textile sector, include aesthetic appeal, comfort, fantasy design (color changing), wound monitoring, smart wetting properties, and protection against extreme environmental variations. In recent decades, shape memory polyurethane (SMPU) fibers have aroused much attention because, in the form of fiber, SMPUs are more easily applied in textiles. SMPUs use their soft-segments as transition segments for the shape memory effect (SME) [14–21]. However, although many researchers have tried to develop the fibers from pellet, unfortunately it is too difficult to create monofilaments due to the specific properties of polyurethanes such as mechanical strength, viscosity, flexibility or elasticity [22–26].

The aim of this chapter was to prepare a kind of novel polyurethane fibers (*Figure 6.1*) with shape memory effect through thermal stimulus. From these fibers produced by melt spinning from different shape memory polyurethanes pellets, knitted fabric samples were then created.

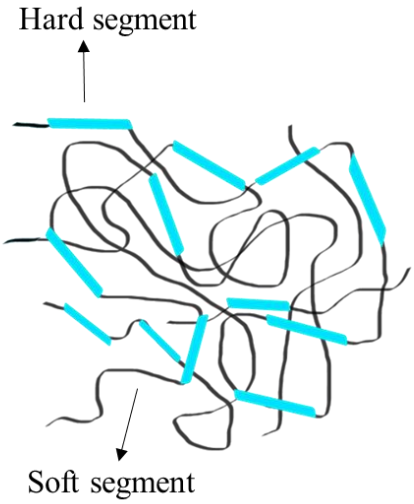

Figure 6.1. *Schematic representation of a polyurethane fiber*

Previously to the preparation of fibers, SMPUs were synthesized using the prepolymer method as explained in *Chapter II* [27,28], with a soft-segment glass transition temperature close to the body temperature. Moreover, a commercial polyurethane, named DIAPLEX MM4520, was also evaluated in order to make comparative studies between this polyurethane and the synthesized SMPUs. All the SMPUs were characterized by different techniques such as thermogravimetric analysis (TGA), differential scanning calorimetry (DSC), dynamic mechanical analysis (DMA) and tensile test. On the other hand, shape memory capabilities of the developed fabrics were measured by thermomechanical analysis (TMA).

In this chapter, the applications of shape memory polyurethanes in textiles and the clothing sector are elucidated. Furthermore, the associated constraints on fabrication of textiles and their potential applications in the near future are discussed. Therefore, the obtained results show that these fibers could be attractive candidates for potential applications, such as breathable fabrics, moisture management textiles and biomedical wearable devices (*Figure 6.2*).

Figure 6.2. *Applications of the fibers produced*

6.2. Preparation of SMPU fibers and fabrics

In this section, and considering that the employed materials (polyol, diisocyanates, chain extender...), the polyurethane synthesis and characterization methods have already been described in *Chapter II*, only the preparation of the SMPU fibers and fabrics are explained. Fibers and fabrics were prepared in the department of Textile Technology, faculty of textiles at University of Borås (Sweden). *Table 6.1* shows the different shape memory polyurethanes that are studied in this chapter.

Table 6.1. *SMPUs used for producing fibers and textiles (n = 4.5, 3 and 2.5)*

Sample code	Polyol	Diisocyanate	BD
PTMG1000TDI	1	5.5	4.5
PTMG650TDI	1	4	3
PTMG650MDITDI	1	3.5*	2.5
MM4520		Commercial sample	

*50% weight of TDI and 50% weight of MDI

First, shape memory polyurethane pellets were dried in a vacuum oven for 1 hour at a temperature of 70ºC. After that, the SMPU fibers were prepared by a melt spinning method. For this purpose, a piston spinning machine was utilized (FOURNÉ Polymertechnik, Germany) followed by two godet rolls and a winding unit (*Figure 6.3*). Depending on the type of polyurethane, a different set of processing parameters, such as piston temperature (T_{pist}), volumetric flow rate (V_{pist}) of polymer melt and roller speeds (v_{r1}, v_{r2}), was used [29,30] (*Table 6.2*). In order to get monofilaments, a spinneret with a 0.5 mm diameter was attached at the outlet of the piston spinning machine. Before inserting the polymer in the piston machine, it was heated for 1.5 hours and then about 50 g of the polymer were used for each batch. After introducing the polymer into the piston machine, it took about 30-40 min before starting the actual spinning when the polymer strands started to come out of the spinneret. A specific speed of both take-off roller (r_1) and drawing roller (r_2) was adjusted according to the required draw down ratio. Samples with the same processing conditions were prepared to make drawn fibers with different draw ratios (DR= v_{r2} / v_{r1}). In this work, the used draw ratio was equal to 1 in the solid-state

over the two godet rolls. In this case, the first roll was heated to an appropriate temperature (T_{r1}) (around the glass transition temperature of each polymer, which is 38ºC for synthesized polyurethanes and 45ºC for the commercial one) and the second roll had the room temperature (T_{r2}) (25ºC) [31]. After drawing, the fibers were collected on bobbins at the take-up unit.

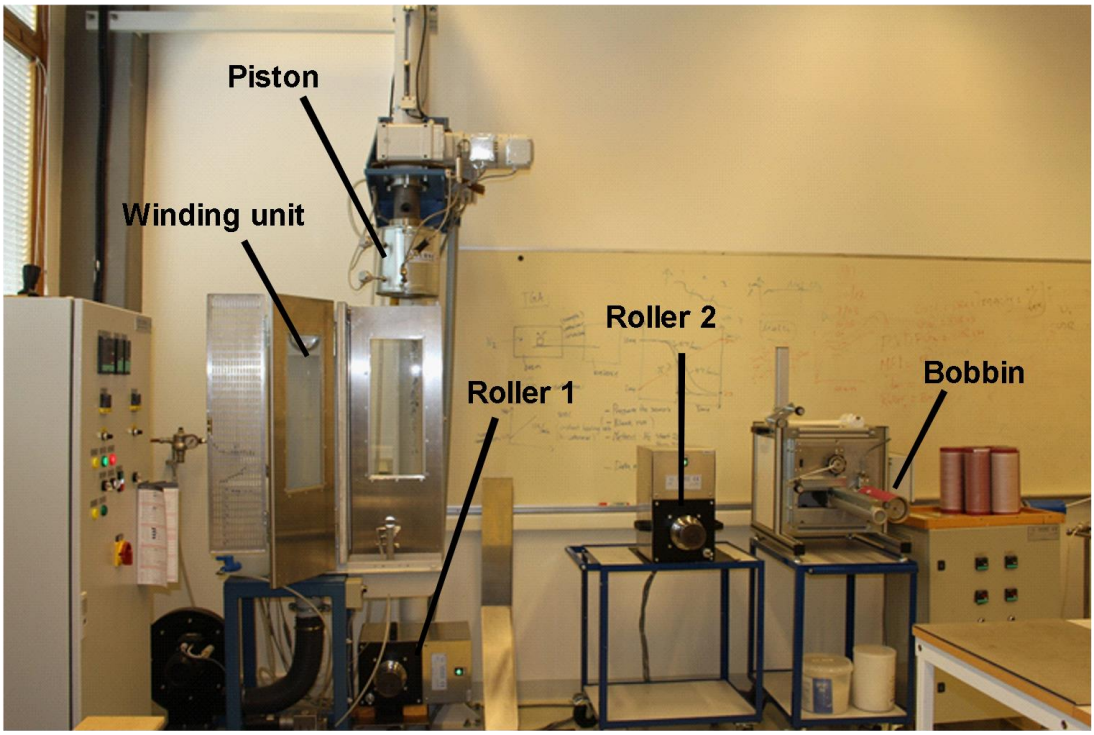

Figure 6.3. *Piston spinning machine used to produce fiber*

Table 6.2. *Summary of the suitable conditions for the piston spinning*

Sample code	Piston		Godet 1		Godet 2	
	V_{pist} ($cm^3 \cdot min^{-1}$)	T_{pist} (ºC)	v_{r1} ($m \cdot min^{-1}$)	T_{r1} (ºC)	v_{r2} ($m \cdot min^{-1}$)	T_{r2} (ºC)
PTMG1000TDI	0.6	190	10	40	10	25
PTMG650TDI	0.8	190	10	40	10	25
PTMG650MDITDI	0.7	205	10	40	10	25
MM4520	0.7	210	10	40	10	25

Once the fibers were produced, the textile structures were made in a Dubied hand driven knitting machine (*Figure 6.4*). The pattern of knitting is shown in *Figure 6.5*, and *Figure 6.6* shows the real fiber and fabric structure.

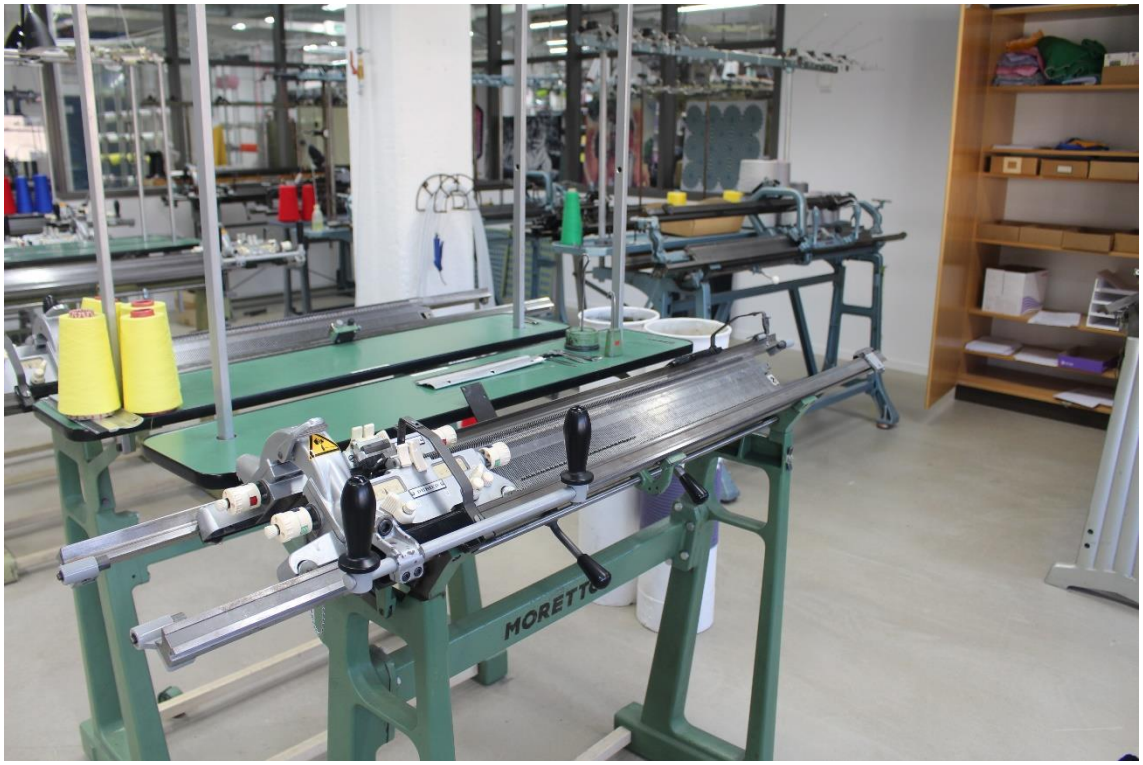

Figure 6.4. *Knitting machine used to produce fabrics*

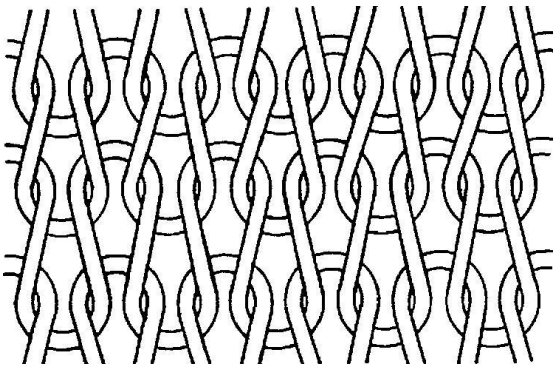

Figure 6.5. *Schematic representation of the polyurethane textile in a knitting machine*

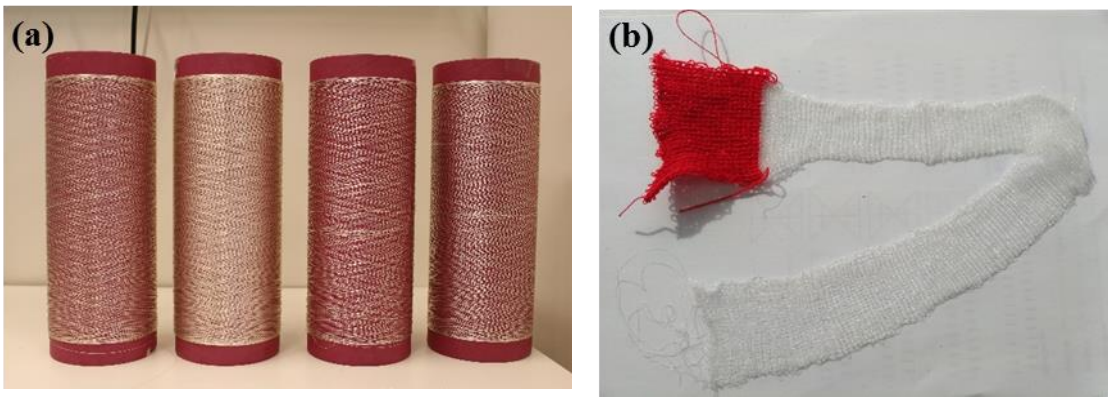

Figure 6.6. *Filament yarn (a) and fabric (b) from shape memory polyurethane produced in laboratory*

Fibers and fabrics were characterized using the same characterization techniques described in *Chapter II* such as thermogravimetric analysis (TGA), differential scanning calorimetry (DSC), dynamic mechanical analyses (DMA) and thermomechanical analyses (TMA). Polyurethane fibers were measured on a TA-Instruments DMA Q800, specific for fibers, at University of Borås, in a temperature range between -40 to 150ºC. Moreover, optical microscopic images of all polyurethane fibers were acquired using a Nikon SMZ800 at University of Borås. Finally, the tensile tests were carried out according to ISO 527 standard in a Tinius Olsen H10KT testing machine with extensometer in order to evaluate the mechanical properties of the fibers. Five dumbbell-shaped specimens were examined for each sample in the machine direction of the fibers. The gauge length was 100 mm while the test speed was 10 $mm \cdot min^{-1}$. The capacity of used load cell was 10 N.

6.3. Results and discussion

In order to evaluate the performance of the self-made fibers and fabrics, comparison experiments were carried out between polyurethane fibers, fabrics and pellets.

6.3.1. Thermogravimetric analysis (TGA)

The thermal stability of the synthesized and commercial polyurethanes, in the form of both pellet and fiber, was evaluated by TGA and derivative thermogravimetric (*DTG*) analysis. The initial decomposition temperatures ($T_{5\%}$), defined as the temperature at 5% weight loss; the temperatures at the maximum degradation rate ($T_{max,1}$, $T_{max,2}$ and $T_{max,3}$) for each degradation step, obtained from the minimum in DTG curves; and the weight percentages of residue remaining at the end of the degradation (*wt% residue*) are listed in *Table 6.3*. As an example, *Figures 6.7.a* and *6.7.b* show respectively the TGA and DTG curves for the PTMG650TDI in the form of both fiber and pellet. In *Figure 6.7.a* it can be seen a weight loss between 290 and 450ºC, which can be attributed to the decomposition of the SMPUs. On the one hand, the 5% weight loss of the SMPU pellets occurred between 284.6 and 323.8ºC. On the other hand, the 5% weight loss of the SMPU fibers occurred between 281.5 and 304.2ºC, which indicates that the thermal stabilities of all fibers are high enough for their use in textiles [32]. *Table 6.3* also shows that the wt% residue increases in polyurethane fibers in comparison with polyurethane pellets.

Therefore, it was demonstrated that the composite fibers were successfully fabricated and possessed stable thermal properties, which were determined by the network structure.

Table 6.3. *Thermal properties of synthesized and commercial polyurethanes*

Sample code		$T_{5\%}$ (ºC)	%wt residue	$T_{max,1}$ (ºC)	$T_{max,2}$ (ºC)	$T_{max,3}$ (ºC)
PTMG1000TDI	Pellet	284.6	2.54	322.4	414.9	-
	Fiber	281.5	5.88	307.2	418.1	-
PTMG650TDI	Pellet	285.9	1.06	328.7	418.7	-
	Fiber	284.2	3.92	319.3	408.0	-
PTMG650MDITDI	Pellet	296.1	4.43	332.7	360.4	425.7
	Fiber	293.9	8.61	317.0	340.3	425.3
MM4520	Pellet	323.8	9.05	341.4	380.0	426.1
	Fiber	304.2	11.39	315.1	360.7	409.5

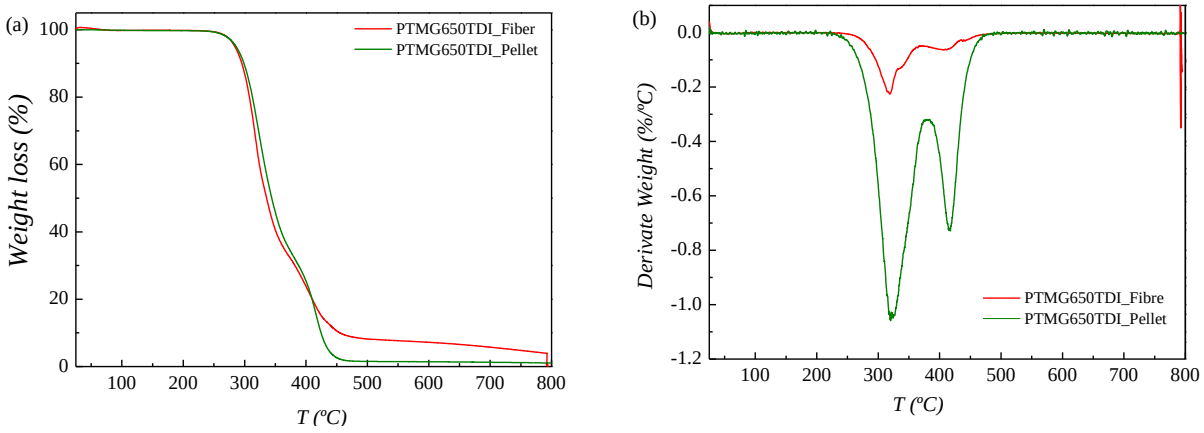

Figure 6.7. *Comparison of TGA (a) and DTG (b) curves for PTMG650TDI pellet and fiber polyurethanes.*

6.3.2. Differential scanning calorimetry (DSC)

In this study, the thermal properties of shape memory polyurethanes were tested by DSC. The comparison between DSC curves of the PTMG650TDI pellets and polyurethane fibers are shown, as an example, in *Figure 6.8*. Moreover, the detailed results of the DSC tests about all pellets and fibers are summarized in *Table 6.4*. The orientation of the developed soft-segments due to elongation during spinning increased the transition temperature, T_g. Therefore, the glass transition temperatures ($T_{g,DSC}$), measured in the second heating cycle, of the polyurethane fibers and pellets are similar to each other, except for those of PTMG1000TDI (deviation of 20ºC), although SMPU fibers showed a slightly higher T_g than that one for PU pellets due to elongation [11,33]. For example, for the commercial polyurethane MM4520, the T_g for the pellet form is 37.8ºC and for the fiber form is 39.7ºC. The same trend occurs for the synthesized ones, where T_g of PTMG650MDITDI pellets is 9.2ºC and for the fiber form is 9.9ºC. This result indicates that once the pellet entered into the piston spinning to produce fibers, the domains of the polymer are more ordered in the new fibers than in the original pellet, so that glass transition temperature is higher. It is evident that all polyurethanes are amorphous because of the absence of endothermic peaks as reported in literature [10,32].

Table 6.4. *Glass transition temperature and elastic modulus of synthesized and commercial polyurethanes*

Sample code		$T_{g,\ DSC}$ (ºC)	E'(MPa)	$T_{g,\ DMA}$ (ºC)
PTMG1000TDI	Pellet	-27.4	2068	37.9
	Fiber	-5.1	2592	61.3
PTMG650TDI	Pellet	6.6	2176	37.5
	Fiber	6.7	4718	59.2
PTMG650MDITDI	Pellet	9.2	2793	37.2
	Fiber	9.9	4483	59.5
MM4520	Pellet	37.8	3147	52.5
	Fiber	39.8	3125	64.3

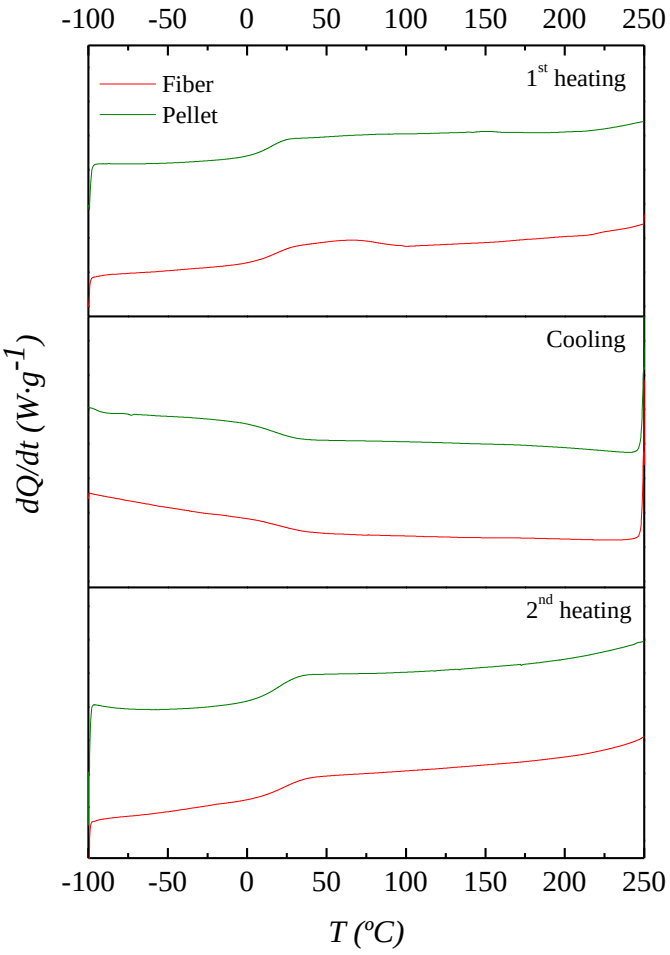

Figure 6.8. *Comparison of differential scanning calorimetric analysis of PTMG650TDI pellet and fiber polyurethanes*

6.3.3. Dynamic mechanical analysis (DMA)

The elastic modulus (*E'*) and loss tangent (*tanδ*) of both the prepared shape memory fibers and pellets over the temperature range from -40ºC to 100ºC are presented, as an example, for PTMG650TDI polyurethane in *Figure 6.9.* As shown in *Table 6.4*, dynamic mechanical analysis proves that the pellets synthesized previously in our laboratory [28] (PTMG1000TDI, PTMG650TDI and PTMG650MDITDI) exhibit a glass transition temperature close to 37-38ºC. Therefore, these SMPUs were chosen for this study because the similarity between its T_g*s* and body temperature made them good candidates for its application in textiles. Regarding the pellets of commercial polyurethane, the glass transition temperature of MM4520 (52.5ºC) is higher than the body temperature. Even so, it was contrasted with synthesized polyurethanes due to DIAPLEX is a relevant commercial shape memory polyurethane applied to textiles, so that it is remarkable to compare this material with the ones synthesized in laboratory. As shown in *Table 6.4*, it is observed that the glass transition temperature of fibers is higher than the glass transition temperature of pellets, at approximately 20ºC. This trend of $T_{g,\ fibers}$ higher than $T_{g,\ pellets}$ was coincident with the tendency found in the DSC tests.

Moreover, storage modulus for fibers produced with synthesized polyurethanes is higher than the storage modulus for pellets, whereas in the case of the commercial polyurethane, storage modulus is similar for both fiber and pellets. As an example, in *Table 6.4*, it can be seen that storage modulus of PTMG650TDI pellets is 2176.8 MPa and for fibers this value increases to 4718 MPa. It can be due to the conditions supported by the polyurethane during the piston spinning process, such as drawing, which could change the properties of the final material (fibers) regarding the original one (pellets) [34,35].

6.3.4. Optical microscopy

Figure 6.10 shows the optical microscope images of both PTMG650TDI and MM4520 polyurethane fibers, obtained at a draw ratio equal to 1. It can be seen that the surface in MM4520 fibers is rougher than the one in PTMG650TDI fibers. On the other hand, PTMG650TDI fibers are more flexible and elastic than MM4520 fibers. This is obviously due to the reagents or additives used in the process of synthesis.

Therefore, a thicker and rougher polymer surface was obtained for commercial fibers and a more elastic polymer surface was obtained for PTMG650TDI fibers [36]. Thus, fibers obtained from synthesized polyurethanes present an advantage for future applications in the textile sector greater than the commercial ones.

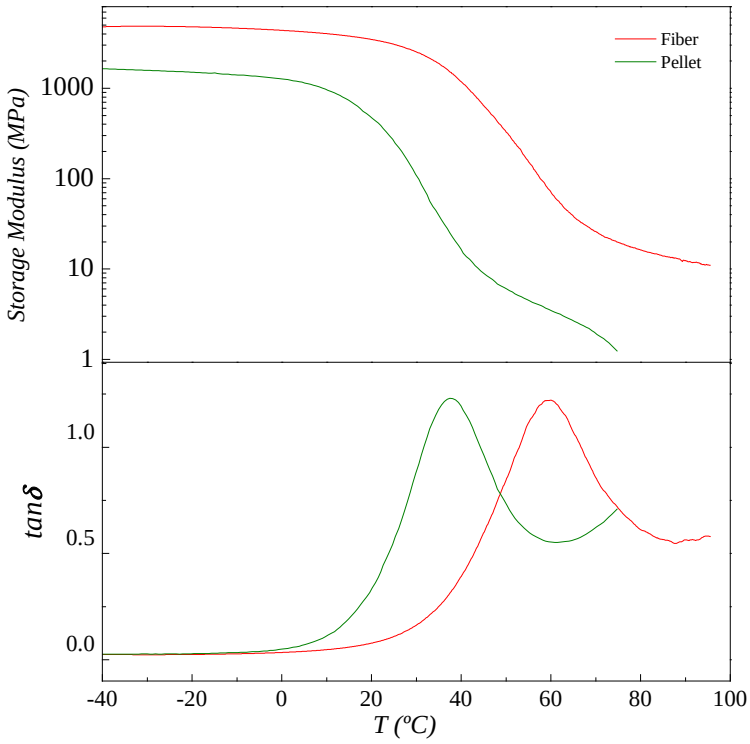

Figure 6.9. *Comparison of DMA curves of PTMG650TDI pellet and fiber polyurethanes*

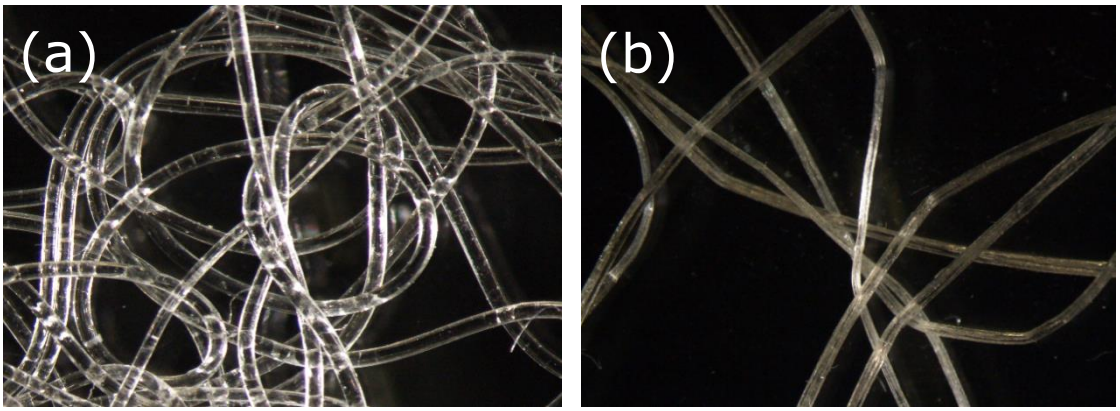

Figure 6.10. *Optical microscopic images of PTMG650TDI (a) and MM4520 (b) polyurethane fibers obtained in piston spinning*

6.3.5. Mechanical testing

The stress–strain curves of all the polyurethane fibers, obtained from both the synthesized and commercial polyurethanes, are presented in *Figure 6.11*. *Table 6.5* shows the tensile strengths (E), elongation at break (ε_b) and fracture toughness (U_T) of all SMPU fibers at room temperature. The commercial SMPU showed a clear yield point, whereas the synthesized SMPUs did not show a clear yield point. Furthermore, the synthesized polyurethanes own more elasticity than the commercial one. In addition, fibers produced from synthesized polyurethanes showed the presence of a neck type deformation and a very long plastic region. On the contrary, the commercial polyurethane presented a lower plastic region [35,37]. Relating tenacity, the commercial polyurethane tenacity increases significantly compared with synthetized ones. It was also observed that elongation at break is higher in synthesized polyurethanes (761% for PTMG1000TDI) than in the commercial polyurethane (64.4% for MM4520). On the other hand, the commercial polyurethane owns a high elastic modulus (0.92 MPa for PTMG1000TDI and 5.30 MPa for MM4520). This may be due to the synthesis procedure of polyurethanes and the type of reagents or additives used during this process, as mentioned before. Depending on the reagents, both the soft and hard-segment content are different. This may be responsible for the lower tenacity and higher elongation because soft-segments tend to orient themselves in the direction of the stretch, whereas the hard-segments remain perpendicular to the stretch direction [38,39]. Hence, the tensile properties of SMPUs synthetized in laboratory are good enough for applications in the textile industry and medical areas, between others. Nevertheless, synthetized polyurethanes are slightly better than DIAPLEX MM4520 due to their elastic properties. Finally, it could be concluded that polyurethane fibers exhibited excellent mechanical properties.

Table 6.5. *Mechanical properties of synthesized and commercial polyurethane fibers*

Sample code	Elastic Modulus E (MPa)	Secant Modulus E* (MPa)	Elongation at break ε_b (%)	Fracture toughness U_T (MJ·m^{-3})
PTMG1000TDI	0.92±0.12	0.92	761.0	227.5
PTMG650TDI	2.49±0.34	2.47	548.3	294.2
PTMG650MDITDI	1.38±0.17	1.39	307.2	62.6
MM4520	8.76±0.12	10.60	64.4	20.5

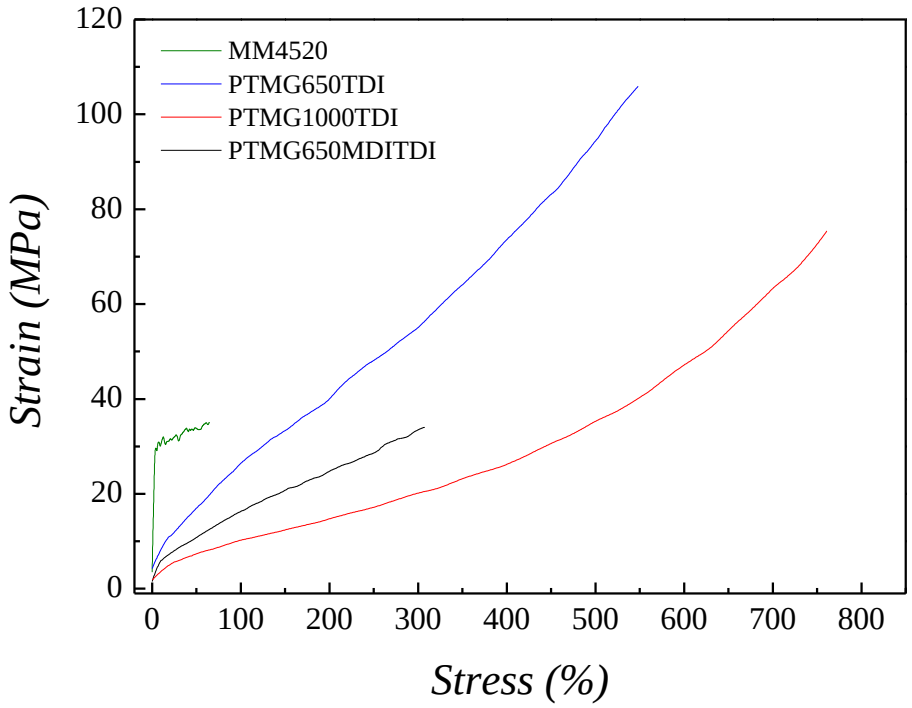

Figure 6.11. *Comparison of tensile test of synthesized and commercial polyurethane fibers*

6.3.6. Shape Memory Behavior

In this chapter, all characterizations of both synthesized and commercial polyurethanes have been performed on fibers produced in a piston spinning machine. In addition, from these fibers, fabrics produced in a knitting laboratory have been selected to evaluate their shape memory effect. This will lead to a better understanding of their performance in the textile field.

Shape memory fabrics are materials that are able to return to a preprogrammed shape because of an external stimulus, generally temperature [40]. The glass transition temperature was assumed to serve as the T_{trans} for the shape memory behavior. Therefore, in this study and as mentioned in the *section 6.2* of this chapter, fabrics were produced by a knitting machine in the department of Textile Technology, faculty of textiles at University of Borås, to test the shape memory behavior of fabrics made from synthesized pellets. *Figure 6.12* shows photographs of two of the developed fabrics. The experimental results are tabulated in *Table 6.6.*

Table 6.6. *Properties of the synthesized shape memory polyurethanes and shape memory fabric*

Sample code		**R_f (%)**	**R_r (%)**
PTMG1000TDI	Pellet	76.9	100
	Plain knit	81.8	100
PTMG650TDI	Pellet	86.4	99.7
	Plain knit	84.7	100
PTMG650MDITDI	Pellet	61.9	98.2
	Plain knit	24.8	99.9
MM4520	Pellet	46.1	87.1
	Plain knit	83.4	100

It is evident that both pellets and fabrics show a shape memory effect, except PTMG650MDITDI which is not able to maintain the fixity shape. *Figure 6.13* suggests that the PTMG650MDITDI fabric cannot fix the temporary elongation completely while cooled from T_{high} to the ambient temperature. It could be seen that shape recovery ratios for the SMPUs, both pellet and fabric, show excellent recovery (more than 99.9% in almost all samples). Relating to shape fixity, the samples of PTMG1000TDI and PTMG650TDI show good and similar shape fixity, regardless if they are pellet or

fabric. As shown in *Figure 6.14*, R_f of PTMG650TDI in the form of pellet is 86.4% and for the fabric form is 84.7%. In the case of commercial polyurethane and PTMG1000TDI, the shape fixity of the fabrics is better than the results obtained from the pellets. This could be explained because soft and hard-segments are both well oriented.

Shape recovery of all samples was excellent because elongation of the fibers occurred during the spinning step and the orientations of the soft and hard-segments were well established except for PTMG650MDITDI.

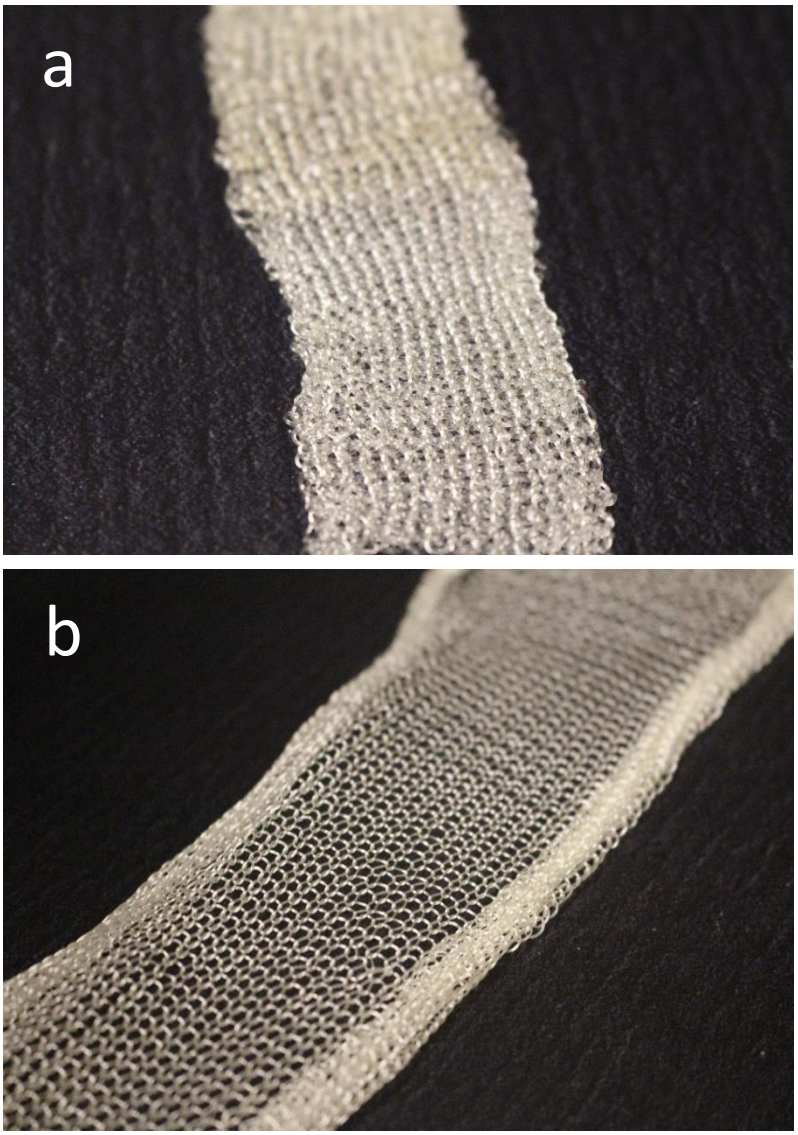

Figure 6.12. *Shape memory fabrics made from PTMG650TDI (a) and DIAPLEX MM4520 (b)*

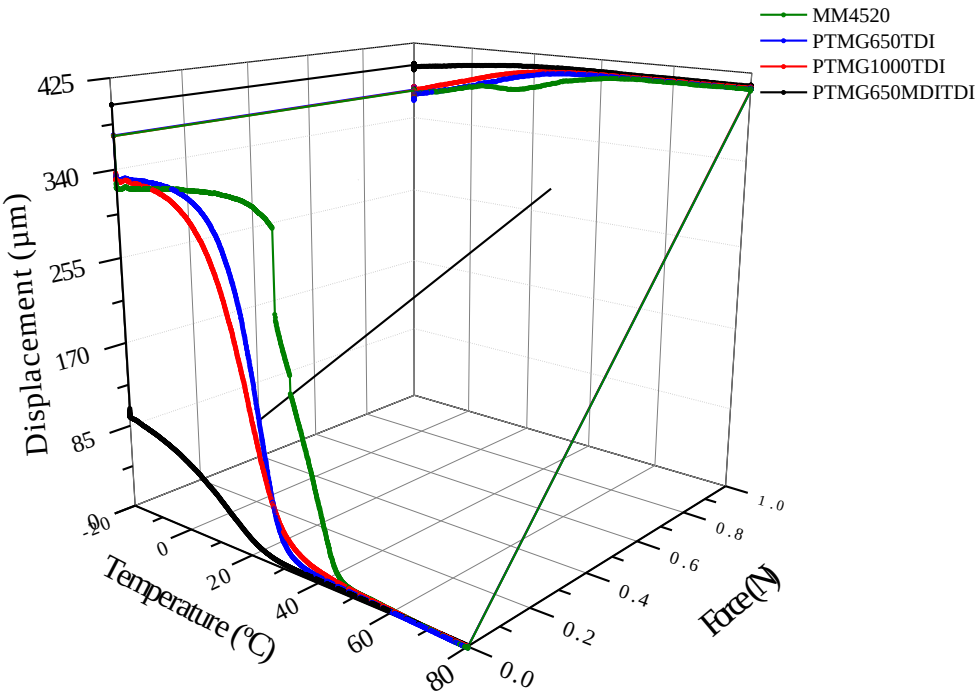

Figure 6.13. *Shape memory behavior of synthetized and commercial fabric polyurethanes*

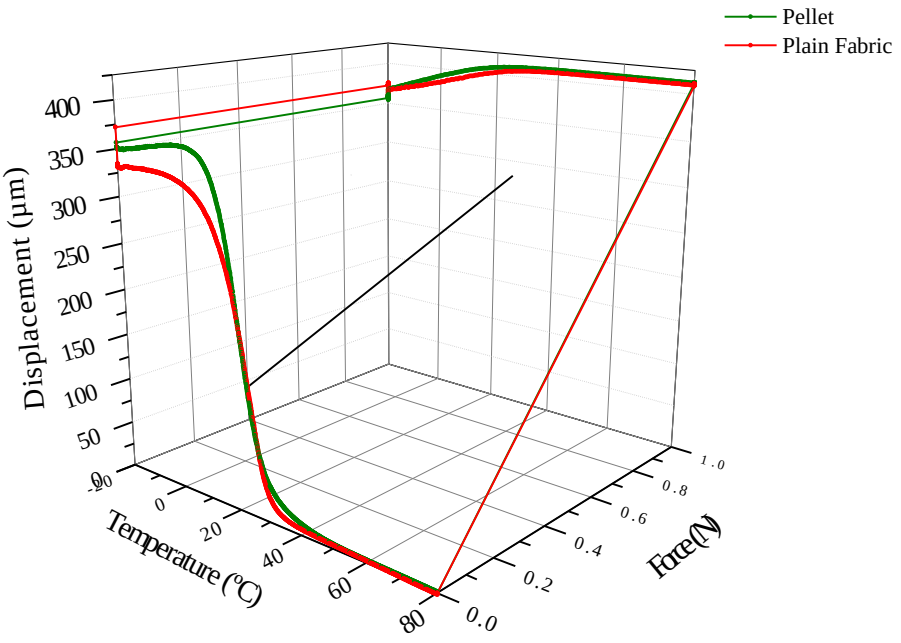

Figure 6.14. *Comparison of shape memory effect for PTMG650TDI pellet and PTMG650TDI plain fabric*

6.4. Conclusions

It is well-known that polymers have gained an important place in day-to-day life because of their specific properties which make them applicable in a wide range of applications. Among them, shape memory polyurethanes are playing an increasingly important role in the textile industry. Previous remarkable research works focused on the design and fabrication of fibers by melt spinning and knitted fabrics of SMPUs. In this chapter, it was demonstrated that synthesized and commercial fibers were successfully fabricated and possesses stable thermal properties. Moreover, the tensile properties of SMPUs synthetized in our laboratory are slightly better than the commercial one. Relating to shape recovery ratios, SMPUs in the form of fabrics show excellent recovery (more than 99.9% in almost samples). Finally, it can be concluded that synthesized polyurethane fibers are good enough for future applications in textile industry or medical areas among others.

6.5. References

1. Zhang P, Li G (2016) Advances in healing-on-demand polymers and polymer composites. Prog Polym Sci 57:32–63.
2. Lexcellent C, Butaud P, Foltête E, Ouisse M (2017) A Review of Shape Memory Polymers Thermomechanical Modelling: Analysis in the Frequency Domain. In: Adv. Shape Mem. Mater. pp 57–80
3. Ashir M, Nocke A, Theiss C, Cherif C (2017) Development of adaptive hinged fiber reinforced plastics based on shape memory alloys. Compos Struct 170:243–249.
4. Chen L, Wang JX, Tang CY, et al (2016) Shape memory effect of thermal-responsive nano-hydroxyapatite reinforced poly-d-l-lactide composites with porous structure. Compos Part B Eng 107:67–74.
5. Ebara M (2015) Shape-memory surfaces for cell mechanobiology. Sci Technol Adv Mater 16:14804–14818.
6. Berg G, McBride M, Wang C, Bowman C (2014) New directions in the chemistry of shape memory polymers. Polymer (Guildf) 55:5849–5872.

7. Memarian F, Fereidoon A, Ghorbanzadeh Ahangari M, et al (2016) The shape memory, and the mechanical and thermal properties of TPU/ABS/CNT: a ternary polymer composite. RSC Adv 6:101038–101047.

8. Ji Y, Schaerlaekens M, Terentjev EM, et al (2009) Innovative Textile Materials, Stiffening Procedures and Fabric-Joining Methods. In: Transform. Cloth. Prod. into a Demand-driven, Knowledge-based, High-tech Ind. Springer, pp 61–93

9. Liu C, Qin H, Mather PT (2007) Review of progress in shape-memory polymers. J Mater Chem 17:1543–1558.

10. Ding XM. M, Hu JL. L, Tao XM. M, Hu CP. R (2006) Preparation of temperature-sensitive polyurethanes for smart textiles. Text Res J 76:406–413.

11. Han HR, Chung SE, Park CH (2012) Shape memory and breathable waterproof properties of polyurethane nanowebs. Text Res J 83:76–82.

12. Maksimkin A, Kaloshkin S, Zadorozhnyy M, Tcherdyntsev V (2014) Comparison of shape memory effect in UHMWPE for bulk and fiber state. J Alloys Compd 586, Suppl:S214–S217.

13. Bashir T, Fast L, Skrifvars M, Persson N-K (2012) Electrical Resistance Measurement Methods and Electrical Characterization of Poly(3,4-ethylenedioxythiophene)- Coated Conductive Fibers. J Appl Polym Sci 2:9903–9910.

14. Li Z, Lu H, Yao Y, Lin L (2017) Thermomechanical performance and shape recovery behaviour of shape memory polymer nanocomposite incorporated with hexagonal boron nitride. Pigment Resin Technol 46:79–83.

15. Xu W, Zhang R, Liu W, et al (2016) A Multiscale Investigation on the Mechanism of Shape Recovery for IPDI to PPDI Hard Segment Substitution in Polyurethane. Macromolecules 49:5931–5944.

16. Chen S, Mo F, Stadler FJ, et al (2015) Development of zwitterionic copolymers with multi-shape memory effects and moisture-sensitive shape memory effects. J Mater Chem B 3:6645–6655.

17. Gu L, Cui B, Wu Q-Y, et al (2016) Bio-based polyurethanes with shape memory behavior at body temperature: effect of different chain extenders. RSC Adv 6:17888–17895.

18. Yildirim E, Yurtsever M, Wilkes GL, Yilgör I (2016) Effect of intersegmental

interactions on the morphology of segmented polyurethanes with mixed soft segments: A coarse-grained simulation study. Polymer (Guildf) 90:204–214.

19. Kim JT, Kim BK, Kim EY, et al (2014) Synthesis and shape memory performance of polyurethane/graphene nanocomposites. React Funct Polym 74:16–21.

20. Niu Y, Zhu Y, Gao R, et al (2014) Synthesis, Characterizations and Biocompatibility of Novel Block Polyurethanes Based on Poly(lactic acid) (PLA) and Poly(3-hydroxybutyrate-co-4-hydroxybutyrate) (P3/4HB). J Inorg Organomet Polym Mater 25:81–90.

21. Li S, Zhao J, Zhang Z, et al (2014) Synthesis and characterization of aliphatic segmented poly(ether amide urethane)s through a non-isocyanate route. RSC Adv 4:23720–23729.

22. Hu J, Meng H, Li G, Ibekwe SI (2012) A review of stimuli-responsive polymers for smart textile applications. Smart Mater Struct 21:53001–53024.

23. Meirowitz R (2010) Microencapsulation technology for coating and lamination of textiles. In: Smart Text. Coatings Laminates. Woodhead Publishing Ltd, Cambridge, pp 125–154

24. Liu N, Zhao Y, Kang M, et al (2015) The effects of the molecular weight and structure of polycarbonatediols on the properties of waterborne polyurethanes. Prog Org Coatings 82:46–56.

25. Benhamou K, Kaddami H, Magnin A, et al (2015) Bio-based polyurethane reinforced with cellulose nanofibers: A comprehensive investigation on the effect of interface. Carbohydr Polym 122:202–211.

26. Mi H-Y, Salick MR, Jing X, et al (2013) Characterization of thermoplastic polyurethane/polylactic acid (TPU/PLA) tissue engineering scaffolds fabricated by microcellular injection molding. Mater Sci Eng C 33:4767–4776.

27. Sáenz-Pérez M, Laza JM, García-Barrasa J, et al (2017) Influence of the soft segment nature on the thermomechanical behavior of shape memory polyurethanes. Polym Eng Sci 1–7.

28. Sáenz-Pérez M, Lizundia E, Laza JM, et al (2016) Methylene diphenyl diisocyanate (MDI) and toluene diisocyanate (TDI) based polyurethanes: thermal, shape-memory and mechanical behavior. RSC Adv 6:69094–69102.

29. Hooshmand S, Soroudi A, Skrifvars M (2011) Electro-conductive composite fibers by melt spinning of polypropylene/polyamide/carbon nanotubes. Synth Met 161:1731–1737.

30. Soroudi A, Skrifvars M (2010) Melt blending of carbon nanotubes/polyaniline/polypropylene compounds and their melt spinning to conductive fibres. Synth Met 160:1143–1147.

31. Manvi KP, Roth D, Seide G, Gries T (2014) Water quenched melt spinning process for thermoplastic polyurethanes. In: Chem. Fibers Int. International business Press, Frankfurt, pp 40–41

32. Zhang F, Zhang Z, Liu Y, et al (2015) Thermosetting epoxy reinforced shape memory composite microfiber membranes: Fabrication, structure and properties. Compos Part A Appl Sci Manuf 76:54–61.

33. Kim Y-J, Matsunaga YT, Nothdurft K, et al (2017) Thermo-responsive polymers and their application as smart biomaterials. J Mater Chem B 5:4307–4321.

34. Meng Q, Hu J (2008) Study on poly (ε-caprolactone)-based shape memory copolymer fiber prepared by bulk polymerization and melt spinning. Polym Adv Technol 19:131–136.

35. Zhu Y, Hu J, Yeung L, et al (2006) Development of shape memory polyurethane fiber with complete shape recoverability. Smart Mater 15:1385–1394.

36. Bashir T, Skrifvars M, Persson N-K (2012) Synthesis of high performance, conductive PEDOT-coated polyester yarns by OCVD technique. Polym Adv Technol 23:611–617.

37. Shishoo R (2002) Recent developments in materials for use in protective clothing. Int J Cloth Sci Technol 14:201–215.

38. Kaursoin J, Agrawal AK (2007) Melt spun thermoresponsive shape memory fibers based on polyurethanes: Effect of drawing and heat-setting on fiber morphology and properties. J Appl Polym Sci 103:2172–2182.

39. Ding X, Hu J, Tao X, Hu C (2006) Preparation of temperature-sensitive polyurethanes for smart textiles. Text Res J 76:406–413.

40. Coyle S, Diamond D (2010) Smart Nanotextiles: Materials and Their Application. In: Encycl. Mater. Sci. Technol. Elsevier, Oxford, pp 1–5

Chapter VII.
CONCLUSIONS AND FINAL CONSIDERATIONS

"Ordu gozoak / ordu garratzak / denetilk du bizitzak. / Baina gaur tori loreak / eta utzi arantzak."

Horas dulces / horas amargas, / de todas se nutre la vida. / Toma hoy esta flor / y olvida sus espinas.

Joxantonio Ormazabal

Chapter VII

CONCLUSIONS AND FINAL CONSIDERATIONS

Shape memory polymers (SMPs) are those able to change their shape upon the application of an external stimulus. Recently, the research on SMPs has been focused mainly on the development of thermally induced SMPs for a wide range of applications such as biomedical, aerospace, electrical, textile and footwear industry.

In this work, a thorough study of shape memory polyurethanes (SMPUs) has been presented. First, numerous synthesis with different experimental conditions of shape memory polyurethanes were performed by the prepolymer method. Soft-segment was composed of poly(ethylene glycol) (PEG) or poly(oxytetramethylene) glycol (PTMG) and hard-segment was composed of a chain extender (1,4-butanediol,

BD) and a diisocyanate: 2,4-toluene diisocyanate (TDI), 4,4'-methylene diphenyl diisocyanate (MDI) or a 50% weight mixture between MDI and TDI. Second, relevant shape memory polyurethane features such as thermogravimetric behavior, thermomechanical properties, permeability, and shape memory effect were characterized. Besides, fibers and fabrics were created from those shape memory polyurethanes with transition temperatures (T_g) close to the body temperature, in order to use them as a final product in footwear sector. Therefore, the objectives proposed in *Chapter I* have been fulfilled and finally, general conclusions have been presented.

Regarding the thermogravimetric analysis, it could be concluded that all the polyurethanes synthesized in this work display a typical two-stage degradation, except those synthesized with a mixture of diisocyanates (TDI+MDI) which present three stages. Anyway, all synthetized SMPUs show good thermal stability with initial decomposition temperatures higher than 275°C.

Furthermore, both differential scanning calorimetry (DSC) and dynamic mechanical analysis (DMA) showed that glass transition temperature of polyurethanes (T_g) increases with the hard-segment content (higher n). Both methods indicated that PEG-based SMPUs own glass transition temperatures lower than PTMG-based SMPUs.

Relating to mechanical properties, both types of polyurethanes show a huge versatility. When the soft phase is very large (low n), the material cannot withstand the applied stress and is easily deformed. On the contrary, at high n values, hard-segments prevent macromolecules moving too far out of position, yielding lower elongation at break (ε_b) values but increasing the elastic modulus (E). Overall, the obtained experimental findings through this work highlight the potential of SMPUs for applications in which a vibration isolation is needed over a wide range of temperatures. These may include manufacturing of soles for footwear, isolators for large industrial equipment and isolation systems for vibration-sensitive instruments such as scanning electron microscopes among others.

Moreover, the study of the shape memory effect showed that almost all SMPU samples were characterized by shape fixity ratios higher than 85% and shape recovery ratios near 99%. Besides, depending on the hard-segment content, the shape memory effect varies between MDI-based SMPUs and TDI-based SMPUs, finding TDI-shape memory properties superior to MDI-based SMPUs. Relating to

SMPUs with TiO_2 nanoparticles, the results demonstrated that the addition of nanoparticles enhances slightly the shape fixity and shape recovery ratios of SMPUs.

This research work has also shown that both water vapor transmission rate and oxygen permeability decrease when the hard-segment content in the polyurethane increases. It is worth remarking that an increase in the molecular weight of the polyol (from 650 to 1000 $g \cdot mol^{-1}$), permeability rises too. To sum up, shape memory polyurethane films have potential applications in different fields such as in textile sector, where they could promote sweat evaporation and humidity control. Moreover, barrier properties of polyurethane films make them promising candidates for food and pharmaceutical packaging applications. However, further studies are needed to improve the synthesis and processing method, for example, in order to increase the dispersion of the nanoparticles in the polyurethanes.

Finally, it was demonstrated that fibers and fabrics were successfully fabricated from synthesized and commercial SMPUs, and possess stable thermal properties. Relating to shape recovery ratios, SMPUs in the form of fabrics showed excellent recovery (more than 99.9% in almost samples). To sum up, it is found that synthesized polyurethane fibers are good enough for future applications in textile industry or medical areas among others.

In conclusion, considering the foregoing, PTMG-based SMPUs could be more promising thermal-induced shape memory polymers than PEG-based SMPUS and, especially, TDI-based SMPUs. These polyurethanes could be able to provide promising applications in several fields as textile, footwear, biomedicine, automotive, aerospace, etc. Thus, the principal advantages of synthesized SMPUs fibers versus commercial ones are the price, the simple process of synthesis and the flexibility to vary their properties such as glass transition temperature.

Future work

This work represents a first approach to get a new generation of synthesized polyurethane fibers that can act as future active materials with applications in textile industry. However, there is still a lot of work to do to get a final application. For future work, the research of shape memory polymers could be continued in the related areas of textile and footwear. Therefore, some further efforts need to be made in the following directions:

- To study the use of different stimuli (electrical, magnetic or chemical), or their combination, to be able to create textile actuators.
- To improve the efficiency of fibers and fabric methods of preparation.
- Two-way recovery of polymers in one cycle and multiple cycles should be researched.
- To synthesize other shape memory polyurethanes in order to obtain a broader variety of properties.
- Novel shape memory polymeric systems should be developed using biocompatible and biodegradable polymers, especially biocompatible SMPUs, with antimicrobial properties.

Moreover, future studies should be focus on trying to obtain final products for commercial purposes to benefit demand for higher quality of life. Finally, other application fields should be explored with new polymers and new functionalities.

Appendices

Appendix A
TGA AND DTG CURVES

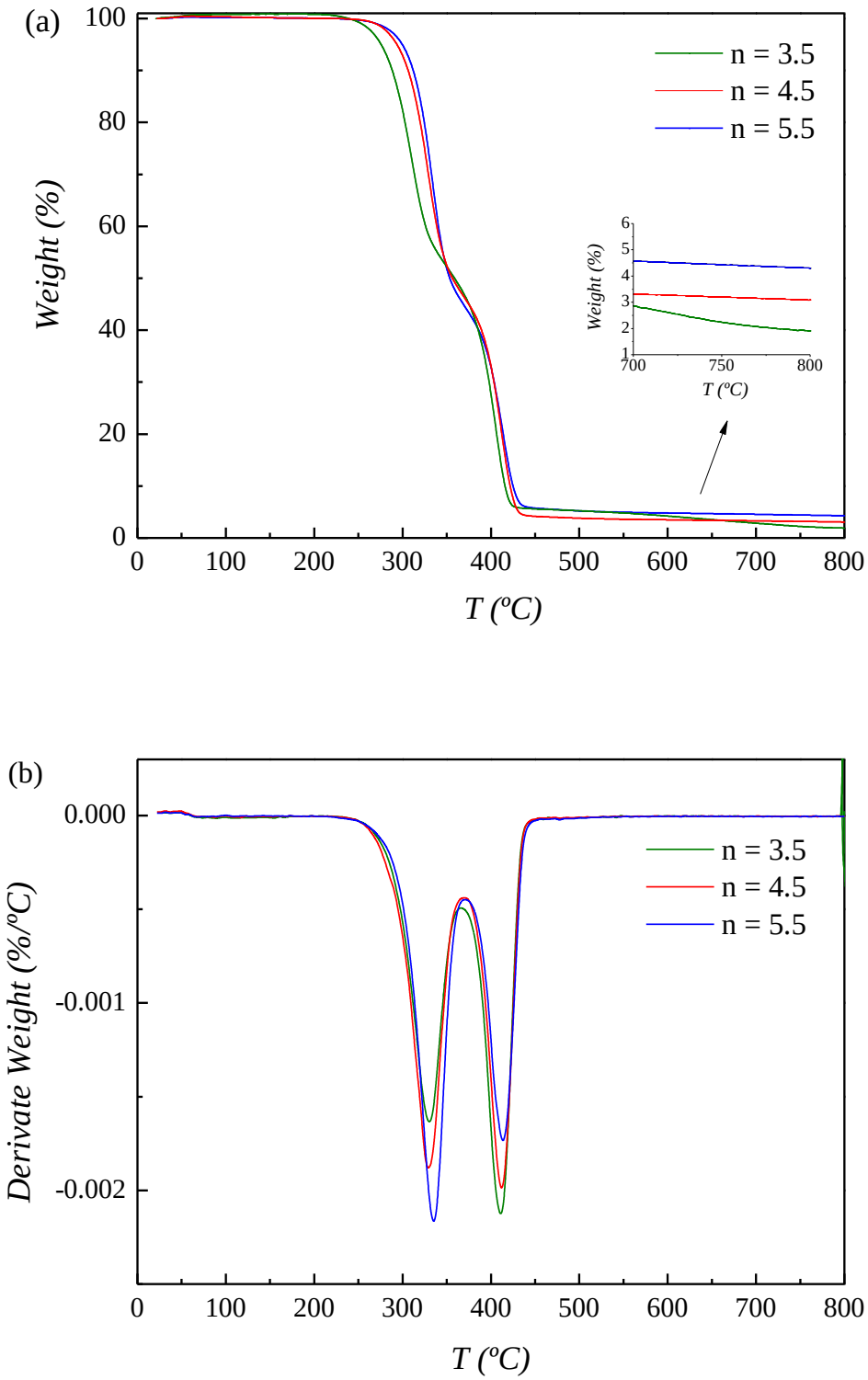

Figure A.1. *TGA (a) and DTG (b) curves for system 1, PEG1000TDI*

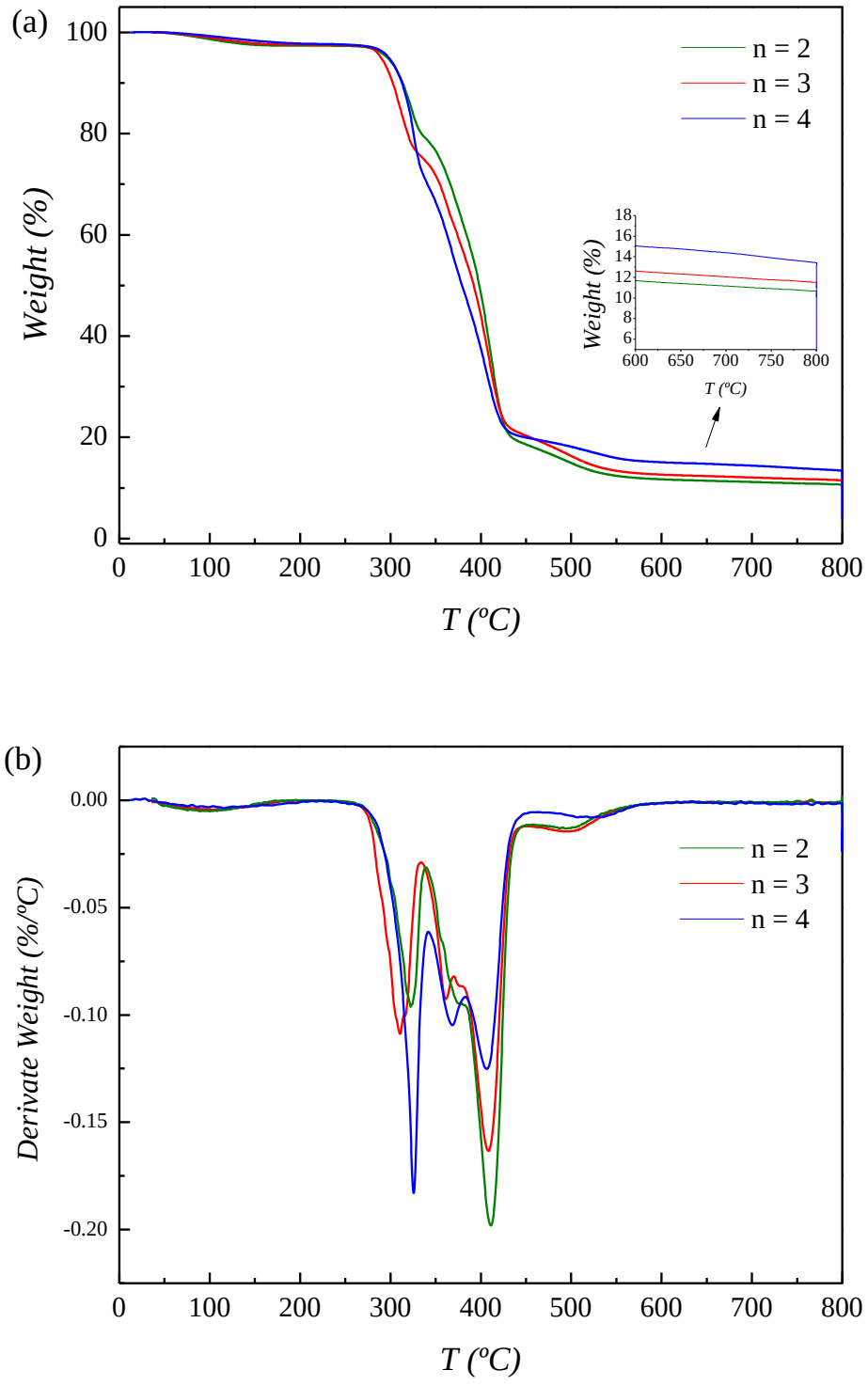

Figure A.2. *TGA (a) and DTG (b) curves for system 2, PEG1000MDI*

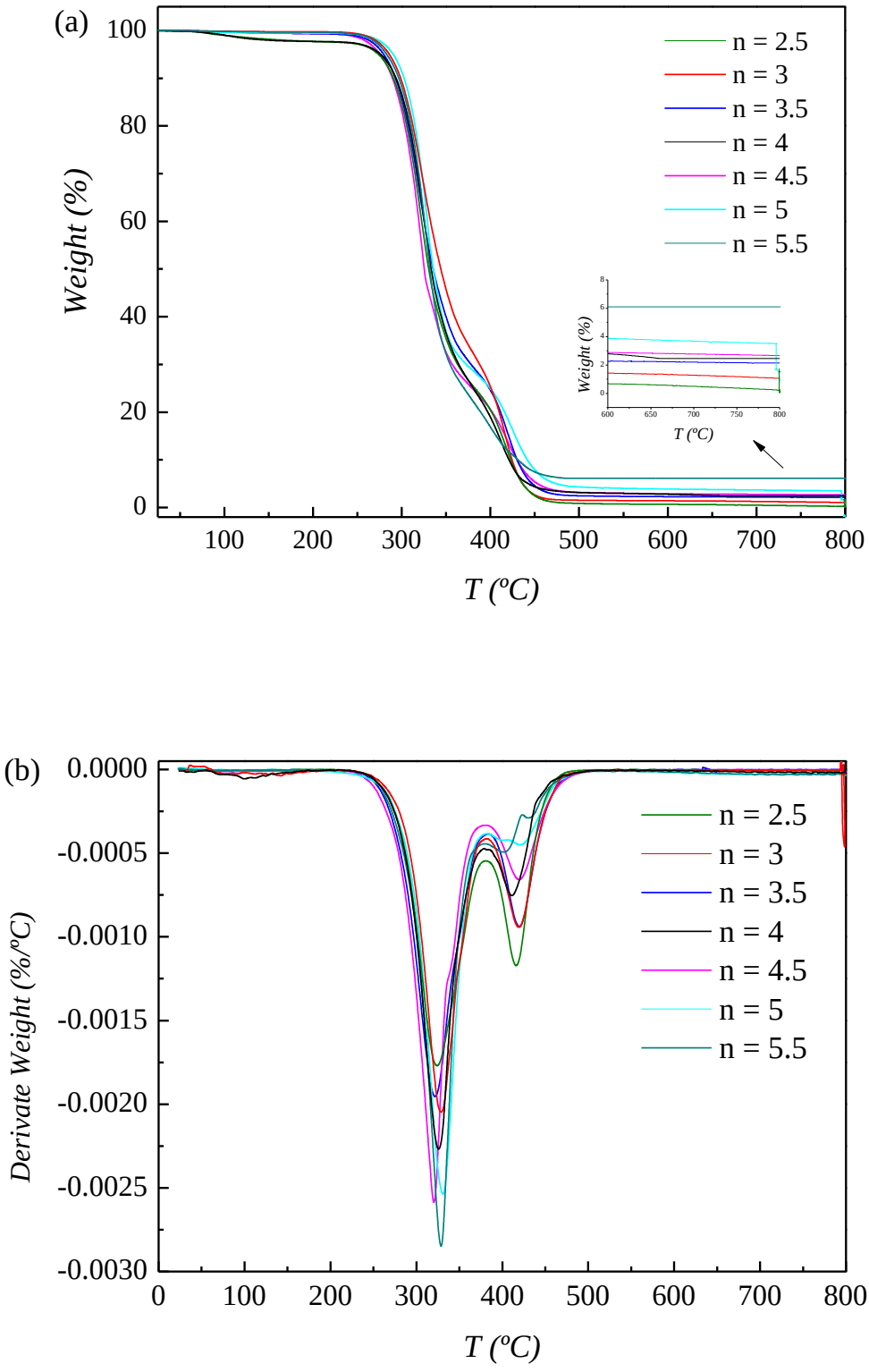

Figure A.3. *TGA (a) and DTG (b) curves for system 3, PTMG650TDI*

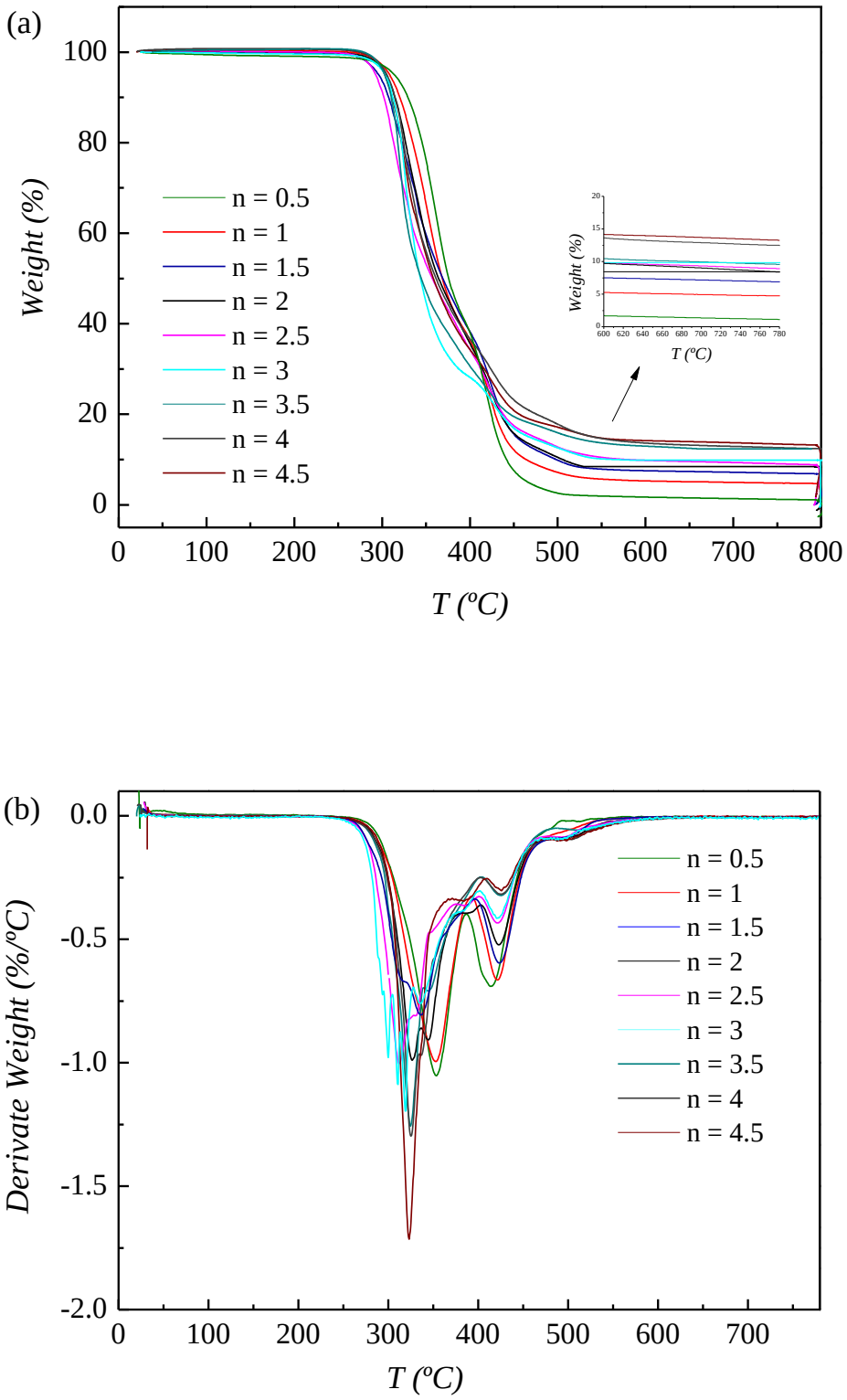

Figure A.4. *TGA (a) and DTG (b) curves for system 4, PTMG650MDI*

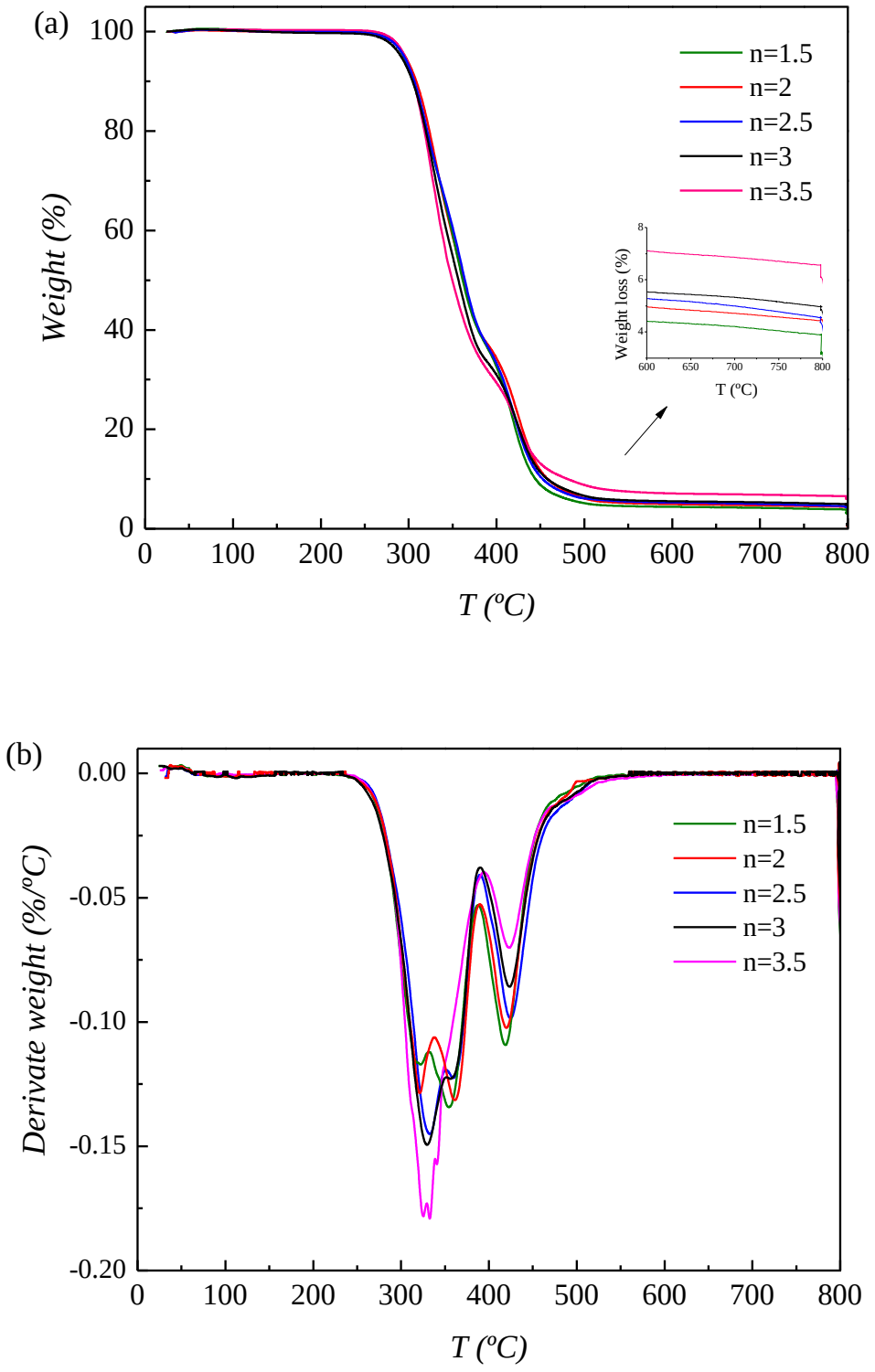

Figure A.5. *TGA (a) and DTG (b) curves for system 5, PTMG650TDI+MDI*

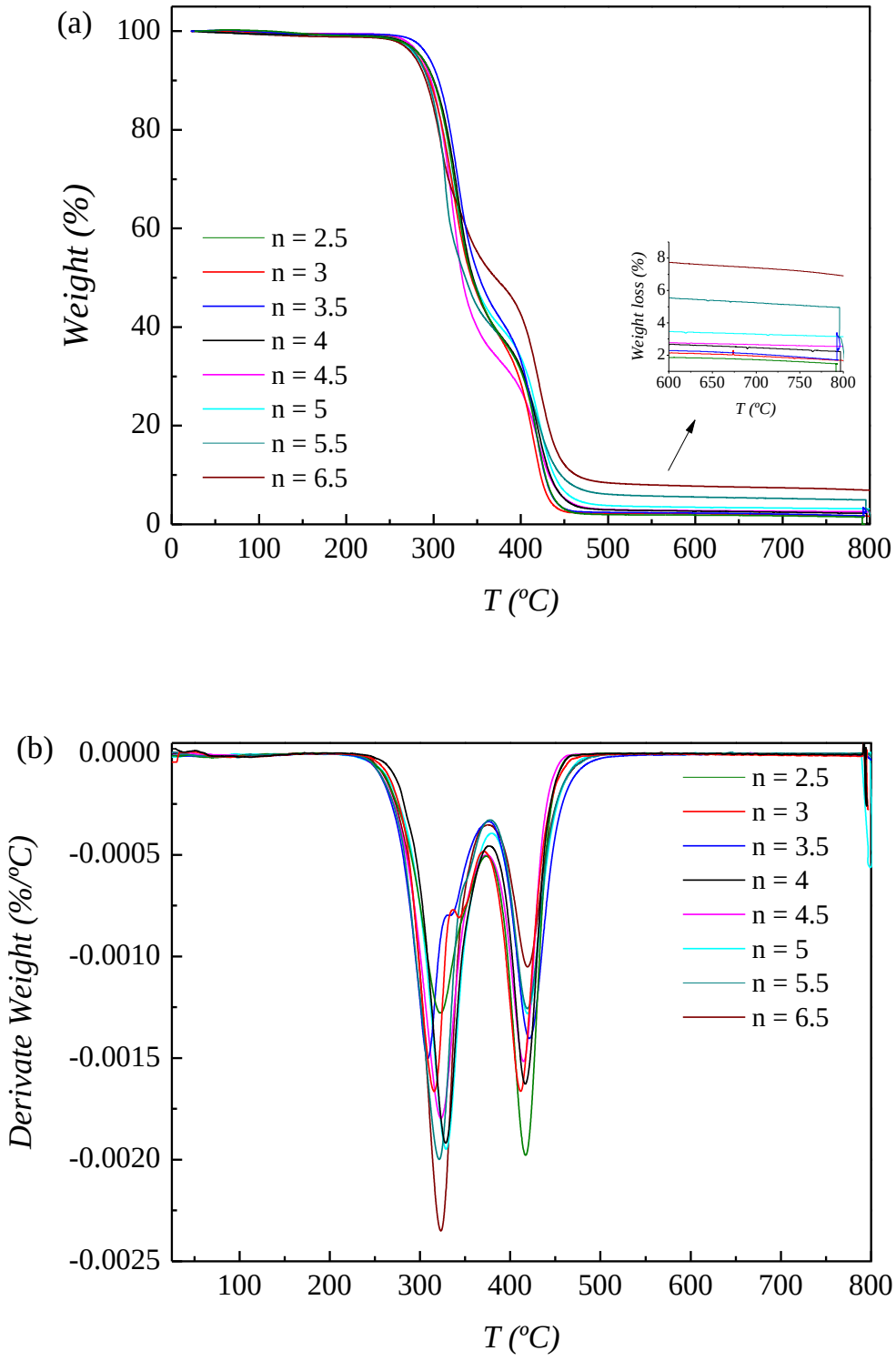

Figure A.6. *TGA (a) and DTG (b) curves for system 6, PTMG1000TDI*

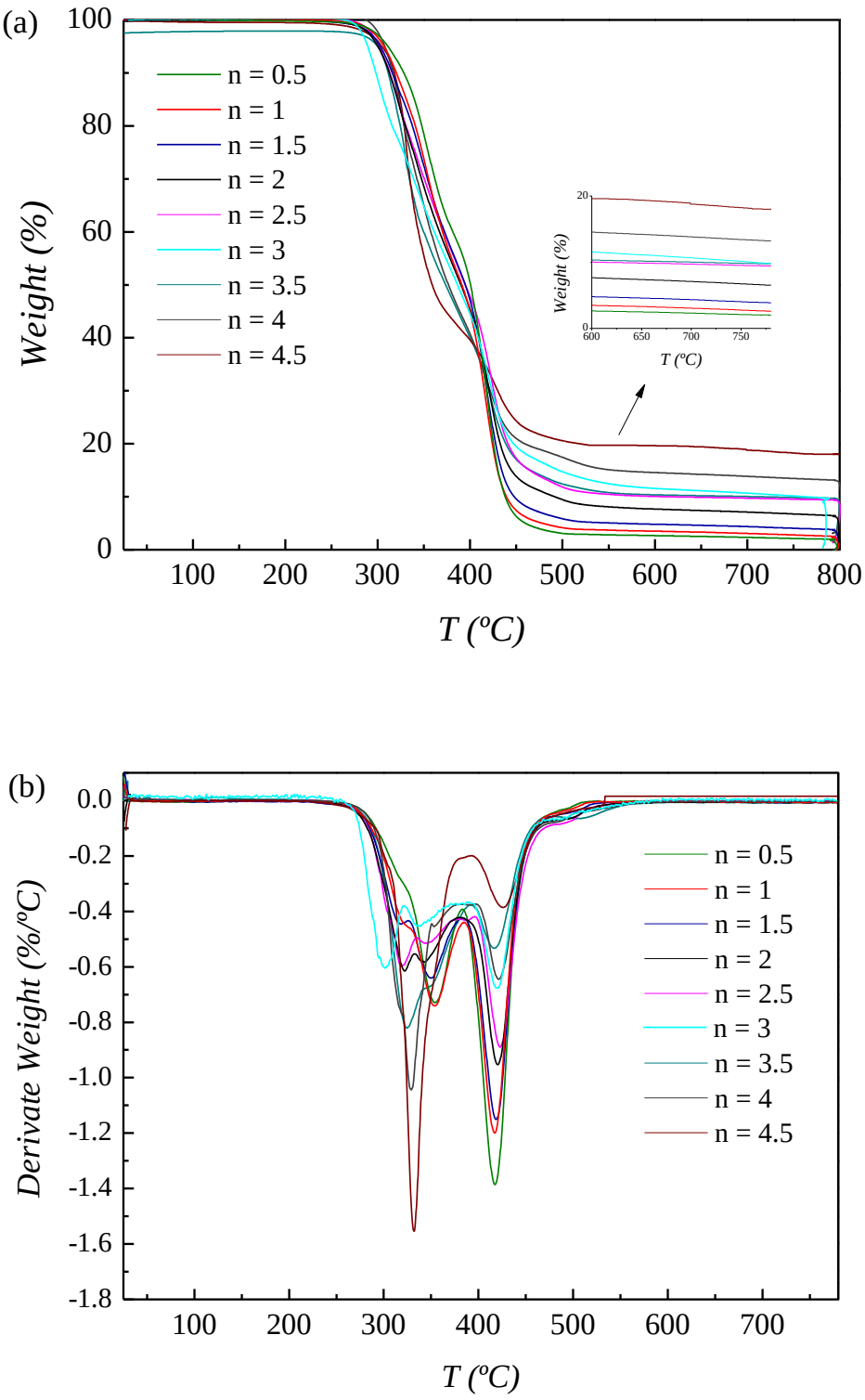

Figure A.7. *TGA (a) and DTG (b) curves for system 7, PTMG1000MDI*

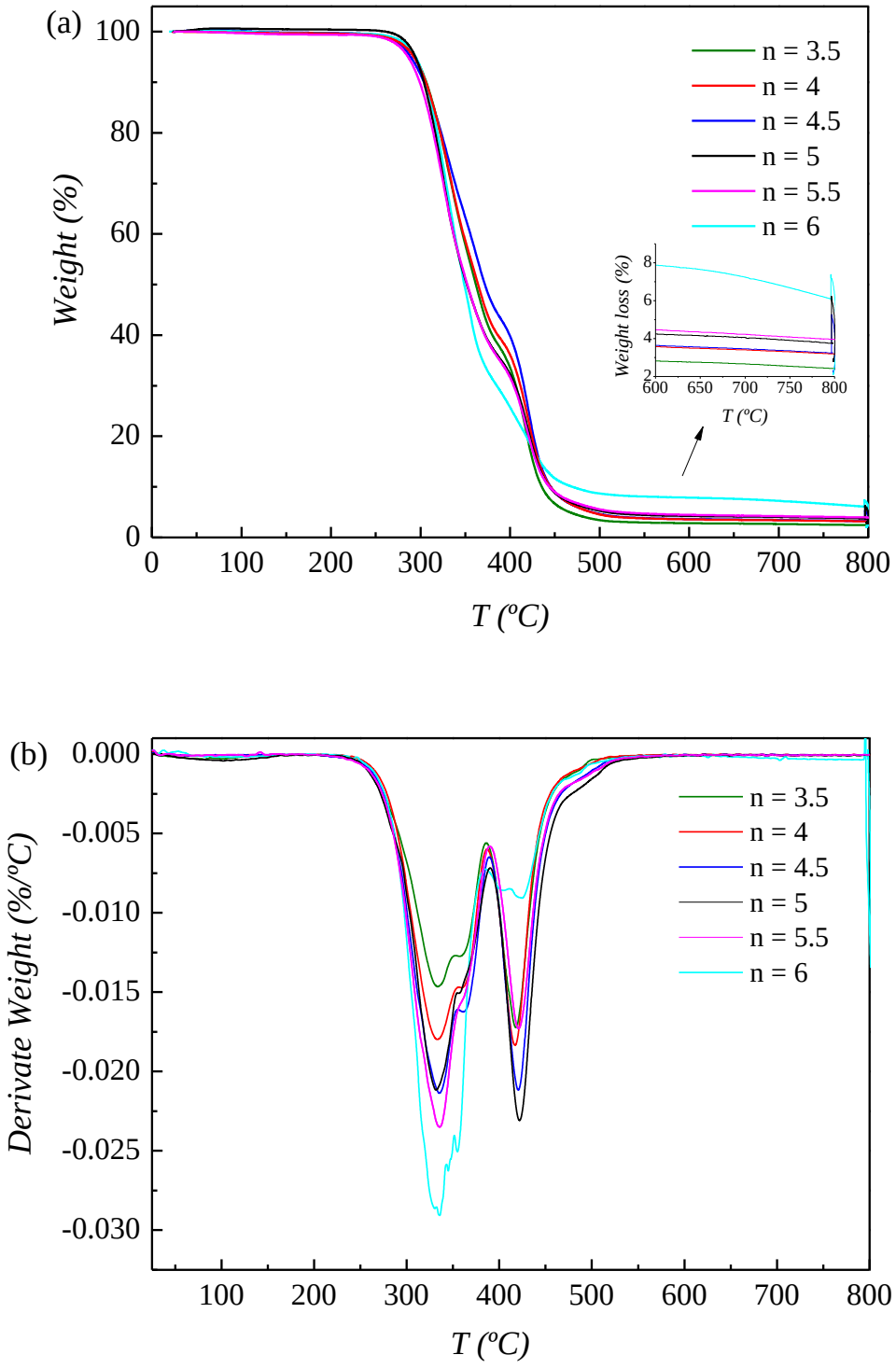

Figure A.8. *TGA (a) and DTG (b) curves for system 8, PTMG1000TDI+MDI*

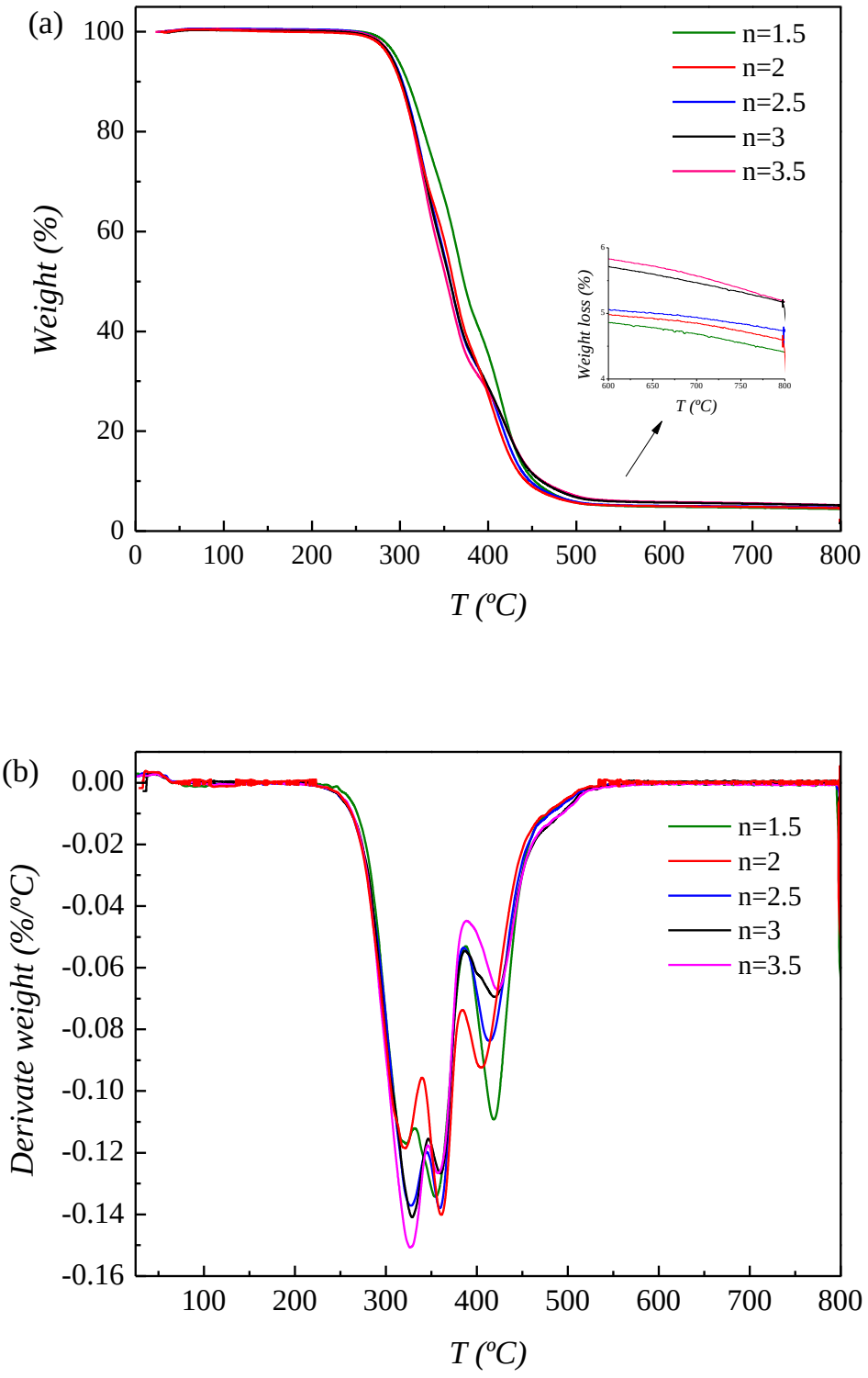

Figure A.9. *TGA (a) and DTG (b) curves for system 9, PTMG650/MDI+TDI/1%TiO_2*

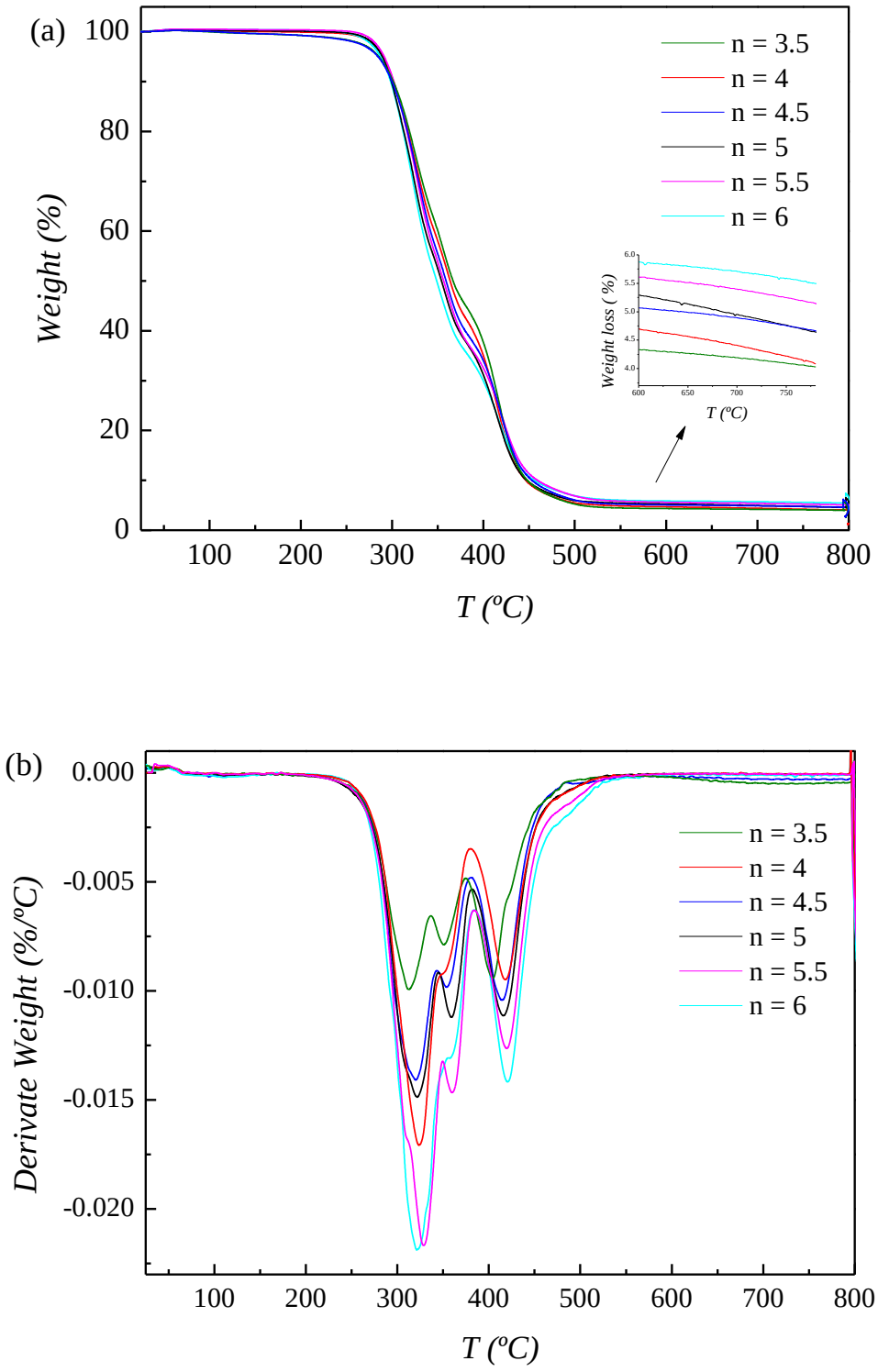

Figure A.10. *TGA (a) and DTG (b) curves for system 10, PTMG1000/MDI+TDI/1%TiO2*

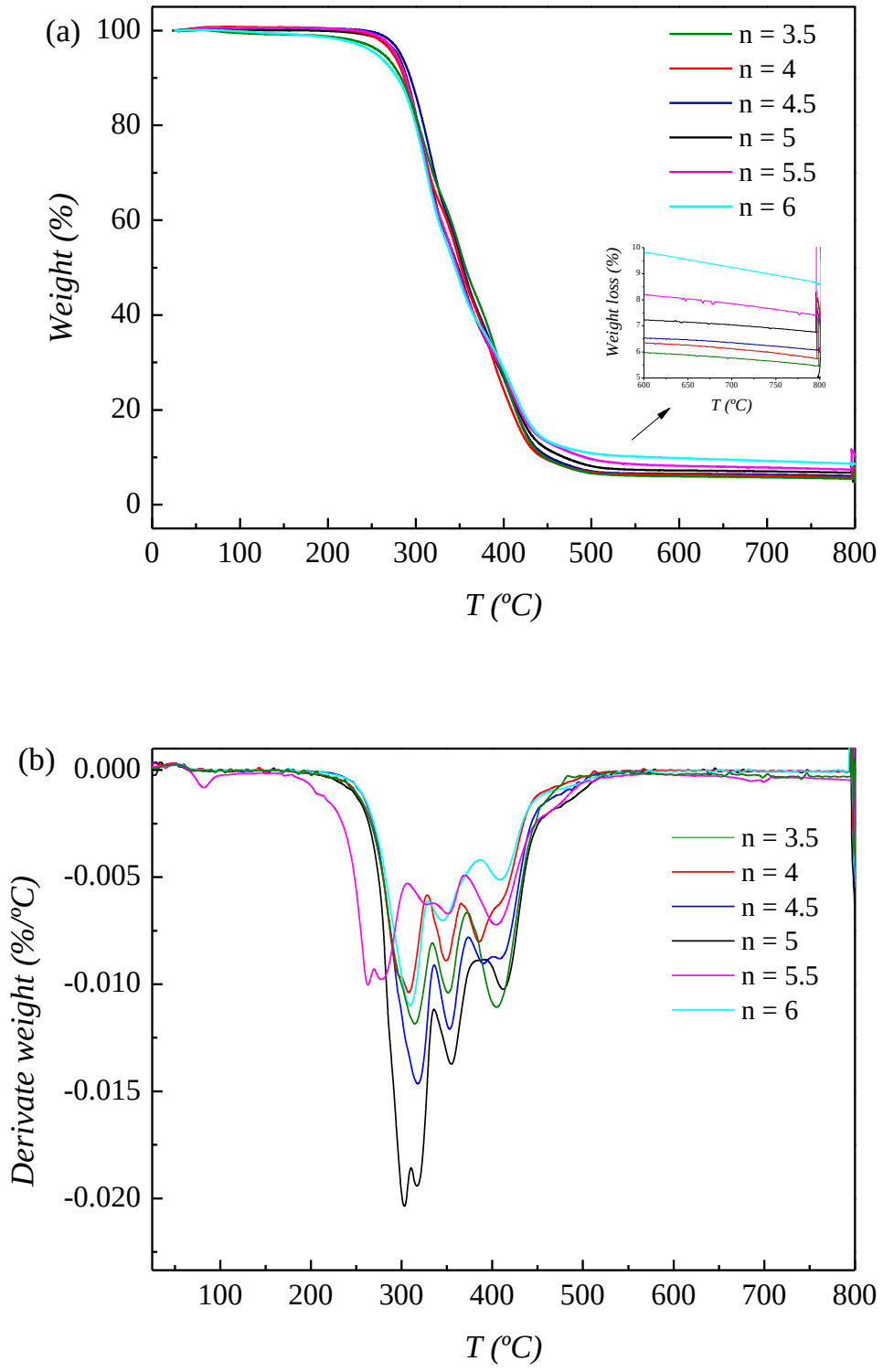

Figure A.11. *TGA (a) and DTG (b) curves for system 11, PTMG1000/MDI+TDI/3%TiO_2*

Appendix B
DSC THERMOGRAMS

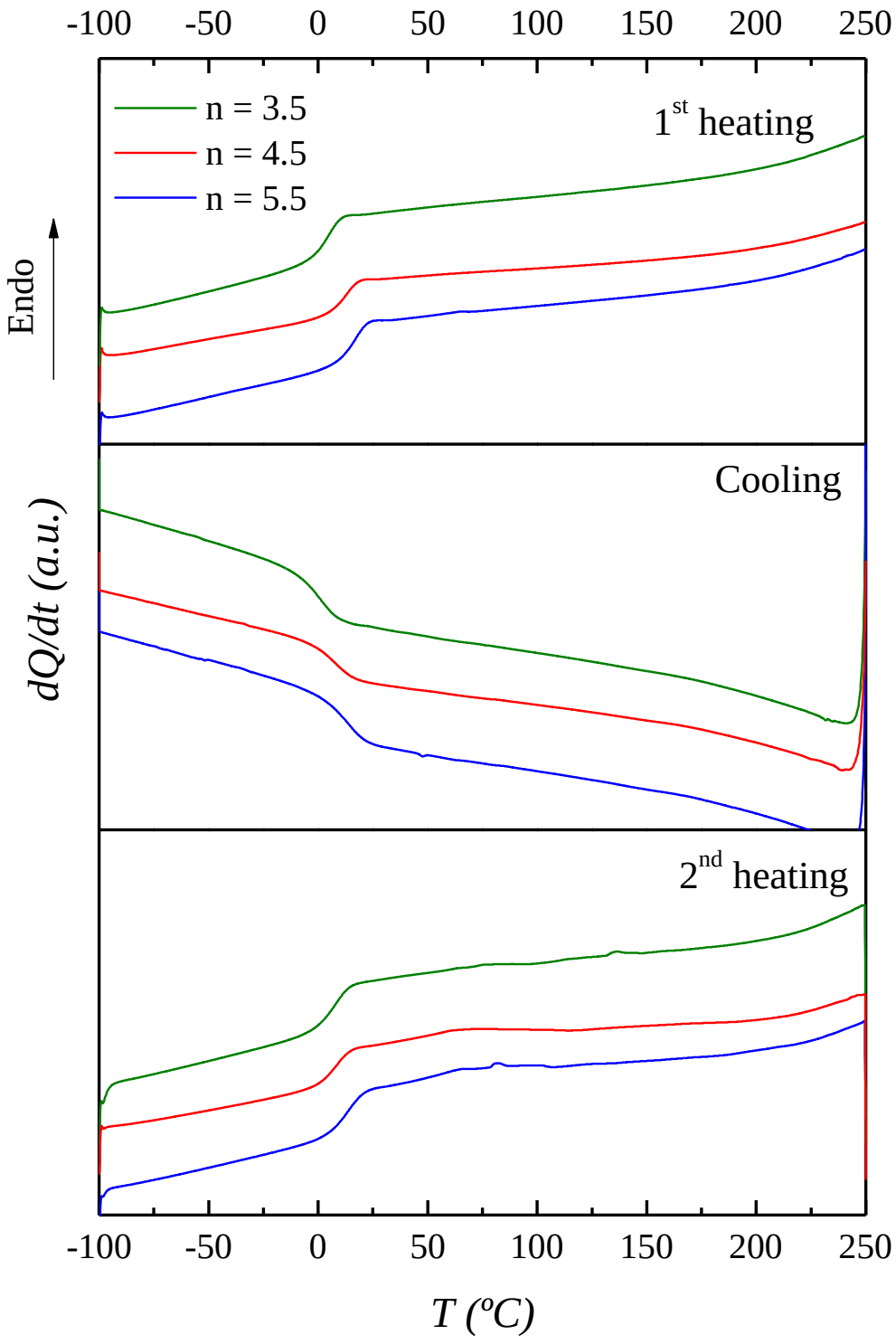

Figure B.1. *DSC curves for system 1, PEG1000TDI*

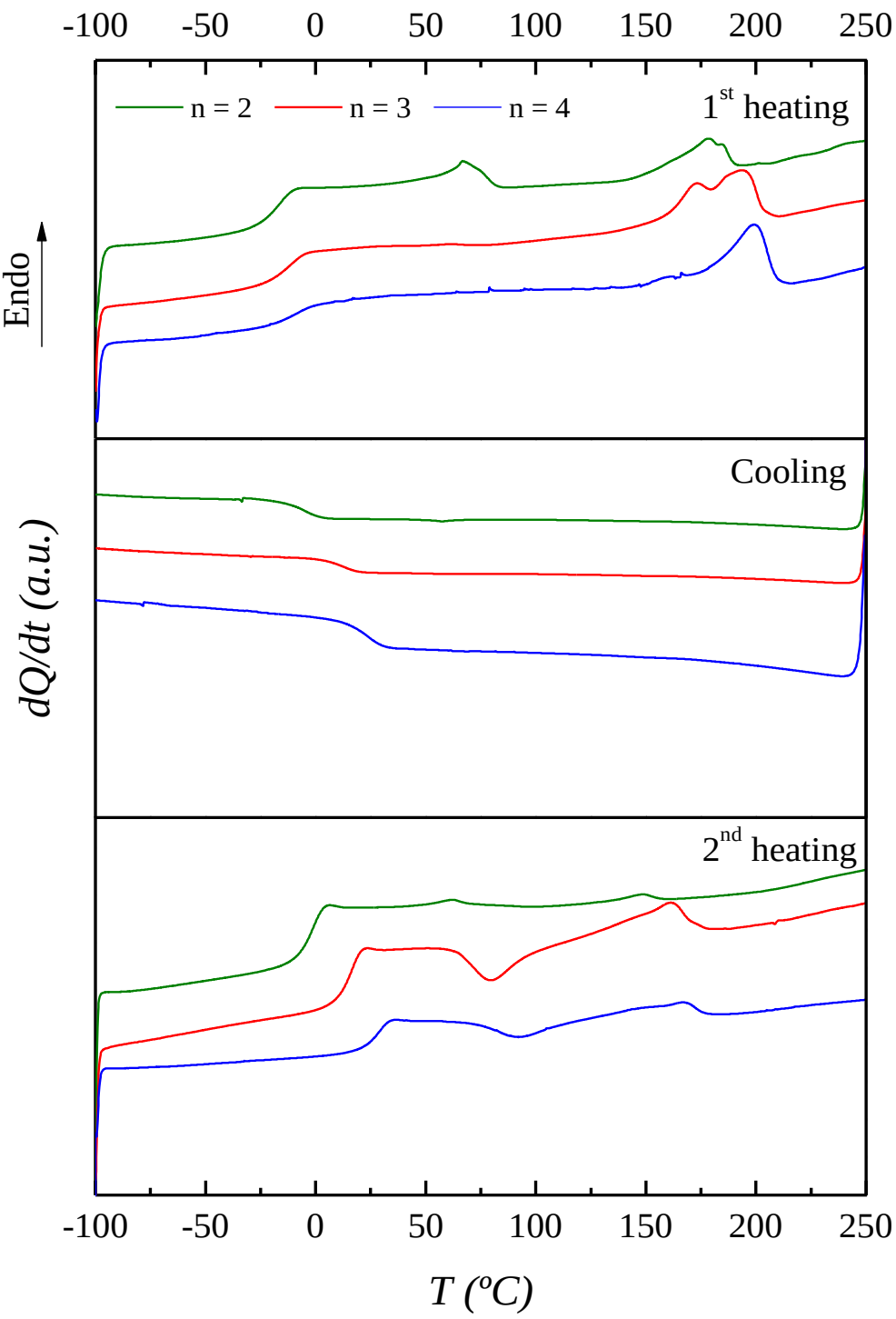

Figure B.2. *DSC curves for system 2, PEG1000MDI*

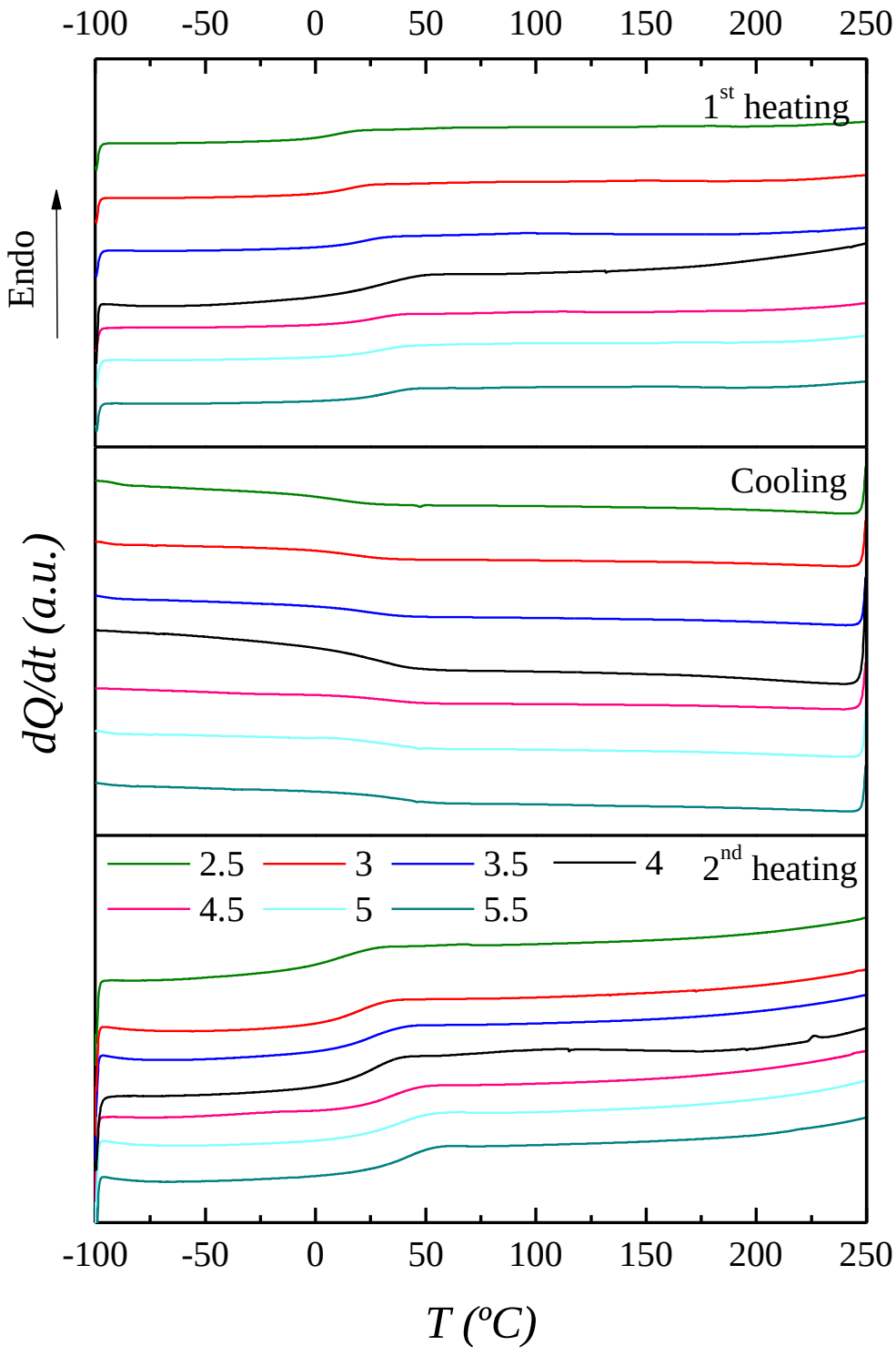

Figure B.3. *DSC curves for system 3, PTMG650TDI*

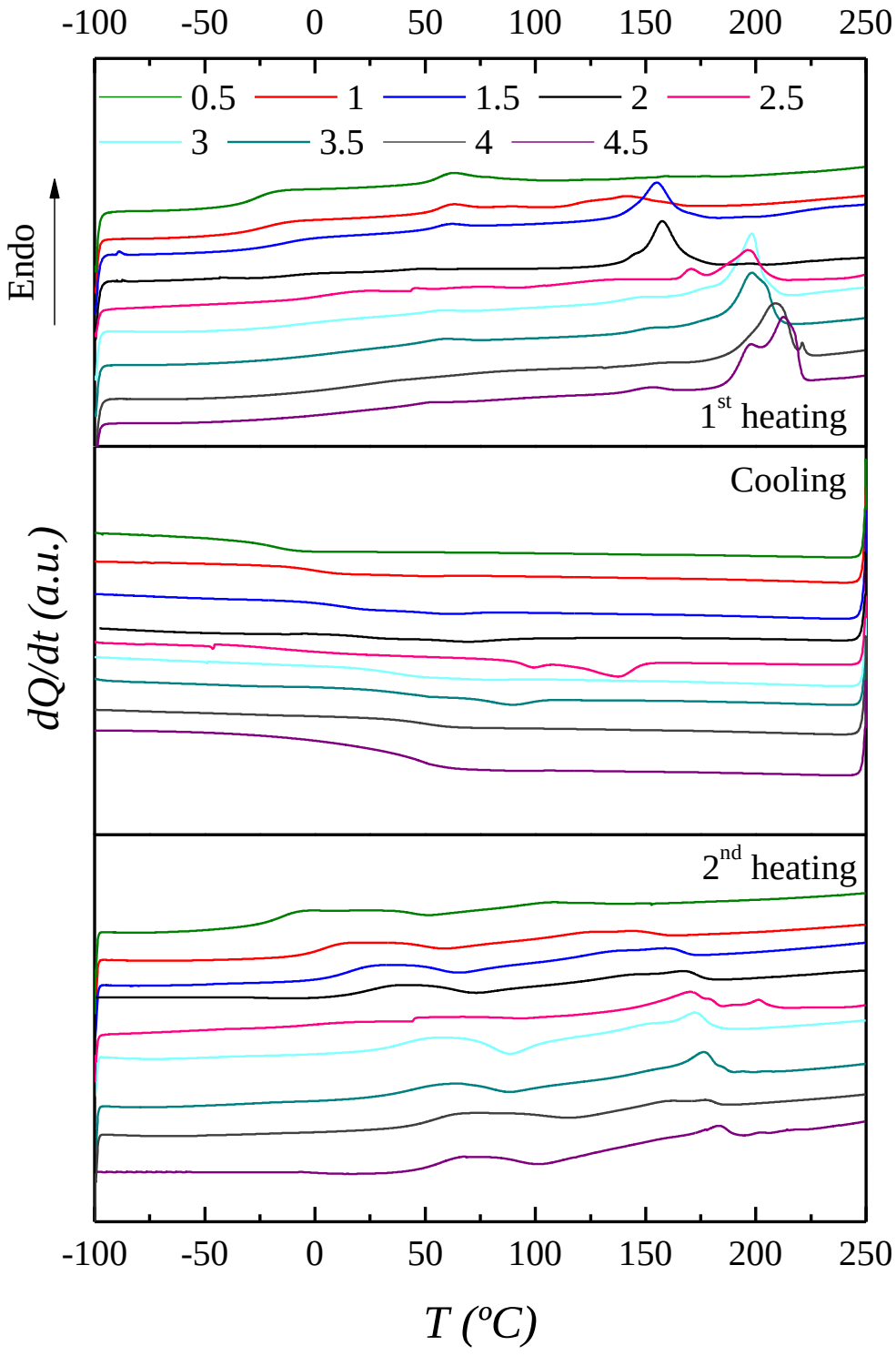

Figure B.4. *DSC curves for system 4, PTMG650MDI*

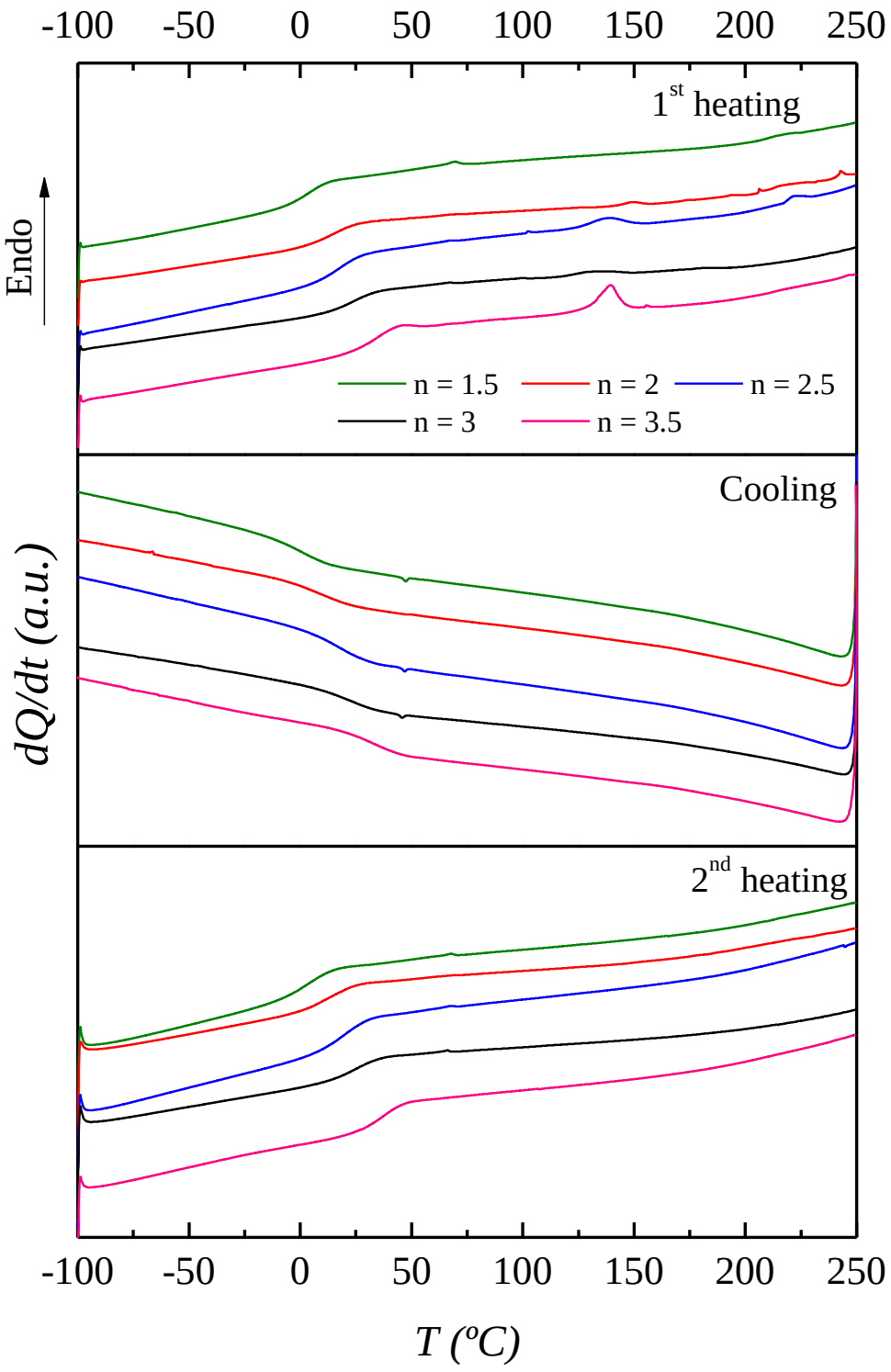

Figure B.5. *DSC curves for system 5, PTMG650TDI+MDI*

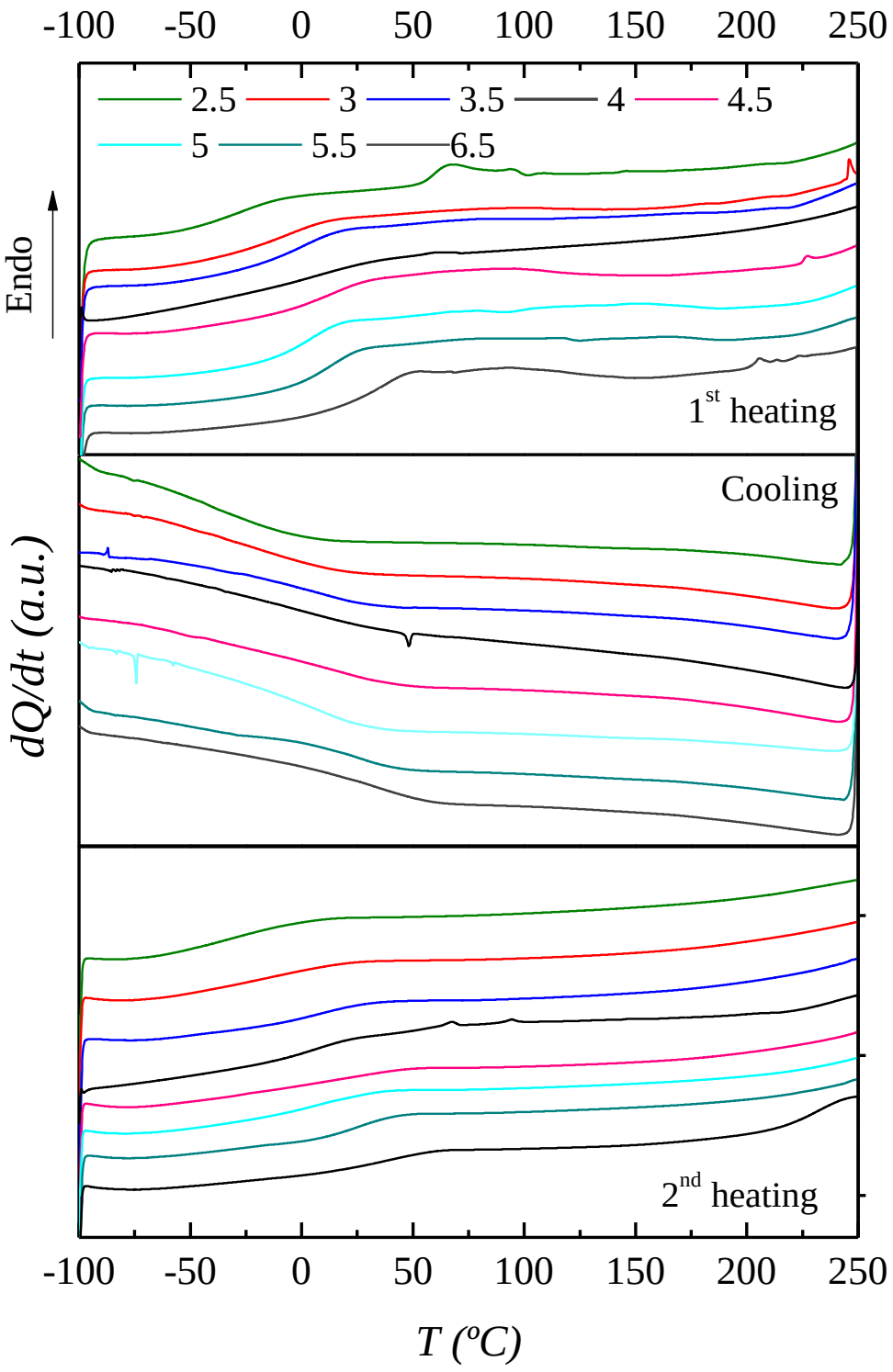

Figure B.6. *DSC curves for system 6, PTMG1000TDI*

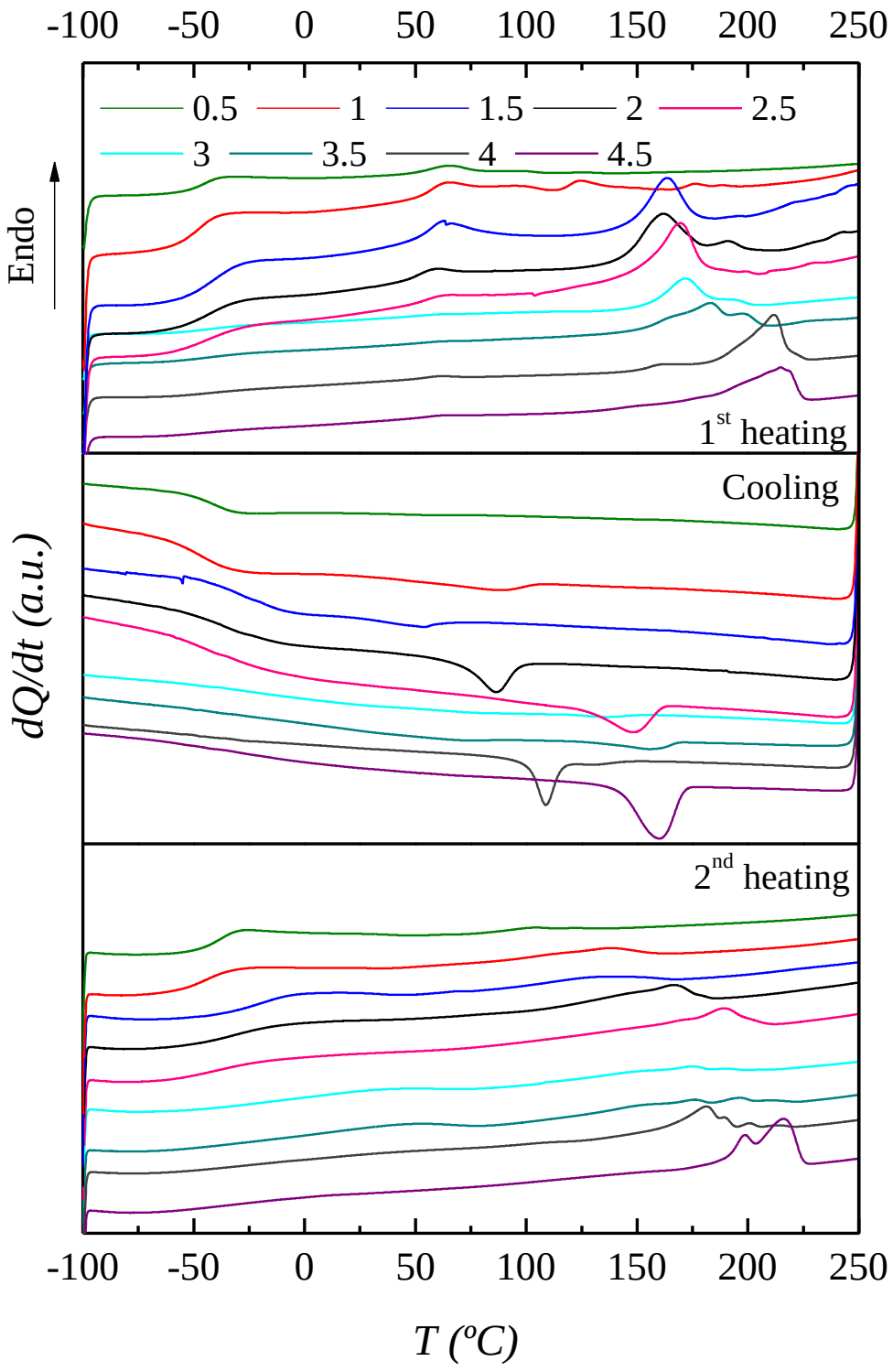

Figure B.7. *DSC curves for system 7, PTMG1000MDI*

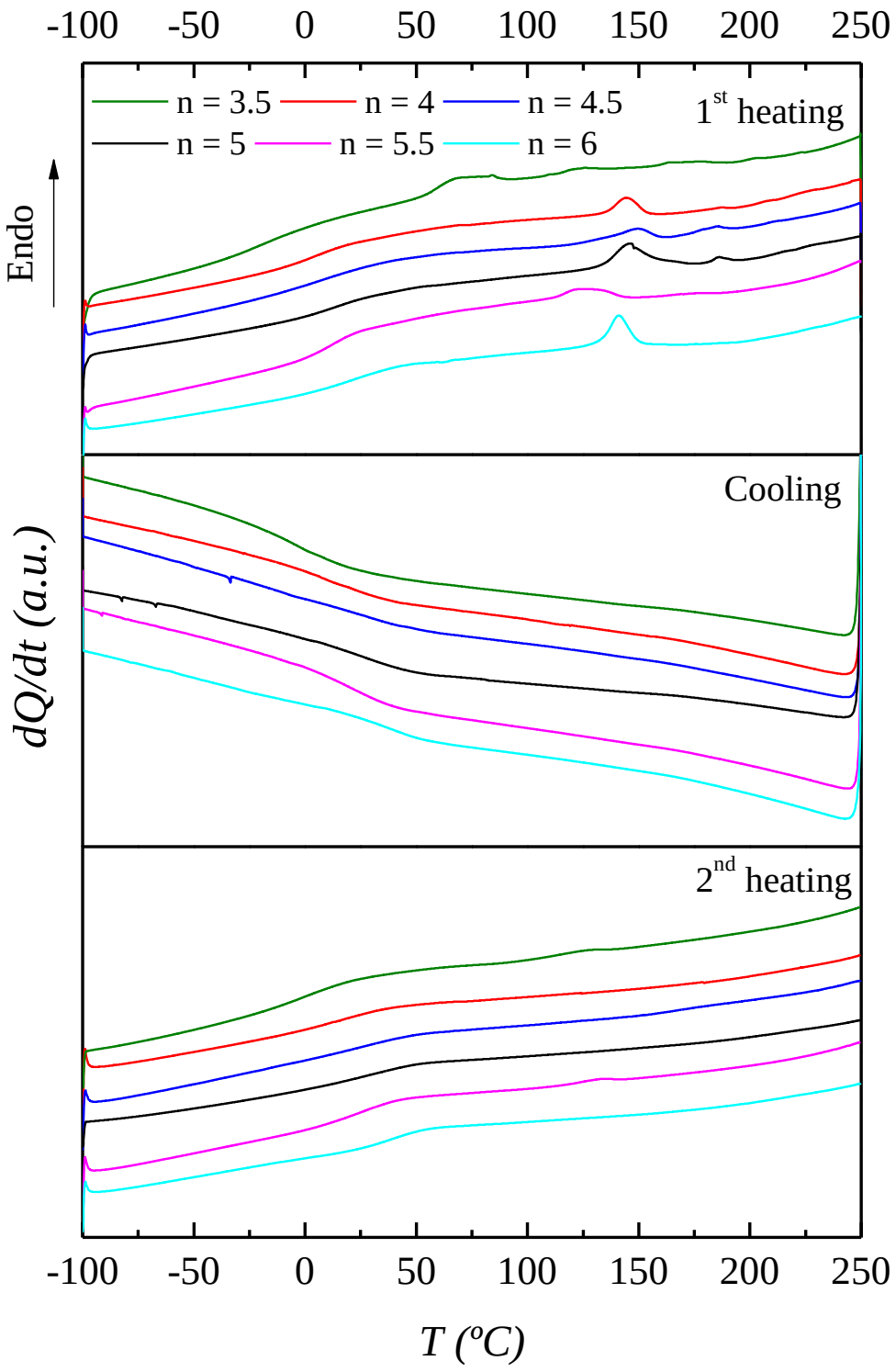

Figure B.8. *DSC curves for system 8, PMG1000TDI+MDI*

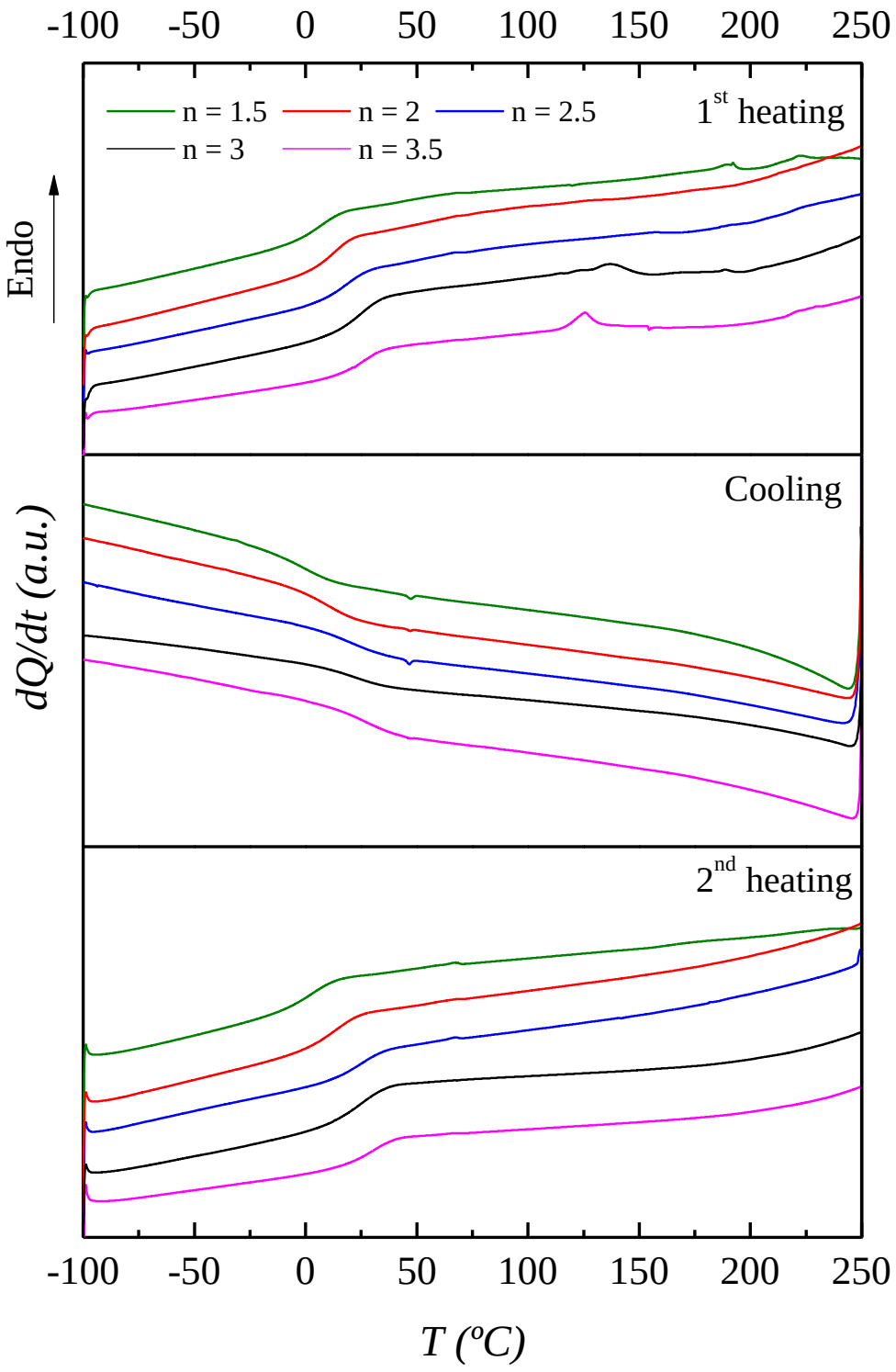

Figure B.9. *DSC curves for system 9, P*TMG650/MDI+TDI/1%TiO_2

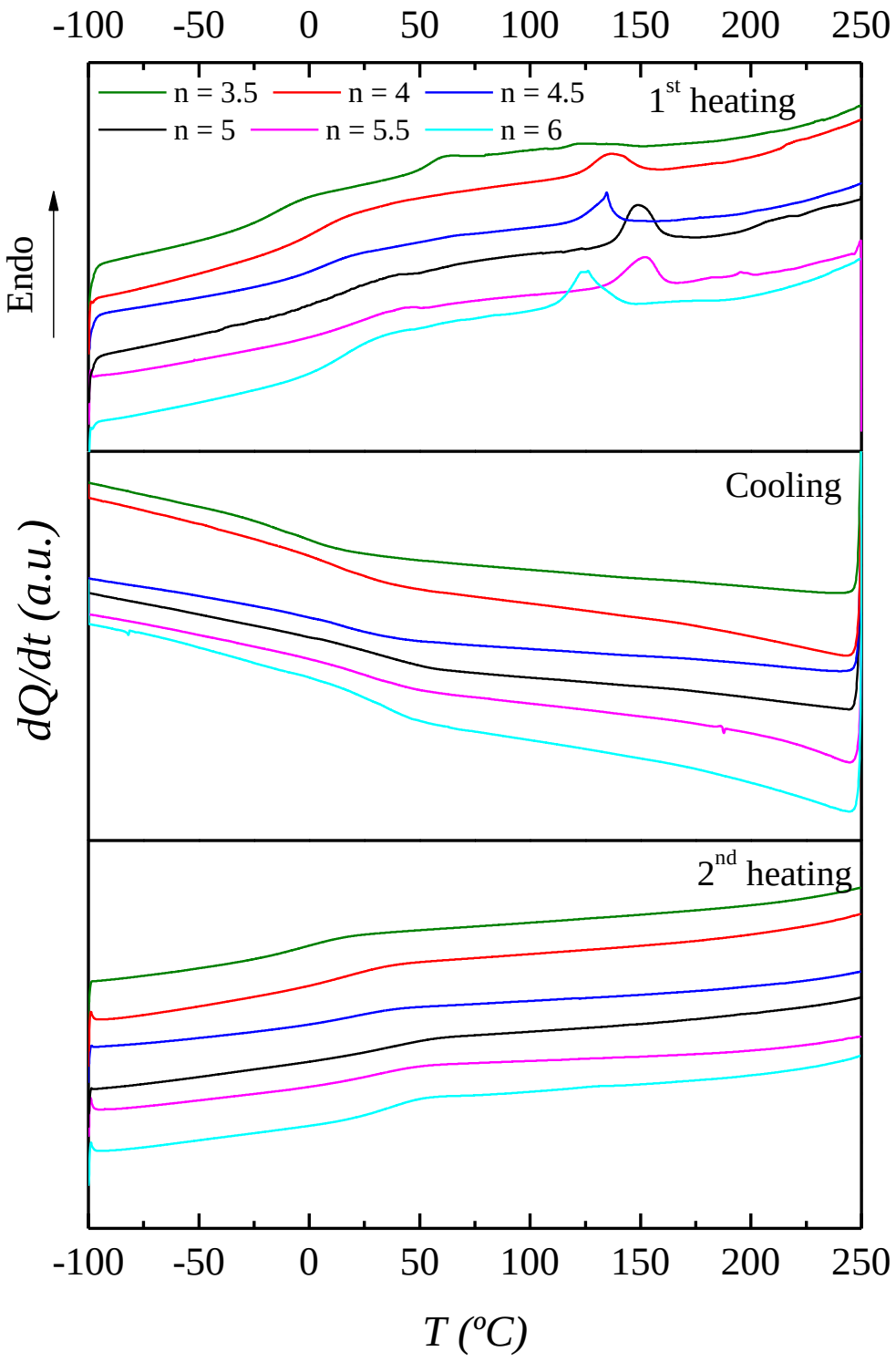

Figure B.10. *DSC curves for system 10, PTMG1000/MDI+TDI/1%TiO2*

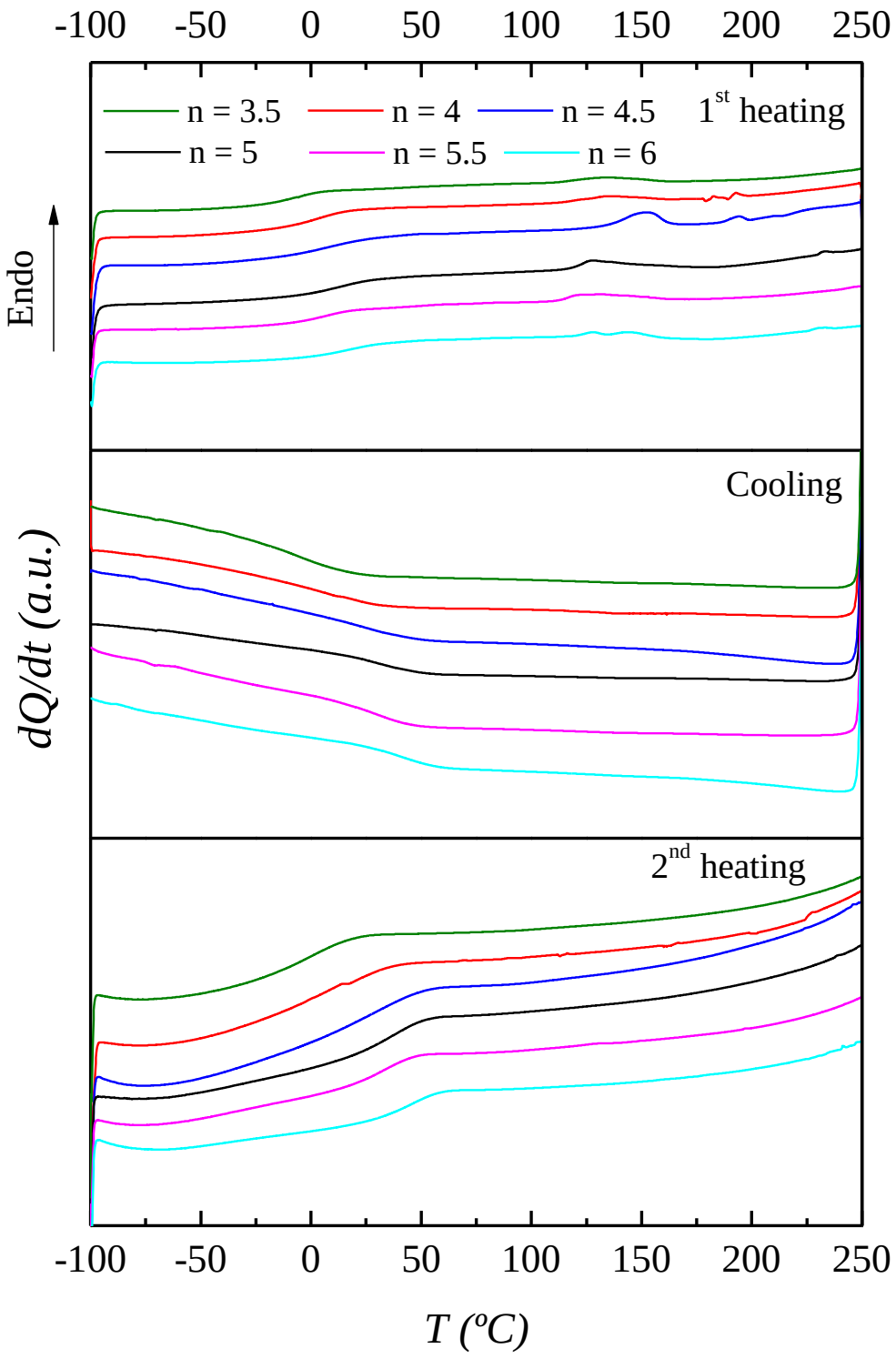

Figure B.11. *DSC curves for system 11,* PTMG1000/MDI+TDI/3%TiO_2

Appendix C
THERMOMECHANICAL BEHAVIOR

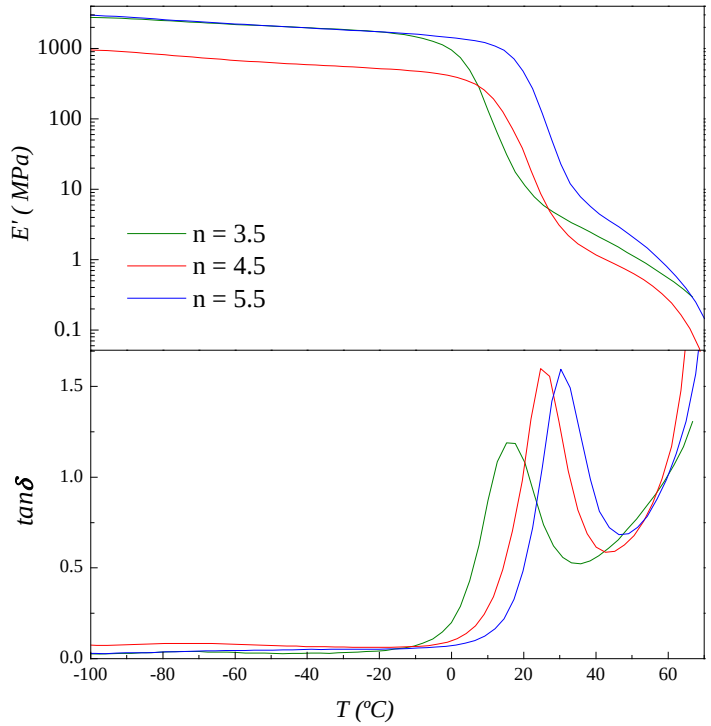

Figure C.1. *DMA curves for system 1, PEG1000TDI*

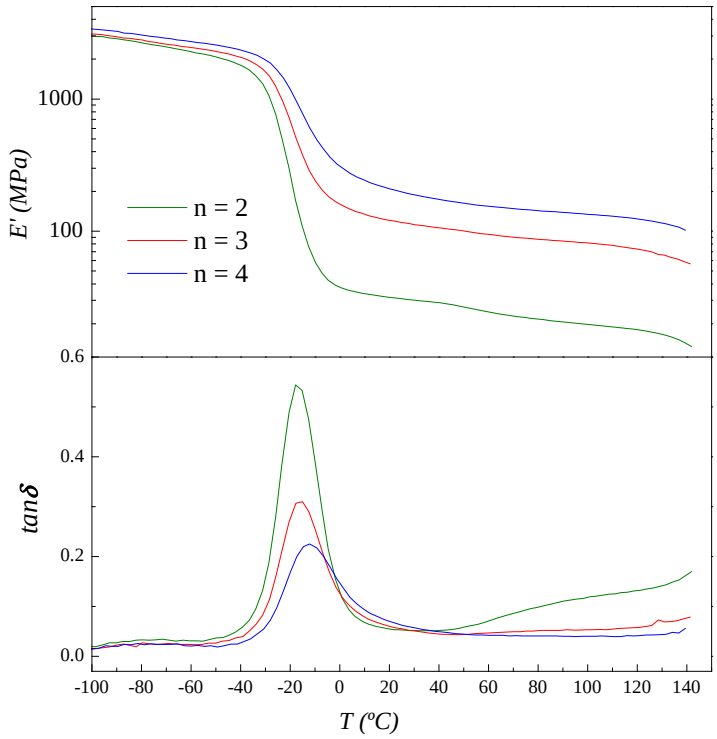

Figure C.2. *DMA curves for system 2, PEG1000MDI*

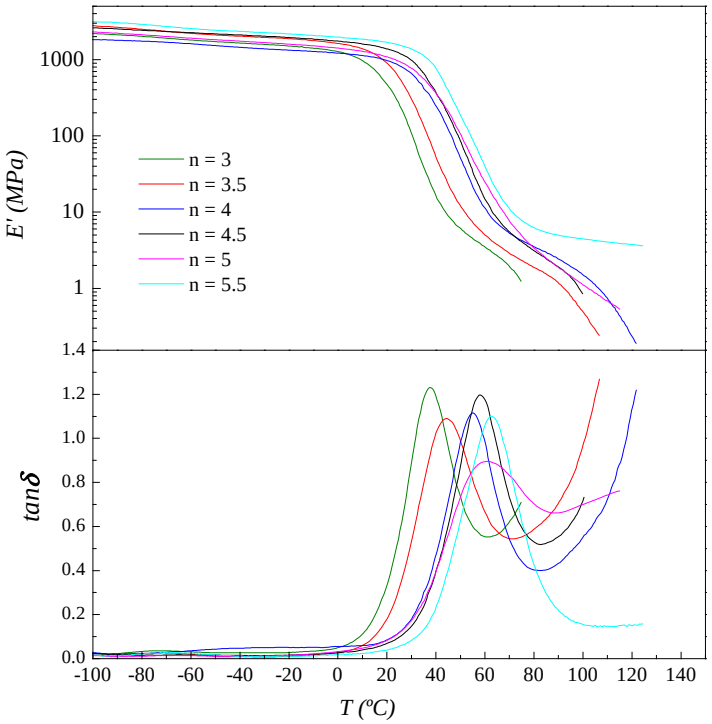

Figure C.3. *DMA curves for system 3, PTMG650TDI*

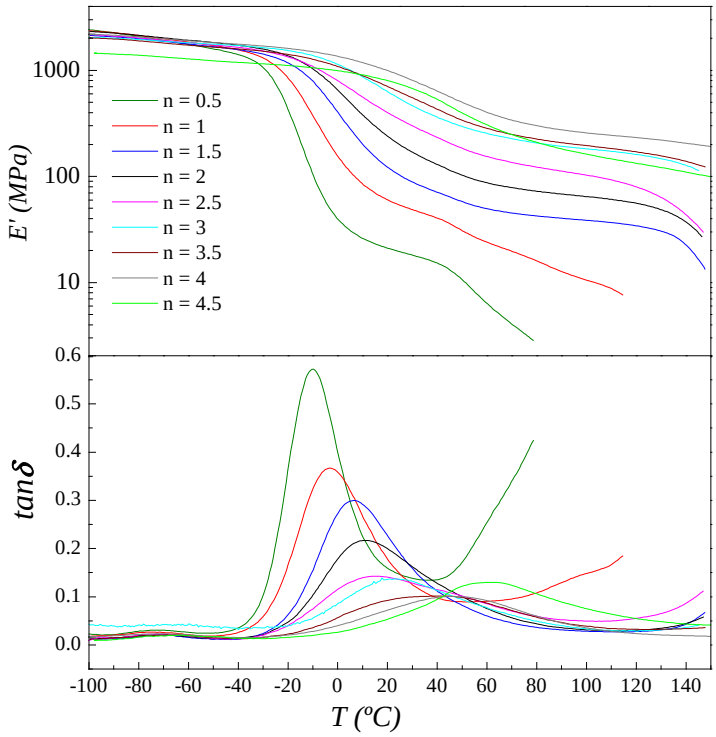

Figure C.4. *DMA curves for system 4, PTMG650MDI*

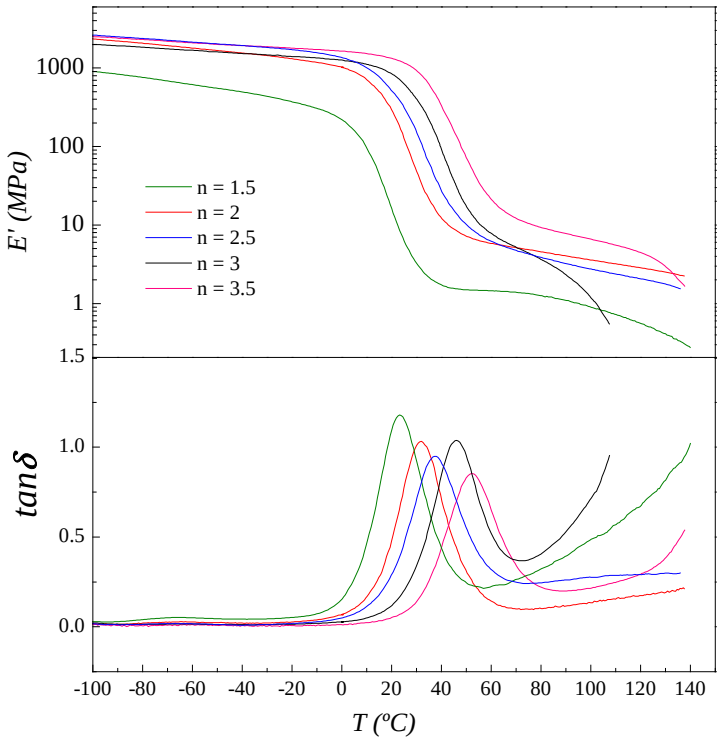

Figure C.5. *DMA curves for system 5, PTMG650TDI+MDI*

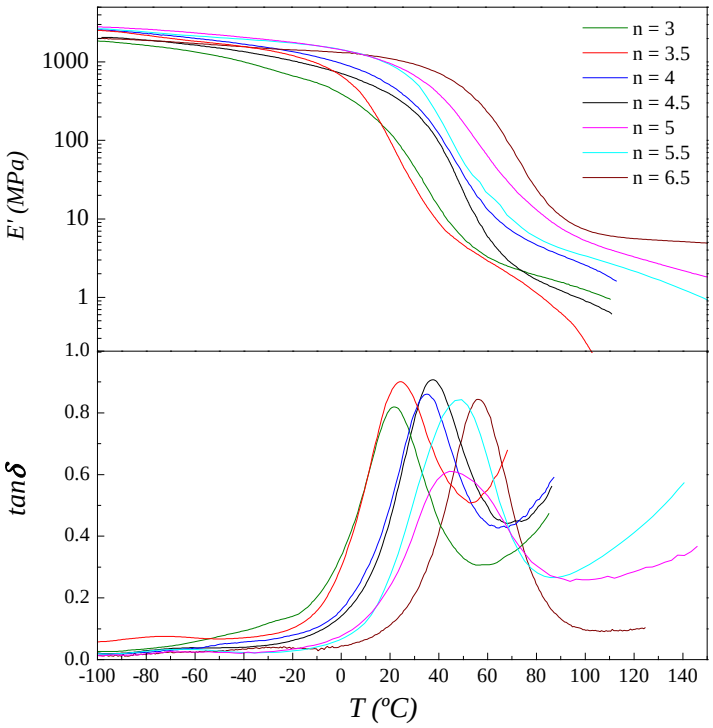

Figure C.6. *DMA curves for system 6, PTMG1000TDI*

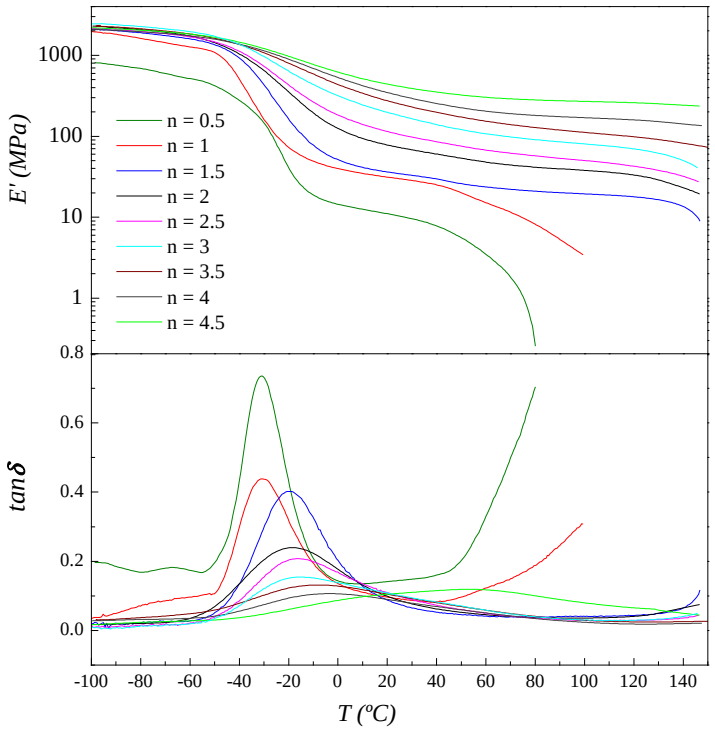

Figure C.7. *DMA curves for system 7, PTMG1000MDI*

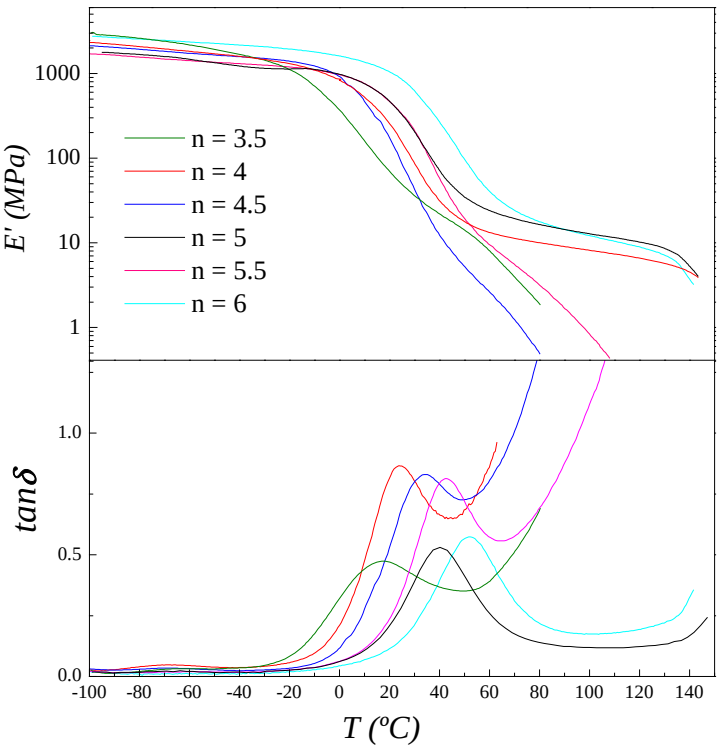

Figure C.8. *DMA curves for system 8, PTMG1000TDI+MDI*

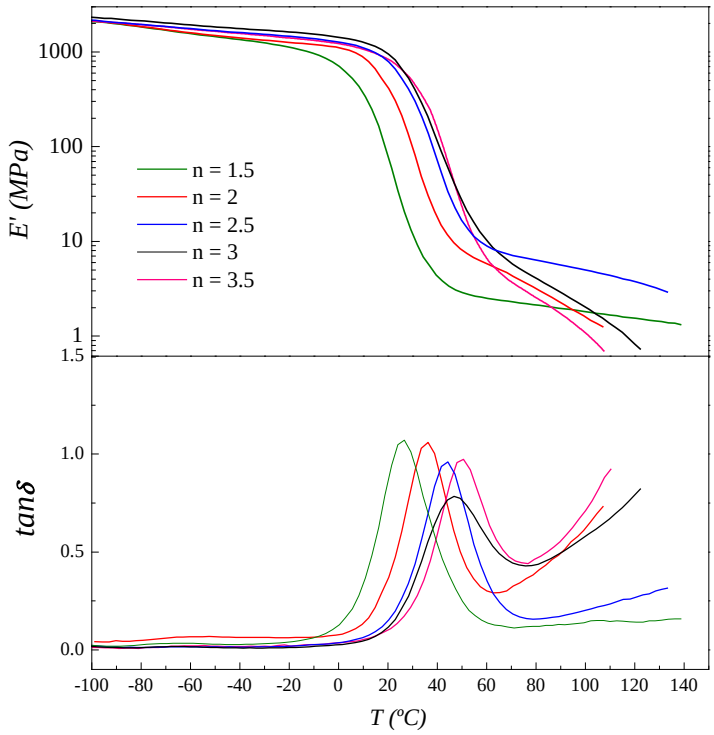

Figure C.9. *DMA curves for system 9, PTMG650/MDI+TDI/1%TiO_2*

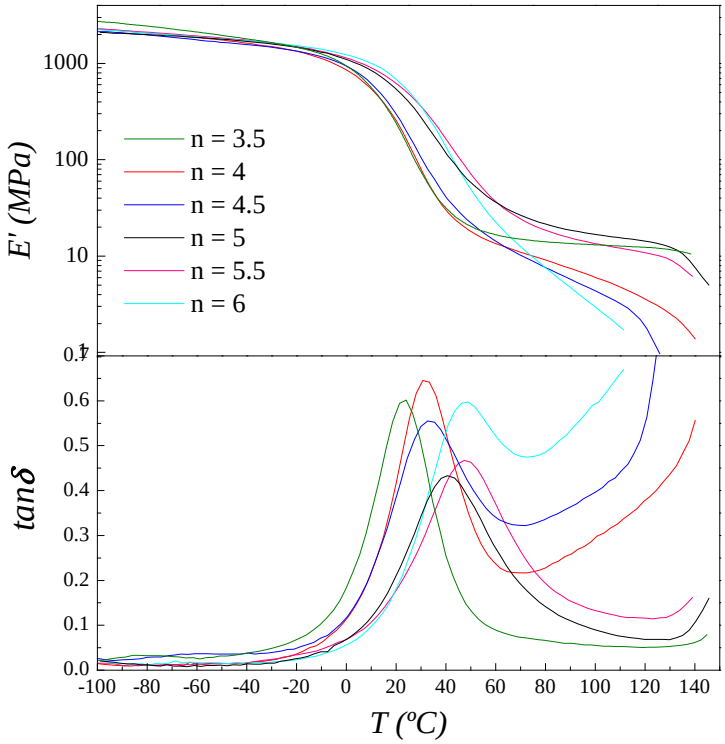

Figure C.10. *DMA curves for system 10, PTMG1000/MDI+TDI/1%TiO2*

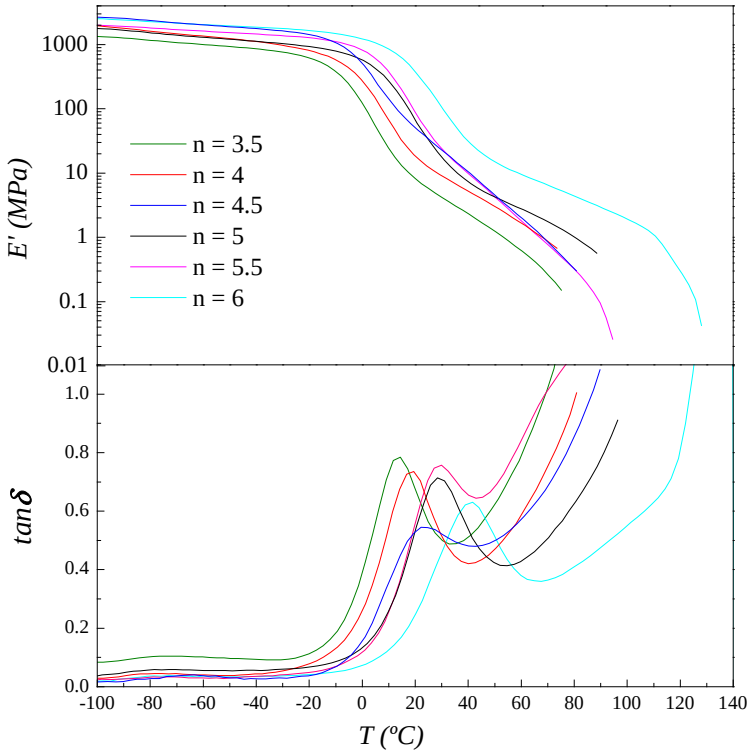

Figure C.11. *DMA curves for system 11, PTMG1000/MDI+TDI/3%TiO_2*

Appendix D
SHAPE MEMORY BEHAVIOR

SHAPE MEMORY BEHAVIOR – ONE CYCLE

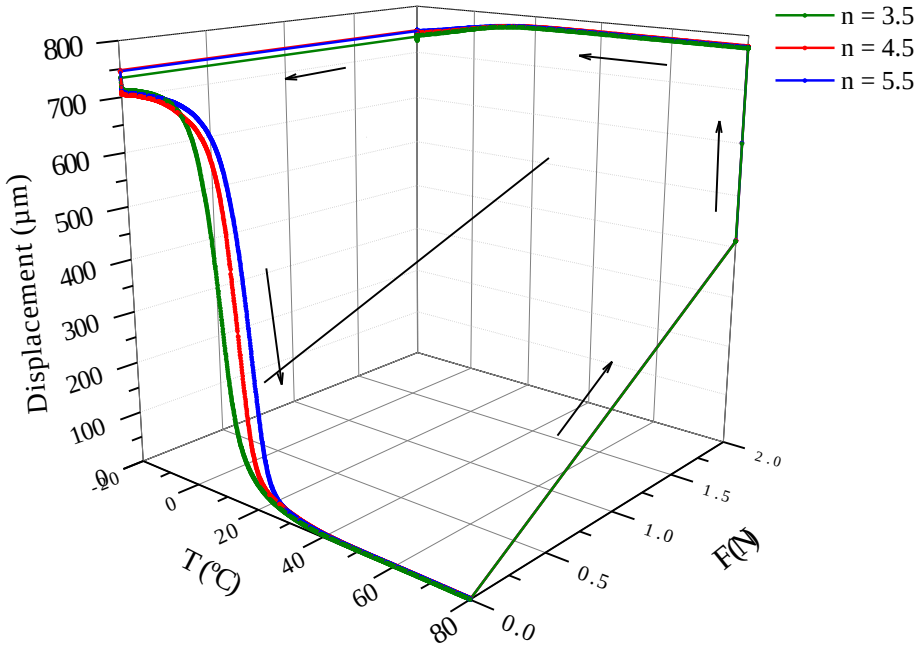

Figure D.1. *Three-dimensional thermomechanical response for system 1, PEG1000TDI*

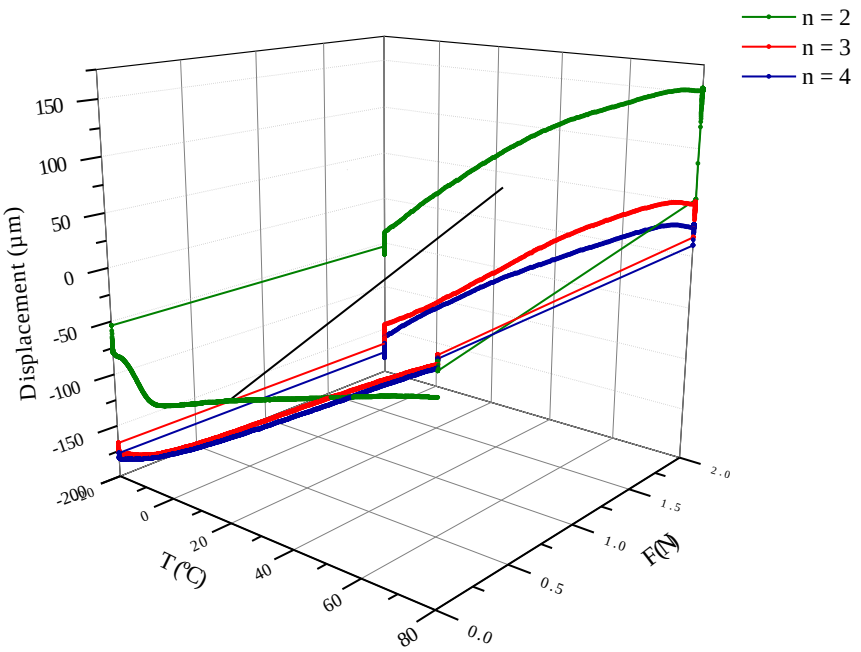

Figure D.2. *Three-dimensional thermomechanical response for* system 2, PEG1000MDI

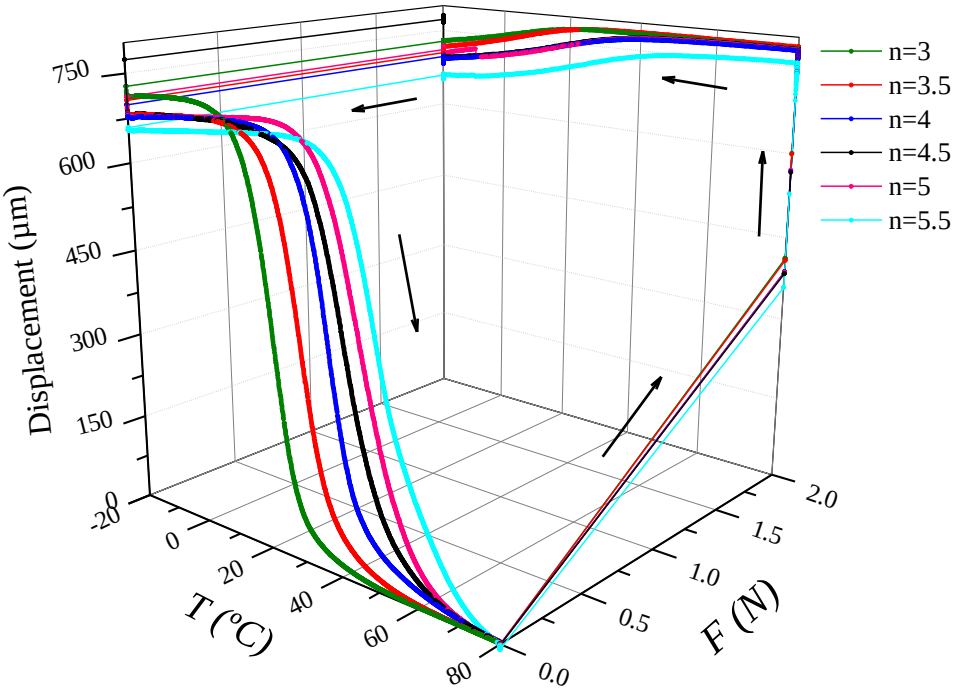

Figure D.3. *Three-dimensional thermomechanical response for system 3, PTMG650TDI*

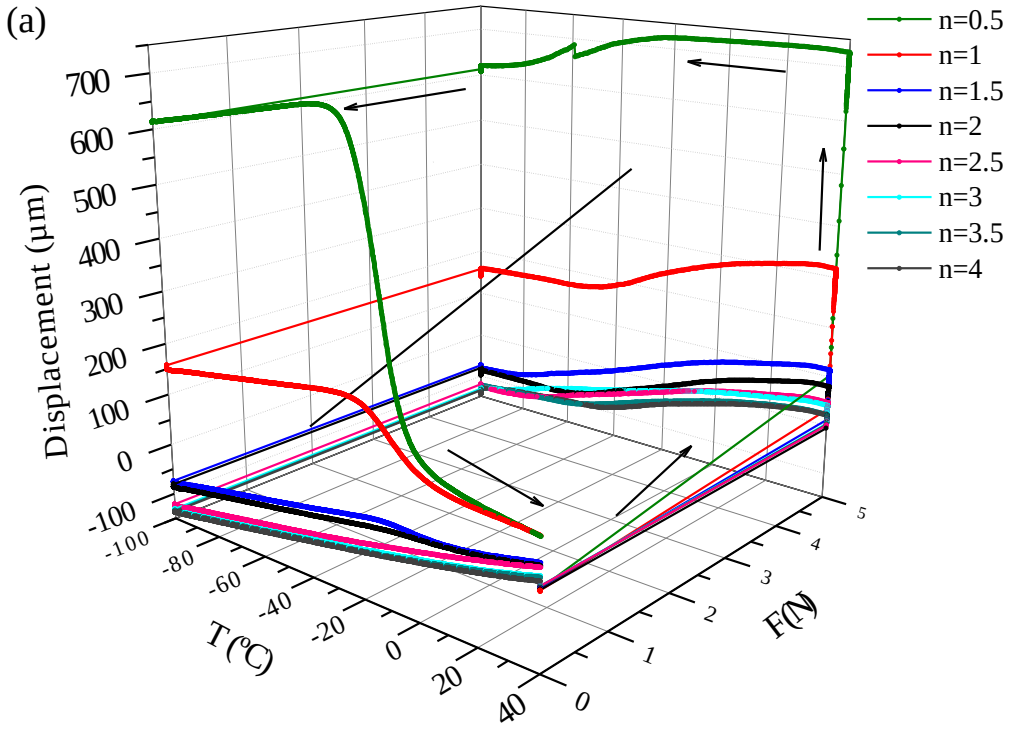

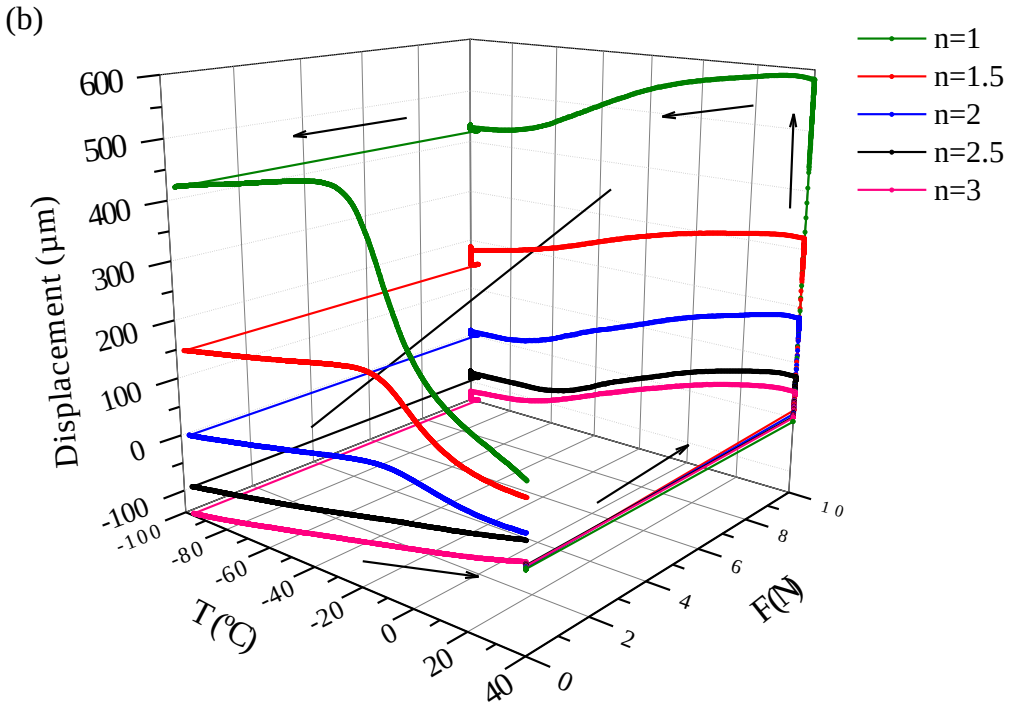

Figure D.4. Three-dimensional thermomechanical response for *system 4, PTMG650MDI, F = 5 N (a) and F = 10 N (b)*

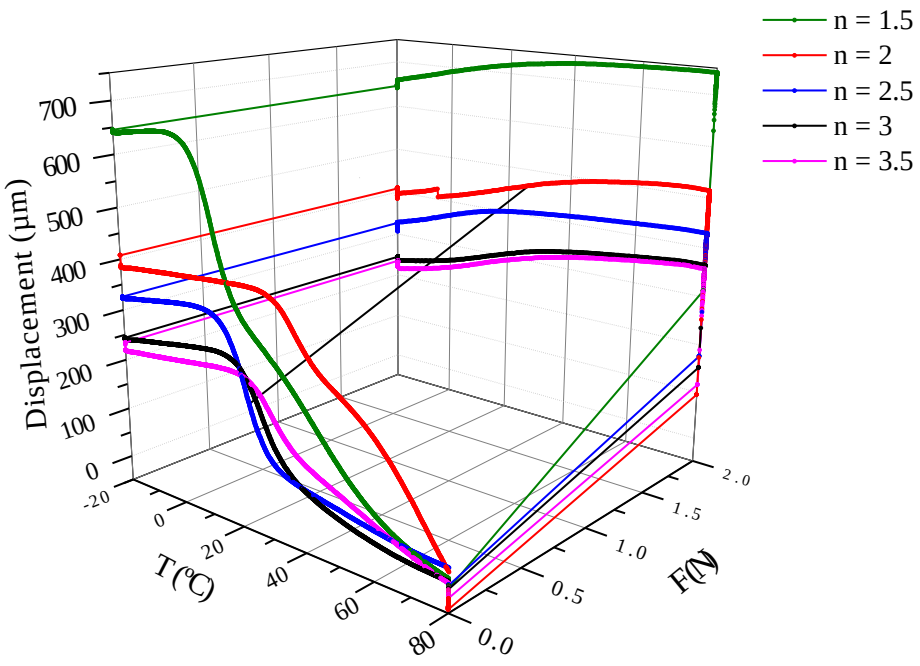

Figure D.5. *Three-dimensional thermomechanical response for system 5, PTMG650TDI+MDI*

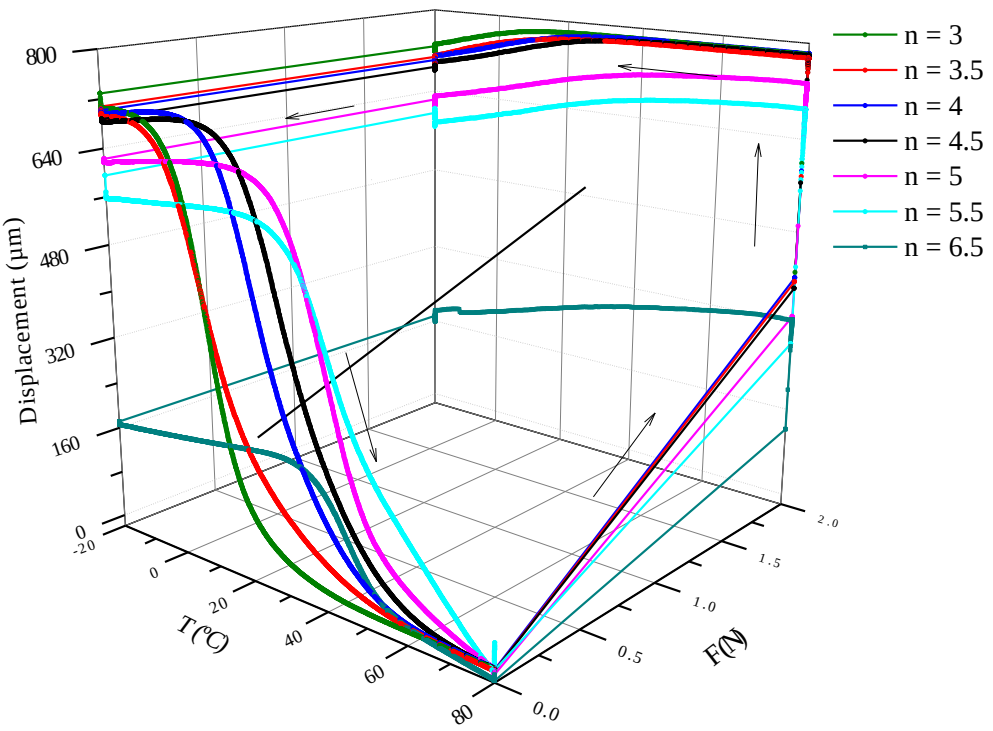

Figure D.6. *Three-dimensional thermomechanical response for system 6, PTMG1000TDI*

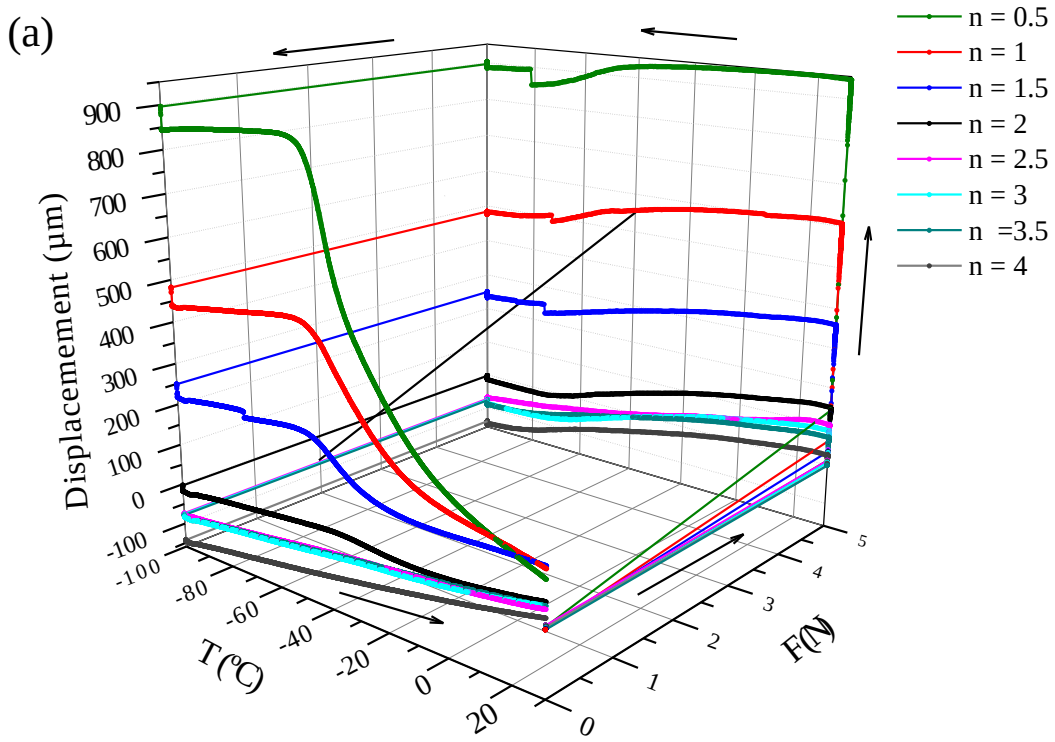

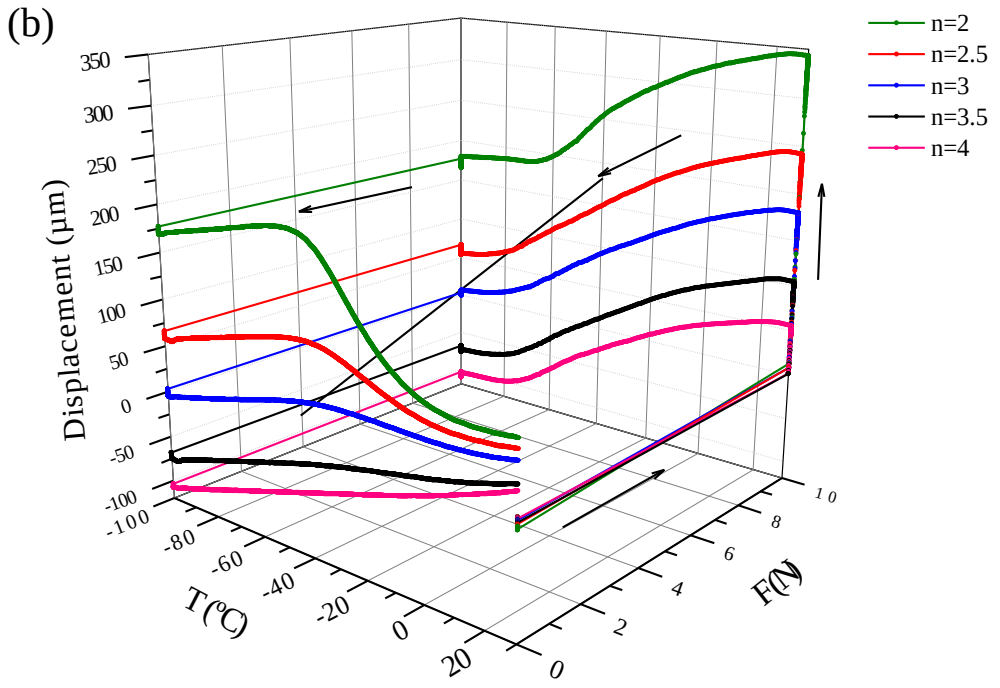

Figure D.7. *Three-dimensional thermomechanical response for system 7, PTMG1000MDI, F = 5 N (a) and F = 10 N (b)*

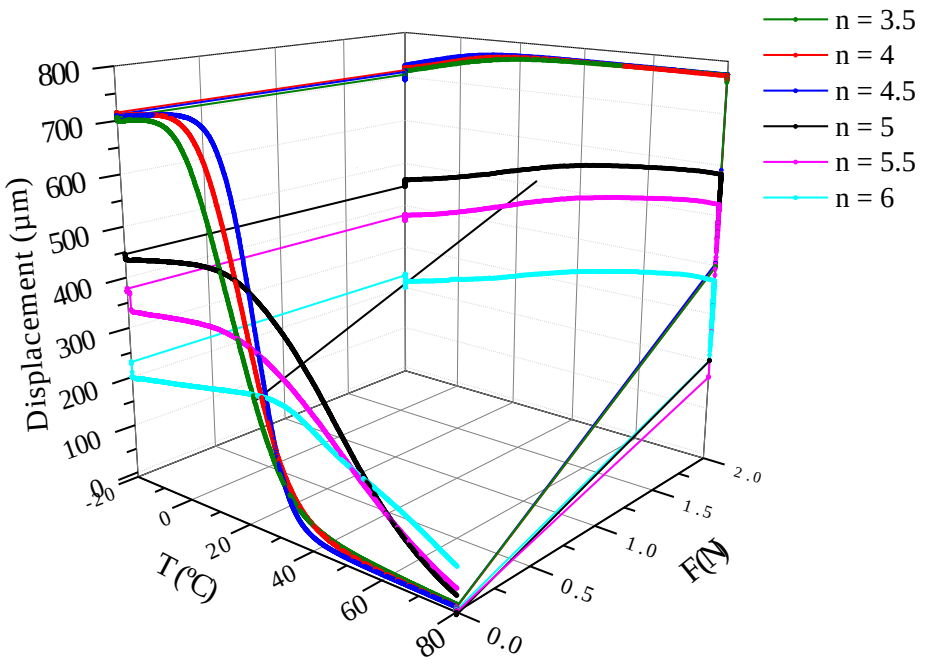

Figure D.8. *Three-dimensional thermomechanical response for system 8, PTMG1000TDI+MDI*

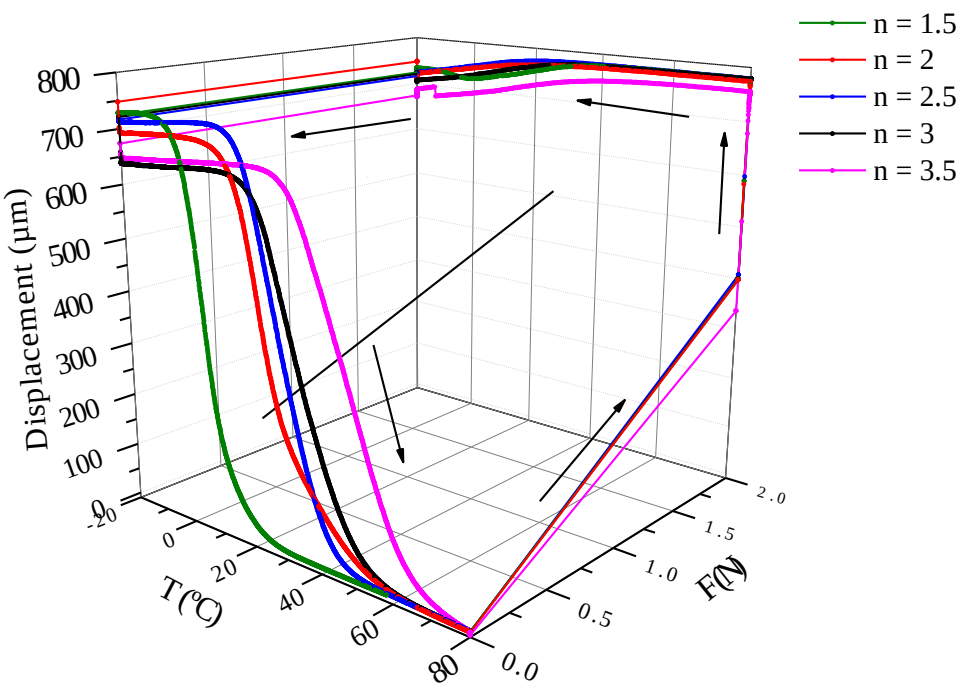

Figure D.9. *Three-dimensional thermomechanical response for system 9, PTMG650/MDI+TDI/1%TiO_2*

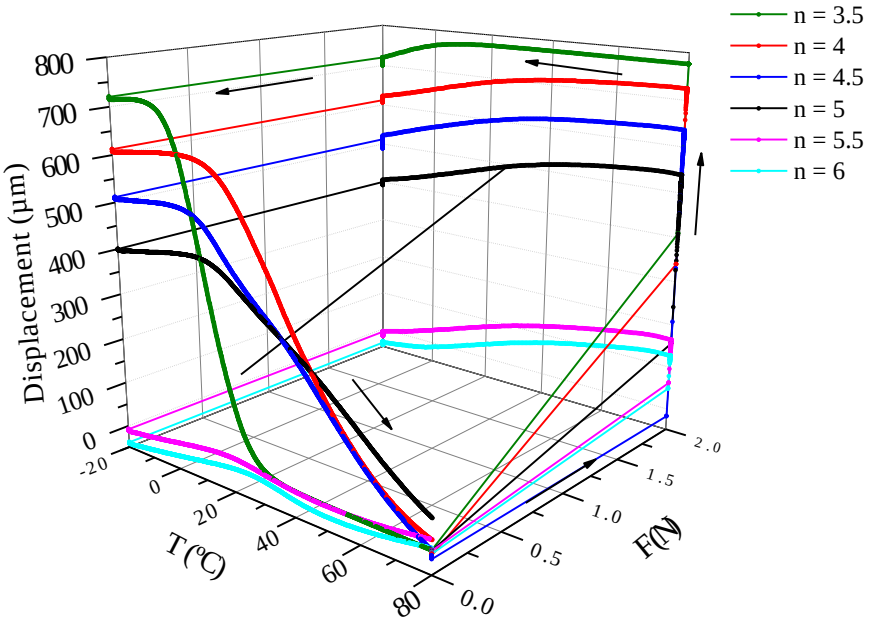

Figure D.10. *Three-dimensional thermomechanical response for system 10,* PTMG1000/MDI+TDI/1%TiO2

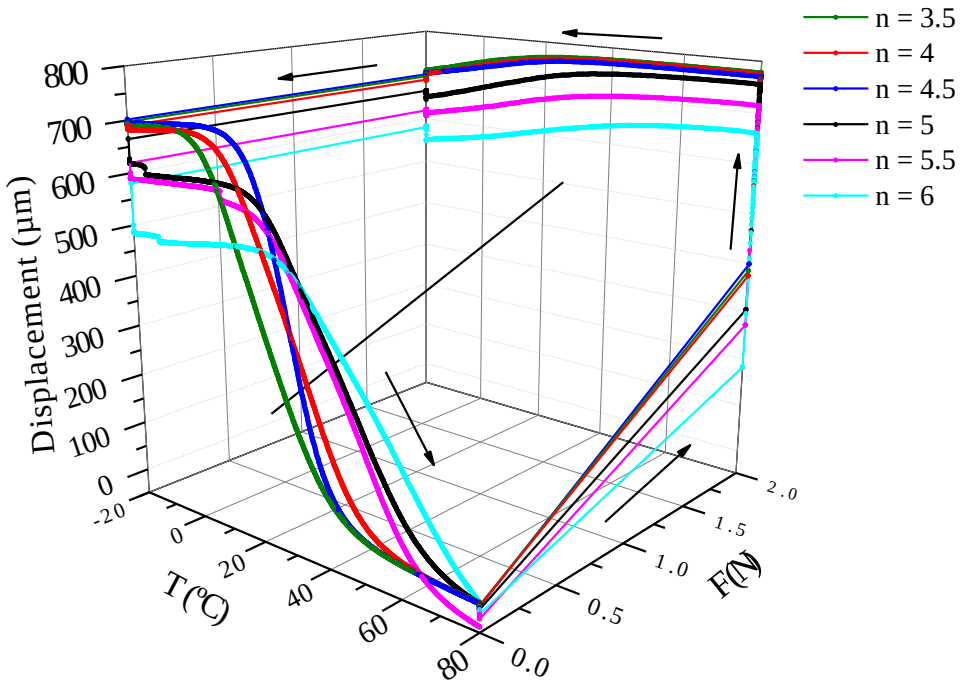

Figure D.11. *Three-dimensional thermomechanical response for system 11, PTMG1000/MDI+TDI/3%TiO_2*

SHAPE MEMORY BEHAVIOR – SIX CYCLES

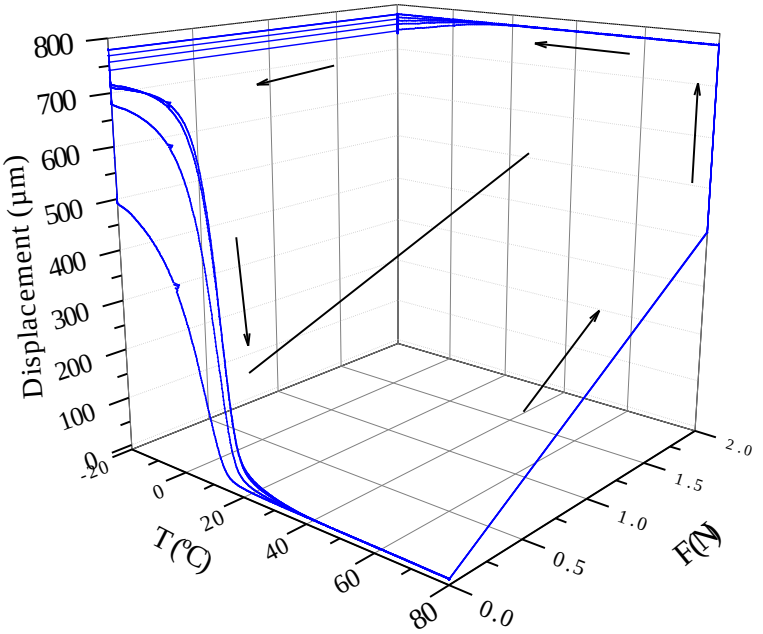

Figure D.12. *Three-dimensional thermomechanical response for system 1, PEG1000TDI – 6 cycles*

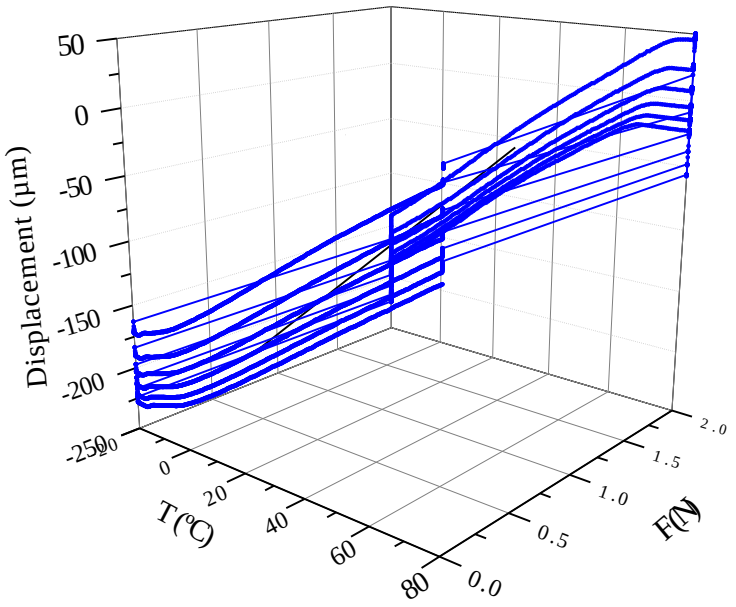

Figure D.13. *Three-dimensional thermomechanical response for* system 2, *PEG1000MDI – 6 cycles*

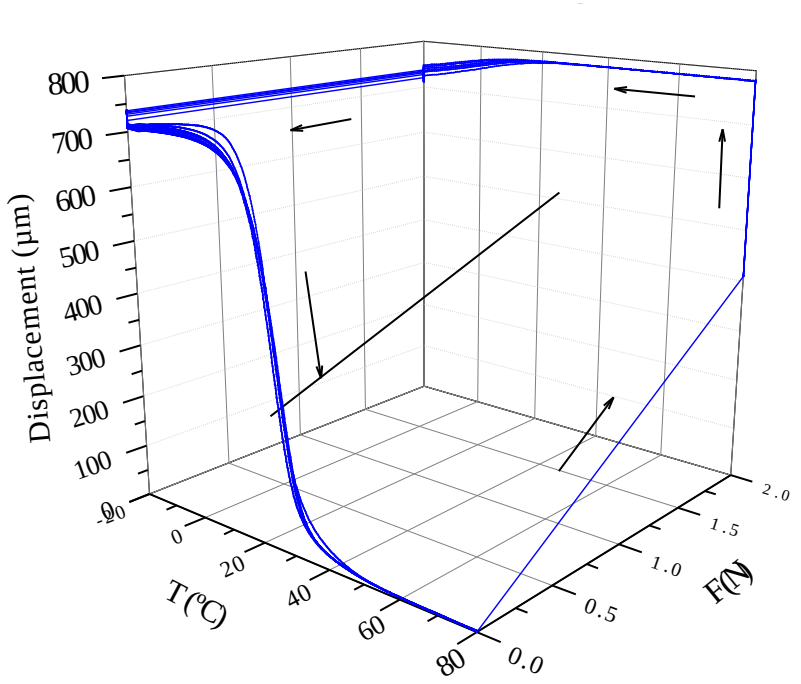

Figure D.14. *Three-dimensional thermomechanical response for system 3, PTMG650TDI – 6 cycles*

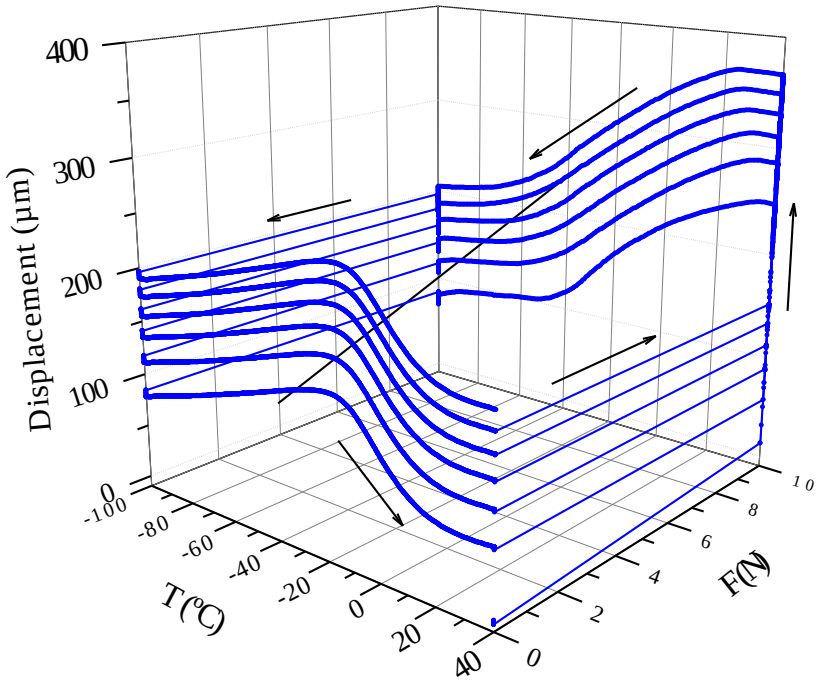

Figure D.15. *Three-dimensional thermomechanical response for system 4, PTMG650MDI – 6 cycles*

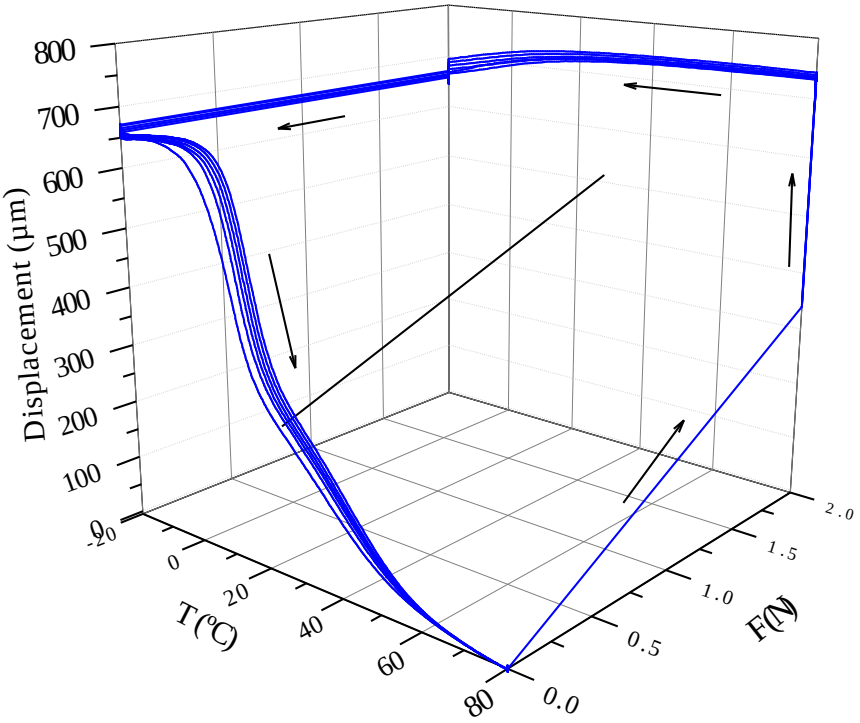

Figure D.16. *Three-dimensional thermomechanical response for system 5, PTMG650TDI+MDI – 6 cycles*

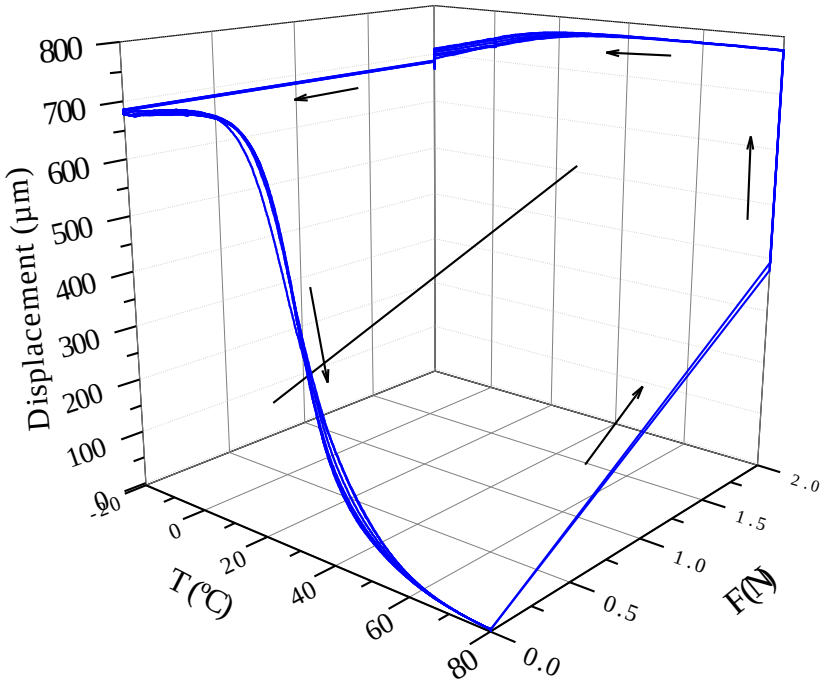

Figure D.17. *Three-dimensional thermomechanical response for system 6, PTMG1000TDI – 6 cycles*

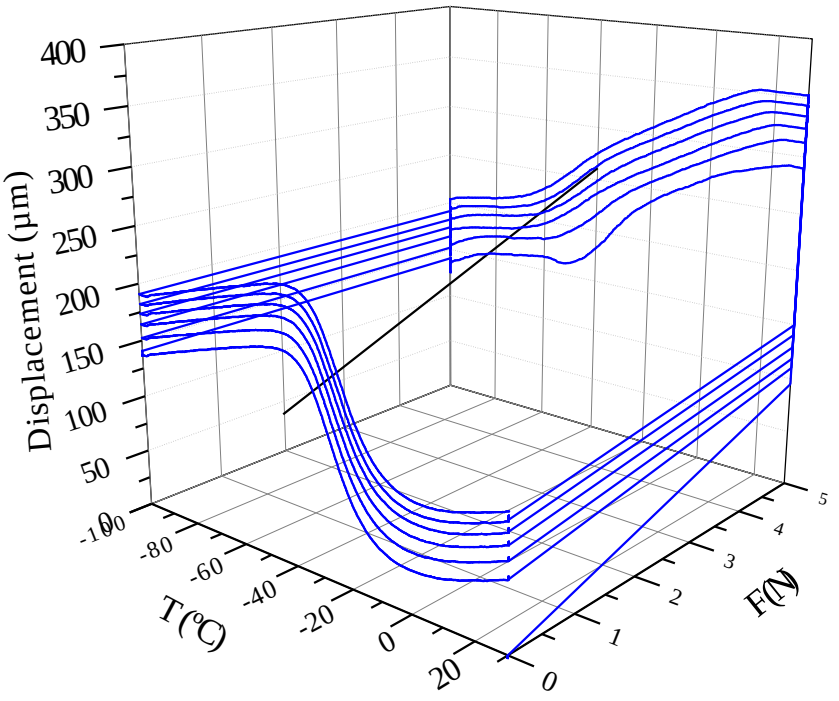

Figure D.18. *Three-dimensional thermomechanical response for system 7, PTMG1000MDI – 6 cycles*

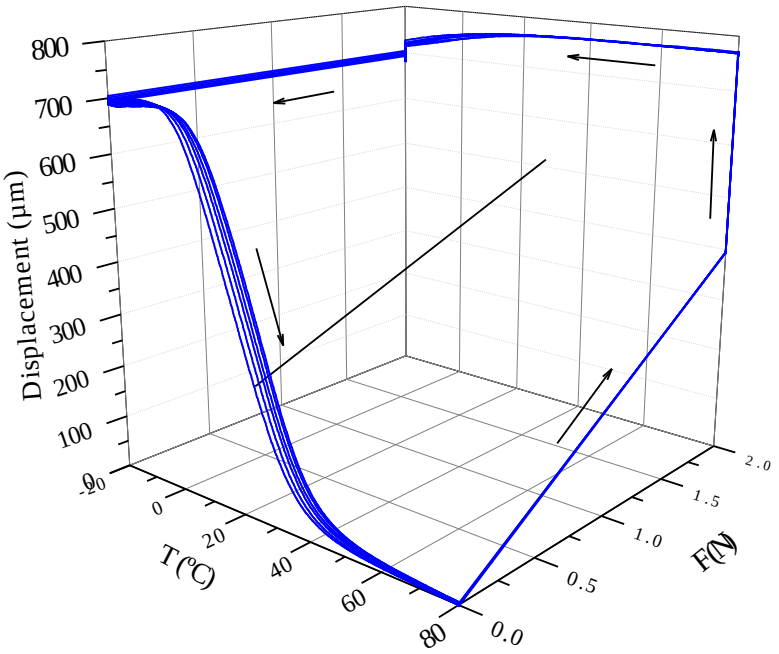

Figure D.19. *Three-dimensional thermomechanical response for system 8, PTMG1000TDI+MDI – 6 cycles*

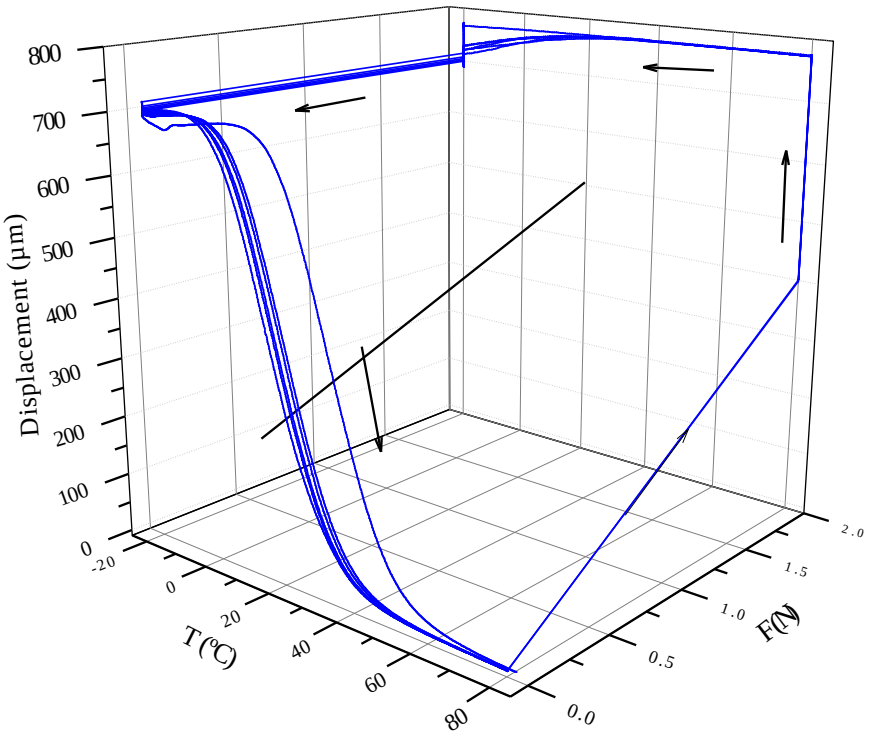

Figure D.20. *Three-dimensional thermomechanical response for system 9, PTMG650/MDI+TDI/1%TiO_2 – 6 cycles*

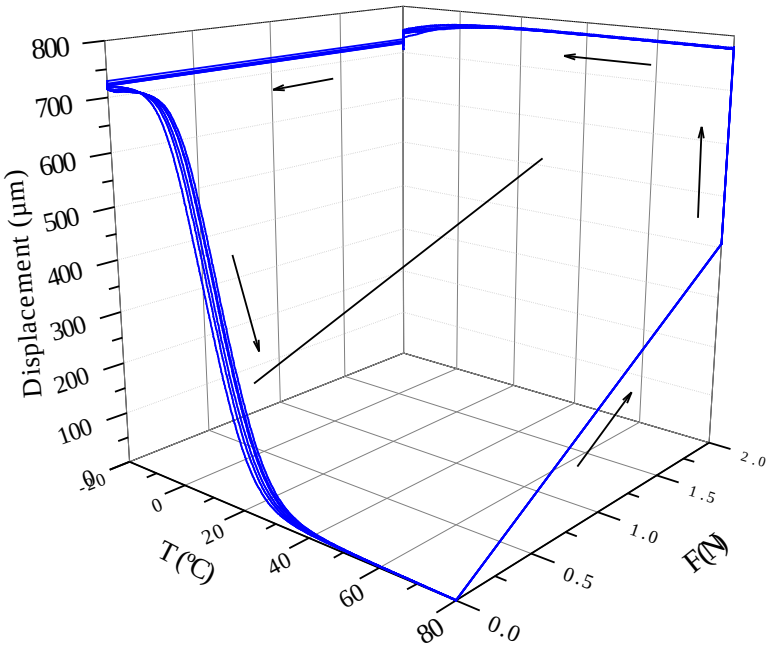

Figure D.21. *Three-dimensional thermomechanical response for system 10, PTMG1000/MDI+TDI/1%TiO_2 – 6 cycles*

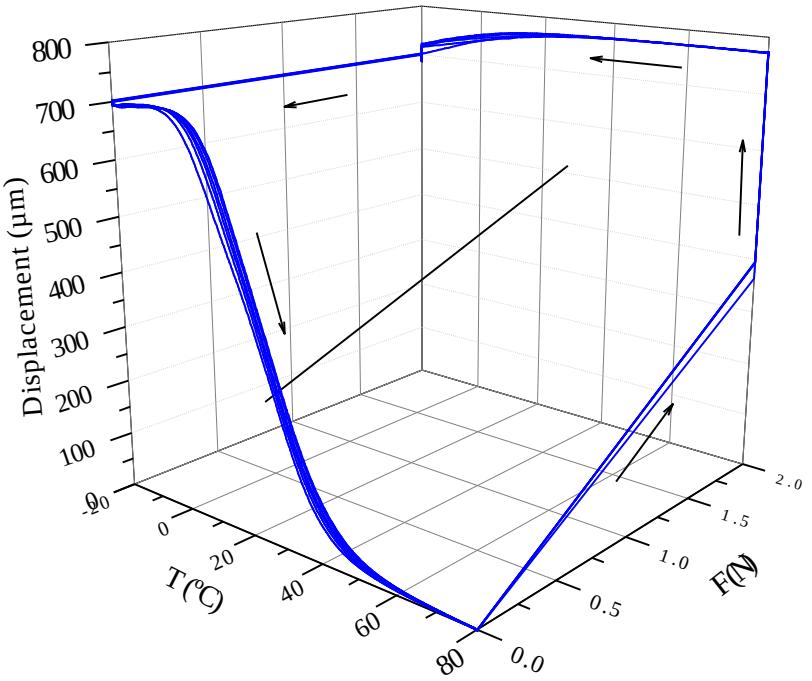

Figure D.22. *Three-dimensional thermomechanical response for system 11, PTMG1000/MDI+TDI/3%TiO_2 – 6 cycles*

Curriculum vitae & Contributions

Míriam Sáenz Pérez

msaenz@ctcr.es

Education

2013-Present PhD, "Shape Memory Polyurethanes. Application in smart fabrics". University of the Basque Country (UPV/EHU)

2013 Master in teacher training of Secondary Education

2012 Master in Chemistry and Polymers, University of the Basque Country (UPV/EHU)

2012 Master of Quality and Environment - EFEM

2011 Chemical Engineering, speciality Process Engineering, University of Zaragoza

Research stay abroad

University of Borås, Sweden (Three months, 2017)

Advisor: Prof. Mikael Skrifvars

Papers

Part of the thesis

1) "Methylene diphenyl diisocyanate (MDI) and toluene diisocyanate (TDI) based polyurethanes: thermal, shape-memory and mechanical behaviour"
   Míriam Sáenz-Pérez, Erlantz Lizundia, José Manuel Laza, Jorge García Barrasa, José Luis Vilas and Luis Manuel León
   RSC Advances
   2016

2) Influence of the Soft Segment Nature on the Thermomechanical Behavior of Shape Memory Polyurethanes"
   Míriam Sáenz-Pérez, José Manuel Laza, Jorge García-Barrasa, José Luis Vilas, Luis Manuel León
   Polymer Engineering and Science
   2017

3) "Novel shape-memory polyurethane fibers for textile applications"
Míriam Sáenz-Pérez, Tariq Bashir, José Manuel Laza, Jorge García-Barrasa, José Luis Vilas, Mikael Skrifvars and Luis Manuel León
Textile Research Jornal
2018 (accept - 22/01/2018)

4) "Water, oxygen and limonene permeability behaviour of shape memory polyurethanes"
Míriam Sáenz-Pérez, José Manuel Laza, Jorge García-Barrasa, José Luis Vilas, Luis Manuel León
(in preparation)

Other articles

1) "Nanopatterned polystyrene-b-poly(acrylic acid) surfaces to modulate cell-material interaction"
Erlantz Lizundia, Míriam Sáenz-Pérez, David Patrocinio, Iskander Aurrekoetxea, Maria dM Vivanco, José Luis Vilas
Materials Science and Engineering C
2017

2) "Physical aging and mechanical performance of poly (L-lactide)/ZnO nanocomposites"
Erlantz Lizundia, Leyre Pérez-Alvarez, Míriam Sáenz-Pérez, David Patrocinio, José Luis Vilas, Luis Manuel León
Journal of Applied Polymer Science
2016

3) "New amphiphilic block copolymers from lactic acid and cholinium building units"
Mehmet Isik, Haritz Sardon, Míriam Sáenz and David Mecerreyes
RSC Advances
2014

Contributions to congresses

1) XIV REUNION DEL GRUPO ESPECIALIZADO DE POLIMEROS GEP (RSEQ, RSEF)
Burgos, España
05/09/2016 – 08/09/2016
"Síntesis y caracterización de poliuretanos con memoria de forma"

M. Sáenz-Pérez, J. García-Barrasa, J.M. Laza, J.L. Vilas, L.M. León

2) MOL2NET International Conference
Online
05/12/2015 – 15/12/2015
"Synthesis and Characterization of Shape Memory Polyurethanes"

Míriam Sáenz-Pérez, J. M. Laza, Jorge García-Barrasa, Luis Manuel León and J. L. Vilas.

3) 5th International Conference on Biobased and Biodegradable Polymers
Donostia- San Sebastián, España
06/10/2015 – 09/10/2015
"Physical aging and mechanical performance of poly(l-lactide)/ZnO nanocomposites and applications of polyelectrolytes"
E. Lizundia, L. Pérez-Álvarez, M. Sáenz-Pérez, D. Patrocinio, J. Luis Vilas, L. Manuel León;

4) IUPAC World Polymer Congress

Virginia Tech, Estados Unidos de América

24/06/2012 – 29/06/2012

"Polymeric Ionic liquids broadening the properties and applications of polyelectrolytes"

David Mecerreyes; Míriam Sáenz Pérez; Ana Fernandes; Ali Aboudzadeh; Raquel Gracia.

5) 'Polymer Blends',

San Sebastián, País Vasco, España

25/03/2012 – 28/03/2012

6) European Combustion Meeting

Cardiff, Reino Unido

28/06/2011 – 01/07/2011

"Effect of the Gas Residence Time on Soot and PAH Formation during the Acetylene Pyrolysis"